Stability and Comparability of

EUROPEAN WIND–WAVE CLIMATE REGIMES

FOR OFFSHORE RENEWABLE ENERGY

Historical Assessment and Near-Term Projection

PONNI MAYA

$$\frac{\partial N}{\partial t} + \nabla \cdot (\mathbf{c}_g N) = \frac{S_{in} + S_{ds} + S_{nl}}{\sigma}$$

Stability and Comparability of European wind–wave Climate Regimes for Offshore Renewable Energy

Historical Assessment and Near-Term Projection

Dissertation

for the purpose of obtaining the degree of doctor
at Delft University of Technology
by the authority of the Rector Magnificus,
Prof. dr. ir. H. Bijl,
chair of the Board for Doctorates
to be defended publicly on
Thursday, 25 June 2026, 12:30

by

Ponni MAYA

This dissertation has been approved by the promotors.

Composition of the doctoral committee:

Rector Magnificus	chairperson
Prof. dr. A. V. Metrikine	Delft University of Technology, promotor
Dr. ing. J. A. Á. Antolínez	Delft University of Technology, promotor
Dr. L. Cagigal	Universidad de Cantabria, Spain, external adviser

Independent members:

Prof. dr. T. S. van den Bremer	Delft University of Technology
Prof. dr. D. M. Greaves	University of Oxford, United Kingdom
Dr. A. M. Semedo	IHE Delft Institute for Water Education
Prof. dr. M. I. Marcos Moreno	University of the Balearic Islands, Spain

Reserve member:

Prof. dr. ir. A. J. H. M. Reniers	Delft University of Technology

This dissertation forms part of a broader research effort aimed at improving the understanding and assessment of offshore wind and wave energy resources in the context of climate variability and change. It is funded by the Offshore Engineering Section, CEG, TU Delft, and partially supported by the EU-SCORES project under the European Union's Horizon 2020 research and innovation programme (grant agreement No 101036457).

Keywords: wind–wave climate regimes, Climate variability and stability, Machine learning, CMIP6 climate models, Offshore renewable energy

Cover by: Ponni MAYA

ISBN/EAN: 978-94-6518-356-5

An electronic copy of this dissertation is available at https://repository.tudelft.nl/.

Quiescent

Contents

Summary

In planning offshore renewable energy systems—such as offshore wind farms, wave energy devices, or hybrid installations—engineers and policymakers intervene in marine environments governed by coupled wind and wave processes. These processes respond to atmospheric forcing on short time scales (days, seasons) as well as on longer climate time scales (years, decades). For instance, a change in large-scale atmospheric circulation can immediately alter regional wind fields, which in turn modifies wave generation and propagation. Over longer periods, such changes can reorganise spatial patterns of wind–wave variability and affect the persistence and stability of offshore energy resources. The success of climate-informed offshore development therefore depends, at least partially, on our ability to predict how coupled wind–wave systems respond to changes in atmospheric forcing. We essentially aim to answer questions such as: how stable are wind–wave conditions across seasons and years? Which patterns persist, and which reorganise under climate variability? How reliably can climate models represent the wind–wave regimes that underpin offshore wind, wave, and hybrid energy potential, and how may these regimes reorganise under near-term climate forcing in the coming decades?

To answer such questions, a quantitative framework is needed. In this thesis, a framework is developed that sets relations between variables that represent the coupled wind–wave climate, such as significant wave height, mean wave period, wind speed, and wave and wind direction. These relations (in this case, the feature definitions and their joint covariance structure) are derived from physical consistency in the atmosphere–wave system and from statistical principles that capture how the variables co-vary across space and time. Hence, given an initial description of the historical climate (here, ERA5 reanalysis for 1979–2014) and the conditions defining the domain of interest (here, the European seas and their seasonal, interannual cycles), the framework describes the organisation and evolution of wind–wave variability in terms of a small number of coherent regimes. Principal component analysis reduces the multivariate complexity, and clustering groups locations with similar long-term behaviour, producing regimes that can be interpreted as open-ocean, transitional, and enclosed or semi-enclosed wind–wave climates.

A key requirement for a climate analysis framework is robustness. In this context, robustness means that the identified wind–wave patterns are well defined and vary smoothly with changes in the underlying data and methodological choices. Because climate datasets and models represent simplified versions of the coupled atmosphere–ocean system, this requirement is not always guaranteed. When important aspects of joint wind–wave variability are not adequately captured, the resulting classifications can become unstable. Such instability may appear as artificial spatial shifts, inconsistent regime boundaries, or patterns that are difficult to interpret in physical terms.

The first part of this thesis examines situations in which representations of wind–wave

climate variability become unreliable. The focus is on cases where wind and wave conditions are analysed separately, or where variability is reduced to long-term mean statistics. While such simplifications are adequate for certain applications, other questions depend on how wind and waves co-vary across seasons and years, and on how this joint variability is organised in space. In these cases, commonly used descriptions of wind–wave climate can fail. Frameworks that reproduce mean conditions may nevertheless misrepresent persistence, seasonal contrasts, or transitions between different wind–wave states. This thesis shows that such limitations arise under a broader range of conditions than is often assumed. Moreover, alternative descriptions that do not explicitly account for joint wind–wave behaviour are affected in a similar way.

This study is organised in four parts. The first part considers wind–wave variability at the scale of large-scale atmospheric forcing, focusing on coherent patterns that govern offshore conditions. The second part extends this view by explicitly accounting for spatial variability, where changes occur between neighbouring regions. In particular, this study examines how differences between open-ocean, transitional, and enclosed seas shape wind and wave characteristics. Spatial contrasts arise from variations in exposure, fetch, bathymetry, and regional atmospheric circulation, which influence both the magnitude and persistence of wind–wave conditions. The analysis shows that descriptions which neglect this spatial structure, or treat it only implicitly, may lead to misleading interpretations. While large-scale behaviour can appear consistent, accounting for spatial variability reveals limitations that are not evident in simpler representations.

The third and fourth parts of this thesis focus on addressing the limitations that arise when wind–wave climate variability is evaluated across different datasets and under future climate forcing. In particular, the work addresses the lack of a stable reference for comparing reanalysis data and climate-model simulations, which appears to be one of the most critical challenges in coupled wind–wave assessment. Existing approaches are widely used in practice, computationally efficient, and often sufficient for describing mean conditions. For this reason, the aim is not to replace these approaches, but to establish a consistent framework in which their limitations can be identified and interpreted. The core idea underlying this strategy is that inconsistencies arise when spatial patterns and joint wind–wave behaviour are redefined for each dataset or period. By fixing the wind–wave regime structure using a historical reanalysis reference, changes in climate-model output and future projections can be interpreted relative to an unchanged multivariate space. This allows spatial persistence and physical reorganisation to be distinguished in a consistent manner. This approach is designed to preserve comparability across datasets and periods by interpreting future changes relative to a fixed historical reference, rather than redefining wind–wave structure for each scenario.

To address the remaining sources of ambiguity, the framework is extended beyond regime identification to include resolution sensitivity, atmospheric forcing selection, and dynamical wave modelling. Rather than modifying the regime structure itself, this extension tests whether the framework remains consistent when key modelling assumptions change. In particular, differences in climate-model resolution and wind forcing are treated explicitly, and their influence on wind–wave behaviour is evaluated within the same fixed multivariate reference space. A crucial element of this extension is that it accounts for physical processes acting at smaller spatial and temporal scales-not by redefining wind–wave regimes, but by propagating atmospheric forcing through a spectral wave model. By relaxing the implicit assumption that climate-model winds are equally suitable for wave modelling, and instead selecting wind forcing objectively before wave simulation, the approach captures sources of variability and instability that are not apparent in purely statistical analyses. This allows uncertainty associated with atmospheric forcing to be separated from uncertainty arising within the wave model itself.

The proposed regime-based framework satisfactorily reproduces the dominant patterns of coupled wind–wave variability across reanalysis data and selected CMIP6 climate-model simulations. It also captures the evolution of wind–wave behaviour across seasons and regions

in cases where variability remains organised within the historical regime structure. However, when changes in atmospheric forcing, model resolution, or regional dynamics become more pronounced, the interpretation of regime behaviour becomes less straightforward. Overall, we find that uncertainty in coupled wind–wave climate analysis is ubiquitous. We expect that the representation of additional processes and modelling choices beyond those examined here-particularly within larger multi-model ensembles and next-generation efforts such as CMIP7-will reveal yet unknown domains of uncertainty in wind–wave regime behaviour.

Samenvatting

Met het ontwikkelen van offshore hernieuwbare energieinfrastructuur-zoals offshore windparken, golfenergie-installaties of hybride systemen-grijpen ingenieurs en beleidsmakers in in mariene omgevingen die worden gevormd door gekoppelde wind- en golfprocessen. Deze processen reageren op atmosferische forcering op korte tijdschalen (dagen, seizoenen), maar ook op langere klimaattijdschalen (jaren, decennia). Zo kan een verandering in grootschalige atmosferische circulatie de regionale windvelden direct beïnvloeden, wat leidt tot veranderingen in de generatie en voortplanting van golven. Op langere tijdschalen kunnen dergelijke veranderingen de ruimtelijke patronen van wind–golfvariabiliteit veranderen en de continuiteit en stabiliteit van offshore energiebronnen beïnvloeden. Het succes van klimaatgeïnformeerde offshore ontwikkelingen hangt daarom, ten minste gedeeltelijk, af van ons vermogen om te voorspellen hoe gekoppelde wind–golfsystemen reageren op veranderingen in atmosferische forcering. In essentie richt dit onderzoek zich op vragen als: hoe stabiel zijn wind–golfcondities over seizoenen en jaren? Welke patronen blijven bestaan, en welke veranderen onder invloed van klimaatvariabiliteit? En hoe betrouwbaar kunnen klimaatmodellen de wind–golfregimes representeren die ten grondslag liggen aan offshore wind-, golf- en hybride energiepotentieel—en hoe kunnen deze regimes de komende decennia wijzigen onder invloed van de verwachtte klimaatforcering?

Om dergelijke vragen te beantwoorden is een kwantitatief raamwerk noodzakelijk. In dit proefschrift wordt een raamwerk ontwikkeld dat relaties vastlegt tussen variabelen die het gekoppelde wind–golfklimaat representeren, zoals significante golfhoogte, gemiddelde golfperiode, windsnelheid en golf- en windrichting. Deze relaties-in dit geval de definitie van kenmerken en hun gezamenlijke covariantiestructuur-zijn afgeleid uit de fysische samenhang van het atmosfeer–golfsysteem en uit statistische principes die beschrijven hoe deze variabelen gezamenlijk variëren in ruimte en tijd. Uitgaande van een beschrijving van het historische klimaat (de ERA5-heranalyse voor de periode 1979–2014) en de randvoorwaarden die het studiegebied definiëren (de Europese zeeën en hun seizoens- en interjaarlijkse cycli), beschrijft het raamwerk de samenhang en evolutie van wind–golfvariabiliteit in termen van een beperkt aantal coherente regimes. *Principal component analysis* reduceert de multivariabele complexiteit, waarna clustering locaties met vergelijkbaar langetermijngedrag groepeert. Dit resulteert in regimes die kunnen worden geïnterpreteerd als open-ocean-, overgangs- en ingesloten of semi-ingesloten wind–golfklimaten.

Een essentiële vereiste voor een klimaat-analyseraamwerk is robuustheid. In de context van deze thesis betekent robuustheid dat de geïdentificeerde wind–golfpatronen goed gedefinieerd zijn en op een vloeiende manier variëren bij veranderingen in de onderliggende gegevens en methodologische keuzes. Aangezien klimaatgegevens en -modellen vereenvoudigde representaties vormen van het gekoppelde atmosfeer–oceaansysteem, is aan deze vereiste niet altijd voldaan. Wanneer belangrijke aspecten van de gezamenlijke wind–golfvariabiliteit onvoldoende

worden weergegeven, kunnen de resulterende classificaties instabiel worden. Dergelijke instabiliteit kan zich uiten in kunstmatige ruimtelijke verschuivingen, inconsistente regimegrenzen of patronen die moeilijk fysisch te interpreteren zijn.

Het eerste deel van dit proefschrift onderzoekt situaties waarin representaties van wind-golfklimaatvariabiliteit onbetrouwbaar worden. De focus ligt op gevallen waarin wind- en golfcondities afzonderlijk worden geanalyseerd, of waarin variabiliteit wordt gereduceerd tot langetermijngemiddelde statistieken. Hoewel dergelijke vereenvoudigingen voor bepaalde toepassingen toereikend zijn, zijn deze niet toereikend voor vraagstukken waarvoor de manier waarop wind en golven gezamenlijk variëren over seizoenen en jaren, en hoe deze gezamenlijke variabiliteit ruimtelijk is georganiseerd, van belang is. In dergelijke gevallen kunnen gangbare beschrijvingen van het wind–golfklimaat tekortschieten. Raamwerken die gemiddelde condities correct reproduceren, kunnen desondanks continuiteit, seizoenscontrasten of overgangen tussen verschillende wind–golftoestanden verkeerd weergeven. Dit proefschrift toont aan dat dergelijke beperkingen optreden onder een breder scala aan omstandigheden dan doorgaans wordt aangenomen. Bovendien blijken alternatieve beschrijvingen die niet expliciet rekening houden met gezamenlijk wind–golfgedrag op vergelijkbare wijze te worden beïnvloed.

Dit proefschrift adresseert deze problematiek in vier samenhangende delen. Het eerste deel richt zich op situaties waarin beschrijvingen van wind–golfklimaatvariabiliteit onbetrouwbaar worden, met name wanneer wind- en golfcondities afzonderlijk worden geanalyseerd of worden teruggebracht tot langetermijngemiddelden. Het tweede deel breidt deze analyse uit door expliciet rekening te houden met ruimtelijke variabiliteit en contrasten tussen open oceaangebieden, overgangszones en ingesloten zeeën. Het derde en vierde deel richten zich op de evaluatie van wind–golfvariabiliteit over verschillende datasets en onder invloed van verwachte klimaatforcering, met bijzondere aandacht voor vergelijkbaarheid tussen heranalyse- en klimaatmodeluitvoer.

Het derde en vierde deel van dit proefschrift richten zich op de beperkingen die ontstaan wanneer wind–golfklimaatvariabiliteit wordt geëvalueerd over verschillende datasets en onder invloed van verwachte klimaatforcering. In het bijzonder wordt ingegaan op het ontbreken van een stabiele referentie voor het vergelijken van heranalysegegevens en klimaatmodelsimulaties, wat een van de meest kritische uitdagingen blijkt te zijn binnen de beoordeling van gekoppelde wind–golfsystemen. Bestaande benaderingen worden in de praktijk veelvuldig toegepast, zijn wat betreft benodigde rekenkracht efficiënt en vaak toereikend voor het beschrijven van gemiddelde condities. Om deze reden is het doel niet om dergelijke benaderingen te vervangen, maar om een consistent raamwerk te ontwikkelen waarin de beperkingen kunnen worden geïdentificeerd en geïnterpreteerd. Het centrale uitgangspunt van deze strategie is dat inconsistenties ontstaan wanneer ruimtelijke patronen en gezamenlijk wind–golfgedrag voor elke dataset of periode opnieuw worden gedefinieerd. Door de wind–golfregimestructuur vast te leggen op basis van een historische referentie, kunnen veranderingen in klimaatmodeluitvoer en toekomstige projecties worden geïnterpreteerd ten opzichte van een onveranderde multivariabele ruimte. Dit maakt het mogelijk om ruimtelijke continuiteit en fysieke verandering op een consistente wijze van elkaar te onderscheiden. Deze benadering is ontworpen om vergelijkbaarheid tussen datasets en perioden te waarborgen door toekomstige veranderingen te interpreteren ten opzichte van een vaste historische referentie, in plaats van de wind–golfstructuur voor elk scenario opnieuw te definiëren.

Om de resterende bronnen van ambiguïteit te adresseren, wordt het raamwerk uitgebreid voorbij regime-identificatie, door resolutiegevoeligheid, de selectie van atmosferische forcering en dynamische golfmodellering expliciet mee te nemen. In plaats van de regimestructuur zelf te wijzigen, wordt met deze uitbreiding getoetst of het raamwerk consistent blijft wanneer fundamentele modelleringsaannames veranderen. In het bijzonder worden verschillen in klimaatmodelresolutie en windforcering expliciet behandeld, en wordt de invloed op wind–golfgedrag geëvalueerd binnen dezelfde vaste multivariabele referentieruimte. Een cruciaal onderdeel

van deze uitbreiding is dat rekening wordt gehouden met fysische processen die op kleinere ruimte- en tijd schalen optreden-niet door wind–golfregimes opnieuw te definiëren, maar door atmosferische forcering door te geven aan een spectraal golfmodel. Door de impliciete aanname dat klimaatmodelwinden in gelijke mate geschikt zijn voor golfmodellering los te laten, en in plaats daarvan windforcering vooraf op objectieve wijze te selecteren, maakt deze benadering bronnen van variabiliteit en instabiliteit zichtbaar die in zuiver statistische analyses niet aan het licht komen. Hierdoor kan onzekerheid die samenhangt met atmosferische forcering worden onderscheiden van onzekerheid die binnen het golfmodel zelf ontstaat.

Het voorgestelde op regimes gebaseerde raamwerk reproduceert op overtuigende wijze de dominante patronen van gekoppelde wind–golfvariabiliteit in zowel heranalysedata als geselecteerde CMIP6-klimaatmodelsimulaties. Daarnaast beschrijft het de evolutie van wind–golfgedrag over seizoenen en regio's in gevallen waarin de variabiliteit binnen de grenzen van de historische regimestructuur blijft. Wanneer veranderingen in atmosferische forcering, modelresolutie of regionale dynamiek echter sterker worden, wordt de interpretatie van regimegedrag minder eenduidig. In het algemeen blijkt onzekerheid in de analyse van gekoppeld wind–golfklimaat alomtegenwoordig te zijn. Het is de verwachting dat de representatie van aanvullende processen en modelleringskeuzes-buiten de in dit proefschrift onderzochte aspecten-met name binnen grotere ensemble modellen en toekomstige initiatieven zoals CMIP7, zal leiden tot het blootleggen van nog onbekende onzekerheden met betrekking tot wind–golfregimes.

Preface

You are holding in your hands the result of a journey in which I learned as much about wind and waves as about the way I work and think as a researcher. Along this journey, I experienced curiosity and enthusiasm, moments of joy and relief, periods of doubt, frustration, and uncertainty, as well as effort, fatigue, patience, and quiet confidence. Like many long journeys, it was shaped not only by intention and work, but also by chance—echoing a simple understanding found in teachings attributed to Gautama Buddha: that progress unfolds through balance, effort, and change. Great journeys are rarely linear and are often shaped by circumstance.

A decisive moment in this journey occurred on 02-02-2022—a date that remains an easy marker of arrival—when I came to the Netherlands. By then, I was certain that I loved working with the ocean and climate. My path toward this work did not follow a single, clear direction. I was first deeply affected by the 2019 flood in Kerala, where I was born, which drew my attention to the scale and consequences of extreme hydrometeorological events. This experience led me to apply for a master's programme in physical oceanography, where I was given the opportunity to continue my training.

During my master's thesis at the Indian Institute of Tropical Meteorology, I worked closely with climate-modelling data, further strengthening my interest in the links between the ocean, atmosphere, and climate. At the time, I did not anticipate that this trajectory would extend beyond familiar academic and geographic boundaries. It therefore remained an open question when, through an unexpected email during the COVID-19 pandemic, I was invited to apply for a PhD position far from home—a moment that quietly reshaped the course of this journey.

During the PhD phase, while working with ocean and climate data, I noticed that maps of the same region often looked different depending on how they were produced. Understanding why this happens became the central motivation for the research presented in this dissertation. This book seeks to explain aspects of that question by examining how wind–wave variability is represented, interpreted, and classified across different data sources and methodological choices.

You may be reading this work for different reasons. You may have a personal connection with me and no background in ocean or climate science. Although this dissertation is necessarily technical, the introduction was written with you in mind. To offer a more intuitive sense of the subject, I include a short reflection that acknowledges water as a source of life, strength, and continuity—beyond data and models.

Ye, Waters, are beneficent: so help ye us to energy,
That we may look on great delight.

Give us a portion of the sap, the most auspicious that ye have,
Like mothers in their longing love.

To you we gladly come, to whose abode ye send us on;
And, Waters, give us procreant strength.

The Waters be to us for drink, Goddesses for our aid and bliss:
Let them stream to us health and strength.

Within the Waters—Soma thus hath told me—dwell all balms that heal,
And Agni, he who blesseth all.

O Waters, teem with medicine to keep my body safe from harm,
So that I long may see the Sun.

- Rigveda, X.9 (Hymn to the Waters),
translated by Ralph T. H. Griffith (1896)

After the Introduction, the book continues through the scientific chapters until the Acknowledgements. If the subject itself sparks your curiosity, you are welcome to ask me about it—I would be happy to talk about it for hours.

For readers with a background in science—particularly in oceanography, meteorology, or climate science—the core research is presented in Chapters 2–6. These chapters follow a logical progression, but they are written to stand on their own and can be read independently, as each is structured as a self-contained article.

In writing this book, I have tried to follow the principle expressed by Antoine de Saint-Exupéry, that "perfection is achieved, not when there is nothing more to add, but when there is nothing left to take away." For this reason, I hope you find value in it—whether you read it in full, skim through the text, linger over the figures, turn first to the acknowledgements, or simply allow it to take its place on your bookshelf.

PONNI Maya
Delft, January 2026

1

Introduction

"The more I learn, the more I realize
how much I do not know."

- Socrates

"The word climate, however, denotes first and foremost
a specific property of the atmosphere, but this property
depends on the perpetual interactions of a fully and deeply
moving ocean, of currents of contrasting temperatures,
furrowed sea surface with the heat-radiating dry Earth,
which is manifoldly structured, elevated, coloured,
naked, or covered with woods and herbs."

- Alexander von Humboldt, Kosmos (1845–1862)

1.1 Context

"How inappropriate to call this planet Earth when it is clearly Ocean," remarked Arthur C. Clarke. This observation reflects a fundamental characteristic of the climate system: the dominant role of the ocean in storing and redistributing energy. With a heat capacity approximately 1,100 times greater than that of the atmosphere and a water mass exceeding it by more than five orders of magnitude, the ocean acts as the primary regulator of Earth's climate *[Trenberth et al., 2009, Talley, 2011]*.

The ocean interacts continuously with the atmosphere through exchanges of momentum and energy. Atmospheric winds transfer momentum to the ocean surface, generating surface waves and modifying upper-ocean conditions *[Phillips, 1977, Holthuijsen, 2010]*. Wave characteristics respond rapidly to changes in wind forcing and therefore provide a direct expression of atmospheric variability on short timescales. At the same time, surface waves influence air–sea exchanges by modulating momentum transfer and turbulent processes, forming a physical coupling between atmospheric circulation and oceanic response *[Cavaleri et al., 2012]*.

Wind and wave conditions exhibit pronounced variability across both space and time. Seasonal shifts in large-scale circulation produce systematic changes in wind strength and direction, leading to corresponding variations in wave conditions. Interannual climate variability alters the frequency and persistence of dominant wind–wave states, while extreme atmospheric events generate short-lived but dynamically distinct wave conditions. Regional factors, including basin geometry, coastline orientation, and bathymetry, further shape how atmospheric forcing is expressed in the wave field *[Hemer et al., 2013]*.

Taken together, these features indicate that wind–wave variability is organised rather than random. Capturing this organisation requires treating wind and wave conditions as a coupled system, rather than analysing individual variables in isolation. Such a perspective enables recurring patterns, spatial coherence, and transitions between characteristic states to be identified and meaningfully compared across regions and timescales.

Ocean surface waves encompass a wide range of physical processes operating over different temporal and spatial scales. As illustrated in Figure 1.1, this spectrum includes capillary waves, gravity waves, infragravity waves, long-period motions, and tides, each governed by distinct forcing mechanisms and physical dynamics. Not all of these processes are equally relevant for wind-driven climate-scale behaviour.

This thesis focuses on wind-generated gravity waves, which occupy the central portion of the wave spectrum and respond directly to atmospheric forcing. These waves are produced through momentum transfer from the wind to the ocean surface and evolve on timescales from seconds to several tens of seconds. Their properties reflect wind speed, duration, and fetch, as well as the broader circulation patterns in which they develop. Wind-generated gravity waves therefore provide a physically consistent basis for analysing coupled wind–wave climate variability.

Processes outside this range, including capillary waves, infragravity motions, and tidal waves, are not considered in detail. These phenomena are driven by different forcing mechanisms, operate on different temporal scales, and require alternative observational and modelling approaches. Excluding them allows the analysis to remain focused on the component of the wave field that is directly linked to wind forcing and relevant for climate-scale interpretation.

wind–wave variability has implications for weather, climate, ecosystems, and human activities. Ocean waves influence coastal erosion, navigation, offshore infrastructure, and air–sea exchanges of energy and gases, while wind patterns govern storm development and large-scale atmospheric circulation. Together, wind and waves form a coupled climate-dependent system that evolves continuously in space and time.

This system cannot be fully described by a single representative state. Long-term averages

provide useful baseline information, but they obscure the variability that governs impacts and long-term decision-making. Seasonal contrasts, interannual fluctuations, extreme events, and regional differences often exert a stronger influence on infrastructure performance and risk than mean conditions alone *[Young et al., 2011, Aarnes et al., 2017]*. Variability is therefore a defining characteristic of the wind–wave climate.

Understanding how this variability is represented across observational datasets and numerical models is essential for interpreting past conditions and placing future change in context. Differences between datasets may arise from physical uncertainty, modelling assumptions, or observational limitations. Distinguishing between these sources of variation is a prerequisite for meaningful comparison of wind–wave climate behaviour.

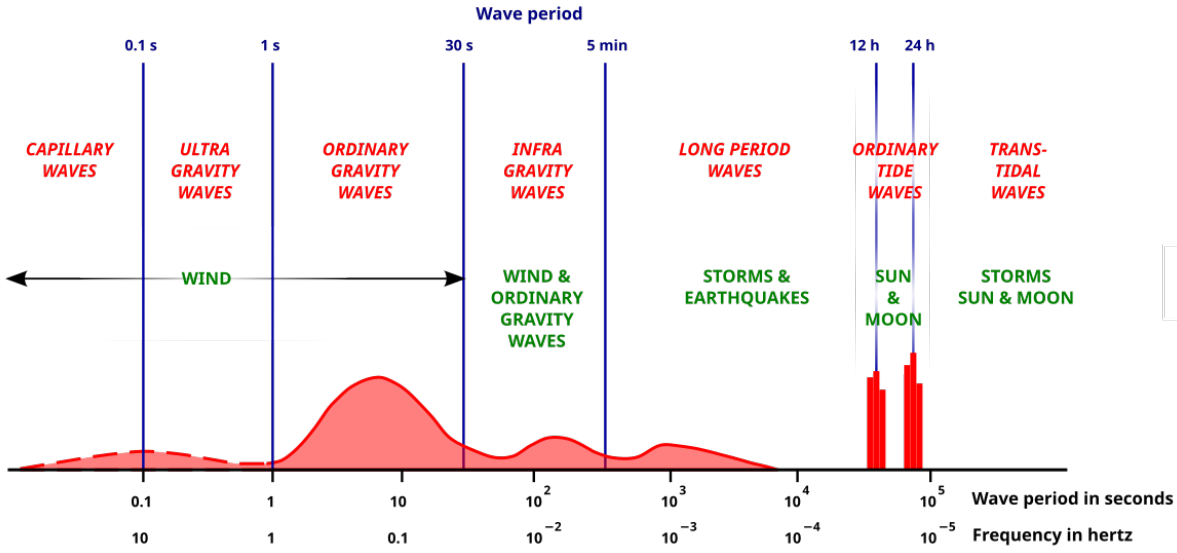

Figure 1.1 Schematic representation of ocean surface wave types across temporal scales and frequencies (Munk [1951]). Wind-generated gravity waves occupy the central portion of the wave spectrum and constitute the primary focus of this thesis. Other wave processes, including capillary waves at high frequencies, infragravity waves at low frequencies, and tidal motions at the longest timescales, arise from distinct forcing mechanisms and are therefore not considered here.

1.1.1 From Observations to Models

Our understanding of the wind–wave climate begins with observation. Measurements from buoys, satellites, and coastal instruments provide direct records of wind and wave conditions, capturing the variability experienced at the ocean surface. Over the past decades, these observations have been combined with numerical weather prediction systems to produce reanalysis datasets, such as ERA5, which offer spatially and temporally consistent descriptions of past atmospheric and oceanic states. These products are often treated as a reference. Yet it is worth pausing to consider what is actually observed. Even the most comprehensive reanalyses remain constrained by the distribution of measurements, the assumptions embedded in data assimilation, and the physical formulations used to interpolate between sparse observations. As a result, reanalysis data are best understood not as an absolute truth, but as a physically informed reconstruction of the past.

Direct observations of the wind–wave climate remain spatially incomplete. Satellite measurements provide broad coverage but sample the ocean surface only along discrete tracks, while in situ observations from wave buoys offer continuous records at fixed point locations. Reanalysis products therefore play a central role by combining these observations with numerical models to produce spatially and temporally coherent representations of past

atmospheric and oceanic states. Climate models, in contrast, are designed to represent the statistical structure and long-term behaviour of the climate system rather than specific events at particular times or locations. Meaningful comparison between observations, reanalysis, and climate simulations must therefore focus on patterns and distributions, rather than point-by-point agreement.

If such datasets exist, why are climate models needed at all? One reason is that observations alone cannot address conditions beyond the historical record. Climate models provide a means to explore how wind and wave behaviour may evolve under changing boundary conditions, offering internally consistent simulations of the coupled atmosphere–ocean system. At the same time, models are simplified representations of reality. Different models emphasise different processes, resolutions, and parameterisations, leading to variations in their depiction of wind and wave climates. This naturally raises a further question: what does it mean for a model to perform well? Agreement with observations in terms of mean values is one criterion, but it is rarely sufficient. Models may reproduce averages while misrepresenting variability, spatial structure, or the frequency of distinct climate states that shape wind–wave behaviour.

In practice, wind–wave climate information is derived from a coupled modelling chain that combines atmospheric climate models with numerical wave models. Global and regional climate models, developed within coordinated efforts such as successive CMIP generations (Figure 1.2), simulate the large-scale atmospheric circulation that governs wind variability over decadal timescales. These simulated winds are commonly used to force spectral wave models, such as WAVEWATCH III (WW3), which resolve the generation, propagation, and dissipation of wind-generated surface gravity waves. The resulting wave simulations therefore reflect a combination of wave-model physics and atmospheric forcing characteristics. Differences in simulated wave climate may arise not only from wave-model parameterisations or resolution, but also from biases, variability, or structural differences in the underlying climate-model winds. Interpreting wind–wave behaviour thus requires treating the atmospheric and wave components as an integrated system, rather than as independent sources of uncertainty.

In this context, differences between observations and models, or among models themselves, should not be viewed solely as shortcomings. Disagreement often highlights the sensitivity of the wind–wave system to atmospheric forcing, regional geography, or modelling choices. Such differences can be informative, revealing which aspects of climate behaviour are robust and which remain uncertain. Rather than focusing exclusively on pointwise comparisons, it becomes useful to consider whether models capture the same underlying patterns of variability observed in reanalysis data. A pattern- or regime-based perspective offers a way to do this, shifting attention from individual values toward recurring structures and behaviours. This approach provides a common language for comparing observations and models, allowing variability, uncertainty, and change to be interpreted within a coherent framework.

1.1.2 The Problem of Comparability and Stability

When multiple datasets are available to describe the wind–wave climate, it is natural to compare them. Yet what does it actually mean to compare two datasets in a meaningful way? Two products may report similar long-term average wave heights over a region and still portray very different seasonal behaviour, extremes, or spatial gradients. In such cases, agreement in one metric can mask divergence in others. Comparability, therefore, is not simply a matter of numerical proximity, but of whether different datasets describe the same underlying climate behaviour. This distinction becomes particularly important when observations, reanalysis products, and climate-model simulations are placed side by side, each shaped by different data sources, assumptions, and representations of physical processes.

A closely related question concerns stability. When can a wind–wave pattern be considered stable, and in what sense? Stability does not imply that conditions remain unchanged, nor

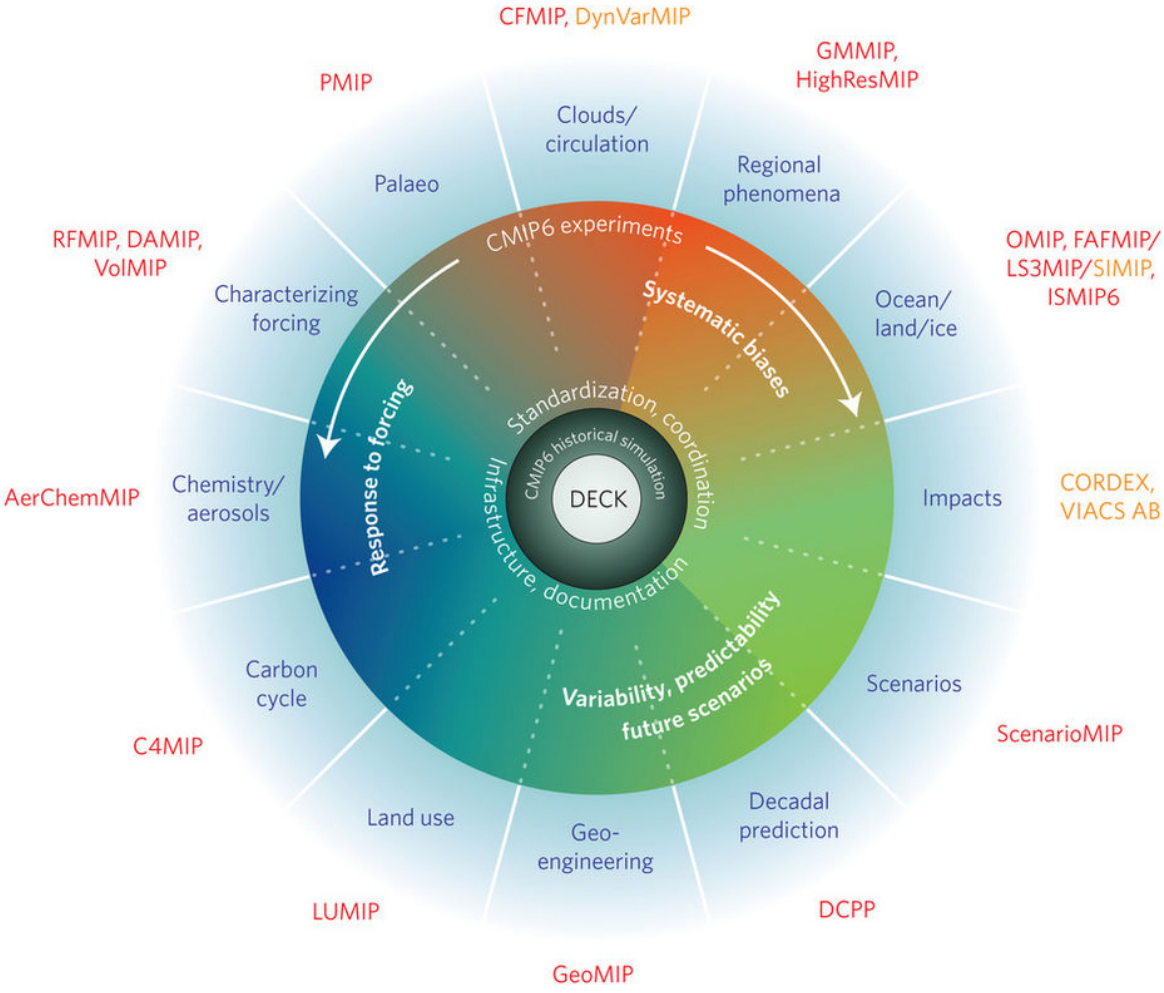

Figure 1.2 Schematic overview of the CMIP6 framework, illustrating the coordinated set of model intercomparison projects designed to investigate climate-system response to external forcing, systematic biases, internal variability, and future scenarios. The central DECK experiments provide a common reference for model evaluation, while specialised MIPs focus on specific components and processes of the climate system, including atmospheric circulation, ocean–land–ice interactions, aerosols and chemistry, and regional phenomena. Atmospheric circulation simulated within CMIP6 constitutes the primary source of wind forcing for wave-modelling applications, thereby linking large-scale climate variability to wind–wave behaviour. Figure adapted from CMIP6/IPCC documentation.

that variability is absent. Rather, it refers to the persistence of characteristic spatial structures, recurring patterns, or relationships between wind and waves over time. For example, a region may consistently exhibit stronger wind–wave coupling than its surroundings, even as mean conditions fluctuate from year to year. In another area, the same pattern may weaken, shift, or fragment under different atmospheric conditions. Stability, in this sense, is about the continuity of structure rather than the constancy of values.

Comparability and stability cannot be taken for granted across datasets. Reanalysis products integrate observations within a modelling framework, while climate models simulate the climate system based on prescribed physics and boundary conditions. Each approach carries its own strengths and limitations, and each filters variability in different ways. Disagreement between datasets, therefore, does not necessarily indicate that one is correct and another is flawed. Instead, such differences often reflect structural uncertainty: uncertainty arising from how the climate system is observed, represented, and simulated. Recognising this shifts the focus from seeking perfect agreement to understanding which aspects of wind–wave behaviour are robust and which remain sensitive to data and modelling choices.

1.1.3 Why a Regime-Based Perspective

Analyses of wind–wave climate variability often begin with point-wise statistics, long-term means, or trends computed at fixed locations. Such approaches are valuable, but they can offer a fragmented view of a system that is inherently organised. Averages may smooth over transitions, and trends may differ in sign or magnitude depending on the period or region considered. This raises a natural question: when variability is large and spatially structured, what aspects of the climate system should be compared? Is it the exact value at a given point, or the broader pattern in which that value sits?

A regime can be understood as a recurring, physically coherent state of the climate system, characterised by a consistent relationship between wind and wave conditions over a given region. Rather than describing isolated moments or locations, regimes capture how the system tends to organise itself under certain atmospheric conditions. For example, similar wind–wave configurations may reappear seasonally or under particular circulation patterns, even if their intensity varies from one year to the next. From this perspective, the exact magnitude of wind speed or wave height becomes less central than the persistence of the underlying structure. Can patterns remain stable even when amplitudes change? In many cases, they can, and it is this stability of structure that regimes are intended to capture.

Viewing wind–wave variability through regimes also provides a practical way to compare observations, reanalysis products, and climate models. Different datasets may disagree on absolute values while still reproducing similar spatial organisations or transitions between states. A regime-based perspective allows such similarities to be identified without requiring point-by-point agreement. Because regimes focus on coherent behaviour rather than local noise, they are less sensitive to small-scale discrepancies, resolution differences, or short-term fluctuations. This makes them a useful lens for interpreting variability and change, helping to distinguish shifts in the organisation of the wind–wave climate from changes in intensity alone.

1.1.4 Relevance for Renewable Energy Planning under Climate Variability

When wind–wave behaviour is viewed through a regime-based lens, climate variability can be described in terms of recurring states and their transitions over time. This perspective is particularly relevant for renewable energy planning, where decisions are shaped not only by long-term average conditions, but also by how often certain states occur, how persistent

they are, and how they shift across seasons and years. A stable average wind or wave climate may conceal a distribution of conditions that clusters into distinct regimes, each associated with different operational or environmental contexts. What does a representative mean value imply if the system alternates between contrasting states for much of the time?

Planning decisions are therefore sensitive to variability and structure, not just magnitude. Two regions may exhibit similar average wind or wave energy levels, yet differ substantially in seasonal dominance, persistence of favourable conditions, or exposure to intermittent extremes. In one case, energy-relevant conditions may be spread evenly throughout the year; in another, they may be concentrated within a narrow seasonal window or linked to specific circulation patterns. These differences influence how consistently energy can be harnessed and how systems respond to variability, even when mean conditions appear comparable.

A regime-based understanding supports planning by providing context for such differences. By framing wind–wave behaviour in terms of dominant states and their variability, it becomes possible to interpret uncertainty as part of the climate structure rather than as unexplained noise. This does not offer precise predictions of future conditions, nor does it remove uncertainty. Instead, it provides a way to assess robustness, to recognise which aspects of the climate are persistent, and to anticipate how shifts in dominant regimes may affect long-term planning considerations. In this sense, the value of a regime-based perspective lies in interpretation and risk awareness, rather than in exact forecasts.

1.2 Scientific Motivation

Near-surface wind and wave conditions are fundamental expressions of the coupled ocean–atmosphere system. Together, they regulate air–sea momentum exchange, ocean mixing, and energy transfer, while shaping coastal processes and influencing offshore infrastructure, navigation, and marine ecosystems *[Hemer et al., 2010, Waterhouse et al., 2014, Reguero et al., 2015, Dodet et al., 2019]*. At regional to basin scales, wind–wave variability reflects the combined influence of atmospheric circulation, storm-track dynamics, fetch, and local bathymetry, and plays a central role in determining offshore renewable-energy potential and operational reliability *[Young et al., 2011, Casas-Prat and Sierra, 2013, Morim et al., 2019, Olauson, 2018]*.

In recent decades, substantial progress has been made in describing wind and wave climate using reanalysis datasets and numerical models. Reanalyses such as ERA5 provide spatially and temporally consistent representations of historical surface winds and waves, constrained by observations and widely adopted as reference datasets for marine climate studies *[Hersbach et al., 2020]*. At the same time, climate-model ensembles coordinated through CMIP6 form the basis for assessing internal climate variability, uncertainty, and future change under different forcing scenarios *[Eyring et al., 2016, Zelinka et al., 2020]*. Together, these datasets underpin contemporary assessments of wind and wave variability, trends, and extremes across European seas *[Young et al., 2011, Bonaduce et al., 2019, Meucci et al., 2024]*.

Despite these advances, existing analyses of wind and wave climate remain fragmented in both concept and methodology. Many studies focus on individual variables-such as wind speed or significant wave height-or examine wind and waves separately, even though they arise from the same atmospheric forcing and evolve in a coupled manner *[Semedo et al., 2011, Janssen, 2004, Reguero et al., 2015]*. Trend analyses and climatologies are commonly performed on a grid-point basis or through spatial averaging, approaches that obscure coherent regional behaviour and mask the joint structure of wind–wave variability *[Casas-Prat and Sierra, 2013, Morim et al., 2019]*. As a result, physically meaningful spatial patterns that persist across seasons and years are often difficult to identify and compare consistently across datasets.

These limitations become more pronounced when extending analyses from reanalysis

products to climate-model simulations. Climate models differ in spatial resolution, physical parameterisations, and coupling strategies, all of which influence the representation of storms, wind fields, and wave growth processes *[Stopa and Cheung, 2014, Ardhuin et al., 2010, Haarsma et al., 2016]*. Conventional model-evaluation approaches-based on grid-cell statistics, bulk performance metrics, or basin-averaged comparisons-struggle to distinguish physically meaningful discrepancies from noise and bias, particularly when spatial patterns differ between models *[Gleckler et al., 2008, Akinsanola et al., 2021]*. Consequently, model performance is often assessed without a stable spatial or dynamical reference, limiting confidence in both historical benchmarking and future projections.

A further challenge arises in translating climate-scale wind and wave information into offshore renewable-energy assessments. Wind and wave energy resources depend not only on mean conditions but also on their seasonal persistence, interannual variability, and joint behaviour *[Reguero et al., 2015, Olauson, 2018]*. Evaluations that treat wind and wave energy independently fail to capture their natural complementarity and may misrepresent the stability of hybrid offshore energy systems *[WindEurope, 2022, Sardana et al., 2024]*. In addition, the selection of climate-model wind forcing for wave simulations is often based on subjective choices or isolated performance metrics, without accounting for the multidimensional nature of wind variability that propagates into wave models *[Martinez and Iglesias, 2022, Lobeto et al., 2021, Meucci et al., 2024]*. This disconnect complicates the assessment of uncertainty and limits the credibility of climate-driven wave and energy projections.

Taken together, these challenges highlight the need for a unified framework that can represent joint wind–wave variability in a physically interpretable and statistically robust manner, while remaining transferable across reanalysis data, climate-model simulations, and energy-relevant diagnostics. Such a framework must provide a fixed reference space in which wind–wave behaviour can be compared consistently, allowing spatial coherence to be preserved rather than redefined for each dataset or modelling configuration. It must also support the evaluation of model resolution effects, uncertainty propagation, and regime stability under climate forcing, without conflating methodological differences with physical change.

This thesis is motivated by the need to formalise and apply such a framework. By adopting a regime-based, multivariate representation of wind–wave climate defined in reanalysis space and applying it consistently across climate-model simulations, near-term projections, and offshore renewable-energy assessments, the work seeks to improve comparability between datasets, strengthen confidence in climate-model-based analyses, and provide physically meaningful insight into the stability and evolution of offshore wind and wave resources across European seas.

1.3 Knowledge Gaps

Despite extensive literature on wind and wave climate, several structural knowledge gaps remain that limit consistent interpretation, model evaluation, and application to offshore renewable energy.

Gap 1: Lack of a unified framework for joint wind–wave variability. Most existing studies analyse wind and wave characteristics separately or focus on single parameters, despite their shared atmospheric forcing and coupled evolution *[Semedo et al., 2011, Janssen, 2004, Reguero et al., 2015]*. Multivariate assessments remain limited in scope, often restricted to wave-only parameters or short temporal windows *[Fairley et al., 2020]*. As a result, there is no widely adopted framework that captures coupled wind–wave behaviour in a physically interpretable manner across large spatial domains and long timescales.

Gap 2: Absence of a fixed spatial reference for cross-dataset comparison. Comparisons between reanalysis products and climate-model simulations are typically performed using grid-point statistics or basin-averaged metrics, which are sensitive to resolution and model-specific spatial structures *[Casas-Prat and Sierra, 2013, Bonaduce et al., 2019]*. This approach obscures coherent regional behaviour and makes it difficult to distinguish physical differences from artefacts of spatial representation. A stable, dataset-independent spatial reference for evaluating wind–wave variability is largely missing.

Gap 3: Limited understanding of resolution effects on coupled wind–wave regimes. While higher-resolution climate models are known to improve the representation of storms and coastal processes, few studies have examined how horizontal resolution influences the spatial coherence and variability of joint wind–wave regimes *[Haarsma et al., 2016, Stopa and Cheung, 2014, Meucci et al., 2024]*. In particular, controlled comparisons between standard-resolution and high-resolution simulations within a consistent regime framework remain scarce.

Gap 4: Weak integration of climate evaluation with energy-relevant diagnostics. Wind and wave energy assessments are often derived independently from climate-evaluation studies, using metrics that do not explicitly account for regime-scale variability, seasonal persistence, or joint behaviour *[Reguero et al., 2015, Olauson, 2018]*. This separation obscures how climate uncertainty propagates into wind and wave energy estimates and limits the climate context available for offshore renewable-energy studies.

Gap 5: Lack of objective, multivariate approaches for selecting climate-model wind forcing for wave simulations. Climate-model selection for wave modelling is frequently based on subjective judgement or single-metric performance, despite evidence that wind variability is multidimensional and region-dependent *[Goyal et al., 2021, Martinez and Iglesias, 2022]*. Machine-learning approaches offer promising alternatives, but their integration into climate-to-wave modelling chains remains limited, particularly for regional applications.

Gap 6: Insufficient assessment of regime stability and reorganisation under near-term climate forcing. While future projections often focus on changes in mean or extreme conditions, fewer studies examine how coherent wind–wave regimes reorganise, persist, or transition under climate change *[Morim et al., 2019, Casas-Prat et al., 2024b]*. Understanding regime-scale stability and redistribution is essential for interpreting future offshore renewable potential and climate-aware planning.

1.4 Conceptual Framework

This thesis examines how joint wind–wave variability is described and compared across reanalysis data, climate model simulations, and offshore renewable energy assessments. Although wind and waves are commonly studied together, existing analyses often rely on spatial definitions, metrics, or classifications that differ between datasets and modelling systems. This makes it difficult to compare variability consistently, evaluate model performance across resolutions, or track changes through time without introducing uncertainty related to changing spatial representations.

To avoid this, the thesis uses a regime-based approach in which joint wind–wave behaviour is analysed within a fixed multivariate climate space. This space is defined using long-term ERA5 reanalysis data and captures recurring patterns of atmospheric forcing and ocean response across European seas. The resulting regimes represent typical wind–wave conditions

and their variability across seasons and years. The analysis focuses on spatially coherent behaviour at regional scales rather than on individual grid points or isolated events.

These ERA5-derived regimes are then used as a reference for evaluating climate model simulations. Model outputs are projected onto the same regime space, allowing their wind–wave characteristics to be examined without redefining spatial patterns for each dataset. This makes it possible to compare different CMIP6 experiments and resolutions within a common framework, and to separate differences related to model configuration from those caused by changes in spatial classification.

Within this framework, wind and wave energy metrics are analysed at the regime level. This allows variability, seasonal behaviour, and wind–wave complementarity to be examined in regions that reflect underlying physical behaviour rather than administrative boundaries. Based on these characteristics, regimes are grouped into Primary, Secondary, and Hybrid Hotspot zones to support regional-scale offshore energy assessment.

Here, the term *hybrid* refers to the combined characterisation of wind and wave climate properties within a regime, and does not imply hybrid energy technologies or infrastructure.

Uncertainty is addressed step by step. Variability is first characterised using regimes derived from reanalysis data. Climate model uncertainty is then examined by evaluating how well different CMIP6 configurations reproduce these regimes. Uncertainty related to atmospheric forcing is further reduced through an objective, machine-learning–based selection of wind datasets. Finally, the effects of these choices are tested using high-resolution regional wave simulations driven by selected raw climate model winds. This approach examines uncertainty directly, rather than masking it through bias correction.

The same framework is applied to near-term climate projections. By projecting future simulations onto the fixed ERA5 regime space, changes in wind–wave conditions are interpreted relative to an unchanged reference. Regime transitions, spatial shifts, and changes in seasonal behaviour are used to describe how wind–wave patterns evolve under climate forcing and how these changes affect offshore energy potential.

In this thesis, the term stability refers to how consistently coupled wind–wave behaviour can be represented and compared across datasets, model resolutions, atmospheric forcing configurations, and future climate conditions. In Chapters 2–4, stability is examined through the persistence, coherence, and distinctness of multivariate wind–wave climate regimes identified from ERA5 reanalysis and climate-model simulations. In Chapters 5–6, the focus shifts to the atmospheric forcing used for wave modelling, examining whether raw climate-model wind fields remain comparable with satellite observations and reanalysis datasets and whether they reproduce physically meaningful wave behaviour in dynamical wave simulations. Together, these analyses link the statistical representation of wind–wave climate variability with its dynamical propagation in wave modelling.

1.5 Objectives and Research Questions

The objective of this thesis is to develop and apply a physically interpretable, multivariate, regime-based framework to characterise coupled wind–wave climate variability across European seas. The framework is designed to be robust across space, seasons, and timescales, transferable between reanalysis data and climate-model simulations, and relevant for offshore renewable-energy assessment. In addition, the thesis aims to evaluate the reliability of climate-model forcing for wave modelling and to assess how uncertainty in atmospheric forcing propagates into wave-climate and energy estimates under historical and near-term climate conditions.

To this end, the following research questions are addressed.

RQ1. How can coupled wind–wave climate variability be described within a physically interpretable, regime-based framework that is robust across space, seasons, and timescales, and suitable for offshore energy and engineering applications?

(a) How can joint wind and wave statistics be formulated to represent coupled wind–wave climate variability across European seas?

(b) What spatially coherent wind–wave regimes can be identified from long-term ERA5 reanalysis using a multivariate spatio-temporal clustering approach?

(c) To what extent are the identified regimes internally coherent and mutually distinct in multivariate feature space?

(d) How do the wind–wave regimes differ in their seasonal and interannual variability of wave height, wave period, wind speed, and directional characteristics?

(e) Under which large-scale atmospheric circulation patterns is regime-level wind–wave variability most strongly conditioned?

RQ2. How reliably can CMIP6 EC-Earth3 climate simulations reproduce the spatial coherence, variability, and energy relevance of European wind–wave climate when evaluated using a fixed ERA5-derived multivariate regime framework, and how does model resolution influence confidence in regime representation and offshore renewable-energy classification?

(a) To what extent can an ERA5-derived multivariate wind–wave regime framework be transferred to independent EC-Earth3 historical simulations (ScenarioMIP and HighResMIP, 1979–2014) to enable consistent regime-scale benchmarking?

(b) How consistently do EC-Earth3 ScenarioMIP and HighResMIP reproduce the large-scale spatial organization of ERA5 wind–wave regimes, and where are the dominant regime disagreements located (e.g., coastal and transition zones)?

(c) How does horizontal resolution (ScenarioMIP $\sim 1^\circ$ vs HighResMIP ~ 50 km) alter regime boundaries, coastal transitions, and the representation of mesoscale wind–wave structure within the fixed ERA5 regime space?

(d) How does regime-membership confidence, quantified using softmax probabilities in the ERA5 PCA space, vary across regions and between EC-Earth3 configurations, and what does this reveal about spatial uncertainty and ambiguity?

(e) How well do EC-Earth3 simulations reproduce ERA5 patterns of seasonal and regime-scale variability in wind energy density and wave power, and how do biases differ between ScenarioMIP and HighResMIP?

(f) How do depth-resolved energy–stability classes (Primary, Secondary, Hotspot, Low) for wind, wave, and hybrid resources distribute across European seas, and how are these zones structured when aggregated by jurisdictional (EEZ) and ecological (MEOW) regions?

RQ3. How will European coupled wind–wave regimes—and the associated hybrid offshore wind–wave renewable potential—reorganise under near-term climate forcing (2020–2050), when future EC-Earth3P-HR projections are mapped onto a fixed, physically interpretable ERA5-derived multivariate regime framework?

(a) To what extent can future EC-Earth3P-HR wind–wave conditions (2020–2050) be consistently projected onto a fixed ERA5-derived principal-component space, enabling direct comparison with historical conditions (1979–2014) without redefining regime geometry?

(b) How do European wind–wave regimes reorganise under near-term climate forcing in terms of regime transitions, centroid migration, and changes in spatial footprint, and what does this reveal about spatial persistence versus dynamical redistribution within the fixed regime framework?

(c) Which changes in significant wave height and near-surface wind speed drive the observed future regime transitions, and how do these anomalies relate to shifts in atmospheric forcing and wave-generation processes across European seas?

(d) How does the seasonal coherence of wind–wave regimes evolve under future climate forcing, as quantified by the Seasonal Regime Stability Index, and do seasonal states become more or less consistent with their annual mean behaviour?

(e) How do offshore wind and wave energy resources evolve within the historical regime structure under future forcing, as measured by changes in deep-water wave power and hub-height wind energy?

(f) How does a hybrid classification combining energy magnitude and seasonal stability reorganise Primary, Secondary, Hotspot, and Low wind–wave resource zones under future climate conditions?

(g) What insights does a regime-based, multivariate framework provide into future offshore renewable potential, resource stability, and climate-aware planning across European seas?

RQ4. How can CMIP6 wind forcing be objectively selected for wave modelling, and does that selection translate into credible regional wave-climate simulations when dynamically downscaled through a spectral wave model?

(a) How accurately do CMIP6 historical near-surface wind simulations reproduce observed and reanalysis wind climatology across seasons and regions relevant for wave modelling?

(b) Do conventional single-metric evaluations adequately discriminate between CMIP6 wind models, or do they obscure important magnitude and seasonal errors relevant for wave generation?

(c) Can a multi-metric, machine-learning–based framework (KD-tree nearest-neighbour ranking) objectively identify the most suitable CMIP6 wind forcing for a given region?

(d) Does the objectively selected CMIP6 wind forcing, when used without bias correction, produce a regional wave hindcast that reproduces observed wave-climate statistics?

(e) How do biases in climate-model wind forcing propagate into simulated wave heights and wave power, and which physical processes dominate the resulting errors?

(f) Is a wave modelling framework driven by objectively selected CMIP6 winds suitable for regional wave-climate analysis and for providing climate context relevant to offshore renewable-energy studies at climate timescales?

Aim of the Dissertation

The aim of this dissertation is to develop and apply a physically interpretable, multivariate, regime-based framework to describe coupled wind–wave climate variability across European seas, to examine its robustness and transferability across reanalysis data, climate-model simulations, and near-term future projections, and to consider its relevance for offshore renewable-energy assessment under climate change.

1.6 Methodological Overview

Figure 1.3 provides an overview of the methodological framework used throughout this thesis. ERA5 reanalysis data are first used to construct a fixed multivariate regime space that characterises coupled wind–wave climate variability across European seas. This regime framework is then transferred to CMIP6 EC-Earth3 historical simulations to evaluate model fidelity and resolution effects, and to near-term future projections to examine regime persistence, transitions, and changes in spatial footprint under climate change. Within this fixed regime structure, wind and wave energy metrics and stability diagnostics are derived, and hybrid energy zones are classified. In parallel, an objective multi-metric selection of CMIP6 wind forcing is performed and validated through regional wave modelling using WW3, providing a consistent link between climate-model forcing, wave-climate simulation, and renewable-energy assessment.

1.7 Dissertation Structure

In order to address Research Question 1, Chapter 2 develops a multivariate, physically interpretable framework to describe coupled wind–wave climate variability across European seas. Using ERA5 reanalysis data for the period 1979–2014, joint wind and wave statistics are formulated and principal component analysis followed by unsupervised clustering is applied to identify spatially coherent wind–wave regimes. The internal coherence, mutual distinctness, and seasonal and interannual variability of these regimes are analysed, along with their modulation by large-scale atmospheric circulation patterns. This chapter establishes a fixed, regime-based reference representation of the European wind–wave climate.

To address Research Question 2, Chapter 3 extends the ERA5-derived regime framework to climate-model simulations and evaluates its transferability and robustness across model configurations. EC-Earth3 CMIP6 ScenarioMIP and HighResMIP historical simulations (1979–2014) are projected onto the fixed ERA5 principal-component space, enabling regime-scale benchmarking without redefining regime geometry. Spatial agreement, regime-membership confidence, and the influence of horizontal resolution on coastal transitions and mesoscale structure are assessed. The framework is further applied to evaluate wind, wave, and hybrid wind–wave energy classes and their climate-defined stability (temporal persistence), providing a consistent basis for comparing energy-relevant conditions across models.

Research Question 3 is addressed in Chapter 4 by applying the fixed ERA5-based regime framework to near-term future climate projections. EC-Earth3P-HR simulations for the period 2020–2050 are projected onto the historical regime space to quantify regime transitions, centroid migration, and changes in spatial footprint. These changes are interpreted through projected anomalies in wind speed and wave height, shifts in seasonal coherence are assessed using a Seasonal Regime Stability Index, and future wind, wave, and hybrid energy potential is evaluated within the historical regime structure. This chapter examines how coupled

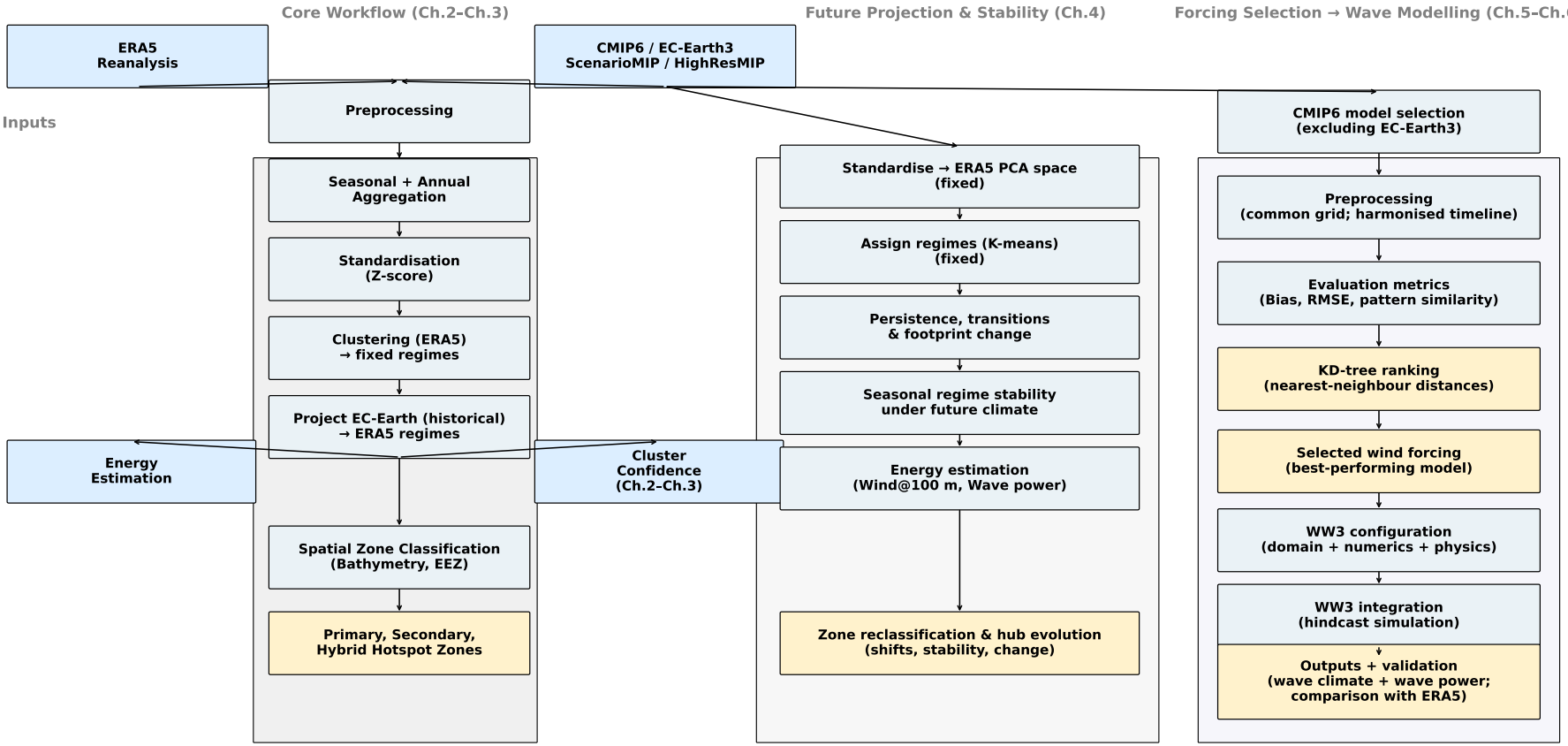

Figure 1.3 Schematic overview of the methodological framework adopted in this thesis. ERA5 reanalysis data are used to define a fixed multivariate regime space describing coupled wind–wave climate variability across European seas. This framework is subsequently applied to CMIP6 EC-Earth3 historical simulations and near-term future projections to assess transferability, regime persistence, and regime reorganisation under climate change. Within the fixed regime structure, wind and wave energy metrics and stability diagnostics are derived, and hybrid energy zones are classified. In parallel, an objective multi-metric selection of CMIP6 wind forcing is evaluated through regional wave modelling using WW3.

wind–wave regimes reorganise under climate forcing and the implications for future offshore resource stability.

Research Question 4 is addressed in Chapter 5, which develops an objective framework for selecting CMIP6 wind forcing suitable for wave modelling. Historical near-surface wind simulations are evaluated using multiple performance metrics, and the limitations of conventional single-metric model assessment are demonstrated. A KD-tree–based multi-metric ranking approach is applied to identify regionally optimal wind forcing, thereby reducing uncertainty in atmospheric inputs used for wave-climate simulations.

In Chapter 6, the suitability of the objectively selected CMIP6 wind forcing is assessed through regional wave-climate simulations dynamically downscaled using a spectral wave model. Historical wave conditions forced by the selected winds are simulated using WW3 and evaluated against reanalysis and observational benchmarks. The propagation of wind-forcing biases into wave statistics and wave power estimates is examined, and the suitability of the resulting simulations for climate-scale wave and renewable-energy applications is assessed.

Finally, Chapter 7 synthesises the findings across all chapters in a unified discussion, examining the robustness, physical interpretability, and limitations of the proposed framework. Chapter 8 concludes the dissertation by summarising the main contributions, directly addressing the research questions, and outlining recommendations and directions for future research.

2

Multivariate Spatio-Temporal Clustering Approach to Classify wind–wave Variability in European Seas

"What we know is not much.
What we do not know is immense."

- Pierre–Simon Laplace, (1814)

"The first step in wisdom is to know the things themselves;
objects are distinguished and known by classifying them
methodically and giving them appropriate names."

- Carl Linnaeus, (1758)

This chapter develops a multivariate spatio-temporal clustering framework to characterize joint wind–wave regimes across European seas using ERA5 reanalysis (1979–2014). Seasonal and annual statistics of significant wave height, mean wave period, wind speed, and wave and wind direction are computed on a 0.5° grid and used to describe the coupled wind–wave climate at the basin scale. Dimensionality is reduced using Principal Component Analysis, retaining thirty components that capture 99% of the variance, and MiniBatch k-means clustering is applied to identify nine coherent regimes with persistent

spatio-temporal signatures, where each location is characterised by its multi-year evolution rather than by a single climatological snapshot. The resulting regimes naturally group into open-ocean, transitional, and enclosed or semi-enclosed categories based on their internal variability, directional spread, and geographic exposure. Open-Atlantic regimes exhibit higher wave and wind levels with pronounced winter maxima in wave height, wave period, and wind speed. Enclosed and semi-enclosed basins display lower amplitudes and reduced variability, while transitional shelves and the southern Mediterranean show intermediate behaviour characterised by moderate wave-period levels and a seasonal rotation of both wave and wind directions, reflecting the combined influence of locally generated seas and remotely forced swell. Dispersion analyses highlight a clear Atlantic–Mediterranean partition, with transitional shelves forming a dynamical bridge between open-ocean and enclosed basins. A teleconnection analysis further shows that the NAO and AO exert primary control on Atlantic regimes, while SCAND, EA, and POLEUR modulate the variability and directional persistence of transitional and enclosed seas. The classification provides a coherent climatological framework for understanding European wind–wave conditions and provides transferable regime units for subsequent benchmarking and interpretation in later chapters.

This chapter is based on:

Maya, P., Parker, K., Cagigal, L., Metrikine, A. V., & Antolínez, J. A. A.
Multivariate spatio-temporal clustering approach to assess wind–wave variability in European seas.
Ocean Engineering and Science, under review.

2.1 Introduction

Near-surface wind–wave conditions, referring here to 10 m atmospheric winds and surface gravity waves at the ocean–atmosphere interface, are key components of the coupled ocean–atmosphere system. They shape coastal erosion, sediment transport, and energy transfer, and also affect offshore infrastructure and marine ecosystems *[Reguero et al., 2015, Waterhouse et al., 2014, Dodet et al., 2019]*. At larger scales, they contribute to ocean mixing, nutrient upwelling, and carbon cycling *[Hemer et al., 2010, Waterhouse et al., 2014, Liang et al., 2018]*. Wind–wave variability arises from atmospheric circulation, storm activity, and local geography *[Hurrell and Deser, 2010, Casas-Prat and Sierra, 2013]*. Understanding their seasonal and inter-annual variability improves knowledge of regional climate, supports coastal and offshore planning, and places observed trends in broader context. With shifting storm patterns and more frequent extremes, it is important to identify spatial patterns and long-term changes in wind–wave conditions *[Morim et al., 2019, Young and Ribal, 2019]*.

Several studies have examined wind–wave variability in different regions, often focusing on individual parameters such as wave height *[Reguero et al., 2015, Morim et al., 2019]*, wave period *[Hemer et al., 2010]*, or wind speed *[Young et al., 2011, Young and Ribal, 2019]*. In European seas, research has reported seasonal and inter-annual trends in specific basins *[Casas-Prat and Sierra, 2013, Benetazzo et al., 2014]*, investigated dual-use solutions such as wave farms for energy and coastal protection *[Rodriguez-Delgado et al., 2019]*, and linked long-term changes in wave energy to shifting climate patterns *[Morim et al., 2019, Young et al., 2011, Bergillos et al., 2019]*. Other studies have analyzed storm impacts on coastal conditions *[Bonaduce et al., 2019, Lobeto et al., 2021]* and the influence of regional features such as pressure gradients and stratified sea surface temperatures on variability *[Varlas et al., 2020, Martínez-Asensio et al., 2016]*. These works also highlight basin-scale contrasts: while the North Sea experiences strong winter wind forcing, the Mediterranean shows gradual shifts in wave direction *[Casas-Prat and Sierra, 2013, Morim et al., 2019, Elshinnawy and Antolínez, 2023]*. Despite these insights, most analyses rely on spatial or temporal averaging, which can obscure local interactions between wind and waves. Joint assessments remain limited, especially those seeking to derive long-term, spatially coherent regimes from the combined behaviour of wind and wave parameters across different European basins. Ignoring such co-variability risks overlooking key links between atmospheric forcing and ocean response *[Semedo et al., 2011, Janssen, 2004, Guanche et al., 2013, Sarmiento et al., 2019]*.

Some recent studies have applied clustering techniques to wave data to identify dominant regimes or classify coastal environments *[Fairley et al., 2020]*. Although these methods provide useful summaries, they are often limited to wave-only parameters and short-term snapshots, typically excluding wind input or broader multivariate behavior. Other approaches rely on gridded trend analyses or regional averages, which may overlook coherent spatial structures and mask interactions between variables *[Semedo et al., 2011]*. A complementary approach focuses on classifying large-scale weather patterns (synoptic climatology) and examining their influence on wave conditions, offering a link between atmospheric circulation and wave variability *[Pérez et al., 2014]*. However, such studies generally emphasize the wave response

to atmospheric patterns (geostrophic wind) without explicitly characterizing joint wind–wave variability. As a result, there is limited understanding of how joint wind–wave conditions co-vary across regions and how consistent these patterns remain over time. There remains a need for a framework that can classify such combined behavior in a way that captures both spatial coherence and temporal dynamics. ERA5 reanalysis data *[Hersbach et al., 2020]*, widely used in marine climate studies, provides wind and wave fields generated by the ECMWF Integrated Forecast System, where model simulations are constrained through data assimilation of in-situ measurements and satellite altimeter observations, offering consistent multi-decadal coverage of surface conditions. Its spatial and temporal resolution makes it a suitable basis for investigating long-term wind–wave variability across large geographic domains.

This study proposes a novel, data-driven framework to classify and jointly evaluate wind–wave regimes using long-term reanalysis data. The methodology builds a high-dimensional feature set from seasonal and annual statistics of key wave and wind parameters, covering the mean regime and associated variability at each grid point and reduces its complexity using principal component analysis (PCA). By horizontally stacking principal components over a multi-decadal period, we extract temporally enriched spatial signatures and apply K-means clustering to identify coherent wind–wave regimes. Within each cluster, we assess intra- and inter-annual variability. This approach differs from conventional map-based, grid-cell analyses, which evaluate each location independently and therefore do not capture how wind and wave variables co-vary across space or form coherent regional patterns. By grouping grid points with similar multivariate behaviour, the classification reduces point-level noise and reveals spatial structures that are not visible in single-variable maps, trend fields, or pointwise comparisons. The resulting regimes provide stable units that can be analysed consistently across seasons and decades. While demonstrated here for the European seas, the framework can be applied to other basins. To support interpretation, we also examine how major climate oscillations relate to the identified regimes across seasons. This link to large-scale climate modes is included as part of the study objective, allowing the regime behaviour to be interpreted in terms of known atmospheric circulation patterns rather than as a purely statistical classification.

The remainder of this paper is organized as follows. Section 4.2 describes the ERA5 dataset and the preprocessing steps, including seasonal and annual aggregations. It also outlines the use of PCA and clustering to reduce data complexity and identify patterns, together with the approach for quantifying intra- and inter-cluster variability. Section 6.5 presents the results of the spatio-temporal analysis, highlighting regional trends in wind–wave dynamics and differences across clusters. This section also integrates climate oscillation indices to examine their influence on regime behavior. Finally, Section 5.4 summarizes the key insights, notes limitations, and outlines directions for future research.

2.2 Data and Methodology

The approach involves five main steps: (1) extracting wind and wave parameters from ERA5 (1979–2014) and deriving 10-m wind speed and direction from the u, v wind components (see Section 2.2.2); (2) aggregating seasonal (DJF, MAM, JJA, SON, with December assigned to the following DJF year) and annual statistics, using the sample standard deviation and circular averaging/dispersion for directional variables (see Section 2.2.2.1); (3) standardizing all features and applying Principal Component Analysis (PCA) to reduce dimensionality (see Section 2.2.3); (4) performing K-means clustering ($k = 9$) to identify spatial regimes (see Section 2.2.4); and (5) evaluating intra- and inter-cluster variability and linking clusters and variables to large-scale climate oscillations via (circular) Spearman correlations (see Section 2.2.6). Figure 4.1 summarizes the workflow, including preprocessing and clustering.

Subsequent sections describe each component in detail.

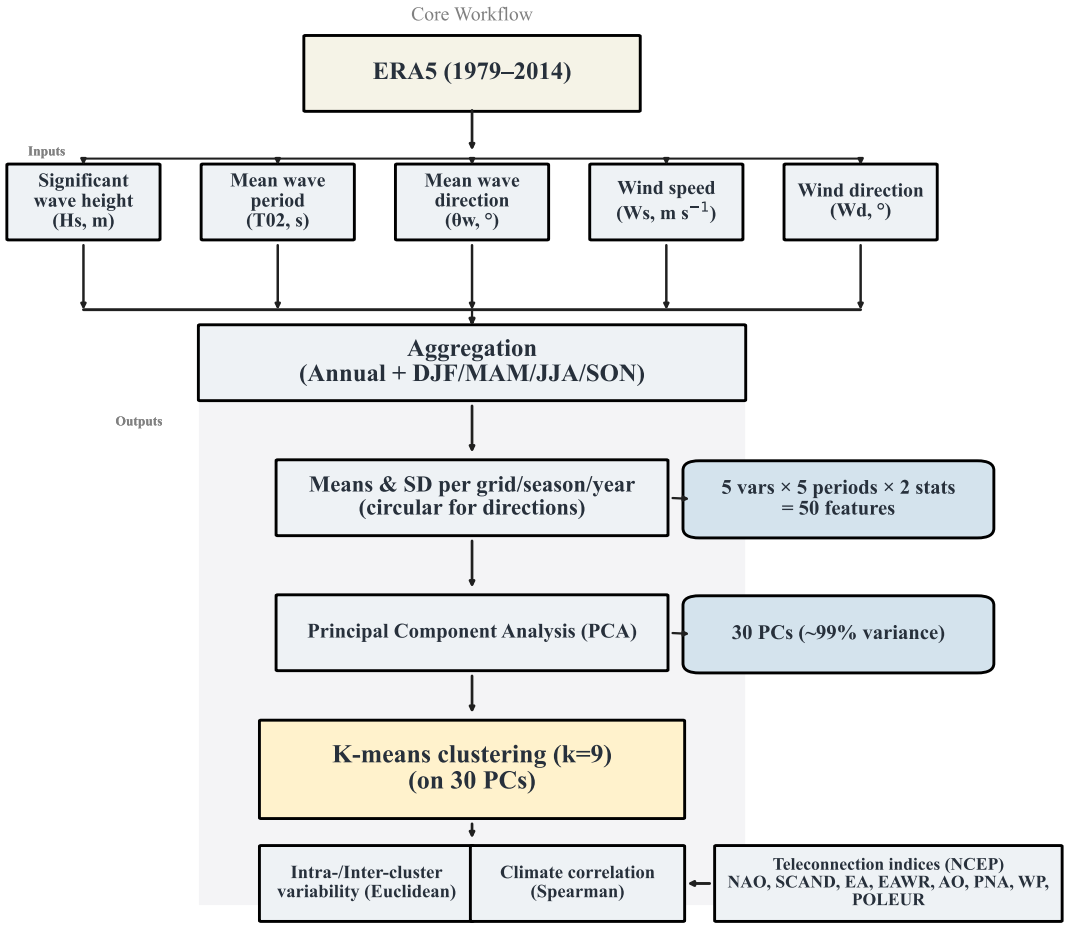

Figure 2.1 Overview of the methodology workflow. ERA5 fields (1979–2014) are aggregated to seasonal and annual statistics (using circular statistics for directions). Fifty features (5 variables × 5 periods × 2 stats) are standardized and reduced via PCA; the first 30 PCs (explaining ∼99% of variance) are clustered with k-means ($k = 9$). Outputs include intra-/inter-cluster variability and correlations with large-scale teleconnection indices (Spearman).

2.2.1 Data Description

We analyse the ERA5 reanalysis (ECMWF) for 1979–2014, which provides a continuous, homogenised reconstruction of near-surface wind and wave conditions based on the Integrated Forecast System with assimilated in-situ and satellite observations. The period 1979-2014 was selected to provide a consistent historical baseline shared across ERA5 and the climate-model experiments used in the subsequent chapters, allowing the ERA5-derived regime framework to be compared directly with CMIP6 historical simulations. The variables are significant wave height (H_s, m), mean wave period (T_{02}, s), mean wave direction (θ_w, °), 10 m wind speed (W_s, $\mathrm{m\,s^{-1}}$), and 10 m wind direction (Wd, °) defined as the direction from which the wind blows at 10 m above the sea surface. Wind quantities are derived from the 10 m zonal and meridional

components (u_{10}, v_{10}). All fields are regridded to $0.5° \times 0.5°$ and aggregated to seasonal (DJF, MAM, JJA, SON) and annual statistics. For each variable, we compute the mean and standard deviation; for wave and wind directions, circular means and circular standard deviations are used. The analysis domain spans 20°W–40°E and 25°N–70°N (Fig. 2.2), covering the dynamically active wind–wave systems of the European seas *[Reguero et al., 2019]*.

The variable set adopted in this study is not intended to represent a fixed or application-specific configuration, but rather a physically based multivariate representation of coupled wind–wave climate variability. The selected parameters describe the dominant atmospheric and wave conditions governing seasonal and inter-annual variability, directional behaviour, and regional wind–wave interactions across the study domain. This formulation allows the framework to characterise the underlying climate structure prior to the introduction of derived or sector-specific metrics. Because the methodology is based on a flexible multivariate framework, additional variables can be incorporated or removed depending on the scientific or operational objective.

2.2.2 Data Preprocessing

2.2.2.1 Seasonal and Annual Aggregation

The dataset was grouped into four standard climatological seasons-DJF, MAM, JJA, and SON-together with annual values. For each variable, we computed seasonal and annual means and standard deviations. Directional parameters (θ_w and Wd) were processed using circular mean and circular standard deviation to account for angular wrap-around. All statistics were derived from hourly ERA5 fields for 1979–2014.

2.2.2.2 Directional Variables (θ_w and Wd_{10})

Directional quantities were treated using circular statistics to avoid discontinuities at the 0°/360° boundary. For any directional series Θ_i, the mean direction was obtained from a vector (trigonometric) average:

$$\Theta_{\text{avg}} = \text{atan2}\left(\sum_i \sin\Theta_i,\ \sum_i \cos\Theta_i\right). \tag{2.1}$$

Circular standard deviation was computed using the resultant-length formulation.

For waves, $\Theta_i = \theta_{w,i}$ corresponds to the native ERA5 mean wave direction. For winds, instantaneous direction was first derived from the 10 m components as

$$Wd_{10,i} = \text{atan2}(v_{10,i},\ u_{10,i}), \tag{2.2}$$

and the same circular averaging was applied to obtain period means.

2.2.2.3 Wind Speed Calculation

Wind speed at 10 m was computed from the zonal and meridional components as

$$U_{10} = \sqrt{u_{10}^2 + v_{10}^2}. \tag{2.3}$$

Wind variables were combined with wave parameters to form a unified dataset for the spatio-temporal analysis. All processing was performed year by year to manage memory usage efficiently.

2.2.3 Principal Component Analysis (PCA)

PCA was used to compress the 50-dimensional feature vector (five variables × five periods × mean/standard deviation) at each grid–cell–year into a smaller set of orthogonal modes that capture the dominant covariance patterns in the wind–wave system *[Jolliffe, 2002]*. This facilitates both noise reduction and efficient downstream clustering of spatio-temporal regimes.

Standardization: Let $\mathbf{x}_{g,t} \in \mathbb{R}^p$ denote the feature vector ($p = 50$) for grid cell g and year t. Each feature was standardized across all grid–cell–year samples,

$$z_j = \frac{x_j - \mu_j}{\sigma_j}, \qquad j = 1, \ldots, p, \tag{2.4}$$

where (μ_j, σ_j) are the sample mean and (sample) standard deviation of feature j. Directional features (mean wave direction and mean wind direction) entered as circular means (in degrees) and circular standard deviations (degrees) computed as described in Sec. 2.2.2.2; after aggregation they are real-valued and were standardized like the linear variables.

PCA estimation: Stacking all standardized samples yields $\mathbf{Z} \in \mathbb{R}^{N \times p}$ with N equal to the number of grid–cell–year observations. PCA was computed via the singular value decomposition (SVD)

$$\mathbf{Z} = \mathbf{U}\,\mathbf{\Sigma}\,\mathbf{V}^\top, \tag{2.5}$$

where columns of $\mathbf{V}$ are the loading vectors (principal directions) and the diagonal entries of $\mathbf{\Sigma}$ give singular values. The principal component (PC) scores are

$$\mathbf{S} = \mathbf{Z}\,\mathbf{V} = [\,\mathbf{s}^{(1)}\ \mathbf{s}^{(2)}\ \ldots\ \mathbf{s}^{(p)}\,], \tag{2.6}$$

with variance explained by component k proportional to σ_k^2. The cumulative variance explained by the first K components is

$$\mathrm{CV}(K) = \frac{\sum_{k=1}^{K} \sigma_k^2}{\sum_{k=1}^{p} \sigma_k^2}. \tag{2.7}$$

Component retention and representation: A scree test and the cumulative variance curve indicated that the first $K = 30$ components account for approximately 99% of the total variance. We therefore retained 30 PCs and discarded the remainder. For each grid cell g and year t, let $\mathbf{s}_{g,t} \in \mathbb{R}^{30}$ be the retained score vector. To preserve temporal evolution in the subsequent clustering, we concatenated yearly scores into a single feature vector per grid cell,

$$\mathbf{S}_g = [\,\mathbf{s}_{g,1979}^\top\ \mathbf{s}_{g,1980}^\top\ \cdots\ \mathbf{s}_{g,2014}^\top\,]^\top \in \mathbb{R}^{30 \times 36}, \tag{2.8}$$

yielding a 1080-dimensional PC-score representation per location. These $\mathbf{S}_g$ vectors formed the input to the k-means clustering in Sec. 2.2.4.

PCA assumes linear superposition and orthogonality of modes. While this is well-suited to variance decomposition and noise reduction, strongly non-linear manifolds may require alternative embeddings (e.g., kernel PCA, autoencoders). In our case, sensitivity tests (varying K and resampling years) showed stable spatial regimes, supporting the chosen configuration.

2.2.4 Clustering Analysis

The classification uses a multivariate feature set composed of the seasonal and annual mean and standard deviation of five variables: significant wave height (H_s), mean wave period (T_{02}), wind speed (W_s), wave direction (θ_w), and wind direction (Wd). These features form the input to the PCA.

We used k-means to identify spatial wind–wave regimes from the PCA representation of ERA5. The method is suitable for this application because it handles large datasets efficiently, performs well in PCA-transformed spaces, and produces centroid-based groups that can be interpreted as representative multivariate conditions *[Jain, 2010, Lloyd, 1982, Jolliffe, 2002]*. Compared with density- or graph-based approaches, which may be sensitive to parameter settings or irregular cluster geometry, k-means provides a consistent and computationally straightforward partitioning of the data *[Xu and Tian, 2015]*. All clustering was carried out using the full-batch k-means++ initialization with multiple restarts to ensure stable solutions.

Uncertainty is also related to the choice of features used as input to the clustering. Tests with alternative feature sets showed that using a single variable (such as H_s alone) produces large-scale regime patterns that are similar to those obtained with the full multivariate set, although differences appear in local boundaries and in the treatment of transitional areas. This indicates that the broad spatial organisation of regimes is not strongly affected by feature reduction, while finer-scale details depend on the selected variables, the temporal aggregation, and the spatial domain.

ERA5 introduces additional uncertainty due to known biases in near-surface wind fields, particularly in semi-enclosed basins, which propagate into the derived wave parameters. These biases influence absolute values, but multi-decadal averaging reduces their effect on the spatial patterns used for clustering.

Clustering input (spatial vectors with temporal memory): Let $\mathbf{s}_{g,t} \in \mathbb{R}^{30}$ denote the retained PC score vector (Sec. 2.2.3) for grid cell g in year $t \in \{1979, \ldots, 2014\}$. To embed interannual evolution in each location's descriptor, we concatenated yearly scores into a single vector

$$\mathbf{S}_g = \left[\, \mathbf{s}_{g,1979}^\top \; \mathbf{s}_{g,1980}^\top \; \cdots \; \mathbf{s}_{g,2014}^\top \right]^\top \in \mathbb{R}^{30\times 36} = \mathbb{R}^{1080}. \tag{2.9}$$

The set $\{\mathbf{S}_g\}$ (one 1080-D vector per grid cell) formed the input to k-means.

Objective function and distance: Given k clusters $\{C_i\}_{i=1}^k$ with centroids $\{\boldsymbol{\mu}_i\}$ in $\mathbb{R}^{1080}$, the within-cluster sum of squares (inertia) minimized by k-means is

$$J \;=\; \sum_{i=1}^{k} \sum_{\mathbf{S}_g \in C_i} \|\mathbf{S}_g - \boldsymbol{\mu}_i\|_2^2, \tag{2.10}$$

i.e., squared Euclidean distance in PC space.

2.2.4.1 Cluster validation and selection

We evaluated k from 2 to 20 using (i) the elbow method (inertia vs. k) and (ii) the silhouette coefficient

$$S \;=\; \frac{b-a}{\max(a,b)}, \tag{2.11}$$

where a is the mean intra-cluster distance and b is the mean distance to the nearest neighboring cluster. Both diagnostics indicated a clear elbow and stable behavior at $k = 9$, which we adopted.

For ERA (30-PC space, $k = 9$) the overall silhouette was $S = 0.260$. Mean silhouettes by cluster were: 0 (0.334), 1 (0.131), 2 (0.416), 3 (0.258), 4 (0.364), 5 (0.166), 6 (0.219), 7 (0.126), 8 (0.273). Clusters 2 and 4 were the most separated, whereas 1 and 7 were comparatively less distinct. Sensitivity checks varying k (6–12), the number of retained PCs (20–40), and random seeds yielded consistent spatial boundaries and labels, supporting robustness.

2.2.5 Cluster Variability Analysis

We quantified within– and between–cluster variability directly in the principal–component (PC) space used for clustering. This keeps the metric consistent with the k-means objective (squared Euclidean distance) and avoids mixing physical units. Let $\mathbf{x} \in \mathbb{R}^p$ denote a grid cell's concatenated PC score vector with $p = 30 \times 36 = 1080$ (Sec. 2.2.4).

2.2.5.1 Centroids in PC space

For cluster k with member set C_k and cardinality $n_k = |C_k|$, the centroid is

$$\boldsymbol{\mu}_k \;=\; \frac{1}{n_k} \sum_{\mathbf{x} \in C_k} \mathbf{x} \;\in \mathbb{R}^p. \tag{2.12}$$

2.2.5.2 Intra–cluster variability

For each member $\mathbf{x} \in C_k$, we measured its deviation from the assigned centroid using the Euclidean (ℓ_2) distance

$$d_{\text{intra}}(\mathbf{x}, \boldsymbol{\mu}_k) \;=\; \|\mathbf{x} - \boldsymbol{\mu}_k\|_2 \;=\; \sqrt{\sum_{j=1}^{p} \big(x_j - \mu_{k,j}\big)^2}. \tag{2.13}$$

The distribution of $\{d_{\text{intra}}(\mathbf{x}, \boldsymbol{\mu}_k) : \mathbf{x} \in C_k\}$ was summarized by n_k, mean, standard deviation, and quartiles to characterize each cluster's internal spread (smaller values indicate more homogeneous regimes).

2.2.5.3 Inter–cluster variability

Between clusters i and j we computed the centroid–to–centroid distance

$$D_{ij} \;=\; \|\boldsymbol{\mu}_i - \boldsymbol{\mu}_j\|_2 \;=\; \sqrt{\sum_{m=1}^{p} \big(\mu_{i,m} - \mu_{j,m}\big)^2}, \tag{2.14}$$

forming a symmetric $k \times k$ distance matrix that measures separation among regimes.

Distances are unitless (PC scores from standardized features). Using Euclidean metrics in PC space aligns with the k-means criterion and provides a consistent basis for comparing intra– vs. inter–cluster structure.

2.2.6 Climate Oscillation Indices

To examine the influence of large-scale climate patterns on regional wind and wave conditions, a set of climate indices was incorporated into the analysis, as summarized in Table 2.1. These indices capture key atmospheric and oceanic modes that can influence variability in near-surface wind speed, wave height, wave period, and wave and wind direction at the air–sea interface through large-scale teleconnections. The selection was based on their relevance to both European and global climate systems.

Table 2.1 Climate Oscillations and Their Definitions.

Climate Oscillation	Definitions
NAO	Represents the atmospheric pressure difference between the Icelandic Low and Azores High, strongly influencing weather and wave dynamics in the North Atlantic Hurrell [1995].
SCAND	Indicates variability in atmospheric pressure over Scandinavia, modulating northern European climate and wind–wave patterns Barnston and Livezey [1987].
EA	Represents oscillations in sea-level pressure over the North Atlantic, impacting European weather systems and precipitation patterns Barnston and Livezey [1987].
EAWR	Characterizes atmospheric pressure anomalies between Europe and western Russia, influencing climate conditions across Eurasia Kutiel and Benaroch [2002].
AO	The northward movement of low-pressure systems or intensification of the westerlies in the Northern Hemisphere Thompson and Wallace [1998].
PNA	Captures pressure variability over the North Pacific and North America, with global teleconnections affecting trans-Pacific climate patterns Wallace and Gutzler [1981].
WP	Reflects atmospheric pressure variability over the Western Pacific, affecting climate dynamics across Asia and the Pacific Barnston and Livezey [1987].
POLEUR	Represents the Polar/Eurasian Pattern, influencing the interaction between polar and mid-latitude atmospheric circulation Barnston and Livezey [1987].

These indices were obtained from the National Centers for Environmental Prediction (NCEP). Seasonal (DJF, MAM, JJA, SON) and annual averages were used to match the temporal resolution of the wave and wind dataset.

2.2.6.1 Correlation metric (Spearman)

We quantified associations using Spearman's rank correlation, ρ_s, for *all* variables. A rank–based measure is appropriate here because (i) the series can be non-Gaussian, skewed, or heteroscedastic; (ii) $n \approx 36$ per period is modest; and (iii) relationships may be monotonic but not strictly linear. Spearman is robust to outliers and equals the Pearson correlation of the ranked variables.

Let $\{x_i\}_{i=1}^n$ and $\{y_i\}_{i=1}^n$ be paired observations and let $R_i = \mathrm{rank}(x_i)$ and $S_i = \mathrm{rank}(y_i)$ (average ranks for ties). Then

$$\rho_s \;=\; \mathrm{corr}_{\mathrm{Pearson}}(R, S), \tag{2.15}$$

which reduces to

$$\rho_s \;=\; 1 - \frac{6\sum_{i=1}^n d_i^2}{n(n^2-1)} \quad \text{when there are no ties,} \tag{2.16}$$

with $d_i = R_i - S_i$. Two–tailed p–values were obtained using the large–sample t approximation, and results with $p < 0.05$ were treated as statistically significant. For each grid cell, climate index, variable, and temporal period, both the correlation coefficient (ρ) and its associated p–value were computed. Only correlations meeting the $p < 0.05$ criterion were included in the analysis and subsequent spatial mapping. For figures, an additional filter (e.g., $|\rho| \geq 0.48$) was applied to display correlations of higher magnitude and improve visual interpretation.

For angular series (wave direction θ_w and wind direction Wd_{10}), we preserved circular geometry by projecting the angle to $\sin\Theta$ and $\cos\Theta$ (with Θ in radians) and computing

$$\rho_{\sin} = \text{Spearman}(X, \sin\Theta), \qquad \rho_{\cos} = \text{Spearman}(X, \cos\Theta), \tag{2.17}$$

where X is the teleconnection index. For reporting we selected the projection with the larger absolute correlation,

$$\rho_{\text{dir}} = \arg \max_{\rho \in \{\rho_{\sin}, \rho_{\cos}\}} |\rho|, \tag{2.18}$$

and used its associated two–tailed p–value. This retains Spearman's robustness while handling the $0°/360°$ wrap–around inherent to angles.

2.3 Results and Discussion

2.3.1 Cluster Identification

Clustering applied to the first 30 principal components of the seasonal–annual ERA5 feature set (capturing ≈99% of variance) produced nine spatially coherent wind–wave regimes across 1979–2014 (Figure 2.2). The resulting domains are Northern European Continental (NEC), Eastern Mediterranean (EMC), Southern Mediterranean (SMC), Southern and Coastal European Seas (SCES), Eastern Atlantic (EAC), Northwestern Atlantic (NWAC), Western European and Northern Sea (WENS), Western Mediterranean and Iberian (WMIC), and the Baltic Sea (BSC). Consistent with their setting, these regimes were grouped into Open Ocean, Transitional, and Enclosed/Semi-Enclosed categories (Table 3.1).

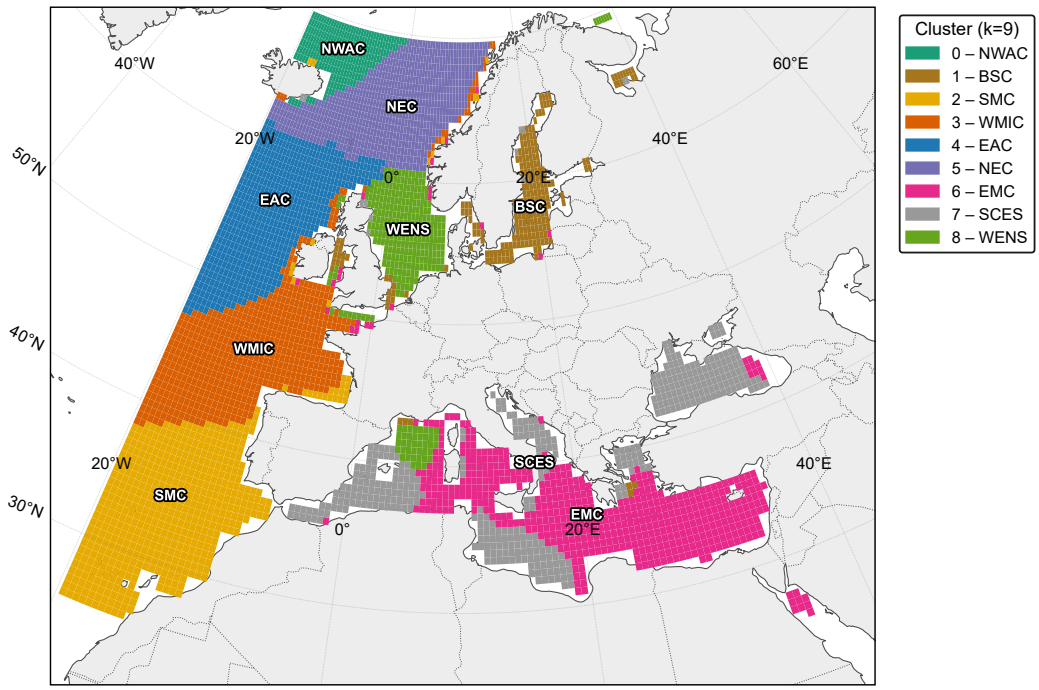

Figure 2.2 ERA5 wind–wave regimes (k=9), 1979–2014. Nine spatial regimes obtained by k-means clustering in the 30-PC space (explaining ≈99% of variance) built from seasonal and annual statistics of H_s, T_{02}, θ_w, W_{s10}, and Wd_{10}. Colours indicate cluster membership; labels denote abbreviations (NWAC, BSC, SMC, WMIC, EAC, NEC, EMC, SCES, WENS).

The robustness of the partition was assessed with complementary diagnostics. The elbow curve (inertia vs. k) showed a clear bend near $k = 9$, and the silhouette analysis supported

Table 2.2 Regional clusters ($k = 9$) and qualitative geographic classification.

Cluster Name (Abbreviation)	Geographic Classification
Northern European Continental Cluster (NEC)	Open Ocean
Eastern Mediterranean Cluster (EMC)	Enclosed/Semi-Enclosed
Southern Mediterranean Cluster (SMC)	Transitional
Southern and Coastal European Seas Cluster (SCES)	Enclosed/Semi-Enclosed
Eastern Atlantic Cluster (EAC)	Open Ocean
Northwestern Atlantic Cluster (NWAC)	Open Ocean
Western European and Northern Sea Cluster (WENS)	Transitional
Western Mediterranean and Iberian Cluster (WMIC)	Transitional
Baltic Sea Cluster (BSC)	Enclosed/Semi-Enclosed

this choice (overall silhouette ≈ 0.26). Sensitivity checks varying k (6–12), the number of retained PCs (20–40), and random seeds yielded nearly identical geographic partitions and label assignments, indicating stable solutions. Taken together, these results suggest that nine clusters provide a defensible balance between within-cluster compactness and between-cluster separation, and they form a reliable basis for the regional and seasonal analyses that follow.

Although displayed on a map, the partition is intrinsically spatio-temporal. Each grid cell is represented by a time-integrated descriptor that embeds its seasonal and annual behavior over 1979–2014 (Sec. 2.2.4). Thus, the regimes are not instantaneous snapshots; they reflect persistent, multi-decadal structure in joint wind–wave variability.

The resulting geography exhibits coherent, non-random "fingerprints" shaped by consistent multivariate signals rather than by coastline geometry or masking. Open-ocean domains (e.g., NEC, EAC) are clearly separated from enclosed basins (e.g., BSC, EMC), while transitional interfaces such as WMIC and WENS emerge where gradients in wind–wave climate are strongest 2.2. These intermediate regions arise from the data-driven signatures in principal-component space, not from spatial proximity alone.

Importantly, the method respects real-world geophysical distinctions without enforcing predefined boundaries. It captures gradients across the domain, enabling a physically interpretable classification. This structure establishes a stable baseline for tracking seasonal and interannual dynamics within each regime and supports further analysis of variability and potential drivers in the sections that follow.

2.3.2 Atlantic–Mediterranean Cluster Separation

Intra-cluster variability was quantified as the Euclidean distance from each grid cell to its cluster centroid in the 30-PC feature space. Figure 2.3 shows the full distributions, and Figure 2.4 summarizes their statistical spread. The most compact regimes are SMC and EAC, with low cluster-mean distances (≈17–18). By contrast, EMC (≈24.1), SCES (≈27.1), and BSC (≈28.0) display broad dispersion, with BSC showing the highest mean distance overall. NEC, NWAC, WENS, and WMIC fall into the intermediate range (≈19–23). Within this group, WMIC lies toward the compact end, while NEC, NWAC, and WENS exhibit greater spread.

The compactness of EAC reflects swell-dominated conditions and long, uniform fetches across the Atlantic, while SMC indicates relatively coherent forcing in the southern Mediterranean. In contrast, EMC, SCES, and BSC exhibit broad variability consistent with semi-enclosed geometry, complex coastlines, and heterogeneous local winds. The particularly high dispersion in BSC is further linked to shallow depth, limited fetch, strong coastal gradients, and

seasonal ice effects. Intermediate regimes reflect mixed forcing: WMIC remains comparatively cohesive, while NEC, NWAC, and WENS show higher variability, with NWAC especially influenced by storm-track activity in the North Atlantic.

Inter-cluster distances (Figure 2.5) confirm separation between regimes. The largest centroid distances occur between EAC–WMIC (≈80.9), EAC–WENS (≈72.9), and EAC–EMC (≈70.3), marking large differences in multivariate wind–wave statistics between the open Atlantic and transitional or eastern Mediterranean regimes. The smallest distance is between WMIC–WENS (≈25.0), reflecting their shared transitional character. Enclosed and semi-enclosed basins are not uniformly similar: EMC is distant from both SMC and SCES (≈64.6 and ≈60.8, respectively), while BSC occupies a mid-range position.

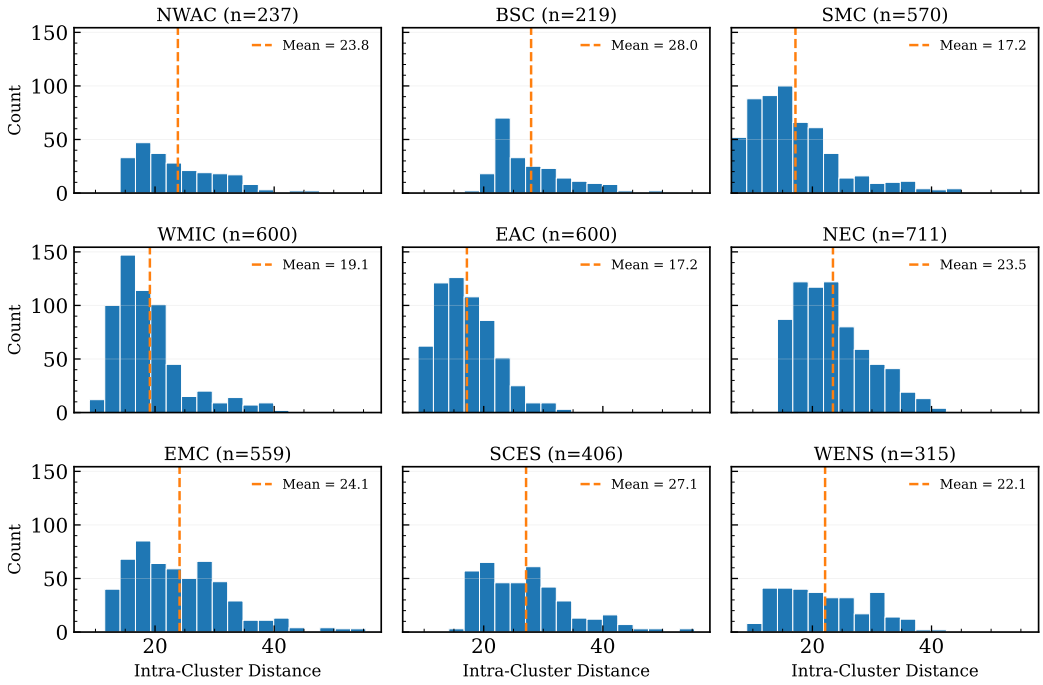

Figure 2.3 Intra-cluster distance distributions (ERA5, k=9). Histograms of Euclidean distances from each grid cell to its cluster centroid in the 30-PC space; the dashed orange line marks the cluster mean. Panel titles list regime and sample size n.

These patterns are consistent with basin-scale forcing. Transitional clusters (WMIC, WENS) are statistically close to EMC but remain well separated from EAC, forming bridges between open-ocean and enclosed basins. The large Atlantic–Mediterranean separations reflect distinct circulation regimes, while the intermediate position of BSC highlights the heterogeneous character of semi-enclosed seas. Boxplots and histograms show that WMIC and WENS occupy intermediate dispersion ranges broader than EAC but narrower than EMC and SCES, consistent with their dual exposure to Atlantic and Mediterranean processes. Among transitional clusters, SMC is comparatively compact.

Together, these results indicate a balanced nine-cluster solution. Compact open-ocean regimes (EAC, SMC) provide consistent baselines for region-specific forecasting of seasonal to interannual conditions. Large inter-basin distances across the Atlantic–Mediterranean divide (EAC–WMIC = 80.9; EAC–WENS = 72.9; EAC–EMC = 70.3) delineate contrasts in wind–wave regimes, informing energy planning where resource potential and design conditions differ substantially. Transitional regimes (e.g., WMIC–WENS = 25.0) identify zones where open-ocean and enclosed-basin processes interact, which is relevant for evaluating combined forcing in siting and operational strategies. Enclosed regimes with broad dispersion (e.g., EMC, SCES, BSC) define areas where local wind and boundary effects dominate, providing

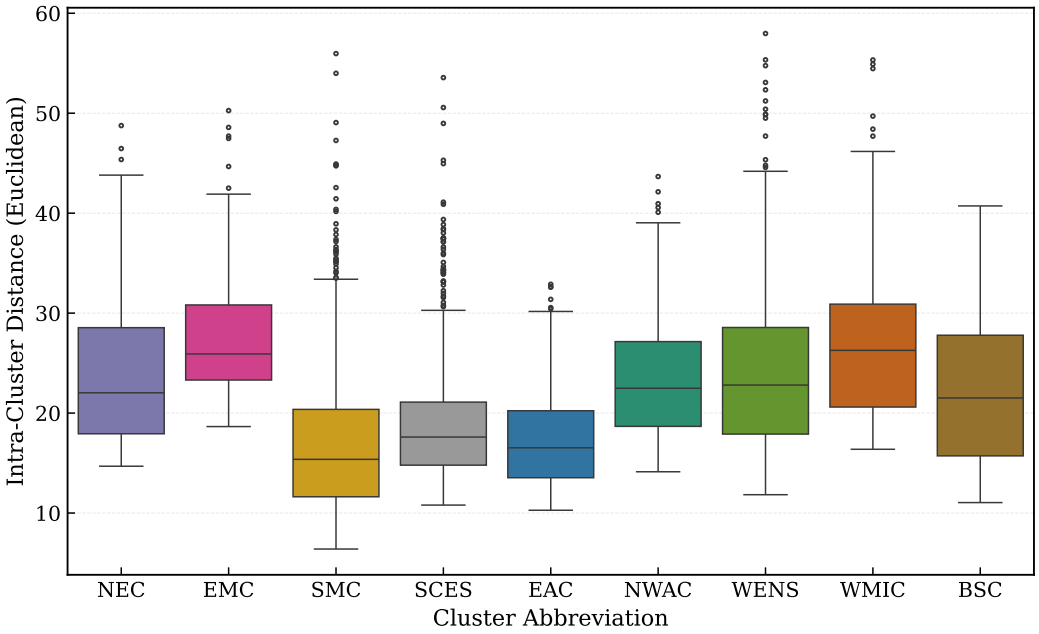

Figure 2.4 Intra-cluster variability by regime (ERA5, k=9). Boxplots of Euclidean distances from each grid cell to its cluster centroid in the 30-PC space (dimensionless); boxes show medians and interquartile ranges, whiskers denote 1.5×IQR, and points indicate outliers.

input for climate-sensitivity assessments that require explicit treatment of heterogeneous responses. The balance of compact, intermediate, and heterogeneous clusters aligned with their open-ocean, transitional, and enclosed classifications supports the nine-cluster framework as a statistically consistent and physically interpretable representation of regional wind–wave regimes.

2.3.3 Spatio-Temporal Variability

2.3.3.1 Long-Term Trends: Annual Mean Significant Wave Height (H_s)

Panel (a) of Fig. 2.6 shows a consistent hierarchy across regimes. Open-Atlantic clusters NWAC, EAC, and NEC exhibit the largest medians, broad interquartile ranges (IQRs), and frequent upper-tail values, with NWAC highest, EAC close behind, and NEC slightly lower. This ranking is consistent across the annual distributions.

Enclosed and semi-enclosed basins (EMC, SCES, BSC) lie at the low end, with compact IQRs and few outliers (Fig. 2.6a). EMC and BSC are most concentrated, while SCES is somewhat wider but remains well below the open-ocean spread.

Transitional regimes (WMIC, WENS) and the southern Mediterranean (SMC) occupy an intermediate band. WMIC has the broadest spread among these, WENS is moderate, and SMC is comparatively tight. The annual standard-deviation boxplots (Fig. 2.7a) mirror this hierarchy: largest dispersion in NWAC/EAC, smallest in EMC/BSC (with SCES slightly higher), and intermediate over WMIC/WENS/SMC.

The open-ocean signal reflects persistent exposure to North Atlantic storm tracks and long-fetch swell, elevating both mean levels and variability in NWAC/EAC; NEC remains elevated but more tempered. In enclosed basins, limited fetch and predominantly local forcing suppress wave growth and compress the distributions. Transition regimes blend these influences: WMIC/WENS carry Atlantic energy but are modulated by shelf processes, while SMC shows relatively uniform regional forcing.

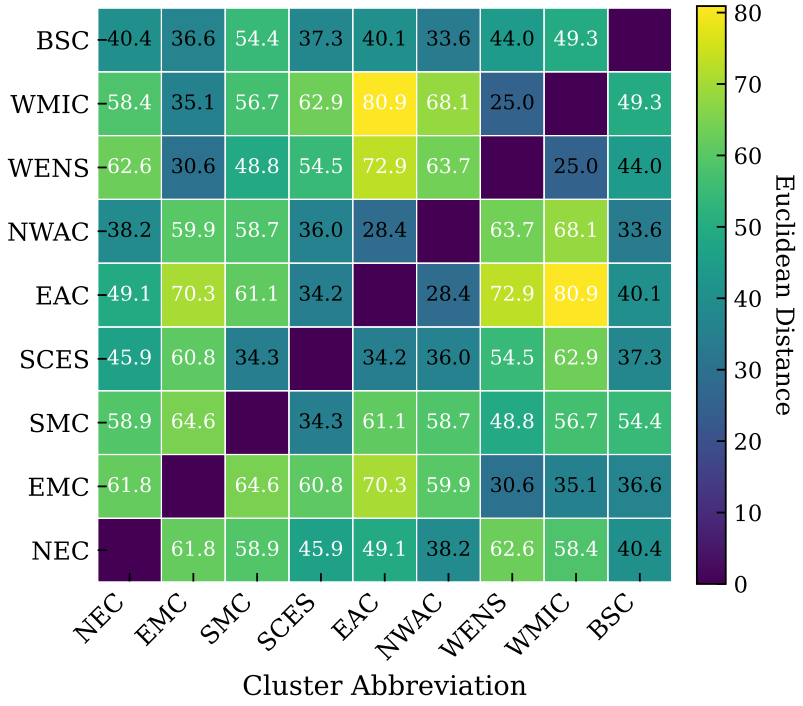

Figure 2.5 Inter-cluster separation (centroid distances; ERA5, k=9). Symmetric matrix of Euclidean distances between cluster centroids computed in the 30-PC feature space (dimensionless). Larger values indicate stronger dissimilarity in multivariate wind–wave statistics; diagonal entries are zero.

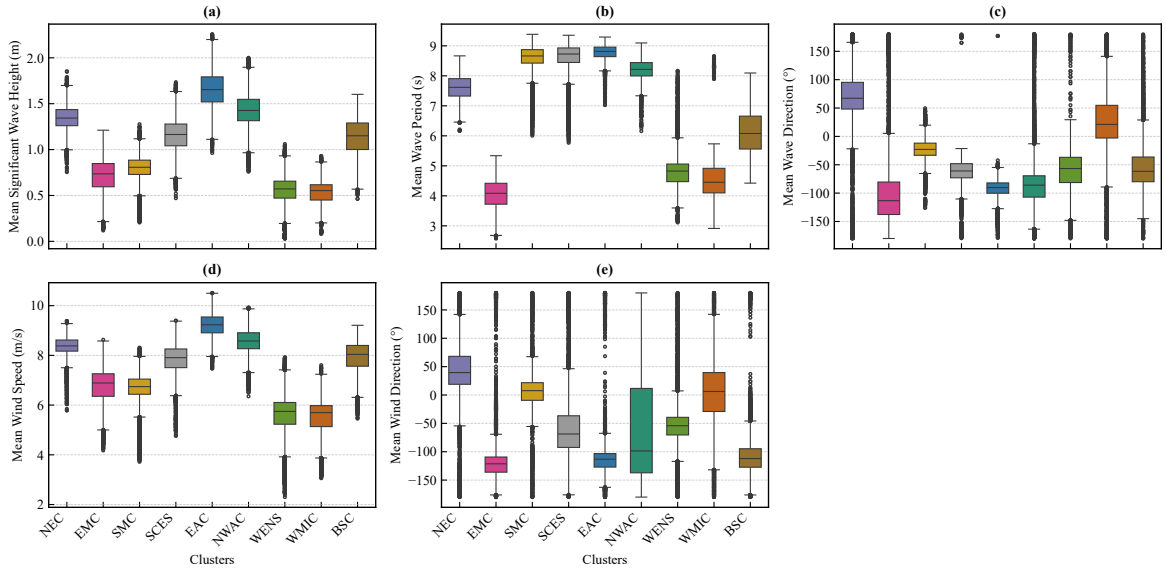

Figure 2.6 Annual mean distributions by cluster (ERA5, 1979–2014; $k = 9$). Boxplots for (a) significant wave height H_s, (b) mean wave period T_{02}, (c) mean wave direction θ_w, (d) 10-m wind speed W_{s10}, and (e) 10-m wind direction Wd_{10}. Boxes show medians and interquartile ranges; whiskers denote 1.5 × IQR; points are outliers. Direction panels use circular means with angles wrapped to $[-180°, 180°)$. Distributions aggregate all grid cells and years within each cluster.

From a metocean standpoint, NWAC/EAC require wider design and operational ranges due to their larger intrinsic variance and heavier upper tails; EMC/BSC offer more stable sea states suitable for sheltered operations. Transition regimes warrant case-specific treatment: neither purely open-ocean nor enclosed, they combine basin-scale exposure with regional heterogeneity. Together, panels (a) in Figs. 2.6 and 2.7 define a clear, physically grounded hierarchy used throughout the analysis.

2.3.3.2 Long-Term Trends: Annual Mean Wave Period (T_{02})

The annual distribution of mean wave period (T_{02}) shows a consistent hierarchy across regimes (Fig. 2.6b). Open-Atlantic clusters-NWAC and EAC, followed by NEC-exhibit the longest periods with broad interquartile ranges and frequent upper-tail values, consistent with persistent swell influence. Enclosed and semi-enclosed basins (EMC, BSC, SCES) display shorter periods with compact spreads, reflecting locally forced seas. Transitional shelves (WMIC, WENS) and the southern Mediterranean (SMC) occupy an intermediate position: medians lie between the open ocean and enclosed groups, and spreads are moderate.

The corresponding annual standard-deviation panel (Fig. 2.7b) reinforces these contrasts. Variability in T_{02} is largest in the open Atlantic (NWAC, EAC), intermediate over the transitional shelves (WMIC, WENS) and SMC, and smallest within the enclosed basins (EMC, BSC, SCES). NEC typically falls between the open Atlantic and transitional groups, reflecting partial continental influence along the Nordic–Barents margins.

Within the Atlantic, NWAC and EAC consistently lead in both median T_{02} and spread, while NEC remains slightly shorter and less variable. Among transitional regimes, WMIC often shows a broader range than WENS, consistent with exposure to both Atlantic swell and Iberian/Mediterranean winds. SMC tends toward the tighter end of the transitional group, with medians closer to the enclosed basins than to the open Atlantic.

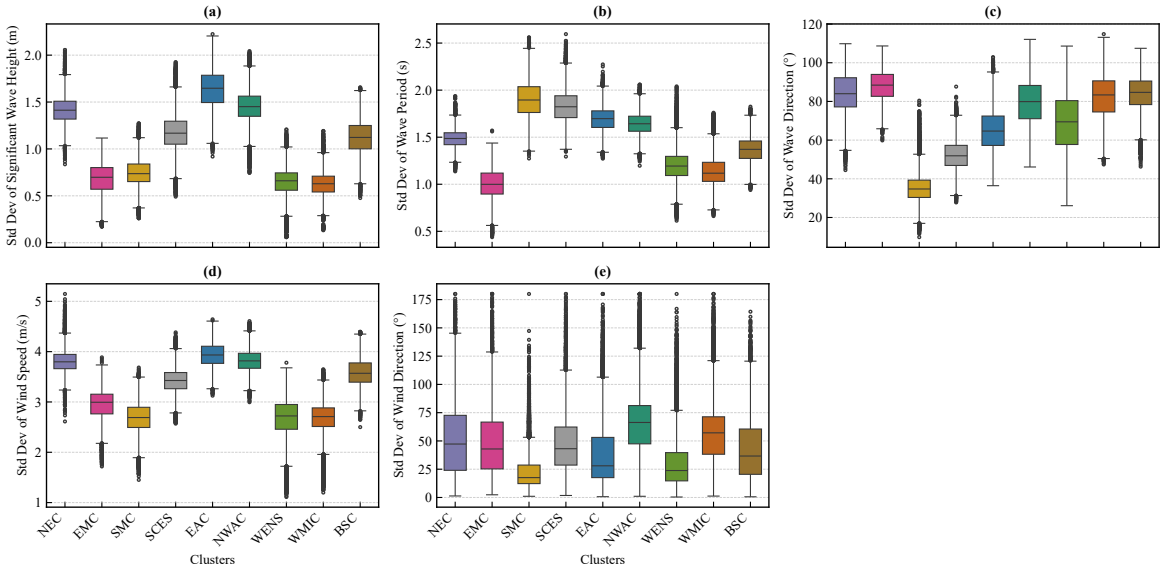

Figure 2.7 Annual variability (standard deviation) by cluster (ERA5, 1979–2014; $k = 9$). Boxplots for (a) $\sigma(H_s)$, (b) $\sigma(T_{02})$, (c) circular $\sigma(\theta_w)$, (d) $\sigma(W_{s10})$, and (e) circular $\sigma(Wd_{10})$. Boxes show medians and interquartile ranges; whiskers denote $1.5 \times$ IQR; points indicate outliers. Directional standard deviations are computed using circular statistics. Distributions aggregate all grid cells and years within each cluster.

The ordering of T_{02} reflects fundamental fetch and forcing controls. Long periods and larger spreads in the open Atlantic arise from recurrent, long-fetch storm systems and the

prevalence of mature swell. Compact, shorter periods in enclosed basins follow from limited fetch and dominant local wind-sea generation. Transitional shelves blend these behaviours: mixed sea–swell conditions produce intermediate medians and moderate variance.

Because mean wave period (T_{02}) modulates wave energy flux and near-bed orbital velocities, these contrasts have practical implications for design and operations. Longer, more variable periods in NWAC and EAC imply wider energy-bearing frequency bands and more stringent fatigue and response checks. By contrast, the shorter, more stable periods in EMC, BSC, and SCES support narrower design spectra and steadier operability envelopes. The transitional shelves require hybrid treatment, with allowance for episodic swell superimposed on locally forced seas.

2.3.3.3 Long-Term Trends: Annual Mean Wind Speed (W_{s10})

Annual 10-m wind speed (W_{s10}) shows a clear spatial ordering across regimes (Fig. 2.6d). Open-Atlantic clusters NWAC and EAC, with NEC trailing, exhibit the highest medians and broad interquartile ranges. Enclosed and semi-enclosed basins (EMC, BSC, SCES) present lower medians with compact spreads. Transitional shelves (WMIC, WENS) and the southern Mediterranean (SMC) occupy an intermediate band.

The annual standard-deviation panel for W_{s10} (Fig. 2.7d) mirrors the mean pattern: variability is largest over NWAC and EAC, intermediate over WMIC, WENS, and SMC, and smallest within EMC, BSC, and SCES. NEC typically sits between the Atlantic core (NWAC/EAC) and the transitional group.

Within the Atlantic, NWAC generally shows the widest spread, consistent with frequent cyclones and strong winter variability, while EAC maintains similarly high medians with slightly tighter dispersion. WENS tends to be windier than WMIC (North Sea exposure), and SMC sits at the lower end of the transitional cohort.

Spatial contrasts in W_{s10} shape wind-sea growth, operability windows, and design envelopes. Higher and more variable winds in NWAC and EAC call for broader environmental design spectra and conservative weather-risk management; tighter, lower-wind climates in EMC, BSC, and SCES support narrower operability bands; transitional shelves require hybrid strategies that accommodate episodic Atlantic influence.

2.3.3.4 Long-Term Trends: Annual Mean Wave Direction (θ_w)

Annual mean wave direction (θ_w) shows coherent, regime-specific centres across all nine clusters (Fig. 2.6c). The open-Atlantic domains NWAC and EAC exhibit tightly grouped medians within a consistent sector, reflecting persistent swell approach from the Atlantic storm track. NEC is similarly well organised but with a slight rotation relative to NWAC and EAC, consistent with Norwegian–Barents Sea exposure. Enclosed and semi-enclosed basins (EMC, BSC, SCES) display compact central angles, strongly constrained by basin geometry and limited fetch. Transitional shelves (WMIC, WENS) and the southern Mediterranean (SMC) occupy intermediate positions: their medians remain stable across years but spread more than the enclosed basins and less than the Atlantic core, evidencing the mixed influence of swell and locally forced seas.

The dispersion panel (Fig. 2.7c) follows the same ordering. Directional variability is largest in the open ocean (NWAC, EAC), reflecting multiple storm approaches and occasional regime shifts, while NEC is moderate. Among the transitional shelves, WMIC typically shows the broadest spread (Atlantic–Mediterranean interface and coastal steering), with WENS somewhat tighter (North Sea shelf orientation). SMC sits in the intermediate-to-low range. The enclosed and semi-enclosed basins (EMC, BSC, SCES) exhibit the smallest dispersion, consistent with short fetch and boundary control.

All direction panels use circular statistics: circular means are reported after wrapping angles to $[-180°, 180°)$, and variability is quantified with a circular spread measure, avoiding artificial widening near the $0°/360°$ seam. The persistent sectoral medians in NWAC, EAC, and NEC indicate stable swell approach at the annual scale, whereas the compact spreads in EMC, BSC, and SCES reflect fetch limitation and boundary effects. Transitional shelves (WMIC, WENS) show mixed signals that are physically credible given their dual exposure. Together, these patterns confirm that the directional climatology encoded by the clusters is geographically coherent and dynamically consistent with known forcing.

2.3.3.5 Long-Term Trends: Annual Mean Wind Direction (W_{d10})

Annual mean 10-m wind direction (W_{d10}) exhibits coherent, regime-specific sectors across the nine clusters (Fig. 2.6e). The open-Atlantic domains NWAC and EAC are westerly centred with broad spreads, consistent with frequent synoptic passages and long storm-track fetch; this variability underpins the elevated H_s and longer T_{02} observed in these regimes. NEC is similarly organised but rotated relative to NWAC and EAC, reflecting Norwegian–Barents exposure. Enclosed and semi-enclosed basins (EMC, BSC, SCES) show compact directional envelopes constrained by basin geometry and limited fetch. Transitional shelves (WMIC, WENS) and the southern Mediterranean (SMC) occupy intermediate positions: medians are stable but spreads exceed those of enclosed basins and are smaller than in the Atlantic core, consistent with mixed local and swell-related forcing.

The variability panel (Fig. 2.7e) follows the same ordering. Directional variability is largest in NWAC and EAC, moderate in NEC, intermediate over WMIC and WENS (with WMIC typically broader given its Atlantic–Mediterranean interface), and smallest in EMC, BSC, and SCES; SMC sits in the intermediate-to-low range. All statistics are circular, with means wrapped to $[-180°, 180°)$ and spread measured using circular dispersion.

These contrasts are operationally relevant. Broader directional variability in NWAC, EAC, and parts of WMIC implies wider metocean load roses, larger yaw/heading excursions, and tighter fatigue allowances. Narrow spreads in EMC, BSC, and SCES support tighter design sectors and more stable operability windows. In transitional shelves such as WMIC and WENS, seasonal wind rotation increases the likelihood of reversals in wave approach and alongshore sediment transport, requiring case-specific coastal planning. SMC, though transitional, behaves closer to enclosed seas, supporting more persistent directional regimes. Because directional spread is greatest where synoptic variability dominates, anomalies linked to North Atlantic modes are most visible in NWAC and EAC and at the Atlantic–Mediterranean interface (WMIC), whereas enclosed basins exhibit higher year-to-year predictability of approach direction. Any long-term displacement of the storm track or westerly jet would be expected to manifest first as shifts in mean sector or dispersion in NWAC and EAC; the cluster climatology here provides a baseline for such monitoring.

2.3.3.6 Short-Term and Inter-Annual Variability

We quantify the seasonal cycle and year-to-year variability using seasonal means and seasonal standard deviations for all variables (Figs. 2.8–2.9). Seasonal means describe the intra-annual structure (DJF, MAM, JJA, SON); seasonal standard deviations summarise interannual spread *within* each season over 1979–2014.

Significant wave height (H_s): Open-Atlantic regimes (NWAC, EAC, NEC) peak in DJF and minimise in JJA, with broad winter distributions (Fig. 2.8a). Enclosed basins (EMC, SCES, BSC) show lower amplitudes and tighter spreads across all seasons. Transitional shelves (WMIC, WENS) are intermediate; SMC is comparatively compact.

Wave period (T_{02}): The seasonal ordering mirrors H_s (Fig. 2.8b): longer periods in DJF for NWAC and EAC (swell-rich conditions), shorter in JJA. Enclosed clusters retain shorter,

less variable periods throughout the year.

Wind speed (W_{s10}): DJF maxima in open-ocean clusters with a marked summer minimum (Fig. 2.8d). Enclosed clusters show muted seasonality; transitional shelves sit between.

Wave direction (θ_w) and wind direction (W_{d10}): Open-ocean clusters retain westerly-dominated sectors, most concentrated in DJF and broader in shoulder seasons (Figs. 2.8c,e). Transitional shelves (WMIC, WENS) exhibit clear seasonal rotation (backing/veering) of prevailing sectors. Enclosed basins maintain narrower, more persistent approach and wind sectors across seasons.

H_s and T_{02} variability: Seasonal standard deviations are largest in DJF for NWAC, EAC, and NEC and smallest in JJA, with enclosed basins lowest in all seasons (Fig. 2.9a–b). Transitional shelves are mid-range; SMC remains relatively low.

W_{s10} variability: The same winter-high/summer-low ordering holds (Fig. 2.9d), strongest over the open Atlantic and weakest in enclosed basins.

Directional variability (circular spread): Directional standard deviations are generally larger outside winter (often MAM/SON) in open-ocean and transitional regimes, and smallest year-round in enclosed basins (Figs. 2.9c,e). Winter sectors are typically tighter over NWAC and EAC, with cluster-specific exceptions (e.g., episodic winter broadening in transitional shelves).

The winter maxima and broad spreads in H_s, T_{02}, and W_{s10} over NWAC, EAC, and NEC reflect the seasonal strengthening and meridional excursions of the North Atlantic storm track, longer effective fetch, and frequent swell incidence. Conversely, the compact seasonal envelopes in EMC, SCES, and BSC arise from geometric confinement and locally forced, short-sea conditions. Transitional shelves (WMIC, WENS) express both behaviours: winter exposure to Atlantic systems and seasonal rotation of prevailing sectors, which broadens directional spread in the shoulder seasons and moderates it in DJF/JJA. The persistently low spread in SMC is consistent with more coherent regional forcing relative to the western/central Mediterranean interface.

Taken together, the seasonal means set the expected cycle (energetic in winter, quiescent in summer) and the seasonal standard deviations indicate where that cycle is most variable from year to year: high over the open Atlantic in DJF, moderate over transitional shelves, and low in enclosed basins. The directional panels confirm that clusters differ not only in energy level but also in *directional persistence* versus *sectoral rotation*, which is central for wave growth, coastal transport, and design load envelopes.

2.3.4 Teleconnection Imprints on Regional Wind–Wave Clusters

We examine cluster-level associations between seasonal and annual wind–wave metrics and two teleconnection sets: Group 1 (NAO, SCAND, EA, EAWR) and Group 2 (AO, PNA, POLEUR, WP). Figures 2.10–2.11 display Spearman rank correlations at the cluster scale. For each variable–season pair within a cluster, the panels report the strongest signed coefficient that is statistically significant (two-tailed $p < 0.05$) and meets a display cutoff of $|\rho| \geq 0.48$; empty cells indicate that no coefficient passed both filters. Signs denote the direction of association, and magnitudes indicate strength.

2.3.4.1 Group 1: NAO, SCAND, EA, EAWR

Figure 2.10 shows a clear, non-uniform teleconnection imprint across the nine regimes. The NAO dominates the open Atlantic: in NEC and EAC it is positively associated with winter and annual wave energy (e.g., H_s-DJF/ANNUAL $\sim$ +0.49–+0.51), while in NEC it also lengthens spring periods (T_{02}-MAM +0.55) and rotates wave approach toward more zonal

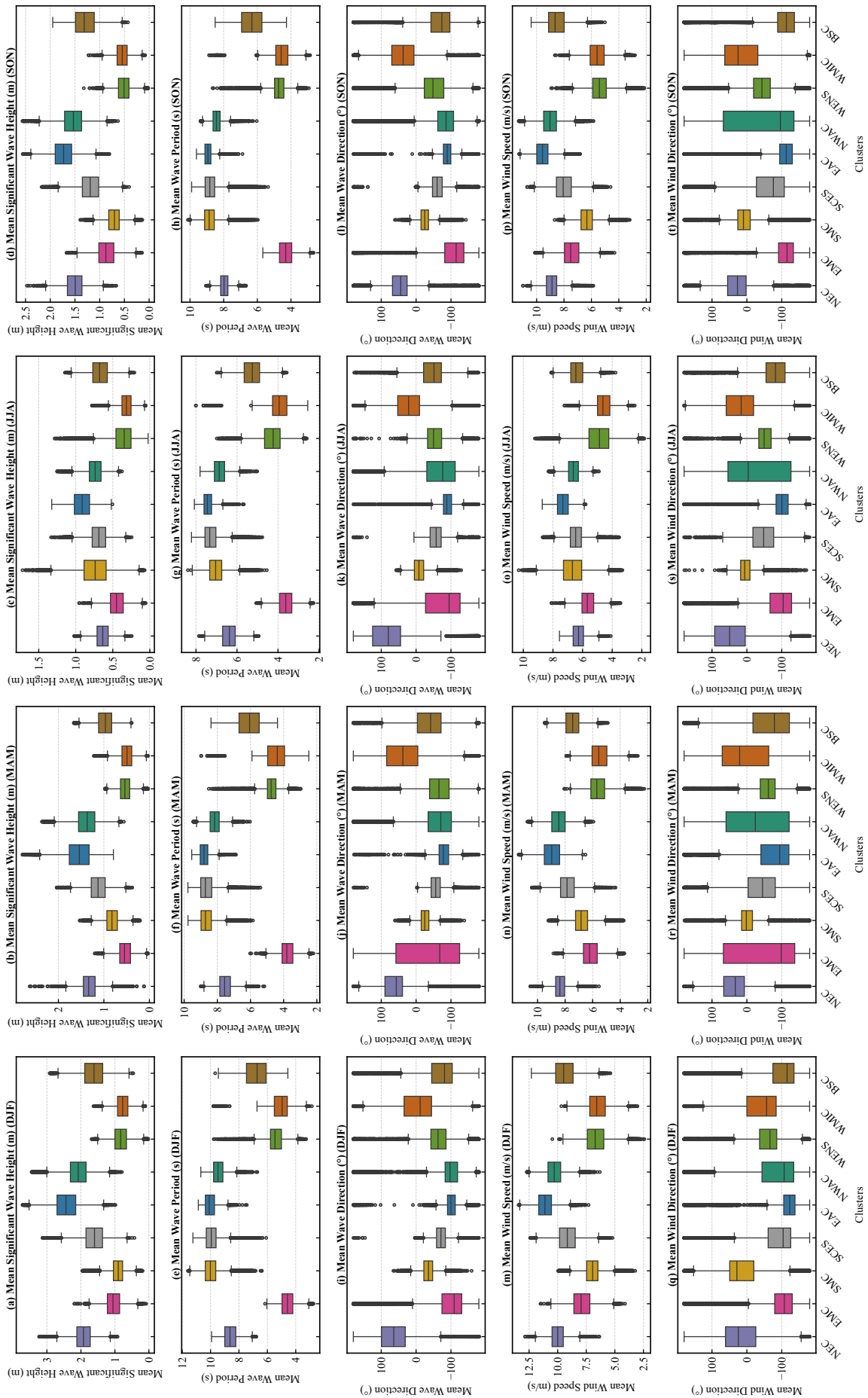

Figure 2.8 Seasonal means by cluster (ERA5, 1979–2014; $k = 9$). Boxplots of seasonal *means* for five variables across the nine clusters. Columns correspond to seasons (DJF, MAM, JJA, SON); rows correspond to (a–d) H_s (m), (e–h) T_{02} (s), (i–l) mean wave direction θ_w (°), (m–p) W_{s10} (m s^{-1}), and (q–t) mean wind direction Wd_{10} (°). Directional means are computed using circular averaging. Boxes show medians and interquartile ranges; whiskers denote $1.5 \times$ IQR; points indicate outliers. Distributions aggregate all grid cells and years within each cluster.

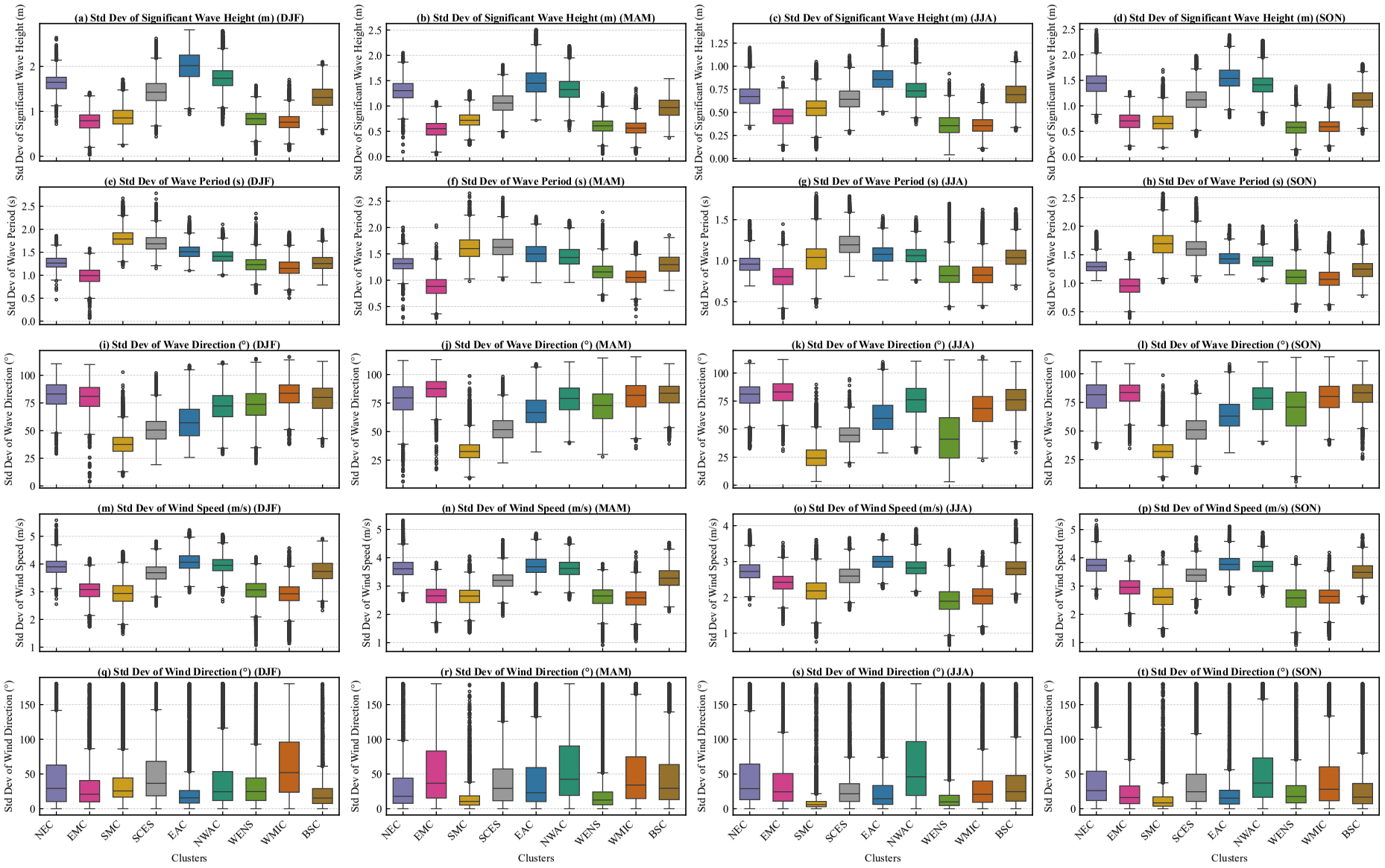

Figure 2.9 Seasonal variability by cluster (standard deviations; ERA5, 1979–2014; $k = 9$). Boxplots of seasonal *standard deviation* for five variables across the nine clusters. Columns correspond to seasons (DJF, MAM, JJA, SON); rows correspond to (a–d) H_s (m), (e–h) T_{02} (s), (i–l) wave direction θ_w (°; *circular* s.d.), (m–p) W_{s10} (m s^{-1}), and (q–t) wind direction Wd_{10} (°; *circular* s.d.). Directional spreads use circular statistics (resultant-length based). Boxes show medians and interquartile ranges; whiskers denote 1.5 × IQR; points indicate outliers. Distributions aggregate all grid cells and years within each cluster.

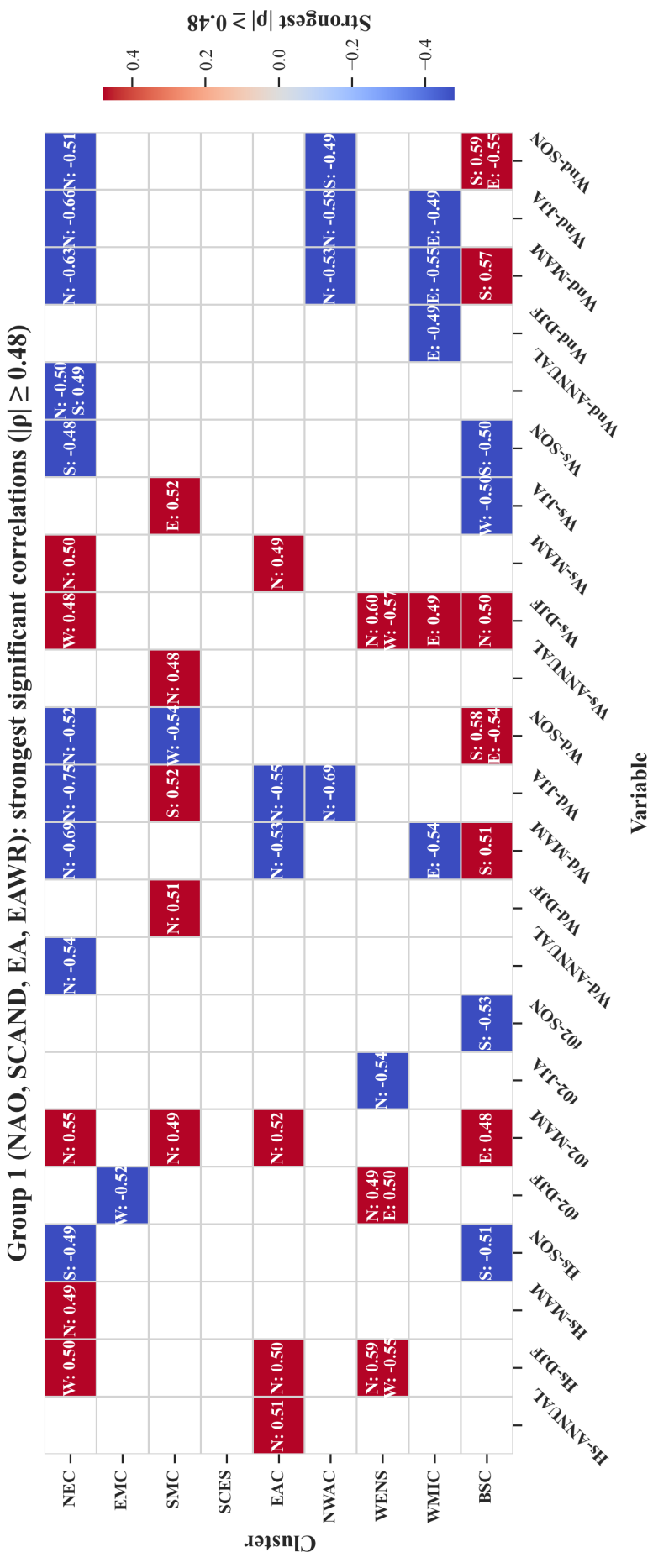

Figure 2.10 Group 1 teleconnections (NAO=N, SCAND=S, EA=E, EAWR=W): strongest significant correlations by regime. For each cluster (rows) and variable/season (columns), the cell reports *all statistically significant* Spearman rank correlation (mean across significant grid cells within the cluster) between that variable and any of the four indices, provided it is significant (two-tailed $p < 0.05$) and exceeds the threshold $|\rho| \geq 0.48$. Color encodes the signed value of ρ (red = positive, blue = negative); empty cells indicate no index met the criterion for that cluster–variable pair. Directional variables (θ_w, Wd_{10}) use the circular Spearman treatment (sin/cos mapping). ERA5, 1979–2014; $k = 9$ clusters.

directions (negative Wd in MAM–JJA, down to -0.75). SMC also shows a spring period signal (T_{02}-MAM $+0.51$). A counterexample is NWAC in summer, where NAO shortens periods (T_{02}-JJA -0.69). On the shelf, WENS exhibits strong but opposing annual signals: NAO enhances H_s and W_s ($+0.59$, $+0.60$), while EAWR suppresses both (-0.55, -0.57). Additional NAO signals are evident in wind direction over NEC/EAC (annual and DJF negative) and in winter wind speed over NEC/NWAC (DJF positive), while SCAND contributes weaker directional effects in SMC, and EA modulates WENS wave direction in autumn (Wd-SON -0.54).

SCAND is most evident in the Baltic (BSC): lower autumn energy (H_s-SON -0.51, T_{02}-SON -0.53) contrasts with higher directional angles in winter (Wd-DJF $+0.51$) and at 10 m in spring and autumn (Wd_{10}-MAM/SON $+0.57$/$+0.59$). Smaller SCAND effects also appear on the Atlantic margin (e.g., NEC H_s-SON -0.49). EA and EAWR act more locally: EA aligns directions in EMC (Wd-MAM $+0.52$) and WMIC (Wd-MAM -0.54), and strengthens late-season winds in SMC (W_s-SON $+0.52$). EAWR reduces annual energy on WENS (as above) and veers SMC summer directions (Wd-JJA -0.54). No signal in SCES exceeds the $|\rho| \geq 0.48$ threshold, consistent with its weak direct teleconnection influence.

These patterns are physically consistent. NAO-linked storm-track geometry explains the coherent energy and direction responses in NEC and EAC, as well as the summer period shortening over NWAC. The WENS dipole (NAO up, EAWR down) reflects its position at a dynamical interface between Atlantic westerlies and Eurasian pressure anomalies. In enclosed and transitional basins, directional adjustments dominate over bulk energy changes (BSC, EMC, WMIC), consistent with fetch limitation and boundary control.

In practice, these teleconnection relationships identify where phase-conditioned metocean statistics should be incorporated into design and operations. We use T_{02} as a proxy for the energy period T_e; where spectra are available, T_e should be used in

$$P \approx 0.49\, H_s^2 T_e. \tag{2.19}$$

During winter NAO phases, the NEC, EAC, and WENS regimes exhibit stronger wind–wave energy and higher load potential; extreme-value estimates and design checks in these regions should therefore be conditioned on NAO state. In the BSC, SCAND primarily affects directionality rather than bulk energy, implying that layout optimization, mooring headings, and port/approach alignment should account for persistent phase-dependent veering or backing. In the southern and western Mediterranean clusters (SMC, WMIC), EA/EAWR exert seasonal control on wave approach, while in WENS they extend to annual energy, producing a dipole response in combination with NAO. Construction windows, access/egress criteria, and routing should thus be evaluated with EA/EAWR phase in mind. More generally, phase-resolved hindcasts-or teleconnection indices used as covariates-can provide conditional design envelopes and operability thresholds for these clusters.

2.3.4.2 Group 2: PNA, WP, POLEUR, AO

Figure 2.11 ($|\rho| \geq 0.48$, $p < 0.05$) shows that AO provides the broadest Group-2 footprint. In NEC and EAC it is strongly positive for energy-bearing metrics (W_s, H_s, T_{02}) and negative for directional variables (wave and wind direction), with signals concentrated in the annual field and the cold season. Additional AO responses appear in NWAC and BSC (positive winter W_s, H_s, T_{02}) and in WMIC (positive winter W_s, H_s only). WENS also registers AO, with negative winter (DJF) signals across W_s, H_s, and T_{02}, alongside directional shifts.

By contrast, PNA, POLEUR, and WP are selective and largely confined to WENS, where they act on wave period (T_{02}): PNA is negative for annual and winter T_{02}, POLEUR is positive for the same seasons, and WP contributes an additional winter (DJF) T_{02} signal. At the cluster-mean threshold used here, EMC and SCES show no Group-2 cells.

The AO pattern is consistent with strengthened zonal westerlies during AO-positive phases: increased surface stress and fetch over the NE Atlantic elevate W_s/H_s and lengthen T_{02}, while the accompanying veer toward W–NW produces negative correlations for wave and wind direction-most clearly in NEC/EAC, and intermittently in NWAC and BSC, with weaker energy-only responses in WMIC.

The WENS sensitivity to PNA/POLEUR/WP is period-centric rather than height-centric, indicating remote modulation of swell input and storm sequencing via jet-stream pathway changes. The opposite-sign T_{02} responses to PNA vs. POLEUR point to competing teleconnection pathways affecting the same transitional shelf. The absence of Group-2 hits in EMC and SCES at $|\rho| \geq 0.48$ suggests that local Mediterranean forcing dominates cluster-mean behavior there, with any remote signals either weaker or spatially heterogeneous enough to average out.

From an engineering standpoint, AO state should be incorporated into winter design checks and operational planning for NEC/EAC, where AO-positive winters are associated with higher loads (greater H_s/W_s) and longer-period seas (larger T_{02}). Secondary AO effects occur in NWAC and BSC, while WMIC shows energy-only responses. In WENS, state-conditioned spectra are advisable: PNA, POLEUR, and WP materially shift T_{02}-especially in DJF-even when H_s changes are modest, with implications for fatigue, mooring tensions, and access windows. Finally, the maps report cluster-mean signals above a strict threshold; finer-scale or weaker teleconnections likely exist but are intentionally suppressed here to emphasize robust, regime-scale responses.

2.4 Summary and Conclusions

We classified multivariate wind–wave regimes across European seas using ERA5 (1979–2014) at 0.5° resolution. Seasonal and annual statistics were computed for significant wave height (H_s), mean wave period (T_{02}), 10-m wind speed (W_{s10}), and wave/wind direction using circular moments. After standardizing features, 30 principal components (≈99% variance) were retained and k-means clustering ($k = 9$) was applied to the spatio–temporal representation. This yielded nine physically interpretable regimes spanning open-ocean, transitional shelf, and enclosed/semi-enclosed basins.

The regimes are spatially coherent, as indicated by compact intra-cluster distances and clear inter-cluster separations, and they are geophysically consistent, with boundaries that correspond to open-ocean, transitional, and enclosed basin settings. Intra-cluster distances reveal clear contrasts in internal cohesion: EAC and SMC are the most compact, NEC and NWAC are intermediate, WMIC and WENS show moderate spread typical of transitional shelves, while EMC, SCES, and BSC exhibit the broadest internal dispersion. Inter-centroid distances emphasize basin contrasts, with the strongest separations between EAC and WMIC/WENS/EMC, and the smallest between WMIC and WENS. Taken together, the patterns indicate a partition that maintains intra-cluster compactness while preserving inter-cluster separation.

Cluster-level correlations ($|\rho| \geq 0.48$, $p < 0.05$) link regime behavior to large-scale circulation. Group 1 indices (NAO, SCAND, EA, EAWR) dominate in the North-East Atlantic and transitional shelves. NAO exerts widespread influence, especially in winter and shoulder seasons, enhancing W_{s10}/H_s, lengthening T_{02}, and rotating approach directions toward zonal sectors. SCAND, EA, and EAWR act more selectively, often in WMIC/WENS and northern basins. Group 2 indices are narrower in scope: AO projects onto W_{s10}, H_s, and T_{02} in NEC/EAC, with secondary signals in NWAC/WMIC/BSC, while PNA, POLEUR, and WP modulate T_{02} in WENS, indicating remote control of swell input and storm sequencing. EMC and SCES show few Group-2 signals, consistent with the dominance of local Mediterranean forcing.

Figure 2.11 Group 2 teleconnections (PNA=P, WP=W, POLEUR=R, AO=A): strongest significant correlations by regime. For each cluster (rows) and variable/season (columns), the cell lists the *largest absolute* Spearman rank correlation(s) between that variable and any of the four indices, provided the correlation is significant (two–tailed $p < 0.05$) and exceeds the threshold $|\rho| \geq 0.48$. Color encodes the signed value of the strongest ρ in the cell (red = positive, blue = negative). If more than one index clears the threshold for a given cell, all are shown on separate lines (e.g., `P:-0.52, R: 0.52`). Directional variables (θ_w, Wd_{10}) use the circular Spearman treatment (sin/cos mapping). ERA5, 1979–2014; $k = 9$ clusters.

Practical implications. (1) *Zoning and siting.* The regimes provide a compact framework for resource assessment and preliminary design: energetic and variable seas in the open Atlantic (NWAC/EAC), intermediate conditions on transitional shelves (WENS/WMIC), and damped, predictable states in enclosed basins (EMC/SCES/BSC). (2) *State-conditioned design and operations.* Where AO/NAO couple to H_s, W_{s10}, and T_{02} (NEC/EAC, intermittently NWAC/WMIC/BSC), winter design seas and maintenance planning should be conditioned on circulation state. In WENS, PNA/POLEUR/WP strongly affect T_{02} even when H_s changes are modest, requiring state-aware spectral definitions in fatigue and access planning. In BSC, SCAND-linked directional persistence supports stable alignment assumptions. (3) *Monitoring.* The maps indicate where seasonal circulation diagnostics are linked to variability in wind–wave conditions. Monitoring indices such as NAO and AO in NEC and EAC, or PNA, POLEUR, and WP for T_{02} in WENS, can therefore provide context for interpreting observed conditions and anticipating short-term fluctuations at the regional scale.

Beyond annual means, the seasonal cycle provides additional structure. Open-Atlantic regimes peak in winter and relax in summer, with broader year-to-year variability than in enclosed basins, which remain compact and predictable across seasons. Transitional shelves combine both influences: winter exposure to Atlantic storms and seasonal rotation of prevailing sectors. Directional contrasts are equally important: broad, variable sectors in NWAC/EAC pose design challenges, narrow envelopes in EMC/BSC/SCES support stable assumptions, and WMIC/WENS highlight the role of seasonal reversals. Together, these results extend the classification from annual averages to dynamic seasonal regimes, directly relevant for design spectra, coastal planning, and long-term monitoring.

Scope and next steps. The reported correlations are statistical and based on cluster means with strict thresholds, which may smooth smaller-scale signals. While k-means assumes spherical geometry, the PCA space and validation metrics support a stable, interpretable solution. Future work should (i) extend to sub-cluster scales, (ii) couple with hindcast/altimetry extremes and spectral partitions, (iii) test nonlinear embeddings and alternative clustering to resolve fine structure, and (iv) propagate regime maps into climate projections to evaluate circulation-dependent shifts in H_s, T_{02}, W_{s10}, and approach direction.

In summary, a compact, data-driven set of regimes captures the dominant multi-decadal wind–wave structure of European seas and identifies where large-scale circulation most strongly conditions marine variability. These results provide both a physical framework and an applied tool for forecasting, offshore design, and climate adaptation.

Acknowledgments

Special thanks are extended to the European Centre for Medium-Range Weather Forecasts (ECMWF) for making the ERA5 reanalysis dataset available, which was instrumental in our analysis. The indices were sourced from the National Centers for Environmental Prediction (NCEP), and their integration significantly enhanced the analysis of climate oscillations. We also appreciate the constructive feedback from our colleagues in the Offshore Engineering and Coastal Engineering groups, whose insights have significantly enhanced the quality of this work.

3

Benchmarking Wind–Wave Resource Variability Across EC-Earth3 Scenario and High-Res Experiments Using ERA5-Derived Climate Clusters

"All models are wrong, but some are useful."

- George E. P. Box (1976)

"The true logic of this world is the calculus of probabilities, which takes account of the magnitude of the probability."

- James Clerk Maxwell, (1845)

Understanding joint wind–wave magnitude and variability is central to both assessing offshore renewable energy potential and evaluating the performance of climate simulations. This chapter applies the ERA5-based nine-regime wind–wave clustering framework of Maya and Antolínez [2025] to EC-Earth3 climate simulations under CMIP6 ScenarioMIP and HighResMIP experiments (1979–2014). The ERA5 principal-component space provides a fixed multivariate reference for projecting EC-Earth3 outputs, enabling consistent regime-scale comparison across model configurations. Softmax probabilities are used to quantify cluster membership confidence and to evaluate spatial consistency between reanalysis and model simulations.Results show that EC-Earth3 reproduces the

large-scale organisation of the ERA5 regimes, with 36.4% of grid points showing full three-model (ScenarioMIP, HighResMIP, ERA5) agreement and nearly 95% exhibiting at least partial consistency across datasets. The mean cluster confidence exceeds 0.9, confirming that the ERA5-derived regime framework is spatially robust across independent simulations. While the coarser ScenarioMIP (∼1°) smooths gradients and broadens regime boundaries, the finer HighResMIP (∼50 km) captures sharper coastal transitions and better resolves mesoscale wind–wave features, yielding closer alignment with ERA5.Seasonal and spatial patterns of wind energy density and wave power are consistent with ERA5, with maxima in the North Atlantic and minima in enclosed basins. Here, the classification framework of Maya and Antolínez [2025] is extended to assess wind and wave energy by incorporating mean energy and temporal stability conditioned on shelf depth. This depth-resolved analysis identifies Primary (high-energy–high-stability) zones in deep-water Atlantic regimes, Secondary classes over transitional shelves, and Hybrid Hotspot zones where wind and wave resources co-occur with higher variability. Integration with ecological (MEOW) and jurisdictional (EEZ) layers highlights the Celtic Seas, North Sea, and Faroe Plateau as stable hybrid resource regions. Overall, the framework provides a transferable basis for evaluating model resolution effects and guiding offshore renewable-energy planning under changing climate conditions.

This chapter is based on:

Maya, P., Parker, K., Cagigal, L., Metrikine, A. V., & Antolínez, J. A. A.
Benchmarking wind–wave resource variability across EC-Earth3 ScenarioMIP and HighResMIP experiments using ERA5-derived climate clusters.
Renewable Energy, under review.

3.1 Introduction

Offshore wind and wave energy are increasingly seen as critical components in meeting Europe's renewable energy targets, particularly in regions with strong and persistent wind–wave conditions and well-established infrastructure Hemer et al. [2010], Reguero et al. [2015], Bonaduce et al. [2019]. Together, these marine sources have the potential to supply over 10% of global electricity demand WindEurope [2022], offering higher capacity than many land-based systems with fewer spatial constraints Olauson [2018]. Their complementary nature also supports hybrid energy strategies, such as the North Sea Wind Power Hub Varlas et al. [2020], Sardana et al. [2024], which aims to improve stability and grid integration. While the potential is evident, realizing this growth requires information on resource variability across both space and time, especially under a changing climate.

Wind and wave climate varies both seasonally and at yearly to decadal timescales due to large-scale weather patterns and cycles. In the Northeast Atlantic, for example, winter wave heights can exceed 6 meters, while summer values often fall below 2 meters Casas-Prat and Sierra [2013], Morim et al. [2019], Shi et al. [2024]. In terms of longer scale variability, a major driver in the Atlantic is the North Atlantic Oscillation (NAO), which changes near-surface wind speed magnitude by up to ±20% across Europe *[Hurrell, 1995, Hurrell and Deser, 2010]*. Apart from natural variability, changes to climate may amplify these patterns, with projected increases in wave height of up to 15% in the North Atlantic and Southern Ocean by the end of the century for high-emission scenarios like RCP8.5 or SSP5–8.5 Reguero et al. [2015], Casas-Prat and Sierra [2013]. To complicate renewable energy development, projected changes are not evenly distributed. For example, the North Sea may see stronger winter winds, while the Mediterranean may experience more persistent shifts in wave direction Casas-Prat and Sierra [2013], Morim et al. [2019].

Wind and wave models serve a key role in understanding renewable energy availability, providing spatially and temporally complete information on current climate, as well as how they may change into the future. Understanding how well models capture historical natural variability is key to improving confidence in future projections and supporting offshore energy planning and engineering design. In this context, and given our reliance on model data, it is essential to assess model performance, biases, and the influence of spatial resolution on wind and wave simulations. A widely used dataset for assessing offshore wind speeds and ocean wave characteristics in Europe is the ERA5 reanalysis, developed by ECMWF Hersbach et al. [2020]. Several studies have used ERA5 to examine either wind or wave parameters separately. For instance, Barbariol et al. [2021] studied seasonal and long-term variability in the Mediterranean using an ERA5-forced wave model. Meucci et al. Meucci et al. [2024] assessed CMIP6 wave simulations against ERA5-based hindcasts. These studies support the use of ERA5 as a consistent reference for wind and wave climatologies. However, only a few studies have jointly analyzed wind and waves, and most classification methods still focus on wave characteristics alone. Fairley et al. Fairley et al. [2020], for example, applied multivariate clustering to ERA5 wave data, without including wind. Some recent work combines climate

model projections of wind and wave to estimate energy potential Meucci et al. [2024], but these typically lack spatial classification and historical validation. There remains a gap in for a consistent framework that jointly analyzes wind–wave behavior over broader spatial domains.

While ERA5 is well-suited for evaluating historical conditions, climate models provide independent, non-assimilated wind and wave fields that are essential for predicting future climate and assessing stochasticity in the climate . The Coupled Model Intercomparison Project (CMIP) provides a standardized framework to evaluate model performance and climate change signals under historical and projected forcing. CMIP5 supported RCP-based future scenarios, and CMIP6 extends this with updated physics, finer resolution in some models, and a wider range of experiments. Two examples of CMIP6 experiments utilized here include ScenarioMIP, which explores different socio-economic pathways, and HighResMIP, which isolates the effect of spatial resolution Haarsma et al. [2016]. Because physical parameterizations are held constant across resolutions, HighResMIP allows resolution effects to be examined directly. HighResMIP historical simulations are often forced with sea surface temperature and sea ice fields from the Climate Forecast System Reanalysis (CFSR) Saha et al. [2010]. This is particularly relevant for wind and wave processes, where spatial resolution influences storm representation and nearshore dynamics *[Stopa and Cheung, 2014, Ardhuin et al., 2010]*. Although CMIP6 shows improvements over CMIP5 in simulating wave conditions Meucci et al. [2024], few studies have compared ScenarioMIP and HighResMIP in a joint wind–wave context. A recent hindcast using MIROC6 for the Northeast Atlantic differed from ERA5 Maya et al. [2023], but no spatial classification was applied. Although CMIP models are often used for future projections, this study focuses exclusively on their historical simulations and benchmarking regime representation. With CMIP6 models forming the foundation of our understanding of how climate may change into the future, validating their ability to reproduce historic spatial patterns is critical for having confidence in their ability to predict future changes.

Conventional spatial analyses often rely on gridded fields to evaluate wind and wave variability. However, such cell-by-cell comparisons can obscure large-scale co-variability and introduce noise due to model-specific biases. To address this, we adopt a fixed clustering framework based on joint wind–wave behavior observed in ERA5. These climate regions capture consistent dynamical regimes and provide a robust spatial reference for evaluating model performance. This approach enables clearer identification of resolution and forcing effects across physically meaningful regions, rather than dispersing them across grids. Building on the framework of Maya and Antolínez [2025], this study applies ERA5-derived clusters as a fixed spatial reference to evaluate the performance of climate model simulations. We project EC-Earth3 outputs, including both climate simulations from CMIP6 ScenarioMIP and HighResMIP, onto nine clusters to compare wind and wave dynamics across models in a consistent spatial context. Within each cluster, we assess seasonal and interannual variability in wind and wave energy, focusing on how model resolution influences representation. By holding spatial clusters fixed, we isolate the effect of model resolution on wind–wave resource variability, rather than confounding it with changing spatial modes. In addition, we introduce a classification scheme that groups regions into Primary, Secondary, and Hybrid Hotspot zones based on energy characteristics. This approach supports regional-scale assessments of renewable energy potential and lays the groundwork for integrating model evaluation into offshore energy planning. Furthermore, as mentioned above, this study attempts to improve our confidence in CMIP6 models by validating their ability to reproduce spatial coherence in joint wind–wave characteristics.

This paper is structured as follows. Section 4.2 outlines the datasets, preprocessing steps, and clustering framework Section 6.5 presents the main findings, including the cross-dataset regime comparison, cluster confidence evaluation, and depth-resolved analysis of wind, wave, and hybrid energy potential. Section 3.3.3 details the spatial energy–stability classification

and its ecological and jurisdictional context. Finally, Section 6.6 summarizes the key outcomes and discusses their relevance for future offshore renewable-energy assessments.

3.2 Data and methods

This section describes the datasets, preprocessing steps, and analytical workflow employed in this study. The analysis integrates all three of the ERA5 reanalysis and EC-Earth3 climate model outputs from CMIP6 ScenarioMIP and HighResMIP experiments to examine multidecadal wind–wave conditions across the Northeast Atlantic and European regional seas (1979–2014). Five core variables were processed at annual and seasonal scales: 10-m wind speed, significant wave height (H_s), mean wave period (T_p), and wind and wave directions. All datasets were standardized and decomposed using Principal Component Analysis (PCA), after which clustering was applied to the ERA5 feature space to identify dominant wind–wave regimes. The resulting ERA5-derived clusters served as the fixed spatial reference for projecting EC-Earth3 simulations, ensuring consistent regime comparison across datasets. Wind and wave energy metrics were subsequently estimated at both grid and cluster levels, and the resulting spatial patterns were evaluated in relation to ecological regions, jurisdictional boundaries, and bathymetry to identify zones suitable for offshore renewable-energy development.

An overview of the workflow is shown in Figure 4.1.

3.2.1 Data Sources

Five datasets were used to characterize joint wind–wave conditions across the Northeast Atlantic and European seas during 1979–2014: ERA5 reanalysis, EC-Earth3 ScenarioMIP and HighResMIP climate simulations, and two WW3 hindcasts forced by the respective EC-Earth3 winds and sea-ice fields. All datasets were limited to 30°W–45°E and 30°N–75°N and interpolated to the ERA5 grid for consistency Maya and Antolínez [2025].

ERA5, produced by the European Centre for Medium-Range Weather Forecasts (ECMWF), is a global atmospheric reanalysis with a horizontal resolution of 0.25° × 0.25° (approximately 31 km) Hersbach et al. [2020]. It assimilates a diverse range of observations, including satellite radiances, scatterometer winds, and in-situ measurements from surface stations, ships, radiosondes, and aircraft. Buoy and altimeter data are also used, particularly for wave height. For this study, ERA5 serves as the reference dataset for model evaluation and historical climate characterization.

EC-Earth3 is a global coupled climate model developed by the EC-Earth Consortium. It combines ECMWF's Integrated Forecasting System (IFS) for the atmosphere with the NEMO ocean model. In this study, two configurations of EC-Earth3 are used: ScenarioMIP and HighResMIP, both following CMIP6 protocols. The ScenarioMIP version uses a T255 atmospheric resolution (1.0°) with a 1° ORCA1 ocean grid and provides 3-hourly outputs of near-surface wind components ('uas', 'vas') and wind direction. The HighResMIP configuration (EC-Earth3P-HR) increases spatial detail with a T511 (50 km) atmospheric grid and a 0.25° ocean grid, also providing 3-hourly wind fields. Neither configuration includes a coupled wave model. Instead, wave parameters are sourced from external WW3 simulations. One WW3 hindcast is forced by ScenarioMIP winds, providing 3-hourly outputs of significant wave height ('H_s'), mean wave period ('T_p'), and wave direction on a 0.5° grid. A second hindcast uses HighResMIP winds to drive WW3 at higher resolution, yielding hourly outputs of 'H_s', mean wave period ('T_p'), and wave direction on a 0.5° (30 arcmin) grid.

The selected wind and wave variables, covering both magnitude and directional components, were bilinearly interpolated to the ERA5 grid to ensure spatial consistency across datasets.

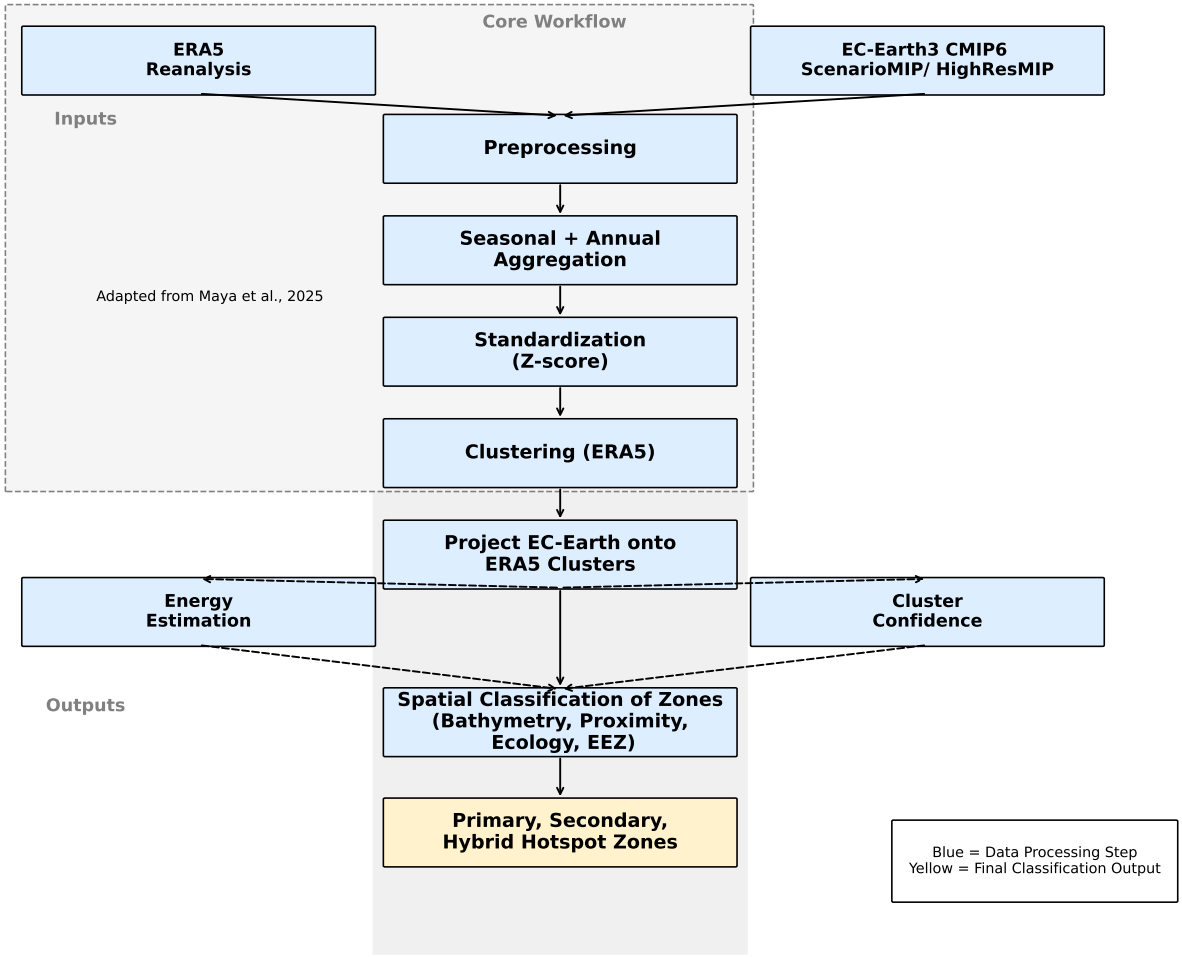

Figure 3.1 Overview of the data and methods workflow. Core steps begin with preprocessing, followed by clustering, projection of EC-Earth3, energy estimation, and classification.

Dataset	Variables Used	Spatial Resolution	Temporal Resolution
ERA5	u10, v10, hs, tp, wind dir, wave dir	0.25° × 0.25°	Hourly
EC-Earth3 (ScenarioMIP)	uas, vas, wind dir	~1.0° (T255)	3-hourly
EC-Earth3P-HR (HighResMIP)	uas, vas, wind dir	~50 km (TL511)	3-hourly
WW3 (Scenario-forced)	hs, tp, wave dir	0.5°	3-hourly
WW3 (HighRes-forced)	hs, tp, wave dir	0.5° (30 arcmin)	Hourly

Note: hs = significant wave height, tp = peak period, uas/vas = near-surface wind components, dir = direction

Figure 3.2 Overview of datasets used in this study, including variables, spatial resolution, and temporal resolution.

These processed variables form the input for variability analysis, energy estimation, and clustering tasks described in later sections.

3.2.2 Temporal Aggregation and Variable Processing

The wind and wave data were aggregated to annual and seasonal scales, with seasons defined as DJF (December–February), MAM (March–May), JJA (June–August), and SON (September–November). At each grid point and temporal aggregation level, the mean and standard deviation were computed for significant wave height (H_s), mean wave period (T_p), 10-m wind speed, wind direction, and wave direction. This step captures both interannual and intra-annual variability.

To account for the circular nature of wave and wind directions, both directional means and directional variability were calculated using circular statistics. The mean direction was obtained using trigonometric averaging:

$$\bar{\theta} = \arctan 2\left(\frac{1}{n}\sum_{i=1}^{n}\sin\theta_i, \frac{1}{n}\sum_{i=1}^{n}\cos\theta_i\right) \tag{3.1}$$

Directional standard deviation was also computed using circular statistics, ensuring consistent treatment of angular variables.

Wind speed was recomputed when needed using the vector magnitude of the u and v components:

$$W_s = \sqrt{u^2 + v^2} \tag{3.2}$$

After aggregation, all variables were interpolated to the ERA5 spatial grid for uniform coverage. Each time series was reshaped such that one feature vector per season or year was available per grid cell, covering all derived variables.

Before dimensionality reduction, all features were standardized using z-score normalization:

$$z_i = \frac{x_i - \mu}{\sigma} \tag{3.3}$$

Principal Component Analysis (PCA) was applied to the standardized ERA5 dataset, retaining components that together explain 99% of the total variance. The same transformation

was then applied to the standardized EC-Earth3 data, allowing all datasets to be represented in a common reduced feature space Maya and Antolínez [2025].

The PCA-transformed data were then reshaped so that each row corresponds to a spatial grid point, and each column to a principal component for a given year. This format was used as input to the clustering framework described in Section 3.2.3.

3.2.3 Projection-Based Clustering in a PCA-Derived Feature Space

To identify spatial regions with distinct wind–wave behavior (referred to here as wind–wave regimes), we applied a clustering framework based on Principal Component Analysis (PCA) followed by unsupervised learning, as described in Maya et al. Maya and Antolínez [2025]. Clustering was applied to PCA-transformed features from ERA5, based on 14 standardized wind and wave variables that capture both annual and seasonal statistics.Before applying the final clustering step, DBSCAN (Density-Based Spatial Clustering of Applications with Noise) was used only as a spatial filter to remove small fragmented cells and narrow land-bridging artefacts that appear near complex coastlines. K-means clustering was then applied with $k = 9$, based on the elbow method and the interpretability of the resulting spatial patterns. The PCA transformation and the K-means cluster centroids derived from ERA5 were then applied to the EC-Earth3 ScenarioMIP and HighResMIP datasets to assign each grid point to the corresponding ERA5-defined regime in the same reduced feature space. Cluster labels were assigned using the ERA5-derived model, allowing consistent spatial comparisons across datasets. To visualize the spatial extent of each regime, alpha-shapes were computed from the clustered grid points. This approach produced flexible boundaries that followed coastal geometry while avoiding connections across land.

This clustering framework provides a consistent regime classification across models and forms the spatial foundation for energy potential, stability, and ecological overlay assessments in later sections.

3.2.4 Cluster Confidence Estimation using Softmax Probabilities

To evaluate the confidence of cluster assignments and assess the robustness of the ERA-based regime framework, we computed softmax-based probability scores Bishop [2006] derived from the Euclidean distances between each grid point and all cluster centroids. This probabilistic measure provides an interpretable indication of how strongly each point belongs to its assigned regime within the PCA-transformed feature space. For each point in the ERA5, EC-Earth3 ScenarioMIP, and EC-Earth3 HighResMIP datasets, the trained K-means model was used to calculate distances to all nine cluster centroids. The softmax transformation was then applied to the negative distances to obtain a normalized probability distribution across clusters. The softmax probability corresponding to the assigned cluster was retained as the membership probability:

$$P_{i,k} = \frac{e^{-d_{i,k}}}{\sum_{j=1}^{K} e^{-d_{i,j}}} \tag{3.4}$$

where $d_{i,k}$ denotes the Euclidean distance between point i and centroid k, and K is the total number of clusters. Higher $P_{i,k}$ values indicate stronger cluster membership and lower classification ambiguity.

3.2.5 Wind and Wave Energy Estimation

Although this thesis does not aim to perform site-specific renewable-energy assessment or infrastructure design, wind and wave conditions are naturally interpreted through energy-related metrics in many offshore applications. To provide a physically intuitive characterisation of the identified regimes, standard bulk wind and wave energy metrics were therefore computed using ERA5 and EC-Earth3 data. These metrics are used here as climate diagnostics that summarise the intensity and variability of wind–wave conditions, rather than as estimates of extractable or deployable energy.

In this study, the terms wave power and wind energy density follow the conventional terminology commonly used in wave-climate and wind-resource literature, respectively. They are used here as bulk indicators of offshore resource intensity rather than estimates of extractable energy.

Wave power (P_{wave}, in kW/m) was computed using the deep-water approximation:

$$P_{\text{wave}} = \frac{\rho g^2}{64\pi} H_s^2 T_p \tag{3.5}$$

where H_s is the significant wave height (m), T_p is the mean wave period (s), $\rho = 1025$ kg/m^3 is seawater density, and $g = 9.81$ m/s^2 is gravitational acceleration. The calculation was based on annual and seasonal mean values.

Wind energy density (P_{wind}, in kW/m^2) was estimated by extrapolating the 10-m wind speed to a hub height of 100 m using the power law:

$$U(z) = U_{10} \left(\frac{z}{10} \right)^{\alpha} \tag{3.6}$$

where $\alpha = 0.11$ for offshore conditions. The extrapolated speed was used to compute energy density as:

$$P_{\text{wind}} = \frac{1}{2} \rho_{\text{air}} U^3 \tag{3.7}$$

with $\rho_{\text{air}} = 1.225$ kg/m^3 representing air density. These computations were repeated for both annual and seasonal timescales.

The resulting outputs were used to examine energy characteristics at two levels. At the grid scale, values were linked to geographic coordinates and cluster identifiers. At the regime level, seasonal mean wind and wave energy were aggregated for each cluster to support comparison across regions and datasets, and to inform the classification of potential energy zones.

3.2.6 Ecological, Economic, and Jurisdictional Data Integration

To support spatial context assessment for offshore renewable energy, the wind–wave cluster datasets were integrated with geospatial layers representing ecological, protected, and jurisdictional boundaries. The following datasets were used: Marine Ecoregions of the World (MEOW) Spalding et al. [2007], the MPAtlas database for marine protected areas (MPAs) Pike et al. [2024], the World Database on Protected Areas (WDPA) Bingham et al. [2019], and Exclusive Economic Zones (EEZs) Shin and Song [2025].

3.2.7 Bathymetry and Coastal Proximity Criteria

To evaluate the spatial suitability of offshore sites for marine renewable energy, we integrated bathymetric depth, coastal proximity, and energy resource characteristics into a structured

classification framework. Bathymetric data were sourced from the GEBCO 2021 global product. Locations with depths less than 200 m were labeled as *Shallow*, while those deeper than 200 m were classified as *Deep*, following EMODnet and IEA-OES offshore classification standards.

Coastal distance was calculated using the Global Self-consistent, Hierarchical, High-resolution Shoreline (GSHHS) full-resolution dataset (GSHHS_f_L1.shp), which was projected to EPSG:3857 for accurate distance estimation. Based on proximity to the shoreline, sites were classified as *Nearshore* (<10 km), *Optimal* (10–50 km), or *Far Offshore* (>50 km).

For each model, annual mean values of wave power (kW/m) and wind energy density (kW/m^2) were used to classify the energy potential at each grid point. Thresholds were informed by the statistical distribution of each dataset and aligned with international guidelines.

$$\mathrm{CoV} = \frac{\sigma}{\mu} \times 100 \tag{3.8}$$

Here, μ represents the mean of the four seasonal mean energy values (DJF, MAM, JJA, SON) at each grid point, and σ represents the corresponding standard deviation. The CoV therefore quantifies the degree of seasonal variability in wave power and wind energy density relative to the mean seasonal state.

To assess seasonal consistency, the Coefficient of Variation (CoV) was computed from seasonal mean wave power and wind energy density time series. Stability was categorized as *Stable* (CoV < 30%), *Moderate* (30–60%), or *Unstable* (>60%).

The CoV metric introduced here is intended as a univariate indicator of seasonal variability in aggregated wind and wave energy characteristics, whereas the Seasonal Regime Stability Index (SRSI) introduced later in Chapter 4 evaluates the persistence and consistency of multivariate wind–wave climate regimes in clustered feature space. The two metrics therefore describe different aspects of variability and stability.

This classification scheme provides a geospatially explicit and interpretable framework for identifying priority zones for offshore renewable energy deployment, accounting for energy magnitude, spatial feasibility, and seasonal reliability.

3.3 Results and Discussion

The ERA5-based nine-regime wind–wave classification established in *[Maya and Antolínez, 2025]* was extended to EC-Earth3 simulations (ScenarioMIP and HighResMIP) to evaluate the spatial consistency of regime representation and the effects of model resolution on cluster geometry. The ERA5 regime structure served as the fixed reference, and EC-Earth3 outputs were projected onto the same principal-component (PC) space to ensure consistent classification across datasets. Figure 3.3 shows the spatial distribution of the nine wind–wave regimes for ERA5, EC-Earth3 ScenarioMIP, and EC-Earth3 HighResMIP for 1979–2014, and Table 3.1 lists their geographic categories. The regime names are used as descriptive identifiers based on the dominant geographical characteristics of the ERA5-derived historical clusters. They do not represent fixed geographical boundaries and may exhibit spatial shifts or changes in extent across different datasets and future climate simulations.

The comparison confirms that the ERA5-based clustering framework *[Maya and Antolínez, 2025]* can be consistently applied to EC-Earth3 outputs for regime-scale evaluation. The nine wind–wave regimes-NWAC, EAC, WENS, WMIC, NEC, SMC, SCES, BSC, and EMC-are reproduced in both ScenarioMIP and HighResMIP (Table 3.1), with spatial differences mainly controlled by horizontal resolution. In ScenarioMIP (T255; 1° grid spacing), reduced horizontal detail smooths coastal gradients and broadens regime boundaries, leading to a northward extension of the EAC region across the open Atlantic and a partial merging of WENS with EAC in the northern sector. The WMIC zone along the Iberian margin and

western Mediterranean becomes narrower, while SCES and BSC are less distinctly represented. The finer TL511 grid (50 km) in HighResMIP resolves mesoscale wind gradients and fetch-limited features more effectively, restoring the narrow NEC and SCES zones and improving the separation between the North Sea (WENS) and Baltic (BSC) regimes. These deviations primarily reflect resolution-dependent representation of near-surface wind gradients and coastal wave growth rather than differences in model formulation. The improved regime delineation in HighResMIP establishes a clearer foundation for analysing regime-membership confidence and resolution sensitivity in the following section.

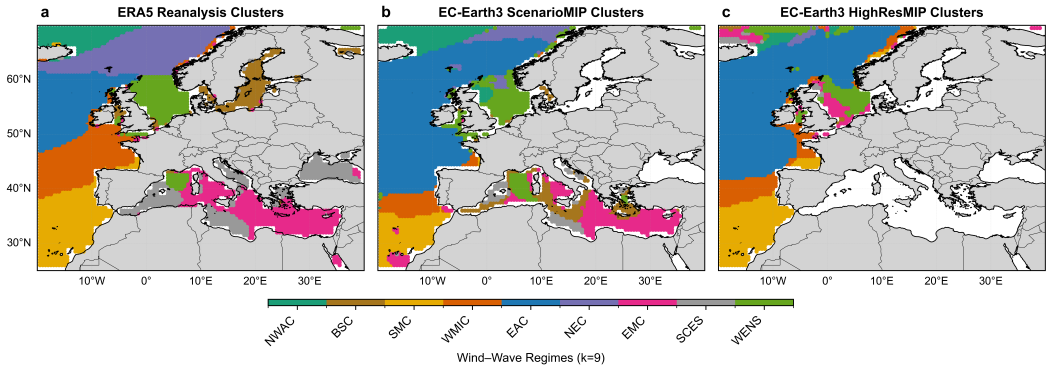

Figure 3.3 Spatial distribution of wind–wave climate clusters across the Northeast Atlantic and European seas (1979–2014). Panel (a) shows ERA5 reanalysis clusters, Panel (b) EC-Earth3 ScenarioMIP clusters, and Panel (c) EC-Earth3 HighResMIP clusters. Clusters were derived by applying K-means clustering ($k = 9$) to PCA-transformed wind and wave parameters, with ERA5 providing the reference cluster structure. Colors denote distinct wind–wave regimes, with abbreviations corresponding to cluster names shown in the legend.

Table 3.1 Regional wind–wave regimes ($k = 9$) and their qualitative geographic classification, adapted from *[Maya and Antolínez, 2025]*.

Cluster Name (Abbreviation)	Geographic Classification
Northern European Continental Cluster (NEC)	Open Ocean
Eastern Mediterranean Cluster (EMC)	Enclosed/Semi-Enclosed
Southern Mediterranean Cluster (SMC)	Transitional
Southern and Coastal European Seas Cluster (SCES)	Enclosed/Semi-Enclosed
Eastern Atlantic Cluster (EAC)	Open Ocean
Northwestern Atlantic Cluster (NWAC)	Open Ocean
Western European and Northern Sea Cluster (WENS)	Transitional
Western Mediterranean and Iberian Cluster (WMIC)	Transitional
Baltic Sea Cluster (BSC)	Enclosed/Semi-Enclosed

3.3.1 Cluster Membership Confidence and Resolution Dependence

The softmax-based confidence analysis quantifies the robustness of the regime classification by evaluating the relative membership probability of each grid point within the ERA5-derived PC space. This provides a measure of how strongly each location is associated with its assigned regime. ERA5 exhibits strong membership strength, with a mean softmax probability of

0.98 and almost all grid points above 0.8, reflecting a persistent and well-defined regime structure over the 1979–2014 period. Regimes such as EAC, NWAC, and SMC exhibit high membership strength, indicating that their wind–wave characteristics form well-defined and internally consistent patterns. In contrast, lower membership values in restricted basins such as the Baltic (BSC) and eastern Mediterranean (EMC) reflect greater variability in local wind forcing and more heterogeneous wave conditions.

For the EC-Earth3 ScenarioMIP experiment, the spatial organization of the ERA5-derived regimes is broadly retained, although the mean confidence decreases to 0.90. Weaker probabilities occur mainly over shallow continental shelves, where the coarse horizontal resolution under-represents wind-stress gradients and coastal variability. In contrast, regimes such as EAC and SMC maintain confidence above 0.9, indicating that synoptic-scale wind–wave dynamics are reasonably reproduced even at standard resolution.

HighResMIP shows higher membership strength overall, with a mean softmax probability of 0.93 and fewer grid points below 0.8. The largest increases occur in open and transitional regions, where finer horizontal resolution produces more internally consistent wind–wave statistics and clearer separation between neighbouring regimes. In contrast, membership values remain comparatively low in semi-enclosed basins such as the Baltic (BSC), NEC, and SCES, reflecting the greater variability and localized forcing typical of these regions rather than model resolution alone.

The comparison between the EC-Earth3 configurations demonstrates the resolution dependence of their ability to reproduce wind–wave spatial coherence within a consistent regime framework.. HighResMIP captures sharper gradients and better-defines open-ocean clusters, aligning more closely with ERA5-derived regimes. The persistence of uncertainty along coasts emphasizes the need for improved air–sea coupling and process-level parameterisations beyond grid refinement. Increased resolution enhances the dynamical fidelity of large-scale wind–wave regimes, while coastal predictability remains limited by unresolved physical processes.

An inter-model agreement analysis was performed to assess spatial consistency of the ERA5-derived regimes across EC-Earth3 ScenarioMIP and HighResMIP simulations. Among 2,899 collocated grid points, 1 054 (36.4%) exhibited full three-model agreement, 1,696 (58.5%) showed consistency between two models, and 149 (5.1%) differed across all three. Discrepancies were concentrated along regime transition zones and coastal boundaries, where unresolved cells in ScenarioMIP and HighResMIP lead to spatial gaps. The high cross-model agreement ($\approx 95\%$ showing at least partial consistency) confirms that the ERA5-based regime framework is spatially robust and transferable across independent climate simulations.

3.3.2 Cluster-Based Characterisation of Wind–Wave Energy Signatures

Figure 3.5 shows the climatological mean wave power flux (kW m^{-1}) from ERA5 and EC-Earth3 simulations (ScenarioMIP and HighResMIP) for 1979–2014. The spatial distribution follows the ERA5-derived wind–wave regimes. In ERA5, the highest wave power fluxes (> 55 kW m^{-1}) occur along the North Atlantic storm-track extending from the subtropical Atlantic to the Norwegian Basin, where persistent westerly winds generate high wind-sea coupling. Minimum values (< 10 kW m^{-1}) occur in fetch-limited and semi-enclosed basins such as the Baltic (BSC) and eastern Mediterranean (EMC), where wave development is constrained by limited fetch and shallow bathymetry. A seasonal cycle is evident, with DJF and SON showing maximum energy flux and JJA showing minimum values, corresponding to variations in atmospheric baroclinicity and storm-track intensity. The EC-Earth3 ScenarioMIP simulation reproduces this large-scale structure but shows a broader and more energetic open-ocean core exceeding 60 kW m^{-1}, consistent with stronger modeled wind forcing. The HighResMIP configuration produces similar magnitudes but with sharper horizontal gradients

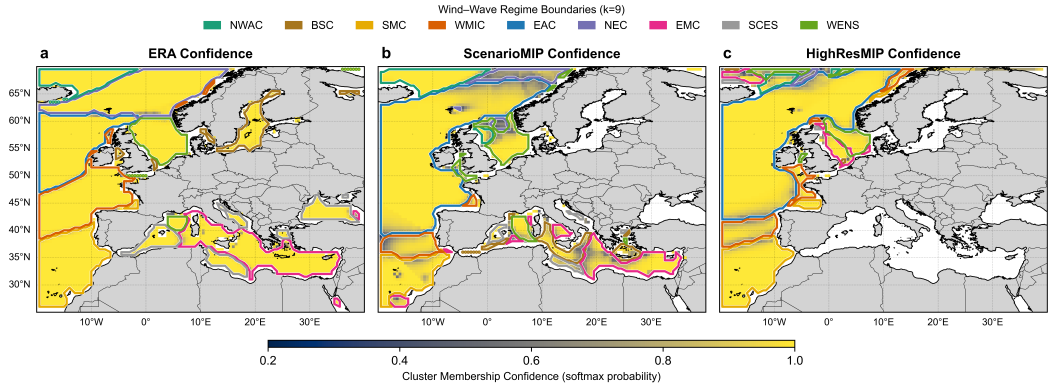

Figure 3.4 Spatial distribution of softmax-based cluster membership confidence for (a) ERA5 reanalysis, (b) EC-Earth3 ScenarioMIP, and (c) EC-Earth3 HighResMIP simulations. The color scale indicates the posterior probability of regime membership, computed from distances to ERA5-trained cluster centroids in the PCA-transformed wind–wave feature space. Bold contours delineate the fixed ERA-defined wind–wave regime boundaries, derived using alpha-shaped polygons to enclose grid points belonging to each of the nine clusters. Panel arrangement and color normalization are identical across all cases to ensure consistent visual comparison of spatial confidence patterns.

and more distinct coastal transitions, particularly along the North Sea and western Iberian shelves, due to its finer horizontal resolution (∼50 km).

The climatological distribution of wave power flux in EC-Earth3 corresponds well with ERA5, indicating consistent representation of the dominant energy pathways associated with extratropical cyclones. ScenarioMIP shows higher mean wave energy in parts of the Northeast Atlantic (> 60 kW m^{-1}), which is consistent with the tendency of coarser-resolution wind fields to produce smoother and more persistent forcing, leading to elevated mean wave energy *[Stopa and Cheung, 2014, Stopa et al., 2016]*. This behaviour reflects the reduced representation of mesoscale variability in T255 winds rather than a systematic strengthening of westerlies. The finer TL511 grid in HighResMIP (∼50 km) captures mesoscale wind gradients and coastal orographic effects more accurately, producing spatial patterns and near-coastal gradients that more closely resemble ERA5. The low wave-energy levels in semi-enclosed basins (BSC, SCES, EMC) across all datasets reflect the dominant influence of limited fetch, shallow bathymetry, and locally driven wind fields in these regions. The differences between the two EC-Earth3 configurations primarily arise from horizontal resolution and the associated representation of near-surface wind variability; the underlying model physics are identical. Increased spatial resolution reduces coastal smoothing and improves the spatial detail of the modeled wave-power field.

Figure 3.6 shows the climatological mean wind energy density (kW m^{-2}) across the Northeast Atlantic and European seas from ERA5 and EC-Earth3 (ScenarioMIP and HighResMIP) simulations for 1979-2014. In ERA5, maximum values (> 1.8 kW m^{-2}) occur in the open-ocean regimes NWAC and EAC, aligned with the North Atlantic storm track, while transitional regimes such as WENS exhibit moderate values between 1.0 and 1.5 kW m^{-2}. Semi-enclosed basins including BSC, SCES, and EMC maintain low energy densities (< 0.5 kW m^{-2}) due to weaker near-surface winds, enhanced surface roughness, and constrained synoptic-scale flow. All datasets show a distinct seasonal cycle, with DJF and SON yielding the highest wind energy densities and JJA the lowest, reflecting the seasonal modulation of mid-latitude storm activity. The ScenarioMIP configuration reproduces the large-scale spatial structure but indicates slightly elevated energy levels (> 2.0 kW m^{-2}) in the open Atlantic and broader high-energy zones, consistent with coarser horizontal resolution (∼1°) and smoother coastal gradients. The HighResMIP simulation produces similar overall magnitudes but displays sharper horizontal gradients and improved representation of nearshore wind intensities along

Figure 3.5 Mean wave power distribution across European seas for the period 1979–2014, based on ERA5 reanalysis and EC-Earth3 climate simulations. The panels represent seasonal averages of wave power (kW/m), including the annual mean, winter (DJF), spring (MAM), summer (JJA), and autumn (SON). The rows correspond to data from ERA5 (top), EC-Earth3 ScenarioMIP, and EC-Earth3 HighResMIP. Colour shading indicates the spatial variation in wave power intensity. Coloured contour lines delineate wave–wind clusters, representing regions with similar regime characteristics. Land is shown in light grey, and areas with no available wave data (typically ocean regions beyond model coverage) are displayed in white. The layout enables a comparative view of wave power patterns across datasets, model resolutions, and seasons.

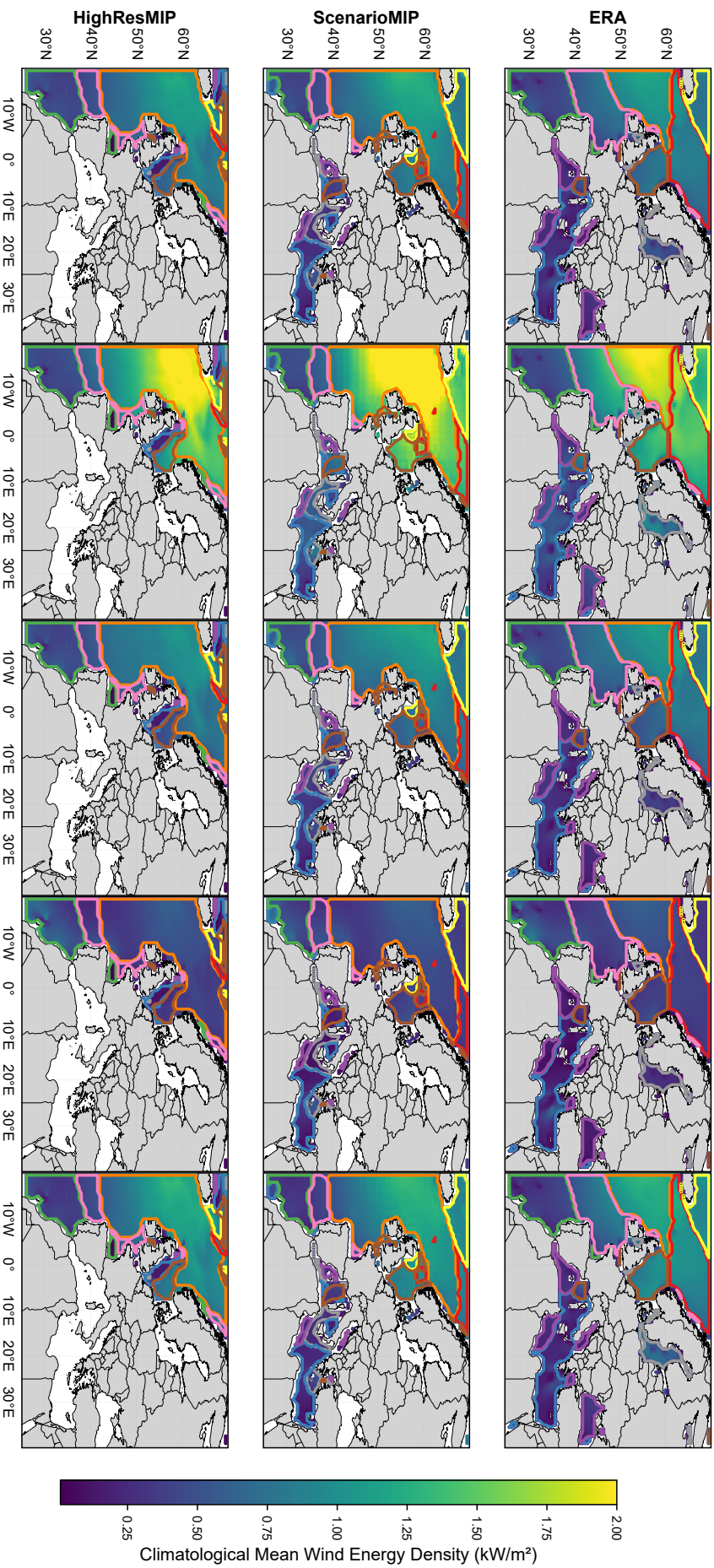

Figure 3.6 Climatological mean wind energy density (kW m^{-2}) across European seas for the period 1979–2014, based on ERA5 reanalysis and EC-Earth3 simulations (ScenarioMIP and HighResMIP). Panels show seasonal means for DJF, MAM, JJA, SON, and the annual average. Rows correspond to ERA5 (top), EC-Earth3 ScenarioMIP (middle), and EC-Earth3 HighResMIP (bottom). Colour shading represents wind energy density at 100 m hub height, extrapolated from 10 m wind speeds using the standard wind energy formulation. Grey areas indicate land; white areas denote missing data.

the Iberian and North Sea coasts.

The climatological distribution of wind energy density in EC-Earth3 simulations is consistent with the ERA5 reference, indicating adequate representation of large-scale atmospheric circulation and storm-track variability. The slightly higher magnitudes in ScenarioMIP result from intensified modeled westerlies and the smoothing associated with its coarse horizontal resolution (∼1°), which increases effective fetch and surface wind stress. The HighResMIP configuration (∼50 km) resolves mesoscale wind gradients and orographic influences more explicitly, reducing open-ocean overestimation and yielding spatial gradients closer to ERA5. Persistent low energy densities (< 0.5 kW m^{-2}) in semi-enclosed basins such as BSC, SCES, and EMC across all datasets highlight the dominant influence of basin geometry, limited fetch, and local atmospheric stability. Differences between the EC-Earth3 configurations primarily reflect resolution-dependent representation of wind-stress gradients rather than variations in model physics.

Figure 3.7 shows the cluster-wise seasonal variability of wave and wind energy densities across ERA5, EC-Earth3 ScenarioMIP, and HighResMIP for the period 1979–2014. All datasets exhibit clear maxima during DJF and SON, consistent with enhanced North Atlantic baroclinicity and storm-track activity, and minima during JJA under weaker westerlies. Open-ocean clusters (EAC, NEC, NWAC) present the highest values, with DJF wave energy exceeding 20 kJ m^{-2} and wind energy reaching approximately 1.75 kW m^{-2} in ERA5. Transitional clusters (WMIC, SMC, WENS) exhibit moderate energy levels (5–12 kJ m^{-2} for wave energy and 0.5–1.25 kW m^{-2} for wind energy), while semi-enclosed basins (BSC, SCES, EMC) remain consistently below 5 kJ m^{-2} and 0.5 kW m^{-2}, respectively.

ScenarioMIP reproduces the seasonal cycle but consistently overestimates wintertime energy densities-often nearly double ERA5 magnitudes in open-ocean regimes. This reflects known EC-Earth3 atmospheric biases, including overly strong westerlies and intensified extratropical cyclones that elevate wind speeds and wave growth. HighResMIP reduces this amplitude bias and shows a narrower inter-cluster spread, particularly in coastal and transitional regions. Despite these differences, the relative ordering of clusters remains unchanged, indicating that the ERA-derived regime framework is robust when applied to EC-Earth3 simulations.

The seasonal and spatial characteristics of wind and wave energy densities across the nine regimes reflect the expected response of the wave field to large-scale atmospheric variability. The elevated DJF and SON values correspond to stronger storm-track activity and higher wind speeds in the North Atlantic, whereas JJA exhibits consistently lower magnitudes across all datasets. ScenarioMIP overestimates energy levels in open-ocean regimes, which is consistent with the tendency of coarser-resolution models (1°) to smooth wind-stress gradients and generate stronger effective forcing. HighResMIP (50 km) captures mesoscale wind features more explicitly, producing narrower seasonal ranges and closer agreement with ERA5. Semi-enclosed regimes (BSC, SCES, EMC) remain low across all datasets, reflecting their limited exposure to North Atlantic storm forcing. Overall, the primary differences between ScenarioMIP and HighResMIP are resolution-dependent, while the consistent inter-cluster ranking across datasets supports the robustness of the ERA5-derived regime framework.

3.3.3 Depth-Resolved Classification of Wind, Wave, and Hybrid Energy Stability Regimes

The spatial classification of wind resource potential (Figure 3.8) is based on long-term mean wind energy density at 100 m hub height and its temporal stability, expressed as the inverse coefficient of variation of annual means ($S = 1/\mathrm{CV}$). Both metrics were partitioned using tertile thresholds (33rd and 66th percentiles) and combined to define four energy–stability classes: *Primary* (high energy × high stability), *Secondary* (intermediate combinations),

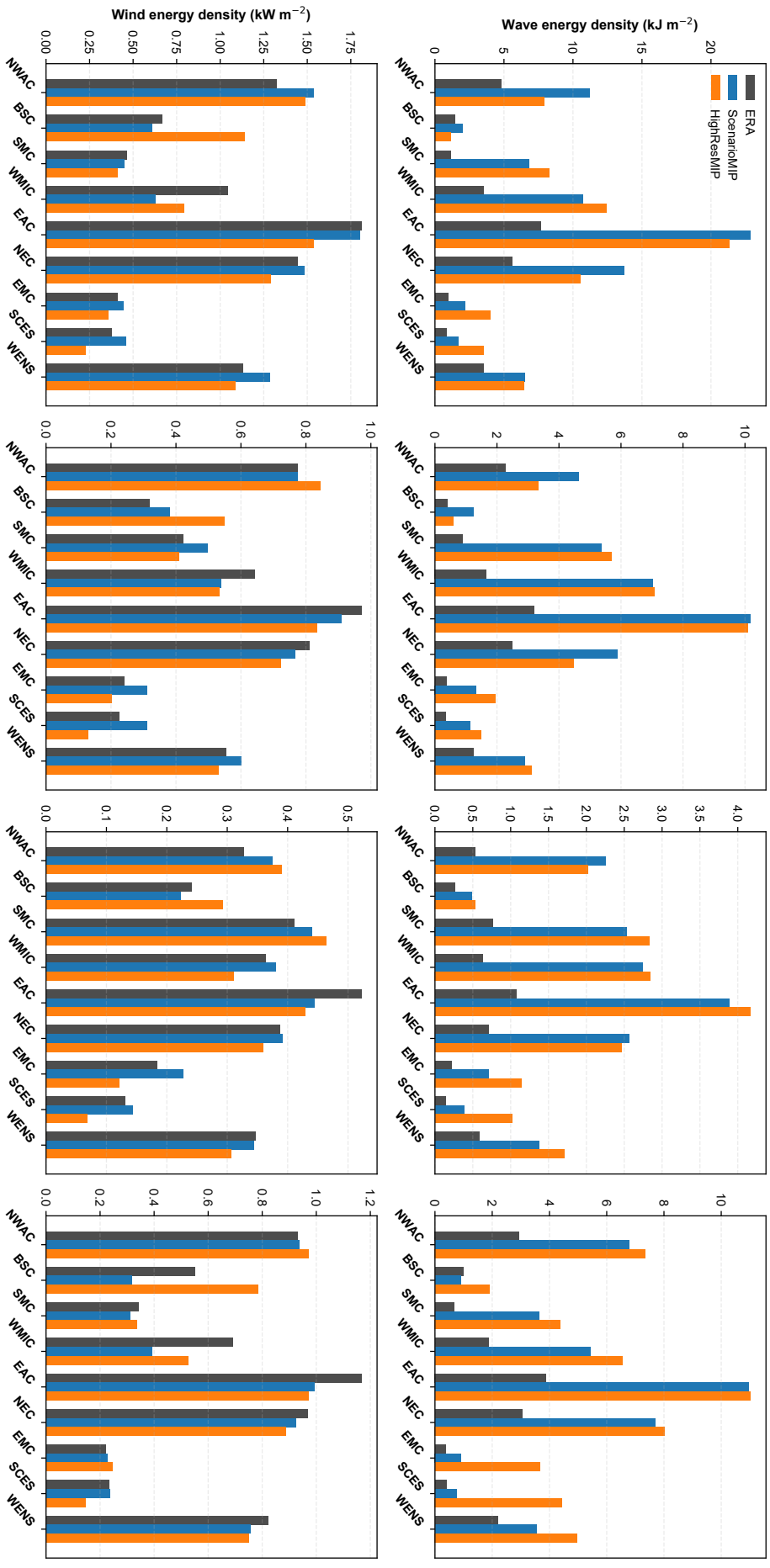

Figure 3.7 Cluster-wise seasonal variability of wave and wind energy density across ERA, ScenarioMIP, and HighResMIP simulations. The top row shows the climatological mean **wave energy density (kJ m^{-2})** and the bottom row shows the corresponding **wind energy density (kW m^{-2})** for four seasons (DJF, MAM, JJA, SON). Bars represent cluster-mean values for the nine ERA-derived wind–wave regimes (NWAC, BSC, SMC, WMIC, EAC, NEC, EMC, SCES, and WENS).

Hotspot (Variable) (high energy × low stability), and *Low* (low energy × low stability).

Primary zones, characterized by mean wind energy density exceeding approximately 1.5 kW m^{-2} and stability above the 66th percentile, are concentrated in deep-water regimes (>200 m) within the Northwestern and Eastern Atlantic clusters (NWAC and EAC). These regions are influenced by persistent westerlies and long fetch, which sustain high kinetic flux with relatively low interannual variability. Transitional-depth regions (50–200 m), including WENS and WMIC, are dominated by *Secondary* and *Hotspot* classes, reflecting intermediate energy levels (0.6–1.2 kW m^{-2}) and enhanced variability associated with mesoscale modulation, boundary-layer shear, and coastal topographic effects. Shallow environments (<50 m) in the Baltic, Black, and eastern Mediterranean seas are predominantly classified as *Low* (<0.5 kW m^{-2}), consistent with weaker near-surface winds, limited fetch, and increased frictional damping.

Across all depth regimes, ERA5 exhibits coherent *Primary* belts aligned with the North Atlantic storm corridor. EC-Earth3 ScenarioMIP reproduces the broad spatial patterns but fragments high-energy areas and expands *Hotspot* zones near coastlines, consistent with its coarser horizontal resolution (∼1°), which smooths near-surface wind-stress gradients and increases effective fetch. In contrast, the HighResMIP configuration (∼50 km) sharpens coastal transitions and preserves regime boundaries, yielding more compact offshore *Primary* patches and clearer deep-to-shallow gradients. These differences indicate that horizontal resolution predominantly controls the representation of near-surface wind gradients and, consequently, the spatial coherence of energy–stability classes.

The resulting depth dependence is physically consistent with expected wind–ocean dynamics: deep waters support high energy and stability under sustained synoptic forcing and uninterrupted air–sea momentum transfer; transitional shelves exhibit greater variability due to mesoscale gradients and coastal influences; and shallow basins remain predominantly *Low*, where limited fetch, enhanced bottom friction, and increased surface roughness constrain energy buildup. Overall, this depth-resolved classification provides a physically interpretable basis for assessing the persistence and variability of wind resources in climate simulations and offers consistent criteria for offshore wind-energy siting across regional scales.

Wave resource classes were derived from the combination of long-term mean wave power and its temporal stability at each grid point. Mean wave power (kW m^{-1}) was estimated following deep-water theory based on significant wave height and energy period. Temporal stability was quantified as the normalized inverse of the coefficient of variation of annual mean wave power, representing interannual persistence of the resource.

Both metrics were partitioned into tertile bands (33rd and 66th percentiles) and cross-combined to define four wave resource classes: *Primary* (high power and high stability), *Secondary* (intermediate combinations), *Hotspot (Variable)* (high power but low stability), and *Low* (low power and/or low stability). This classification was applied consistently across depth regimes and datasets, enabling direct spatial comparison between ERA5 and EC-Earth3 simulations.

Figure 3.9 shows the spatial organization of wave resource potential derived from long-term mean wave power and its temporal stability across three depth regimes for ERA5 and EC-Earth3 simulations. The classification applies percentile thresholds (33rd and 66th) to both metrics and combines them to represent spatial variability in energy magnitude and persistence.

In ERA5, the highest wave power values (>40–50 kW m^{-1}) with strong temporal persistence occur in deep-water regions of the Northwestern and Eastern Atlantic (NWAC, EAC), extending toward the Norwegian and Icelandic Seas. Intermediate-depth regions across the Western Mediterranean and Iberian (WMIC) and Southern Mediterranean (SMC) clusters show moderate wave power (20–35 kW m^{-1}) and variable stability. The northern Atlantic margin and North Sea display high energy but reduced stability, while shallow and semi-enclosed

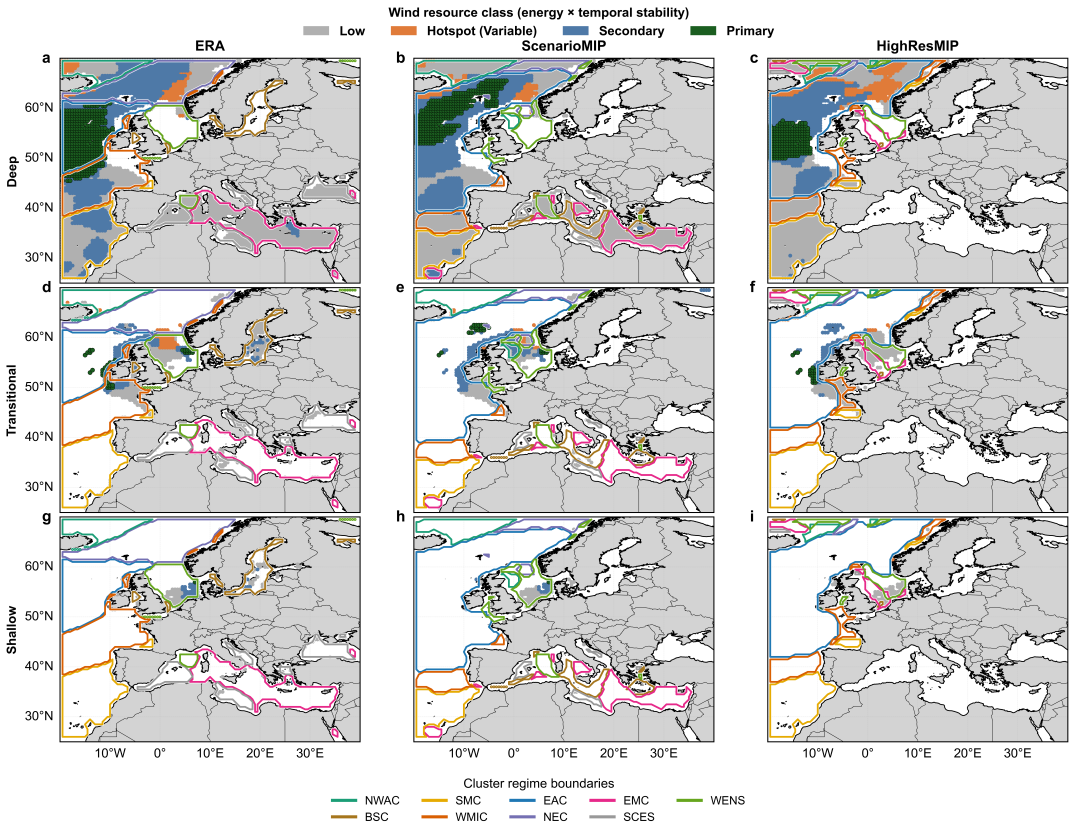

Figure 3.8 Spatial distribution of wind resource classes across three depth regimes for ERA5 reanalysis and EC-Earth3 climate model simulations (ScenarioMIP and HighResMIP). Rows correspond to depth categories (a–c) Deep, (d–f) Transitional, and (g–i) Shallow waters, while columns represent the three datasets. Colours indicate wind resource classes (Primary, Secondary, Hotspot, and Low), and coloured contours denote ERA5-derived wind–wave regime boundaries (e.g., NWAC, WMIC, BSC).

basins such as the Baltic (BSC) and Eastern Mediterranean (EMC) exhibit the lowest wave power (<15 kW m^{-1}) and high interannual variability. The proportion of high-energy, stable zones declines with decreasing depth, consistent with enhanced bottom friction and reduced effective fetch in nearshore environments.

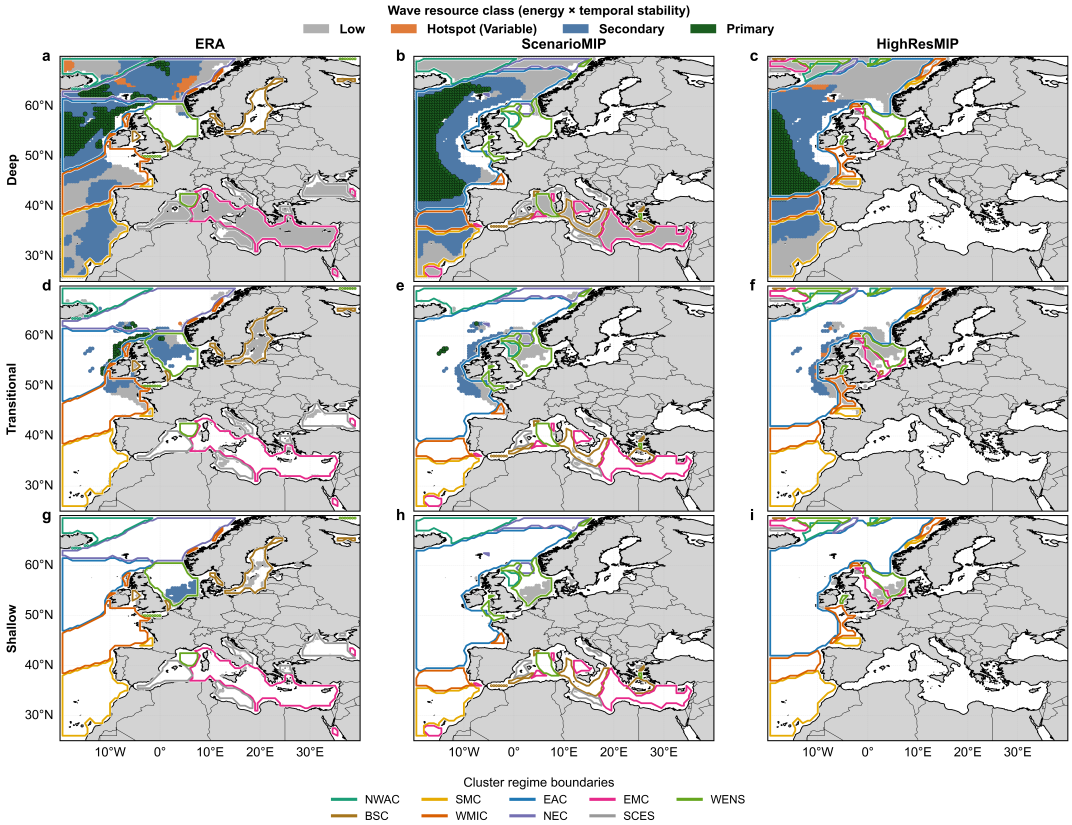

Figure 3.9 Spatial distribution of wave resource classes across three depth regimes for ERA5 reanalysis and EC-Earth3 climate model simulations (ScenarioMIP and HighResMIP). Rows correspond to depth categories (a–c) Deep, (d–f) Transitional, and (g–i) Shallow waters, while columns represent the three datasets. Colours indicate wave resource classes (Primary, Secondary, Hotspot, and Low), and coloured contours denote ERA5-derived wind–wave regime boundaries (e.g., NWAC, WMIC, BSC).

The spatial variability of wave resource potential reflects the combined influence of atmospheric forcing, oceanic fetch, and bathymetric control on wave growth and dissipation. Deep-water regimes in the Atlantic are dominated by persistent westerly forcing, enabling full spectral development and efficient energy transfer, which yields high mean power and strong temporal persistence. Transitional domains such as the Western Mediterranean and Iberian seas are affected by mixed wind–sea and swell conditions, where partial exposure to Atlantic swells and regional wind forcing result in moderate power and stability. In shallow and semi-enclosed basins, limited fetch and depth-induced dissipation constrain wave evolution, producing low and variable power.

Within the EC-Earth3 framework, ScenarioMIP tends to overextend energetic zones due to coarse horizontal resolution, which blends unresolved swell components and smooths fetch-limited gradients. HighResMIP improves the representation of spectral energy gradients and more accurately captures attenuation of wave power across shelf breaks and coastal boundaries. The strong agreement of open-ocean magnitudes across datasets indicates that large-scale atmospheric dynamics primarily govern wave power potential, while discrepancies in enclosed and transitional seas highlight the need for enhanced representation of coastal

and depth-limited processes in global climate wave models.

The hybrid resource classification (Figure 3.10) illustrates the spatial distribution of combined wind–wave energy potential and its temporal persistence across depth regimes and datasets. In ERA5, Primary hybrid zones (jointly high energy and stability) occur mainly in deep-water clusters such as NWAC and EAC, consistent with sustained westerly forcing and large wave fetch. The WENS region shows localized Secondary zones along the North Sea shelf edge, while transitional and shallow waters are dominated by Secondary or Low classes, reflecting weaker joint variability between wind and wave systems. ScenarioMIP reproduces the broad spatial configuration but shows expanded Hotspot areas across the open Atlantic, indicating overestimated interannual variability and reduced temporal stability. The representation of Primary hybrid zones decreases toward shallower depths, with enclosed basins (BSC, EMC) remaining consistently Low in all simulations. The HighResMIP configuration produces a closer spatial agreement with ERA5, particularly over NWAC and EAC, where Primary and Secondary classes are more compact and coherent. Transitional regions such as WENS and WMIC display clearer gradients between Secondary and Hotspot classes, suggesting improved coupling between wind and wave components. Across all datasets, the spatial extent of hybrid potential systematically reduces from deep to shallow regimes, consistent with the attenuation of wave power and increased surface friction in nearshore domains.

The hybrid wind–wave resource classification combines information on both energy magnitude and temporal stability for wind and wave components. At each grid point, a hybrid index was constructed as the mean of the normalized wind energy density and wave power, together with their respective temporal stability scores. Wind energy density ($\mathrm{kW\,m^{-2}}$) was computed from 100 m hub-height wind speeds using a logarithmic power law, while wave power ($\mathrm{kW\,m^{-1}}$) was estimated following deep-water theory based on significant wave height and energy period. Temporal stability for both resources was quantified as the normalized inverse of the coefficient of variation of annual mean values, representing long-term persistence in energy supply.

Both the hybrid energy index and its stability metric were partitioned into tertile bands (33rd and 66th percentiles) and cross-combined to define four hybrid resource classes: *Primary* (high energy and high stability), *Secondary* (intermediate combinations), *Hotspot (Variable)* (high energy but low stability), and *Low* (low energy and/or low stability). This classification was applied consistently across depth regimes and datasets, allowing direct spatial comparison of hybrid wind–wave resource potential between ERA5 and EC-Earth3 simulations.

The hybrid classification reveals that co-located wind–wave resource potential depends on both model resolution and bathymetric context. Compact Primary zones in HighResMIP across NWAC and EAC indicate that finer horizontal resolution better resolves mesoscale wind structures and associated wave growth under strong synoptic forcing. Broader and less distinct hybrid patterns in ScenarioMIP reflect the smoothing of wind gradients and reduced wind–wave synchrony caused by coarse grid spacing. Persistent Low classes in enclosed basins (BSC, EMC) confirm decreased forcing under fetch-limited conditions. Transitional seas, including WENS and WMIC, remain dominated by Secondary classes where partial synchrony produces moderate yet seasonally variable hybrid energy yields. The gradual loss of hybrid stability toward shallow regions reflects depth-dependent dissipation and enhanced boundary-layer turbulence. Overall, model resolution primarily controls spatial coherence of hybrid regimes, but predictability remains constrained by coastal complexity and unresolved sub-grid processes.

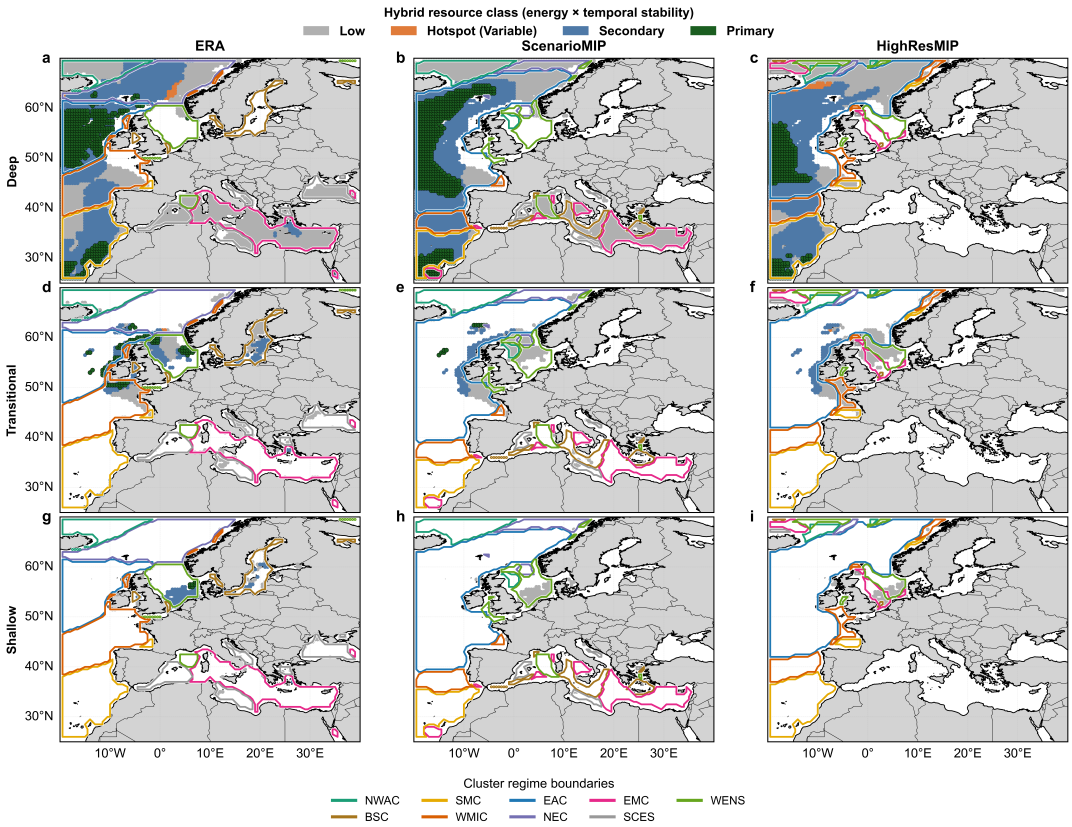

Figure 3.10 Spatial distribution of hybrid (wind–wave) resource classes across three depth regimes for ERA5 reanalysis and EC-Earth3 climate model simulations (ScenarioMIP and HighResMIP). Rows represent depth categories - (a–c) Deep, (d–f) Transitional, and (g–i) Shallow waters - while columns correspond to the three datasets. Colours indicate hybrid resource classes (Primary, Secondary, Hotspot, and Low), and coloured contours denote ERA5-derived wind–wave regime boundaries (e.g., NWAC, WMIC, BSC).

3.3.4 Jurisdictional and Ecological Composition of Energy–Stability Classes

To evaluate the jurisdictional and ecological distribution of offshore renewable energy potential, wind, wave, and hybrid energy–stability classes were aggregated by Exclusive Economic Zones (EEZs) and Marine Ecoregions of the World (MEOW). For each depth regime (Deep, Transitional, and Shallow), the proportion of grid points belonging to four classes-*Primary*, *Secondary*, *Hotspot (Variable)*, and *Low*-was computed for wind energy density, wave power, and the combined hybrid index.

Class definitions were based on joint tertile thresholds (33rd and 66th percentiles) of long-term mean energy metrics and their associated temporal stability indices. The hybrid index was calculated as the normalized mean of wind and wave energy and stability components, representing spatial co-occurrence of both resources. This aggregation was applied consistently across ERA5 and EC-Earth3 (ScenarioMIP and HighResMIP) datasets within the study domain (20°W–40°E, 25–70°N), enabling direct comparison of jurisdictional and ecological patterns across depth regimes.

In Figure 3.11 deep-water regions (> 200 m), both jurisdictional (EEZ) and ecological (MEOW) classifications show dominance of Primary and Secondary classes for wind and wave energy. The Faroe, Iceland, and Canary Islands EEZs record the highest proportions of Primary wind zones, while corresponding MEOW regions-such as the Faroe Plateau and South and West Iceland-exhibit strong wind stability consistent with persistent North Atlantic westerlies. The Azores–Canaries–Madeira region presents a mixture of Primary and Hotspot fractions, indicating intermittently high but less stable conditions. For wave energy, high-energy and persistent regimes are located near Ireland, Spain, and Portugal, whereas eastern basins such as Cyprus and Libya remain dominated by Low stability. Within MEOW regions, the Celtic Seas and North and East Iceland maintain coherent Primary–Secondary wave distributions, while the Levantine and Saharan Upwelling regions remain weak. Deep-water hybrid zones indicate strong joint wind–wave resource potential near the Canary Islands and Faroe Plateau, although hybrid Primary areas are spatially smaller than their single-resource counterparts, suggesting incomplete overlap between the two drivers. Hotspot fractions in the South and West Iceland and Azores–Canaries domains reflect strong seasonal variability driven by storm-track dynamics.

Across transitional waters (50–200 m), the energy–stability distribution shifts toward a predominance of Secondary classes. Denmark, Ireland, and the United Kingdom EEZs retain measurable Primary wind and hybrid shares, while most continental margins (France, Germany, Norway) display Secondary–Low categories. In the MEOW framework, the North Sea and Faroe Plateau remain Secondary-dominated, while the Baltic and Southern Norway regions show reduced persistence. For wave energy, Ireland and the United Kingdom preserve Secondary levels, whereas southern and enclosed basins are largely Low. Hybrid Primary areas occur only in zones where both wind and wave metrics maintain Secondary or higher stability, confirming the dependence of hybrid potential on co-located energy persistence. Transitional Hotspots are concentrated within the Celtic Seas and South and West Iceland, reflecting stronger seasonal modulation compared with deep offshore zones.

In shallow waters (< 50 m), the share of Primary classes declines across all resources, replaced by broader Secondary and Low distributions. Only the Irish EEZ retains a small fraction of Primary wind areas, while France, Germany, and the Netherlands are dominated by Secondary and Low categories. In MEOW regions, the Celtic Seas show limited Secondary wind potential, whereas semi-enclosed basins such as the Adriatic, Aegean, Baltic, and Black Seas are almost entirely Low, reflecting constrained fetch and weaker wind forcing. For wave energy, shallow zones are mostly Low, with isolated Secondary areas near Ireland and the Netherlands. Corresponding MEOW basins display Low wave potential across nearly all

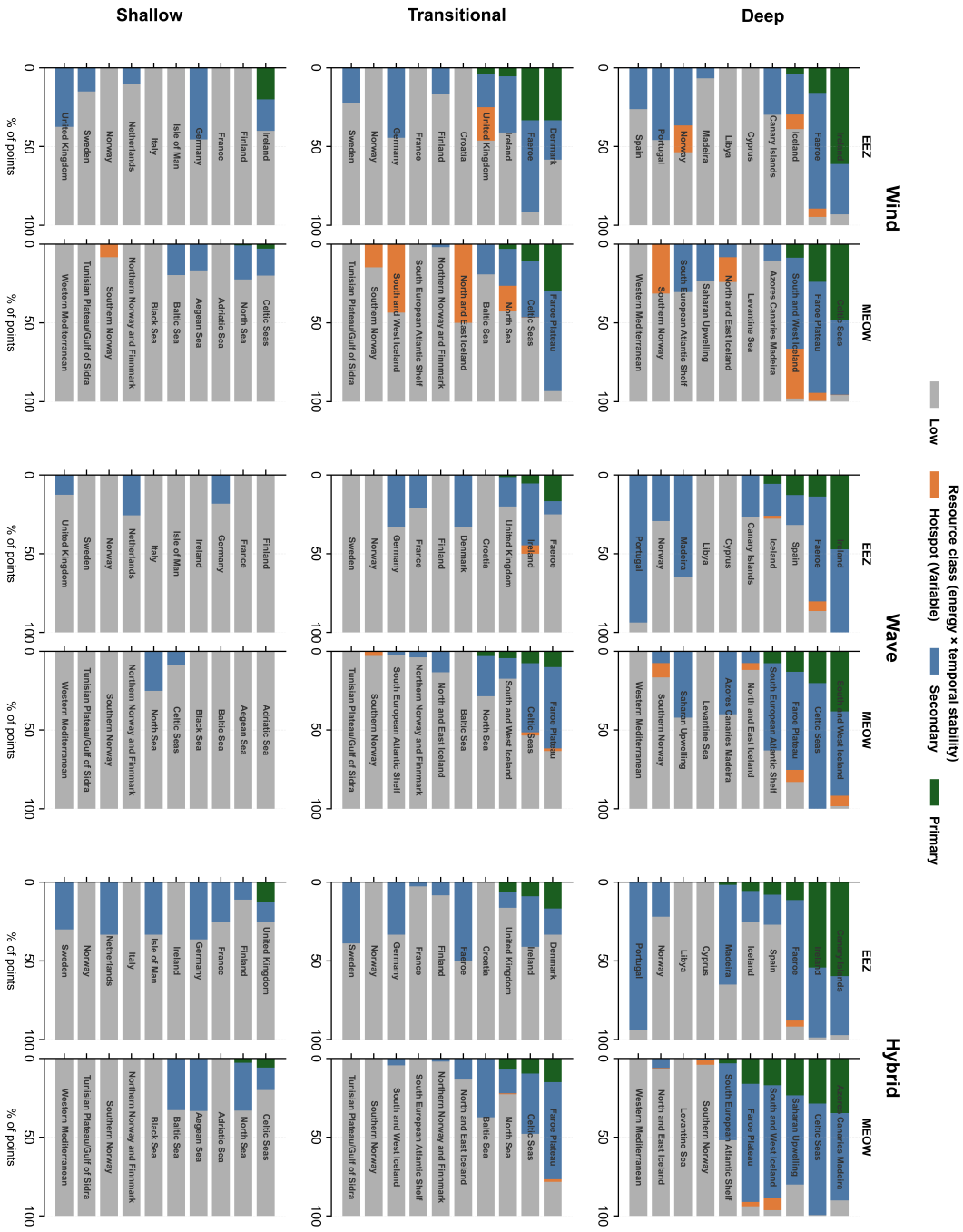

Figure 3.11 Composition of wind, wave, and hybrid resource classes across the top five Exclusive Economic Zones (EEZs) and Marine Ecoregions of the World (MEOW) within each depth regime. Rows correspond to depth categories (Deep, Transitional, and Shallow), while columns represent the resource type (Wind, Wave, and Hybrid). Horizontal stacked bars show the percentage contribution of each energy–stability class (Primary, Secondary, Hotspot, and Low) for ERA5 and EC-Earth3 simulations (ScenarioMIP and HighResMIP).

shallow systems. Hybrid resources show similar patterns: the United Kingdom EEZ retains a narrow Primary segment, while the Celtic Seas contain the only visible Primary hybrid share within shallow ecological zones. Western Mediterranean and Tunisian Plateau regions show exclusively Low hybrid potential. The consistent decline in Primary fractions from deep to shallow regimes indicates depth-dependent energy attenuation and reduced temporal persistence in nearshore environments.

The spatial transition from deep to shallow environments shows a systematic reduction in both energy magnitude and temporal stability. In deep waters, large-scale atmospheric forcing and long-period swell propagation dominate, producing high mean energy densities and relatively stable long-term statistics. These conditions support Primary classifications in exposed North Atlantic regions such as the Faroe Plateau and Celtic Seas. Transitional depths introduce increased spatial heterogeneity, as proximity to coastlines, regional wind variability, and changes in bathymetry modulate the local wind field and wave development. The greater presence of Secondary and Hotspot classes in these zones arises from stronger seasonal variability and localized wind–wave generation rather than any decoupling between wind and wave processes. Shallow waters exhibit predominantly Low and Secondary classes, reflecting the combined influence of limited wave growth, weaker sustained winds, and stronger coastal boundary effects-factors that also influence transitional regions but become increasingly dominant as depth decreases.

EEZ-based aggregation highlights that high-latitude jurisdictions, such as Iceland, Faroe, and Ireland, consistently occupy the upper tier of renewable potential, with substantial Primary or Secondary fractions across wind, wave, and hybrid resources. Mid-latitude zones, including the United Kingdom and Portugal, maintain significant hybrid and wave stability, reflecting favorable wind regimes and exposure to North Atlantic swell. By contrast, enclosed or semi-enclosed EEZs within the Mediterranean and Baltic seas are predominantly Low or Hotspot, indicating constrained resource persistence due to limited fetch and regional atmospheric forcing. Ecological aggregation through the MEOW framework confirms that the Celtic Seas, North Sea, and Faroe Plateau act as consistent hybrid hubs, whereas the Levantine, Aegean, and Black Sea ecoregions remain less stable. These distinctions are relevant for both national energy planning and transboundary ecological management, as they delineate zones where renewable energy extraction can be prioritized without compromising regional environmental coherence. The combined EEZ–MEOW evaluation thus integrates jurisdictional, ecological, and depth-related variability into a unified spatial framework for assessing offshore renewable potential.

3.4 Summary and Conclusion

This study applied an ERA5-derived nine-regime wind–wave classification framework to EC-Earth3 simulations (ScenarioMIP and HighResMIP) for 1979–2014 to assess spatial consistency and resolution dependence across European wind–wave climates. The regime framework was used to contextualize, rather than determine, the renewable energy classifications, allowing spatial patterns in energy density and stability to be interpreted within consistent atmospheric–oceanic regimes. The results demonstrate that the ERA5-based regime structure is transferable to EC-Earth3 outputs, preserving the large-scale organization of wind–wave climates across the Northeast Atlantic and European seas. Quantitatively, 36.4% of collocated grid points exhibited full three-model agreement, 58.5% showed consistency between two models, and only 5.1% differed across all datasets, confirming the robustness of the spatial classification. Cluster-membership confidence remained high (0.98 in ERA5, 0.90 in ScenarioMIP, 0.93 in HighResMIP), with reduced certainty confined to shelf and coastal transition zones where sub-grid processes remain unresolved.

The comparison of climatological energy fields shows that both wave power and wind energy density reproduce the dominant ERA5 storm-track pattern, with maxima in the Northwestern and Eastern Atlantic regimes (NWAC, EAC) and minima in semi-enclosed basins such as the Baltic (BSC) and Eastern Mediterranean (EMC). Seasonal cycles are systematic across datasets, with DJF and SON representing periods of enhanced baroclinic activity and maximum energy flux, while JJA exhibits minima associated with weaker westerlies. The inter-seasonal ranking of regimes (EAC > NWAC > NEC > transitional > enclosed) remains consistent, indicating that the large-scale atmospheric forcing structure is preserved across model configurations. The higher open ocean magnitudes in ScenarioMIP are attributed to its coarse horizontal resolution (1°), which extends effective fetch and smooths mesoscale gradients, while HighResMIP (50 km) resolves wind-stress variability and coastal orographic effects more accurately, producing energy distributions closer to ERA5.

The resource-class maps derived from long-term mean energy and temporal-stability indices reveal a clear depth dependence. Primary zones (high energy × high stability) are concentrated in deep-water Atlantic regimes (NWAC, EAC), Secondary zones dominate transitional shelves (WENS, WMIC), and Low classes prevail in shallow and enclosed seas (BSC, EMC). The share of Primary areas decreases systematically from deep to shallow regimes due to enhanced bottom friction, reduced fetch, and wave transformation processes. ScenarioMIP exhibits broader Hotspot (variable) regions associated with increased temporal variability, while HighResMIP provides sharper coastal gradients and reduced classification ambiguity. The hybrid (wind–wave) potential, represented by a normalized index combining wind and wave energy and their respective stability components, identifies fewer Primary areas than single-resource maps, reflecting the requirement for concurrent persistence of both atmospheric and oceanic drivers. HighResMIP enhances this coherence, but coastal predictability remains limited by sub-grid turbulence and boundary-layer parameterisations.

The jurisdictional and ecological aggregation of energy–stability classes across Exclusive Economic Zones (EEZs) and Marine Ecoregions of the World (MEOW) illustrates consistent spatial patterns. High-latitude Atlantic jurisdictions such as Iceland, the Faroe Islands, and Ireland, and ecological regions including the Celtic Seas, North Sea, and Faroe Plateau, exhibit the highest shares of Primary and Secondary classes, supported by persistent westerly winds and long fetch. Mid-latitude zones (United Kingdom, Portugal) maintain significant Secondary and hybrid fractions, whereas Mediterranean and Baltic EEZs remain dominated by Low or Hotspot classes due to restricted fetch and weaker local forcing. The integrated EEZ–MEOW framework establishes a practical spatial reference for linking jurisdictional boundaries, ecological settings, and depth variability in assessing regional offshore renewable-energy potential.

The framework provides a foundation for extending this analysis toward future scenario-based projections, uncertainty evaluation, and spatial planning of offshore renewable infrastructure.

Acknowledgments

The United States Geological Survey (USGS) is acknowledged for providing access to the CMIP6 MIP simulations used in this study. The European Centre for Medium-Range Weather Forecasts (ECMWF) is acknowledged for making the ERA5 reanalysis dataset available. Bathymetric information was obtained from the General Bathymetric Chart of the Oceans (GEBCO). Additional spatial layers were sourced from the Marine Ecoregions of the World (MEOW) and Exclusive Economic Zones (EEZ) datasets.

4

Assessing Future Transitions in European wind–wave Regimes using a Fixed ERA5-Derived Clustering Framework and EC-Earth3P-HR

"The present state of nature is the effect of its past and the cause of its future."

- Pierre Simon Laplace (1814)

"The important aspect of creativity is seeing the same thing as everybody else, but thinking of something different."

- A. P. J. Abdul Kalam

This chapter investigates how coupled wind–wave regimes across European seas may reorganise under near-term climate forcing by projecting EC-Earth3P-HR simulations (2020–2050) onto a fixed, physically interpretable clustering framework derived from ERA5 (1979–2014). The approach preserves a consistent multivariate reference by mapping future wind–wave fields into the ERA5 principal-component space and classifying

each grid point using the nine historical regime centroids. Future reorganisation is quantified using regime transition diagnostics, including a Regime Transition Index, centroid migration, and changes in regime spatial footprints, thereby separating spatial persistence from dynamical redistribution within the fixed regime geometry. The physical basis of regime change is interpreted through projected anomalies in significant wave height and near-surface wind speed, while changes in seasonal coherence are assessed using a Seasonal Regime Stability Index based on departures of seasonal states from the annual mean in standardised feature space. Finally, the chapter evaluates how offshore wind and wave resources evolve within this regime framework using deep-water wave power and hub-height wind energy proxies, and integrates energy magnitude with stability to classify Primary, Secondary, Hotspot, and Low hybrid wind–wave resource zones. Together, these diagnostics provide a coherent, regime-based view of how the European wind–wave climate and hybrid renewable potential may shift in space, intensity, and persistence over 2020–2050, offering a structured foundation for offshore planning and climate-aware energy assessments.

This chapter is based on:

Maya, P., Parker, K., Cagigal, L., Metrikine, A. V., & Antolínez, J. A. A.
Assessing future transitions in European wind–wave regimes using a fixed ERA5-derived clustering framework and EC-Earth3P-HR simulations.
Journal of Climate, under review.

4.1 Introduction

Offshore wind and wave energy are central components of Europe's strategy for reducing carbon emissions from the power sector. Both are driven by atmospheric circulation, yet they respond differently to variations in wind intensity, storm frequency, and fetch conditions. Winds immediately reflects changes in weather systems, while waves integrate wind forcing over broader spatial and temporal scales, allowing energy to persist even after local winds have weakened. This difference in response time creates a natural complementarity between the two resources, where wave energy can sustain power generation during periods of low wind. Understanding this coupled behaviour is therefore critical for evaluating the long-term stability of offshore renewable systems and assessing how their balance may shift under a changing climate *[Hemer et al., 2010, Reguero et al., 2015, Bonaduce et al., 2019, Olauson, 2018, WindEurope, 2022]*.

Studying how they interact is important for understanding long-term resource stability and for planning reliable offshore systems. Wind–wave processes also affect air–sea exchanges, ocean mixing, and the performance of coastal and offshore structures. With a warming climate, changes in storm tracks and wind fields are expected to alter wave conditions *[on Climate Change , IPCC]*. These shifts can change average and extreme sea states, influencing coastal erosion, navigation, and energy production *[Woolf and Wolf, 2013, Dodet et al., 2019]*.

Across Europe, the open North Atlantic and the semi-enclosed North, Baltic, and Mediterranean Seas show clear contrasts in how wind and waves respond to atmospheric forcing. Local depth and fetch play a strong role in shaping these regional patterns *[Bonaduce et al., 2019, Barbariol et al., 2021, Cieślikiewicz and Cupiał, 2024]*. Understanding such differences is key for estimating future offshore energy potential and exposure in each basin *[Susini et al., 2022, Akpınar et al., 2022, Casas-Prat et al., 2024b]*.

Recent studies have examined long-term variations in surface winds and waves using reanalysis datasets and climate model simulations, with particular focus on European seas. The ERA5 reanalysis provides high spatial and temporal resolution and shows improved consistency with independent observations, including radiosonde and buoy measurements *[Hersbach et al., 2020, Graham et al., 2019, Olauson, 2018]*. Global and regional studies have shown upward trends in wind speed and significant wave height across many mid- and high-latitude oceans, together with a clearer separation between locally generated wind-seas and remotely driven swell systems *[Young et al., 2011, Semedo et al., 2011]*.Projections based on CMIP5 and CMIP6 multi-model ensembles indicate spatially variable future changes and show uncertainty related to external forcing, model configuration, and downscaling methods *[Morim et al., 2019, Meucci et al., 2024, Casas-Prat et al., 2024b]*. Regional investigations across the North, Baltic, and Mediterranean Seas describe variations in wave climate and extremes influenced by bathymetry, coastline geometry, and storm trajectories *[Perez et al., 2015, Bonaduce et al., 2019, Casas-Prat and Sierra, 2013, Toomey et al., 2022]*. Other studies have assessed the contribution of waves to coastal sea-level variability through wave setup and storm surges *[Dodet et al., 2019, Toomey et al., 2022]*.

Analyses of wave energy potential reveal marked spatial and temporal variability, including seasonal and interannual modulation *[Reguero et al., 2015]*. Studies applying extreme-value theory have quantified uncertainty ranges relevant for offshore design *[Kresning et al., 2024]*. Large-scale atmospheric modes such as the North Atlantic Oscillation introduce coherent patterns in wind and wave variability across the North Atlantic–European region, underscoring the need to examine their combined behaviour *[Hurrell, 1995, Thompson and Wallace, 2000, Sardana et al., 2024]*.

While previous studies have advanced the understanding of wind and wave dynamics, most have examined these variables separately. Trend analyses typically focus on either wind speed or wave height without addressing their joint evolution in space and time *[Young et al., 2011, Bonaduce et al., 2019, Casas-Prat et al., 2024b, Lobeto et al., 2024]*. As a result, the coupled behaviour that governs surface energy transfer remains insufficiently characterized, particularly at regional scales where local bathymetry and fetch modify the response to atmospheric forcing *[Cieślikiewicz and Cupiał, 2024, Najafzadeh et al., 2024]*.

Current projections often evaluate mean or extreme conditions independently and do not describe how wind and wave systems evolve together under different circulation regimes. This separation limits the ability to detect consistent changes in coupled dynamics or to assess their relevance for offshore resource stability. A multivariate framework is needed to represent joint wind–wave variability and to enable consistent comparisons between present and future climate conditions.

To address this gap, a regime-based approach was developed by *Maya and Antolínez [2025]* using ERA5 reanalysis data for the period 1979–2014. The method applied Principal Component Analysis (PCA) to five variables-10 m wind speed, significant wave height, mean wave period, and wind and wave directions-and used K-means clustering to identify dominant wind–wave regimes across European seas. Nine physically consistent regimes were identified, representing open-ocean, transitional, and enclosed environments with distinct wind and wave characteristics. The clusters reproduced stable spatial patterns that reflected large-scale atmospheric modes such as the North Atlantic and Arctic Oscillations. This ERA5-based framework established a fixed multivariate reference for examining regional wind–wave variability and its relationship with climate forcing.

The framework was subsequently evaluated using historical EC-Earth3 simulations to assess its robustness across model configurations. Two CMIP6 experiments were analysed: ScenarioMIP, representing standard coupled simulations, and HighResMIP, designed to test the impact of enhanced horizontal resolution on climate processes *[Haarsma et al., 2016]*. Both experiments use the EC-Earth3 model, which couples the IFS atmosphere, NEMO ocean, and WAM wave components to represent air–sea interactions. Model outputs for 1979–2014 were projected onto the fixed ERA5 principal-component space to ensure consistent regime classification across datasets. Both configurations reproduced the nine-regime structure derived from ERA5, confirming the framework's applicability to climate model data. The HighResMIP experiment, however, better captured spatial gradients and regime boundaries-especially in the North and Baltic Seas-and produced wind and wave statistics closer to ERA5. This comparison demonstrated that spatial resolution strongly affects the representation of wind–wave coupling and that the ERA5-based clustering framework provides a robust reference for evaluating model performance across CMIP6 experiments *[Maya and Antolínez, 2025, Bonaduce et al., 2019, Casas-Prat et al., 2024b]*.

Building on these results, this study extends the regime-based framework to future climate projections using the EC-Earth3P-HR model from the CMIP6 HighResMIP experiment. This configuration was selected because it reproduces the nine ERA5-derived wind–wave regimes and their spatial gradients with the highest fidelity during the historical period *[Maya and Antolínez, 2025]*, and its finer atmospheric (40 km) and oceanic (25 km) grids provide improved representation of storm systems, coastal wind fields, and fetch-limited wave growth

[Haarsma et al., 2016]. Using these simulations, the analysis aims to project historical and future wind–wave fields onto the fixed ERA5 PCA space, classify future conditions within the established nine-regime structure, and quantify how regimes reorganise through transitions, centroid migration, and footprint change. The study further examines the physical drivers of these changes by analysing projected differences in significant wave height and surface wind speed. It also assesses shifts in seasonal coherence using the Seasonal Regime Stability Index and evaluates future wind and wave energy potential using deep-water wave power and hub-height wind energy diagnostics. Finally, a hybrid classification integrating energy magnitude with seasonal stability is used to identify Primary, Secondary, Hotspot, and Low resource zones. Together, these steps offer a coherent and physically interpretable assessment of how European wind–wave regimes may evolve under near-term climate forcing between 2020–2050 relative to the historical baseline, and how these changes influence the spatial distribution of future offshore energy potential.

The paper is organised as follows. Section 4.2 describes the datasets used in this study, the preprocessing steps, and the overall workflow applied to project EC-Earth3P-HR outputs into the ERA5-based regime framework. Section 6.5 presents the projected regime transitions together with the associated changes in physical drivers, seasonal stability, and wind–wave energy potential. The final section summarises the key findings and reflects on what they mean for understanding future wind–wave variability and the assessment of offshore resources across European seas.

4.2 Data and Methods

This section outlines the datasets, preprocessing steps, and analytical framework used to evaluate future changes in European wind–wave regimes. The workflow begins with the extraction and preparation of EC-Earth3P-HR wind and wave fields for the historical (1979–2014) and near-future (2020–2050) periods. These fields are then projected onto the fixed ERA5 principal-component space to ensure a consistent multivariate basis for regime classification. Subsequent analyses quantify regime transitions, physical drivers, seasonal stability, and changes in wind–wave energy. The final part of the section describes the hybrid resource classification used to assess future offshore energy potential.

An overview of the workflow is shown in Figure 4.1.

A schematic overview of the methodological workflow is shown in Fig. 4.1. The analysis proceeds in five steps: (1) preprocessing and regional extraction of EC-Earth3P-HR wind–wave fields, (2) projection onto a fixed ERA5-based PCA space, (3) regime classification and transition diagnostics, (4) evaluation of physical drivers and seasonal stability, and (5) estimation of wave and wind energy and the construction of a hybrid resource classification.

4.2.1 Model data in the study region

The analysis focuses on the European and adjacent seas within 20°W–40°E and 25°–70°N. Two periods were considered: a historical baseline (1979–2014) and a near-future period (2020–2050), enabling assessment of wind–wave regime behaviour under projected climate change.

Wind and wave fields were obtained from the EC-Earth3P-HR climate model, the high-resolution configuration of the CMIP6 HighResMIP experiment (T511 atmospheric resolution, ∼40 km; ORCA0.25 ocean grid, ∼25 km). Dynamically consistent wave output was provided by the WAM Cycle 6 wave model. The analysis uses the following variables: H_s, T_{02}, U_{10}, and wind and wave directions (θ_u, θ_w).

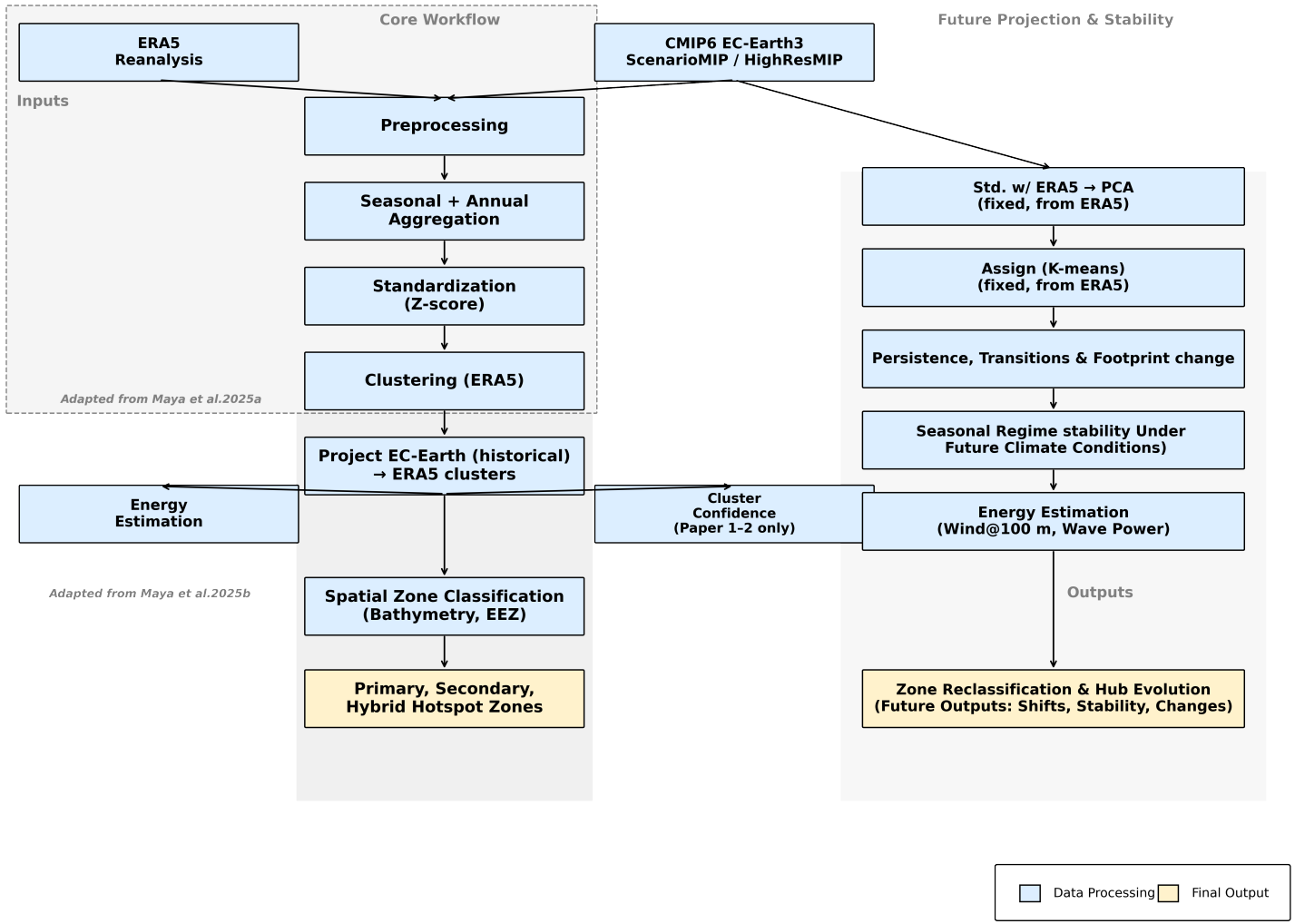

Figure 4.1 Workflow of the data processing and analysis pipeline, including preprocessing, projection into PCA space, regime classification, physical-driver evaluation, and hybrid energy assessment.

Hourly or 3-hourly model outputs were temporally aggregated to monthly means prior to further analysis.

4.2.2 Preprocessing

All EC-Earth3P-HR variables were:

1. spatially subsetted to the study domain,
2. interpolated onto a common 0.25° grid,
3. organized as monthly-mean time series for 1979–2014 and 2020–2050,
4. masked using an ERA5-derived land–sea mask.

No additional statistical bias correction was applied; the analysis is based on internal model consistency and comparison of historical and future anomalies within the same model framework.

4.2.3 Projection into the ERA5 PCA Space

To ensure consistency with the regime structure defined in Paper 1, EC-Earth3P-HR wind–wave fields were projected into the fixed ERA5 principal-component (PC) space. For each monthly field, standardised anomalies were computed and multiplied by the ERA5 loading matrix:

$$\mathbf{Z}_{\mathrm{HR}} = \mathbf{X}_{\mathrm{HR}} \mathbf{W}_{\mathrm{ERA5}}, \tag{4.1}$$

where $\mathbf{W}_{\mathrm{ERA5}}$ contains the fixed PC loading vectors from ERA5. The first N components explaining more than 99% of ERA5 variance were retained.

4.2.4 Regime Classification and Transition Diagnostics

The nine-regime ERA5 clustering solution (from Paper 1) was applied to the projected EC-Earth3P-HR PCs. Each grid point was classified by assigning it to the regime with minimum Euclidean distance to the ERA5 cluster centroids. Transition behaviour between 1979–2014 and 2020–2050 was quantified using three metrics:

- **Regime Transition Index (RTI):** a binary indicator (0 = no change, 1 = change).
- **Centroid migration:** displacement between historical and future centroids, converted from degrees to kilometres.
- **Footprint change:** fractional change in spatial coverage relative to the domain.

These metrics provide complementary information on spatial persistence, latitudinal shifts, and reorganisation of regime areas.

4.2.5 Physical Drivers: Wind and Wave Forcing

Future changes in the underlying wind–wave environment were evaluated using differences in significant wave height (ΔH_s) and 10 m wind speed (ΔU_{10}) between 1979–2014 and 2020–2050. These variables represent the dominant contributors to the PC space used for classification, and their spatial differences provide physical context for centroid shifts and regime expansions or contractions.

4.2.6 Seasonal Regime Stability Index (SRSI)

Seasonal coherence of the wind–wave climate was assessed using the Seasonal Regime Stability Index (SRSI), defined as the Euclidean distance between seasonal-mean and annual-mean states in the standardised (H_s, T_{02}, U_{10}) feature space. The change in SRSI (ΔSRSI) quantifies whether seasonal states become more or less similar to the annual mean under future forcing.

4.2.7 Wave and Wind Energy Diagnostics

Deep-water wave power and hub-height wind energy were computed as:

$$P = H_s^2 T_{02}, \qquad U_{100} = U_{10}\left(\frac{100}{10}\right)^{0.11}, \qquad E = U_{100}^3. \tag{4.2}$$

These energy proxies were calculated for both historical and future periods and sampled on historical regime footprints to quantify regime-specific changes.

4.2.8 Hybrid wind–wave Resource Classification

A hybrid wind–wave resource index was constructed by combining z-scored wave power and wind energy with seasonal stability. Grid points were classified into four categories-Primary, Secondary, Hotspot, and Low-using future-period percentile thresholds applied to both periods. Transitions among hybrid classes were summarized in a row-normalised transition matrix, capturing how combined energy potential reorganises under future forcing.

Within this regime framework, combining normalised wind and wave energy proxies with seasonal stability is meaningful because offshore suitability and operational relevance depend not only on mean resource strength, but also on the consistency with which favourable conditions occur. Although wind and waves are physically distinct and may decouple locally due to swell propagation and fetch limitations, they form a coupled surface climate system driven by atmospheric forcing *[Holthuijsen, 2010, Young, 1999]*. As a result, regions with similar mean wind or wave energy can differ substantially in the persistence and seasonal structure of their co-occurring wind and wave conditions. The hybrid index therefore distinguishes between areas where high energy is associated with stable, repeatable conditions (Primary) and areas where comparable energy levels occur under less persistent, more episodic states (Hotspot). Discrete classes provide an interpretable summary of these contrasts and allow transitions to be tracked consistently across the domain.

This choice avoids introducing distributional adjustments that may unintentionally modify the joint wind–wave structure (covariance and seasonal gradients) used for regime classification. Since regime identity is defined in a multivariate feature space, bias correction applied independently to wind or wave variables can shift points across cluster boundaries and alter diagnosed transitions. The implications of this for regime interpretability are discussed in Section 4.4.1.

4.3 Results and Discussion

4.3.1 Future Regime Transitions and Spatial Reorganization

The nine ERA5-derived wind–wave regimes were projected onto EC-Earth3P-HR simulations for the historical (1979–2014) and near-future (2020–2050) periods to quantify how future conditions reorganize within the fixed PCA–cluster framework. The resulting classification maps (Fig. 4.2) reveal substantial redistribution of grid points across the nine historical

regimes. Across the 2948 overlapping ocean points, 82% retain their historical regime label, while 18% transition to a different label.

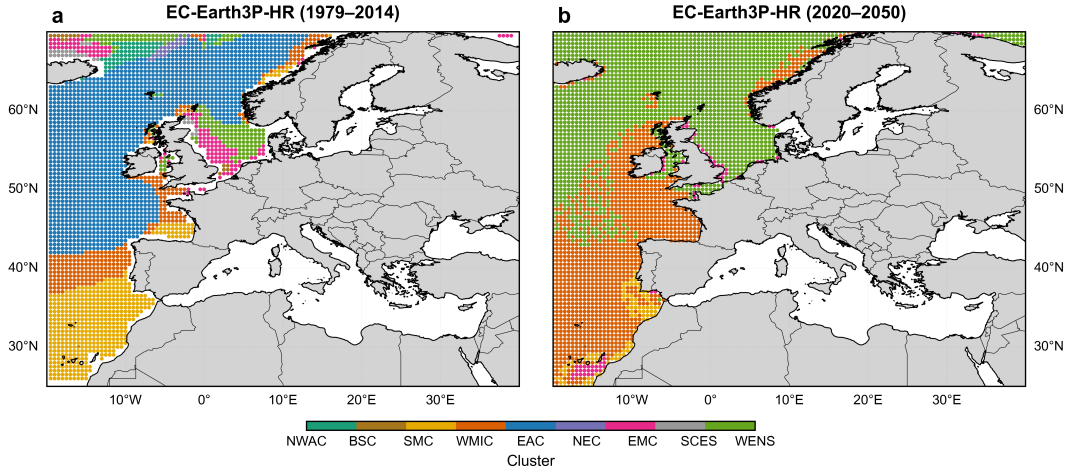

Figure 4.2 Spatial distribution of wind–wave regimes derived from the ERA5-based clustering framework, projected onto EC-Earth3P-HR simulations for (a) the historical baseline (1979–2014) and (b) the near-future period (2020–2050). The comparison shows large-scale preservation of regime patterns alongside regional reorganizations, particularly the expansion of open-ocean and mixed regimes and the contraction of transitional and semi-enclosed basins. Domain extent: 25°N–70°N, 20°W–40°E.

Future conditions occupy only five of the nine historical regimes: WENS, WMIC, SMC, EMC, and EAC. Four regimes-NWAC, NEC, SCES, and BSC-disappear entirely. Among the surviving regimes, WENS and WMIC show large increases in the number of grid points (from 193 to 1977 and from 304 to 1287, respectively), while SMC decreases from 510 to 103 points, EMC from 149 to 92, and EAC from 1646 to only 3 future points. These absolute changes indicate a strong reallocation of grid points within the fixed PCA space rather than a simple physical expansion or contraction of historical spatial domains.

The spatial structure of these transitions is summarized by the Regime Transition Index (RTI; Fig. 4.3), defined as a binary indicator of whether a grid point changes its dominant regime between the historical and future periods. The domain-mean RTI is 0.18, with elevated values concentrated in the Norwegian Sea, the northern entrance of the North Sea, and parts of the Northeast Atlantic shelf. Regions with RTI < 0.1, such as the central North Atlantic and western Mediterranean, exhibit strong regime continuity.

Regime-specific transition probabilities are shown in Fig. 4.4. Historically small or semi-enclosed regimes (SMC, SCES, BSC) exhibit strong consolidation: most of their grid points transition into WMIC or EMC. WENS retains a large fraction of its historical footprint while gaining additional points from neighbouring regimes, contributing to its future dominance. EAC maintains high internal persistence in relative terms but loses almost all of its spatial extent because only 3 grid points are classified as EAC in the future dataset.

4.3.2 Centroid Migration and Regime Footprint Change

Future changes in the wind–wave regime structure were examined by analysing centroid displacement and changes in spatial footprint (Fig. 4.5). Centroid migration indicates how the mean multivariate position of each regime shifts in the PCA space, while footprint change quantifies gains or losses in domain coverage.

WMIC shows the largest centroid displacement, moving more than 1,000 km northeast toward the Bay of Biscay. WENS also migrates northeastward into the northern North Sea.

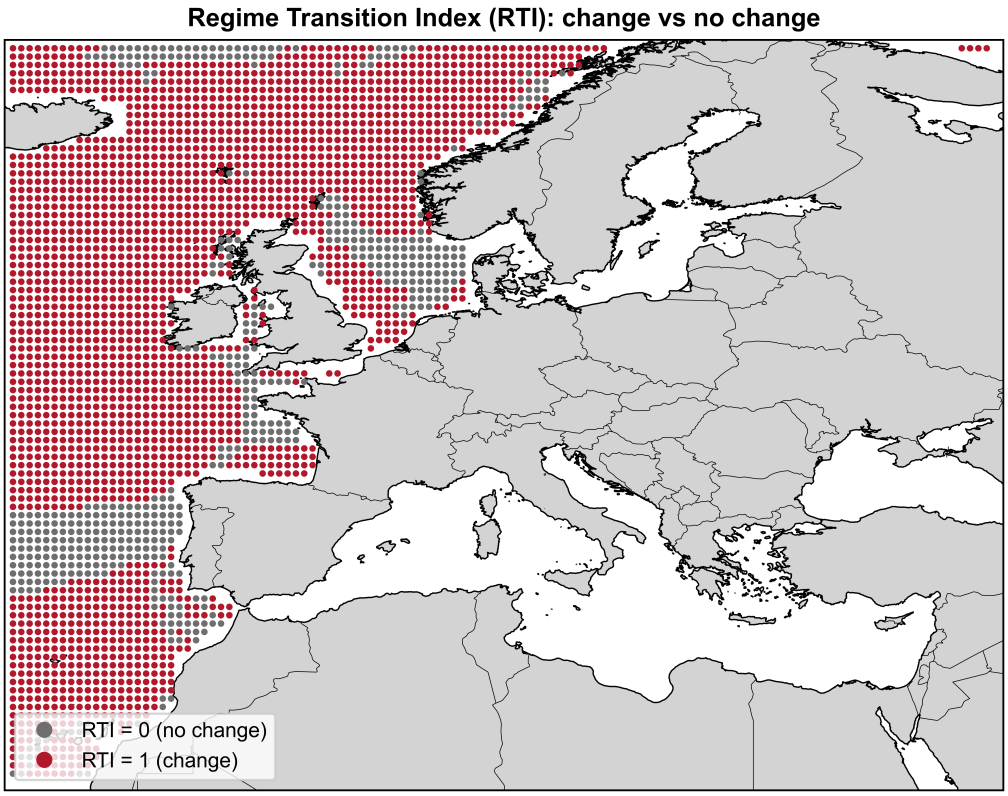

Figure 4.3 Categorical Regime Transition Index (RTI) between historical (1979–2014) and future (2020–2050) EC-Earth3P-HR simulations. RTI = 1 indicates a change in regime identity at a given grid point. High-RTI regions are concentrated along the Norwegian Sea, the northern entrance to the North Sea, and parts of the Northeast Atlantic shelf, whereas the central North Atlantic and the western Mediterranean remain largely stable in terms of regime identity.

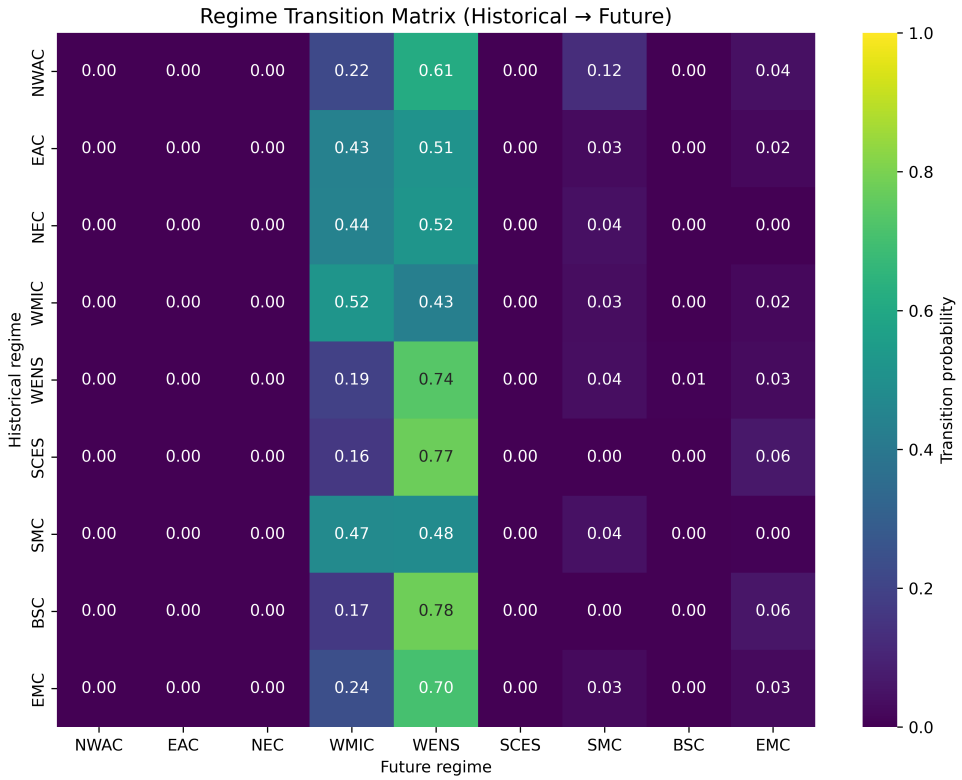

Figure 4.4 Regime Transition Matrix comparing historical and future EC-Earth3P-HR classifications. Rows represent historical regimes; columns show the distribution of their future classifications (row-normalized probabilities). Semi-enclosed and coastal regimes (SMC, SCES, BSC) show strong transitions into WMIC and EMC, while open-ocean regimes exhibit moderate persistence but reduced spatial extent. The matrix highlights a consolidation of the European wind–wave climate into fewer, more spatially coherent regimes under near-term climate forcing.

EMC displays limited centroid movement and reduced spatial extent. Three regimes-NEC, SCES, and EAC-do not have future centroids because their future coverage is negligible.

Footprint changes are consistent with these patterns. WENS expands by +41.6% of the domain and WMIC by +33.9%. SMC contracts by –19.7%, and EAC decreases by –51.1%. The remaining semi-enclosed regimes (BSC, NWAC, NEC, SCES) retain only small or negative future coverage.

These results indicate that WENS and WMIC occupy a larger fraction of the domain in the future classification, while several historically smaller or semi-enclosed regimes show reduced or negligible presence.

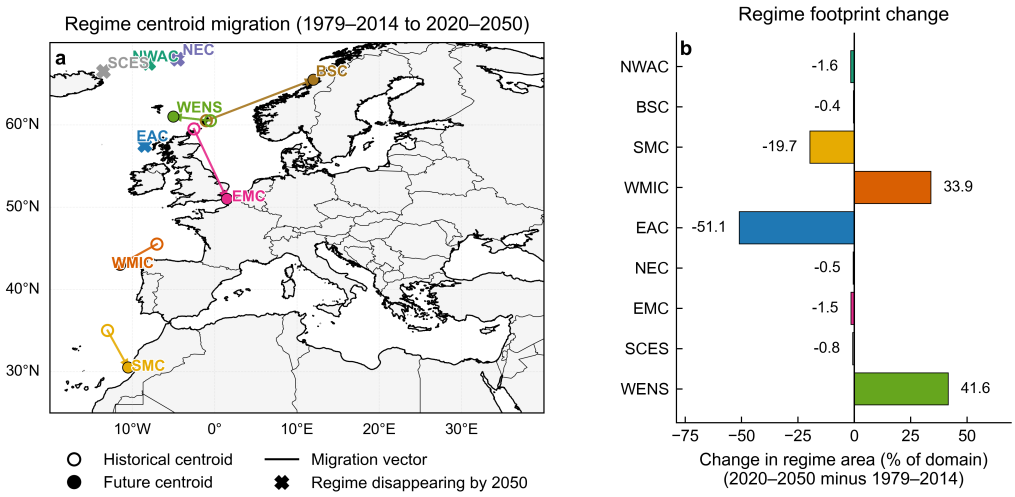

Figure 4.5 Centroid migration and regime footprint changes between the historical (1979–2014) and future (2020–2050) EC-Earth3P-HR simulations. (a) Displacement vectors for historical and future centroids. Asterisks indicate regimes with negligible future coverage. (b) Relative change in regime area as a percentage of the domain.

4.3.3 Physical Drivers of wind–wave Regime Change

Future changes in the wind–wave environment were examined using spatial differences in significant wave height (ΔH_s) and 10 m wind speed (ΔU_{10}) between the historical and future periods (Fig. 4.6). These two variables represent the main contributors to the multivariate regime structure and therefore provide context for the centroid and footprint changes described in Section 4.3.2.

Positive ΔH_s values occur across the northern North Atlantic, with increases generally exceeding 0.6 m in the subpolar region. These areas coincide with the regions where WENS and WMIC expand in the future classification. Negative ΔH_s values appear in the eastern subtropical Atlantic and the western Mediterranean, consistent with reduced future coverage of SMC and EAC.

Changes in 10 m wind speed show a similar spatial pattern. U_{10} strengthens by 4–6 m s^{-1} across the North Sea, Norwegian Basin, and northern Bay of Biscay, while weaker winds are found in parts of the Mediterranean and Iberian coastal zones. Areas of wind strengthening overlap with regions of increased H_s, while areas of wind weakening align with regions showing reduced regime stability in earlier sections.

The ΔH_s and ΔU_{10} anomalies are spatially consistent with the future regime redistribution. Regions with increased wind and wave forcing correspond to the expanded footprints of

WENS and WMIC, whereas regions with reduced forcing correspond to the contraction or disappearance of several semi-enclosed regimes.

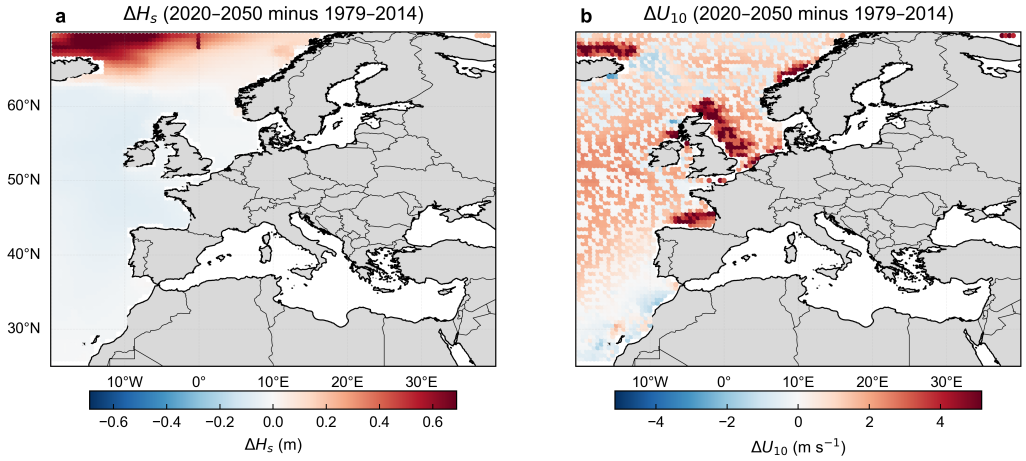

Figure 4.6 Spatial differences in significant wave height (ΔH_s) and 10 m surface wind speed (ΔU_{10}) between historical (1979–2014) and future (2020–2050) EC-Earth3P-HR simulations. Positive values denote increases in wave and wind forcing; negative values indicate regional decreases.

4.3.4 Seasonal Stability and Regime Changes

Seasonal variability in the wind–wave climate was evaluated using the Seasonal Regime Stability Index (SRSI), defined as the Euclidean distance between seasonal-mean and annual-mean wind–wave states in standardized (H_s, T_{02}, U_{10}) space. Positive anomalies in ΔSRSI indicate reduced seasonal stability, while negative values reflect increased similarity between seasonal and annual states. Figure 4.7 shows the spatial distribution of ΔSRSI for winter (DJF), spring (MAM), summer (JJA), and autumn (SON).

Across winter and spring, positive ΔSRSI values appear over large areas of the Northeast Atlantic, particularly west of Ireland and south of Iceland, indicating that seasonal states in these regions diverge more strongly from their annual means in the future period. Smaller positive anomalies extend into the central Northeast Atlantic during both seasons.

Summer exhibits the largest changes. ΔSRSI values exceed 1.5 across the Norwegian Sea and northern North Sea, representing the strongest reduction in seasonal stability among all seasons. Autumn shows weaker but still positive anomalies along parts of the western European shelf.

Negative ΔSRSI values are found in parts of the subtropical eastern Atlantic and the western Mediterranean, indicating increased seasonal coherence in these regions.

The results show reduced seasonal stability in northern and northeastern areas-particularly during summer-while several southern and semi-enclosed basins show little change or increased seasonal uniformity. At the regime level, regions with large positive ΔSRSI values largely overlap with the future footprints of WENS and WMIC, whereas areas associated with SMC- and EAC-type conditions show small or negative ΔSRSI, indicating more seasonally coherent wind–wave states in the subtropical eastern Atlantic and parts of the western Mediterranean.

4.3.5 Future wind–wave Resource Evolution

Projected changes in wind and wave forcing were assessed using deep-water wave power ($H_s^2 T_{02}$) and hub-height wind energy (U_{100}^3), evaluated for both historical (1979–2014) and

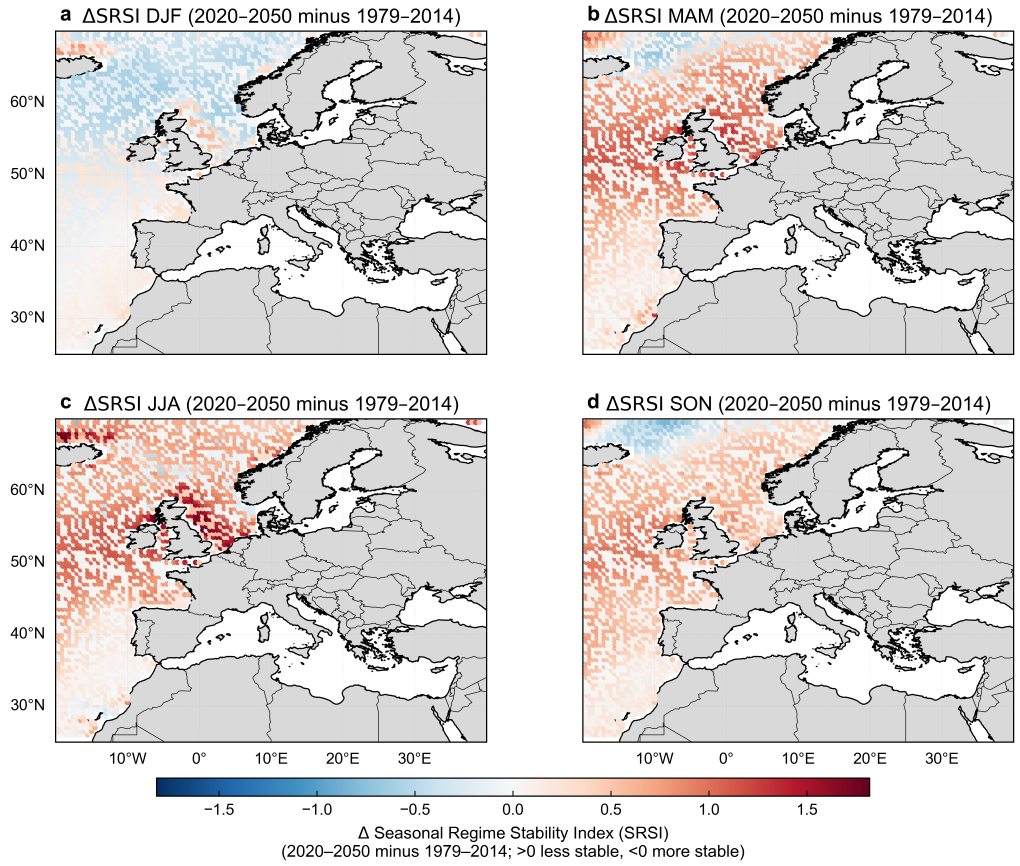

Figure 4.7 Spatial changes in the Seasonal Regime Stability Index (SRSI) between the historical (1979–2014) and future (2020–2050) EC-Earth3P-HR periods for (a) winter (DJF), (b) spring (MAM), (c) summer (JJA), and (d) autumn (SON). Positive anomalies (ΔSRSI > 0) indicate reduced seasonal stability; negative anomalies indicate increased seasonal coherence.

near-future (2020–2050) periods. Figure 4.8 summarises the spatial distribution of these changes.

Both wave power and wind energy exhibit coherent increases across the Northeast Atlantic, northern North Sea, and Norwegian Sea, with positive anomalies extending from the subpolar basin into the entrance of the North Sea. These enhancements reflect regions where future $H_s^2 T_{02}$ and U_{100}^3 exceed their historical climatology. In contrast, parts of the southern European shelf—including the Iberian coastal margin and the western Mediterranean—show small reductions in both metrics.

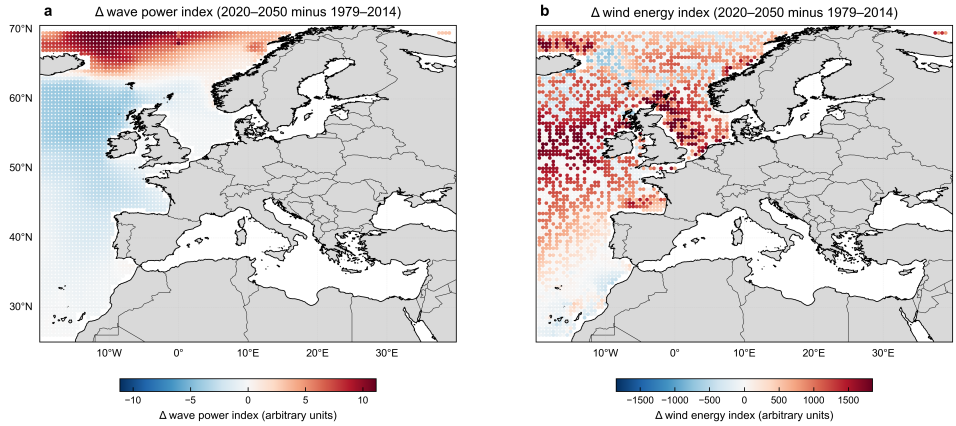

Figure 4.8 Spatial changes in (a) deep-water wave power index ($H_s^2 T_{02}$) and (b) hub-height wind energy index (U_{100}^3) between the historical (1979–2014) and future (2020–2050) EC-Earth3P-HR simulations. Positive values indicate increased offshore energy potential under future forcing; negative values denote declines in wave or wind resource strength.

To understand how these forcing changes manifest within the historical regime structure, future energy values were sampled on the historical regime footprints. Cluster-average differences are shown in Fig. 4.9. Northern and open-ocean regimes (NEC, WENS, WMIC, EMC) exhibit the largest positive changes in both wave and wind energy, consistent with their expanded future coverage and enhanced exposure to stronger winds. Semi-enclosed and southern regimes (SMC, EAC, BSC) show small or negative mean changes, indicating weaker local wind forcing and limited capacity for future wave growth. These contrasts highlight a northward concentration of future energy gain within regions most influenced by storm-track winds.

To integrate both energy magnitude and temporal robustness, a hybrid wind–wave classification was developed using z-scored energy indices together with the Seasonal Regime Stability Index (SRSI). Four hybrid classes—Primary, Secondary, Hotspot, and Low—characterise the combined influence of mean energy and seasonal-to-interannual coherence (Fig. 4.10).

Historically, Primary conditions occupy a small sector of the Northeast Atlantic, whereas Secondary conditions dominate most of the basin. Under future forcing, Primary regions expand into the Norwegian Sea and parts of the subpolar North Atlantic. Hotspot regions, defined by high energy but low stability, increase around the northern British Isles and the northern entrance of the North Sea, aligning with regions of reduced seasonal stability (Section 4.3.4). Low-class areas contract, particularly in southern basins where stability improves or energy increases modestly.

The transition matrix in Fig. 4.11 quantifies how individual grid points shift between hybrid classes. Historical Low sites predominantly transition to the Secondary class, indicating increased energy or stability at the weakest locations. The Secondary class is the most persistent

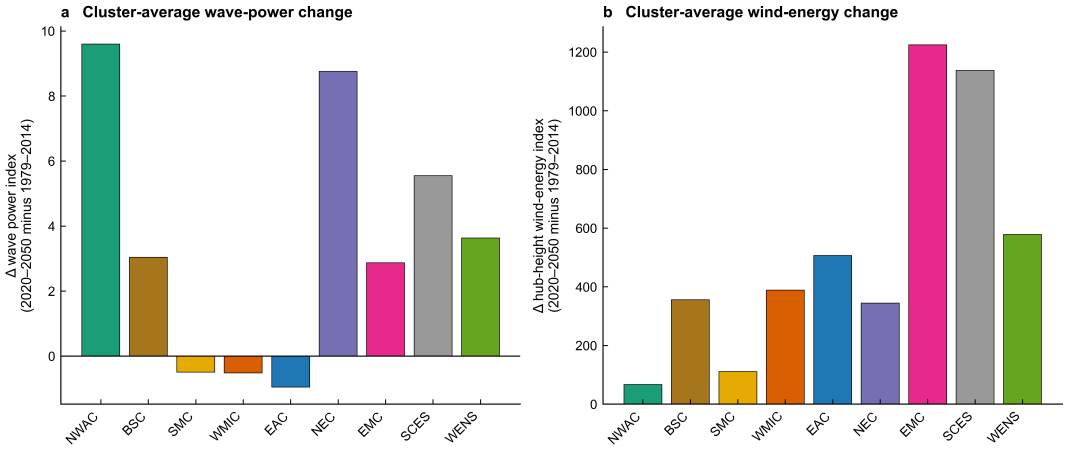

Figure 4.9 Cluster-average changes in (a) wave power index and (b) hub-height wind energy index, computed on historical (1979–2014) regime footprints. Northern and open-ocean regimes exhibit the strongest increases in both metrics, while semi-enclosed and southern regimes show limited or negative changes.

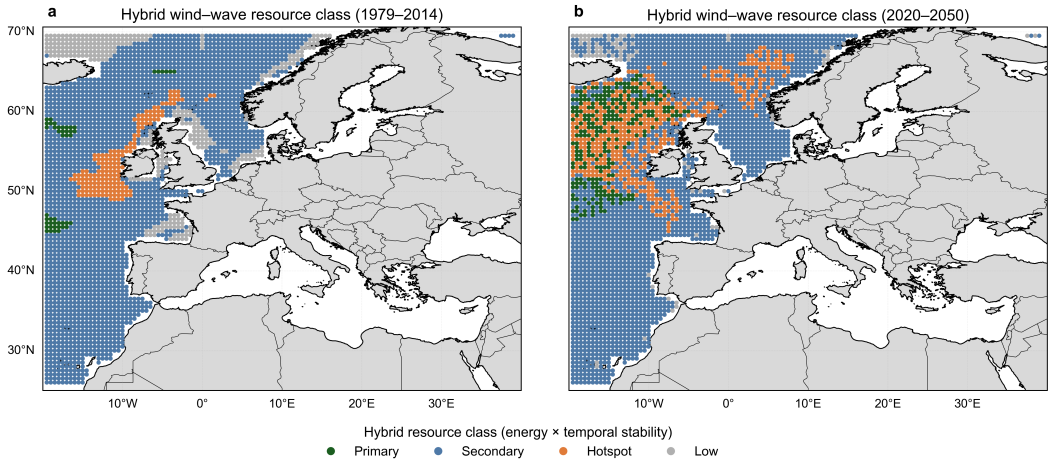

Figure 4.10 Hybrid wind–wave resource classes for (a) the historical (1979–2014) and (b) future (2020–2050) periods, combining normalized energy indices with seasonal stability. Future conditions show increased Primary coverage in northern basins, growth of Hotspot regions around the British Isles, and a contraction of Low-resource areas.

category, with most points remaining Secondary and a notable fraction transitioning to Hotspot. Historical Hotspot points split between remaining Hotspot and reverting to Secondary. Primary conditions show limited persistence and mostly transition toward Secondary or Hotspot categories.

The transitions indicate a reduction in Low classifications and increased representation of Secondary and Hotspot classes in the future, while Primary conditions remain spatially restricted but increase slightly in extent.

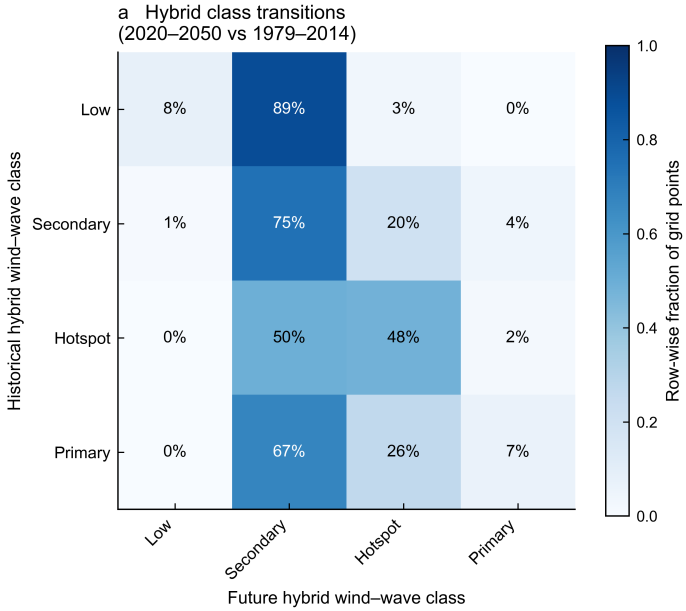

Figure 4.11 Row-normalised transition matrix between historical (1979–2014) and future (2020–2050) hybrid wind–wave resource classes. Values denote the fraction of grid points in each historical class that transition to each future class.

Future wind–wave energy becomes increasingly concentrated in northern offshore corridors, accompanied by reduced seasonal persistence in high-energy regions. Southern basins experience comparatively weak changes. The combined diagnostics indicate a reorganization toward stronger, more variable wind–wave resources in areas most affected by enhanced storm-track activity.

These patterns are consistent with projected changes in North Atlantic atmospheric circulation reported in previous CMIP6-based studies, where enhanced storm-track activity and stronger westerly forcing contribute to increased wave generation and wind-energy potential across northern European basins *[Morim et al., 2019, Meucci et al., 2024, Casas-Prat et al., 2024a]*. In the present analysis, the strongest increases occur in Atlantic-influenced and open-ocean regimes, particularly around the North Sea and Norwegian Basin, where larger effective fetches and persistent wind forcing favour simultaneous increases in wave power and hub-height wind energy. In contrast, semi-enclosed and southern basins exhibit comparatively weak responses, likely due to fetch limitation, reduced storm persistence, and stronger control by regional circulation and coastline geometry. Overall, the results suggest a future reorganization toward increasingly energetic but also more variable wind–wave conditions within northern offshore corridors, while southern regimes remain comparatively stable.

4.4 Summary and Conclusions

This study examined how European wind–wave regimes evolve under near-term climate forcing by projecting EC-Earth3P-HR simulations for 2020–2050 onto the fixed ERA5-based clustering framework. Using a consistent PCA–cluster structure preserves the physical interpretation of the nine historical regimes and enables a direct comparison of future changes without recalibrating the classification. The results reveal that the future wind–wave climate occupies only five of the nine historical regimes, indicating a consolidation of dynamical environments across the domain despite most grid points retaining their original labels.

The most substantial reorganisations arise from the expansion and northeastward migration of the WENS and WMIC regimes. These regimes gain extensive future coverage and become the dominant wind–wave environments, whereas several transitional and semi-enclosed regimes-particularly NEC, SCES, and BSC-contract sharply or vanish. This redistribution reflects a broader poleward shift of mixed and open-ocean conditions linked to strengthened storm-track winds and enhanced wave generation in northern basins.

Changes in significant wave height and surface wind speed support this interpretation. Increased forcing across the Northeast Atlantic, northern North Sea, and Norwegian Basin aligns with the expanded footprints of WENS and WMIC, while weaker forcing in the subtropical eastern Atlantic and western Mediterranean corresponds to reduced representation of SMC- and EAC-type states. Seasonal stability diagnostics further indicate diminished coherence in northern regions-most strongly during summer-and enhanced stability in parts of the southern domain. These seasonal shifts help explain the contrasting persistence and reorganisation of regimes.

Diagnostics of wave power and wind energy show marked increases in the northern basins, particularly within open-ocean and mixed regimes, while southern and semi-enclosed regions exhibit limited or negative changes. Integrating energy magnitude with seasonal stability into a hybrid classification reveals an expansion of Primary and Hotspot zones in northern areas and a contraction of Low-resource regions. Secondary conditions remain widespread but become more variable in several mid-latitude regions.

The analysis indicates a future concentration of hybrid wind–wave potential in northern offshore corridors that experience both strengthened forcing and reduced temporal persistence. These findings underline the importance of considering regime behaviour, stability, and coupled wind–wave dynamics when evaluating offshore resource suitability. Although based on a single high-resolution model, the ERA5-derived clustering framework provides a robust and interpretable basis for assessing future transitions and offers a consistent tool for linking climate-driven changes to offshore planning and adaptation strategies.

4.4.1 Implications for bias-correction practices and interpretability

The regime-based framework used here is intentionally comparative: both historical (1979-2014) and near-future (2020-2050) states are analysed within the same model configuration and classified in a fixed ERA5-derived PCA-cluster geometry. This design supports physically interpretable change diagnostics (RTI, centroid migration, and footprint change) without introducing additional statistical transformations. In this context, bias correction should be applied with caution, because methods that adjust marginal distributions locally can also alter the joint wind–wave structure that defines regime identity.

A key question is whether a given bias-correction approach preserves the *spatiotemporal structure* of the coupled climate signal. If correction modifies spatial gradients, seasonal contrasts, or the covariance between wind and waves, it can shift grid points in feature space and therefore change regime labels and transitions-even when the underlying dynamical

evolution is unchanged. This is particularly relevant in regions where the analysis already indicates reduced seasonal coherence (e.g., the northern basins in summer; Fig. 4.7), because such areas are more sensitive to changes in the joint distribution of wind and wave states. Conversely, bias correction that is explicitly multivariate and structure-preserving may be more compatible with regime-based assessments, as it aims to retain physically meaningful relationships while reducing systematic offsets.

The results emphasize that future resource conclusions depend not only on changes in mean wind or wave magnitude, but also on whether the coupling and persistence of wind–wave states are maintained. For climate-aware offshore assessments, this motivates using correction strategies that either (i) operate on the joint wind–wave space or (ii) explicitly validate that key regime diagnostics (spatial patterns, seasonal stability, and transition statistics) remain consistent before and after correction.

Acknowledgments

The United States Geological Survey (USGS) is acknowledged for providing access to the CMIP6 MIP simulations used in this study. The European Centre for Medium-Range Weather Forecasts (ECMWF) is acknowledged for making the ERA5 reanalysis dataset available. Bathymetric information was obtained from the General Bathymetric Chart of the Oceans (GEBCO). Additional spatial layers were sourced from the Marine Ecoregions of the World (MEOW) and Exclusive Economic Zones (EEZ) datasets.

5

Machine Learning–Based Selection of CMIP6 Wind Forcing

"Information is the resolution of uncertainty."

- Claude E. Shannon

"If you cannot measure it, you cannot improve it."

- Lord Kelvin

This chapter presents a data-driven framework for the evaluation and selection of CMIP6 near-surface wind datasets to support wave climate modelling. Recognising that uncertainties in atmospheric forcing propagate directly into simulated wave characteristics, the analysis focuses on objectively quantifying model performance against observational and reanalysis benchmarks. Multiple statistical metrics, including bias, root mean square error, and cosine similarity, are computed across seasonal and regional domains. To integrate these measurements into a unified and objective ranking, a machine-learning–assisted KD-tree nearest-neighbour approach is applied in multi-metric error space. In this context, information derived from multi-dimensional metrics reduces uncertainty in model choice, while measurement provides the basis for systematic improvement. The selected wind forcing establishes a robust and defensible foundation for the wave climate simulations presented in the subsequent chapter.

This chapter is based on:

MAYA, P., & LAVIDAS, G. (2022). Nearest Neighbor Techniques for the global and regional statistical analysis of high temporal resolution CMIP6 surface wind speed with ECMWF reanalysis and satellite winds. *OTEC: Saga University Institute of Ocean Energy Report*, (27), 113-125.

5.1 Introduction

Climate change is altering global wind patterns, which in turn influence ocean wave climates and affect the viability of offshore renewable energy resources, particularly wave energy *[Morim et al., 2019, Casas-Prat et al., 2024b]*. Because ocean waves are primarily generated by atmospheric wind fields, accurate evaluation and projection of offshore wave energy potential require reliable climate model outputs. Multi-model climate projections, coordinated through the Coupled Model Intercomparison Project (CMIP), provide a standard framework for evaluating and comparing simulations from different modelling centres. In this context, the latest phase, CMIP6, offers improved capability to simulate complex climate processes compared to the previous generation, CMIP5 *[Eyring et al., 2016, Zelinka et al., 2020]*.

Despite the advancements in CMIP6, discrepancies remain due to modelling uncertainties, including differences in physics parameterizations, numerical implementations, and spatial resolution. These factors influence how internal climate variability and responses to external forcing are represented. While internal (natural) variability can be characterised from historical simulations, its future evolution is inherently uncertain and requires comprehensive uncertainty assessment. Scenario uncertainty-arising from differences in assumed future greenhouse gas emissions (e.g., across the Shared Socioeconomic Pathways, SSPs)-further contributes to divergence in simulated climate responses *[Olauson, 2018, Zelinka et al., 2020]*. Together, these sources of uncertainty complicate the reliable assessment of offshore renewable energy potential.

Variability in simulated wind fields propagates through wave models, introducing uncertainty in estimates of wave energy potential *[Meucci et al., 2024]*. Previous studies highlight the importance of selecting appropriate climate models for renewable energy applications, particularly when regional-scale accuracy is required *[Martinez and Iglesias, 2022, Lobeto et al., 2021]*

Climate model evaluation has traditionally relied on statistical comparisons between simulations and observations. Common metrics include mean bias, root mean square error (RMSE), correlation coefficients, and normalized RMSE (NRMSE). While these methods provide useful information on model performance, they can be computationally intensive and are sensitive to the choice of spatial and temporal scales *[Goyal et al., 2021, Akinsanola et al., 2021]*. Moreover, they do not fully represent the multidimensional nature of model uncertainty, which can make it difficult to identify models that perform consistently well across multiple evaluation criteria. Model performance can also vary with the region of interest and the specific requirements of wave energy applications *[Li et al., 2020, Tokarska et al., 2020]*.

Conventionally, climate model evaluations for historical periods relied heavily on statistical comparisons and observational validations, often using performance metrics such as biases, correlation coefficients, root mean square errors (RMSE), and Taylor diagrams (Gleckler et al., 2008). For instance, comprehensive assessments of CMIP3 and CMIP5 models have systematically documented model performance, strengths, and limitations, providing foundational insights into their capability to represent past climate conditions (Flato et al., 2013; Gleckler et al., 2008). However, with increasing model complexity and data dimensionality, traditional statistical methods face limitations in efficiently handling large, multidimensional datasets. To

address these limitations, recent advancements in machine learning offer promising solutions. Algorithms such as decision trees, K-nearest neighbors (KNN), and K-dimensional trees (KD-trees) have emerged as efficient tools for robustly and objectively comparing model outputs against observational data *[Song et al., 2022, Mousa and Hussein, 2022]*. Integrating these machine learning frameworks allows us to systematically and rapidly identify climate models that best replicate observed wind patterns, thereby reducing uncertainty in wave climate simulations.

In this context, the primary objective of this chapter is to systematically evaluate historical wind datasets from the Coupled Model Intercomparison Project Phase 6 (CMIP6). We utilize conventional statistical metrics for baseline comparisons and introduce a KD-tree-based nearest neighbor machine learning approach to address the inherent complexity and dimensionality of climate model data. The added value of this KD-tree-based method lies in its ability to efficiently handle large, multidimensional datasets, objectively ranking models based on multiple simultaneous criteria. This method complements traditional statistical approaches by providing a rapid, robust, and holistic assessment, clearly identifying the closest matches to observed wind conditions and thus enhancing the precision of model selection.

The remainder of the chapter proceeds as follows. Section 5.2 (Methods) introduces the datasets and methodology, detailing the CMIP6 wind models examined, the observational and reanalysis reference datasets used for model validation, and thorough implementation of the KD-tree algorithm for multi-metric evaluation. Section 5.3 presents the evaluation outcomes, comparing each climate model's performance in reproducing historical wind characteristics and providing a detailed analysis of the results.

Within Section 5.3, a particular focus (subsection 5.3.2) is a critical assessment of cosine similarity as one of the performance metrics. This analysis examines the strengths and limitations of using cosine similarity and provides a performance-based ranking of the climate models at both global and regional (Northeast Atlantic) scales. Finally, Sections 5.4 and Section 5.5 synthesize the evaluation's principal findings by identifying the most suitable CMIP6 wind dataset for the Northeast Atlantic and outlining the key conclusions, including a recommendation of the optimal dataset for subsequent wave modeling. These conclusions form the foundation for Chapter 6, where the chosen wind dataset drives wave simulations in the Northeast Atlantic, enabling exploration of climate change impacts on wave energy resources in that region.

5.2 Data and Methods

The model selection criteria are described in Section 5.2.1, where *EC-Earth3* is intentionally excluded to avoid redundancy with earlier chapters. Section 5.2.2 introduces the observational and reanalysis datasets used for reference, along with the preprocessing steps applied. The evaluation metrics-bias, RMSE, and cosine similarity-are defined in Section 5.2.3 to assess model–observation agreement across scales. Finally, Section 5.2.4 outlines the KD-tree–based nearest-neighbor method used to rank models based on their combined performance in metric space.

5.2.1 Selection of CMIP6 Models

The *EC-Earth3* simulations were intentionally excluded from this multimodel assessment, as their performance has already been thoroughly examined in both standard and high-resolution configurations in Chapters 2, 3, and 4. This chapter concentrates on the remaining CMIP6 models to ensure a broader inter-model comparison and to avoid methodological redundancy.

To assess climate model uncertainty in simulating near-surface wind patterns, we selected

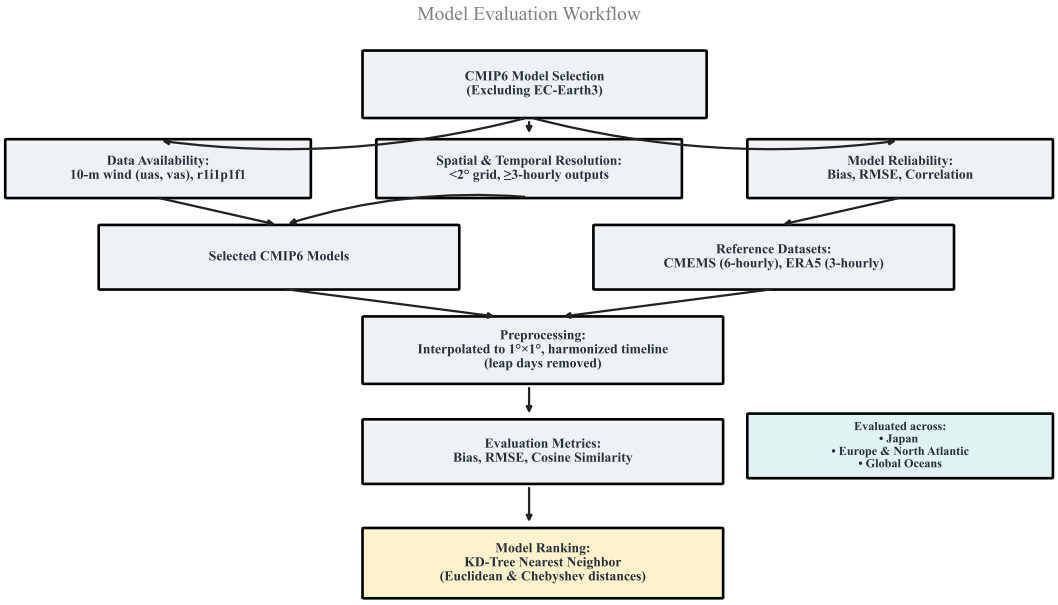

Figure 5.1 Model evaluation workflow. CMIP6 models (excluding EC-Earth3) are selected based on data availability, resolution, and reliability. After preprocessing, model outputs and reference datasets (CMEMS and ERA5) are compared using bias, RMSE, and cosine similarity. Model performance is ranked using KD-tree nearest-neighbor distances in metric space.

a subset of CMIP6 historical model outputs based on the following criteria:

(1) Data availability: Only models that provide both eastward (*uas*) and northward (*vas*) 10-m wind components for the historical period were included. We used the first ensemble member (r1i1p1f1) from each model to maintain consistency across the multi-model ensemble.

(2) Spatial and temporal resolution: We retained only those models that provided wind output at sufficient spatial and temporal resolution to capture regional wind variability and support robust model–observation comparisons. Specifically, models were required to have a horizontal resolution finer than 2° and provide wind components at least every 3 hours. These thresholds ensure compatibility with reference datasets such as ERA5 and satellite-derived products.

(3) Model reliability: We selected models from established climate modeling centers that have been widely used in the literature and have demonstrated consistent performance in previous inter-comparison studies focused on near-surface wind evaluation *[Carvalho et al., 2021, Deng et al., 2021, Zhang and Chen, 2021]*. Model reliability was assessed based on spatial bias, correlation with observations, and root-mean-square error (RMSE) in the historical wind fields. A total of 11 models were retained based on these criteria. The list of selected models and their respective institutions is provided in Table 5.1. All datasets were checked for metadata consistency, completeness of wind components, and temporal continuity before further processing for the period 1992-2014, chosen to ensure overlap between satellite, reanalysis, and all selected model outputs.

The model evaluation is conducted across three spatial domains selected for their relevance to regional and global wind–wave dynamics. The Japan domain spans 30°N–60°N and 125°E–155°E, covering the Japanese archipelago and adjacent oceanic regions influenced by mid-latitude atmospheric systems. The European and North Atlantic domain extends

Table 5.1 CMIP6 Models and Institutions

Model	Institution
IPSL-CM6A-LR	Institut Pierre-Simon Laplace, Paris, France
GFDL-ESM4	NOAA, Geophysical Fluid Dynamics Laboratory, Princeton, USA
MPI-ESM1-2-LR	Max Planck Institute for Meteorology, Hamburg, Germany
AWI-ESM-1-1-LR	Alfred Wegener Institute, Helmholtz Centre for Polar and Marine Research, Germany
MIROC6	Japan Agency for Marine-Earth Science and Technology
IPSL-CM5A2-INCA	Institut Pierre Simon Laplace, Paris, France
MPI-ESM-1-2-HAM	ETH Zurich, Switzerland
GFDL-CM4.gn	NOAA, Geophysical Fluid Dynamics Laboratory, Princeton, USA
GFDL-CM4.gr	NOAA, Geophysical Fluid Dynamics Laboratory, Princeton, USA
CMCC-CM2-SR5	Fondazione Centro Euro-Mediterraneo sui Cambiamenti Climatici, Lecce, Italy
CMCC-ESM2	Fondazione Centro Euro-Mediterraneo sui Cambiamenti Climatici, Lecce, Italy

from 20°N–75°N and 20°W–10°E, encompassing key areas for offshore wind and wave energy development along the western European margin and the eastern North Atlantic basin. The global ocean domain is defined between 60°S–60°N and 0°–360°, excluding the polar regions to focus on mid- and low-latitude ocean basins where wind forcing plays a dominant role in shaping the wave climate.

5.2.2 Observational and Reanalysis Datasets

We used two reference datasets to evaluate and benchmark the CMIP6 near-surface wind simulations:

(1) Satellite-derived Winds (CMEMS): We used the Copernicus Marine Environment Monitoring Service blended ocean surface wind product, which merges calibrated observations from scatterometers and radiometers to produce continuous 10-m height wind fields at 6-hourly intervals from 1992 to 2014. This dataset integrates data from multiple satellite missions-including ESA's ASCAT, NASA's QuikSCAT/RapidScat, and ISRO's OceanSat-2-providing a robust observational record over the global oceans.

(2) Reanalysis Winds (ERA5): We also employed the ERA5 reanalysis from ECMWF, using 10-m wind component data at 3-hourly intervals for the period 1992–2010. ERA5 offers high spatial and temporal resolution and is widely recognized for its reliability in representing wind climatology, making it a suitable secondary benchmark.

To enable consistent comparisons, all model and reference datasets were interpolated to a common $1^\circ \times 1^\circ$ latitude–longitude grid using bilinear interpolation. Temporal resolution differences were reconciled by resampling all datasets to a uniform 6-hourly timeline (matching the satellite product). Leap days (February 29) were removed to standardize time series lengths

across models and reference datasets using a consistent 365-day calendar. These preprocessing steps yielded co-registered spatial and temporal datasets, enabling point-by-point comparisons between models and observations.

5.2.3 Evaluation Metrics

We used a set of standard metrics to quantify discrepancies between CMIP6 models and reference datasets:

- **Bias:** The mean signed difference between modeled and observed wind speeds, highlighting systematic over- or underestimation:

$$\text{Bias} = \frac{1}{n}\sum_{i=1}^{n}(M_i - O_i) \tag{5.1}$$

  where M_i and O_i are modeled and observed wind speeds, respectively.

- **Root Mean Square Error (RMSE):** Measures the typical magnitude of errors, incorporating both bias and variability:

$$\text{RMSE} = \sqrt{\frac{1}{n}\sum_{i=1}^{n}(M_i - O_i)^2} \tag{5.2}$$

- **Correlation (Cosine Similarity):** Assesses the spatial pattern agreement between model and observations, independent of magnitude:

$$\text{Cosine Similarity} = \frac{\sum_{i=1}^{n} M_i O_i}{\sqrt{\sum_{i=1}^{n} M_i^2}\sqrt{\sum_{i=1}^{n} O_i^2}} \tag{5.3}$$

  This ranges from -1 to 1, with 1 indicating perfect alignment of spatial patterns.

Metrics were computed on annual and seasonal scales across all regional domains to assess both mean conditions and variability. These serve as the basis for evaluating model performance in subsequent spatial and statistical analyses.

5.2.4 Machine Learning Approach: KD-Tree Model

To objectively rank the climate models, we employed a K-dimensional tree (KD-tree) nearest-neighbor approach in the space of model error metrics. Each model's performance is represented as a vector of three evaluation metrics-bias (B), root-mean-square error (R), and correlation (C)-computed against observational data. These define a point (B, R, C) in three-dimensional space for each model.

A hypothetical perfect model-one that exactly matches observations-corresponds to the reference point $(0, 0, 1)$, indicating zero bias, zero RMSE, and perfect correlation. We measure each model's deviation from this ideal using two distance metrics:

The Euclidean distance to the reference is defined as:

$$d_{\text{Euc}} = \sqrt{(B-0)^2 + (R-0)^2 + (C-1)^2}, \tag{5.4}$$

and the Chebyshev distance as:

$$d_{\text{Cheb}} = \max\{|B-0|, |R-0|, |C-1|\}. \tag{5.5}$$

The Euclidean distance reflects the combined magnitude of all deviations, while the Chebyshev distance captures the largest single-component error. Smaller values in either metric indicate a model closer to perfect performance.

The KD-tree, originally introduced by *Bentley [1975]*, enables efficient nearest-neighbor searches in this error space. We used the `KDTree` implementation from scikit-learn *[Pedregosa et al., 2011]* to query the tree using the reference point $(0, 0, 1)$. The closest neighbor corresponds to the model with the smallest overall error. Extending this query yields a complete ranking of all models based on their distance from the ideal point. This method is non-parametric and training-free: it requires no fitting or calibration, relying solely on direct error comparisons in metric space.

5.3 Results and Discussion

5.3.1 Seasonal Bias Analysis for the Japan Region

We first evaluated the performance of 11 CMIP6 historical models for the extended Japan coastal region by comparing simulated 10 m wind speeds with satellite-derived CMEMS winds and ERA5 reanalysis. All model outputs and reference datasets were interpolated to a uniform $1^\circ \times 1^\circ$ latitude–longitude grid and resampled to 6-hourly intervals for the period 1992–2014. This preprocessing ensured spatial and temporal consistency between the model and satellite products, which is essential for a valid point-by-point comparison and for integrating the datasets in the subsequent model ranking.

A seasonal breakdown of bias maps (Figures 5.2–5.5) shows that model errors vary substantially with season, reflecting seasonal shifts in the regional wind climate. In winter (DJF; Figure 5.2), many models exhibit pronounced positive biases in the northern offshore areas. For example, MPI-ESM1-2-LR and MIROC6 overestimate wind speeds by about 4–8 m s^{-1} in the northern and eastern parts of the Japan domain. These overestimations, shown as warm-coloured regions in the bias maps, indicate that simulated winter monsoon winds or associated storm systems are too intense in these models. In contrast, winds are underestimated in the southern sectors, underrepresenting the northerly component of the winter monsoon. This north–south dipole bias, with overly strong winds in the north and excessively weak winds in the south, appears consistently across models in winter, highlighting a common limitation in reproducing the regional winter wind patterns.

In spring (MAM; Figure 5.3), biases remain notable but exhibit more complex, model-specific spatial patterns. Many models continue to underestimate wind speeds, although the locations and magnitudes of these errors differ among models. For example, IPSL-CM5A2-INCA, IPSL-CM6A-LR, and MPI-ESM1-2-HAM display pronounced bias anomalies during this season, suggesting challenges in representing the transition from winter to spring circulation. In some cases, winter biases are reduced by spring, but new errors emerge in other parts of the domain, indicating shifts rather than complete improvements in model performance

In autumn (SON; Figure 5.5), biases are again highly model-dependent, similar to the spring patterns. Each model shows distinct regions of overestimation or underestimation, reflecting variability in the seasonal transition from summer to winter circulation. MIROC6, for instance, shifts from underestimating winds in winter to overestimating them in certain areas during autumn, indicating seasonally dependent bias characteristics. Across these varied outcomes, IPSL-CM6A-LR-INCA continues to show relatively balanced biases over most of the domain, with small and spatially uniform deviations that persist across all seasons.

Summer (JJA; Figure 5.4) shows a different behavior-a more coherent bias pattern across the model ensemble. Almost all models systematically underestimate wind speeds in the

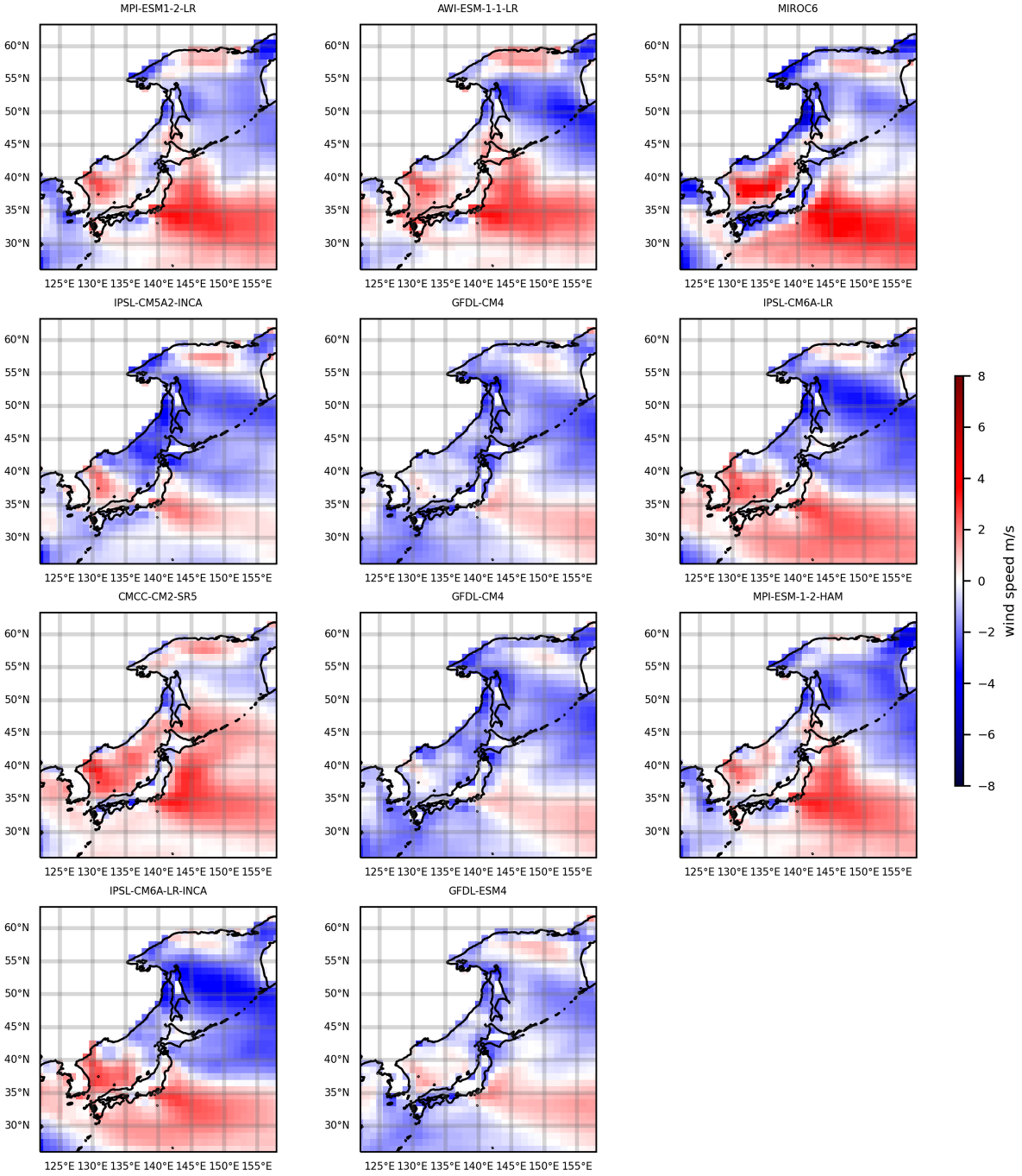

Figure 5.2 DJF wind magnitude biases (in m/s, shaded) computed using CMEMS and CMIP6 wind datasets for 1992–2014. The corresponding model names appear above each figure. Before computation, all data points were regridded to a $1° \times 1°$ latitude–longitude grid through bilinear interpolation and standardized to a uniform calendar using CDO, with leap days removed. We resampled the 11 CMIP6 model datasets to 6-hour intervals to compare them against the satellite-derived CMEMS dataset.

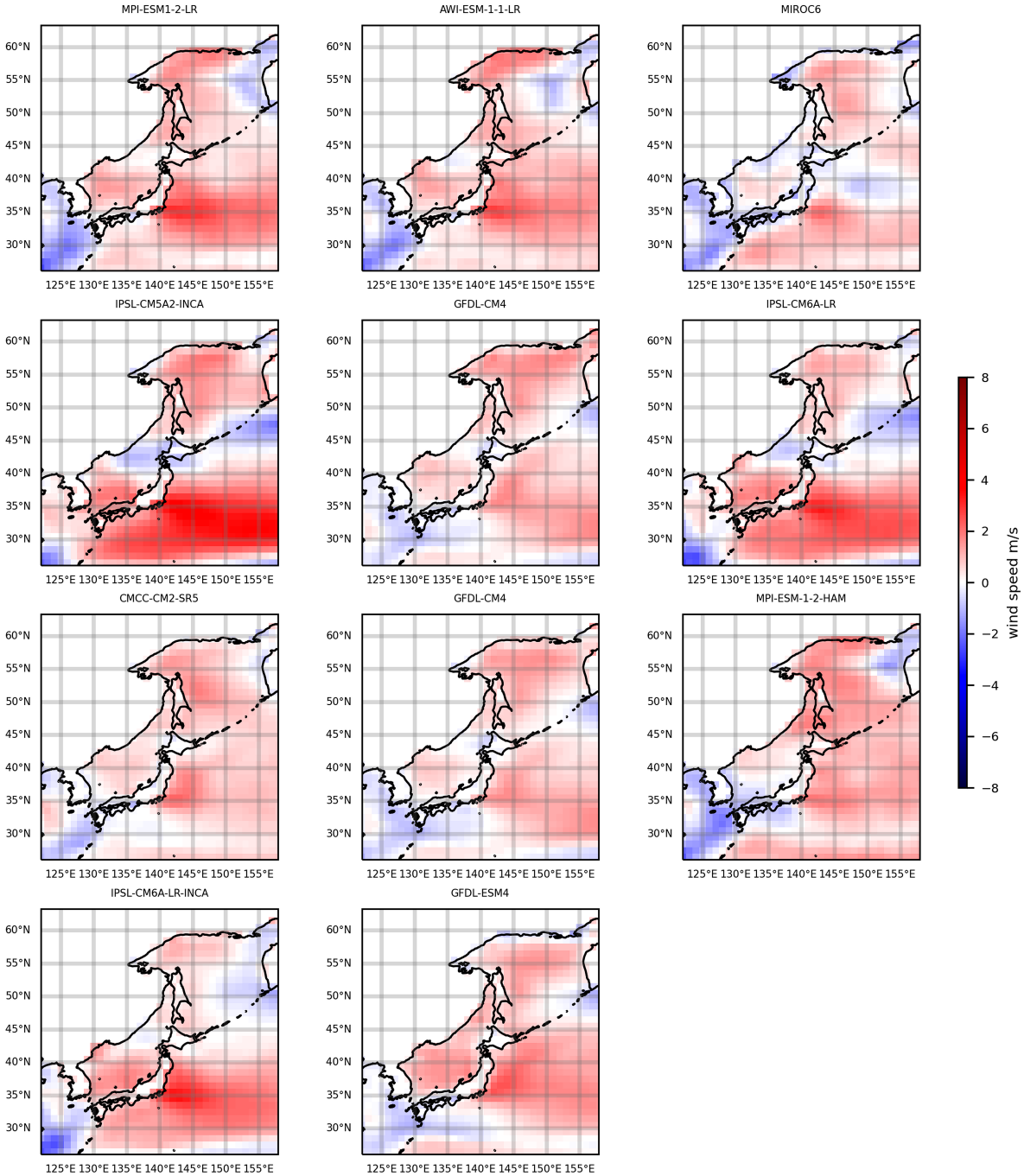

Figure 5.3 Same as Figure 5.2, but for the MAM season for the period 1992–2014.

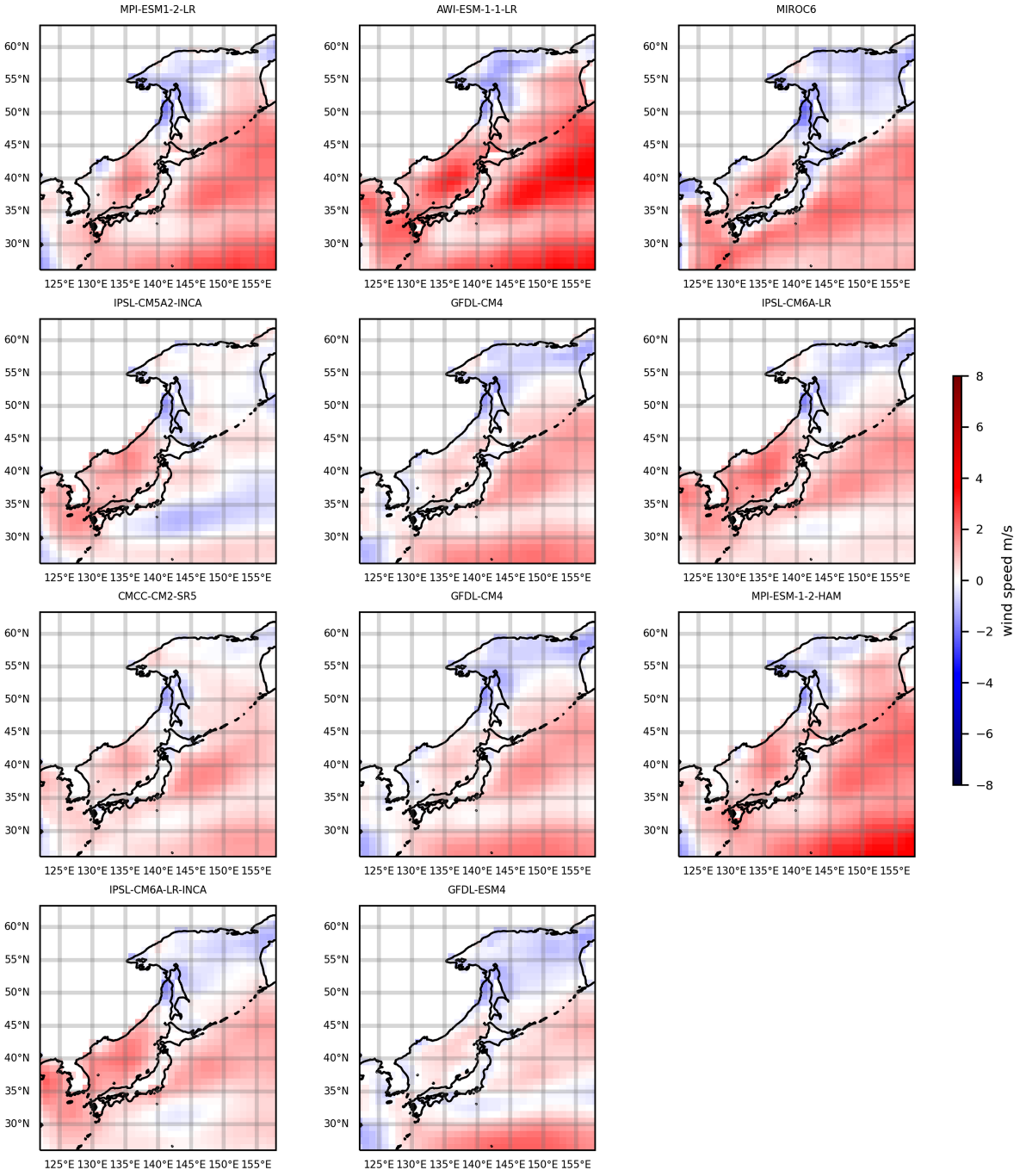

Figure 5.4 Same as Figure 5.2, but for the JJA season from 1992 to 2014.

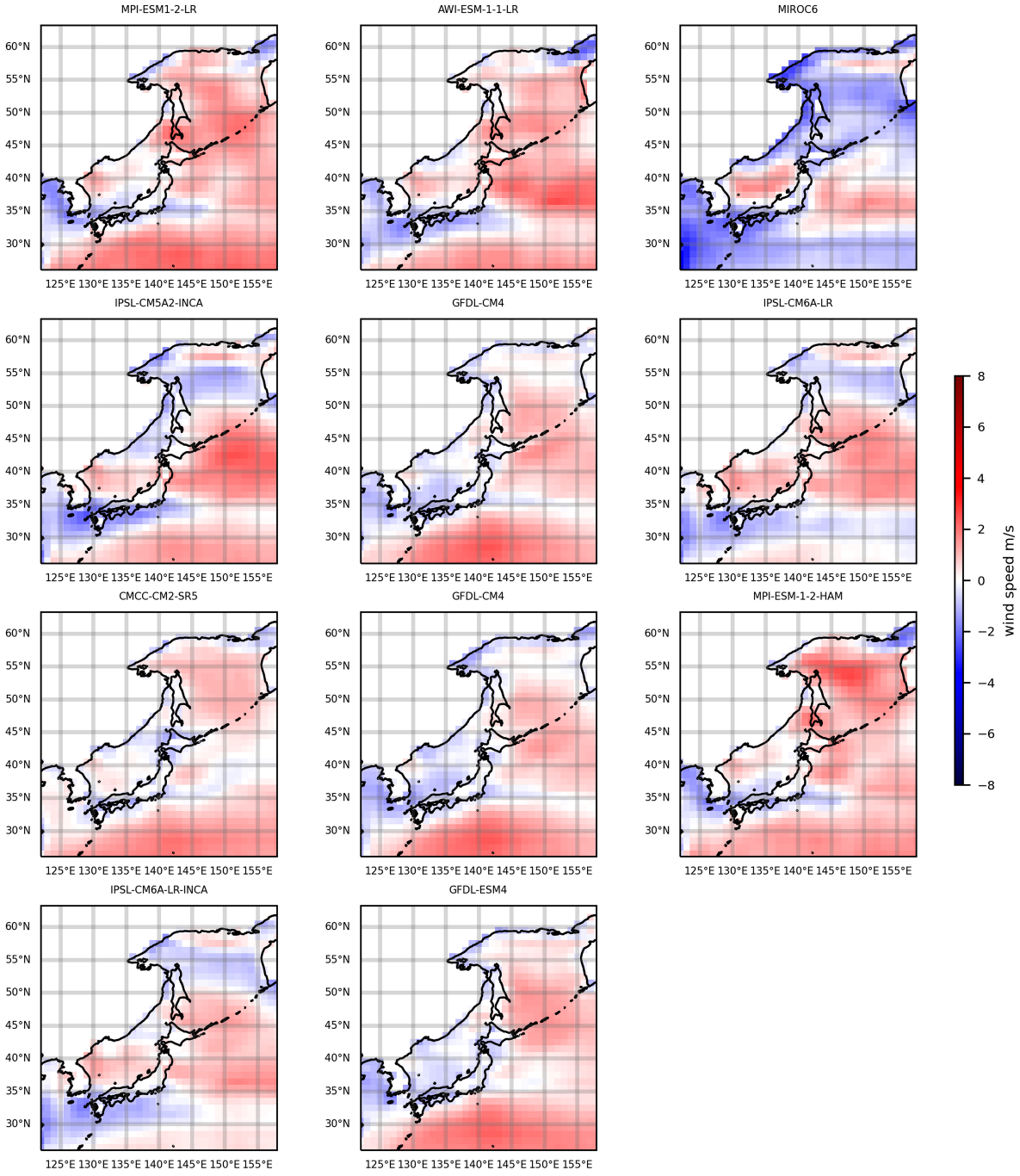

Figure 5.5 Same as Figure 5.2, but for the SON season for the period 1992–2014.

southern and southeastern offshore areas during summer while overestimating winds in the northern part of the domain. Compared to the other selected CMIP6 models, the AWI-ESM-1-1-LR and MPI-ESM-1-2-HAM show significant bias in summer. This consistent bias pattern across models suggests a shared deficiency in capturing the summer monsoonal wind gradient. One plausible cause is biases in simulating convective processes or the subtropical high-pressure system that dominates summer circulation. Notably, the magnitude of biases in summer tends to be smaller than in winter; however, their spatial consistency across models points to common shortcomings in the atmospheric physics or resolution used by the models during the summer season.

One model stands out for its relatively balanced performance amid these seasonal variations: IPSL-CM6A-LR-INCA. Throughout all four seasons, IPSL-CM6A-LR-INCA maintains smaller, more uniform biases across Japan, avoiding the significant positive or negative errors seen in other models. In other words, IPSL-CM6A-LR-INCA does not strongly over- or under-shoot the observed winds in any particular area or season over the selected domain, hinting at its robustness in simulating the regional wind climate. By contrast, every other model exhibits some pronounced weakness in at least one season or location.

This seasonal bias analysis shows that no single model performs equally well across all conditions. Some capture specific seasons or parts of the domain more accurately, while showing larger errors in others. This underlines the need for a seasonal and spatially detailed evaluation when assessing model skill. Looking only at a single season or using spatial averages can hide important errors, as opposite biases may cancel each other out in aggregated values. The strong seasonal and regional differences in the bias patterns reflect the complexity of climate model evaluation and the challenge of identifying a consistently well-performing model from bias maps or a single statistical metric. This points to the need for approaches that combine multiple performance measures to provide a more balanced and objective comparison.

5.3.2 Limitations of Traditional Performance Metrics

Traditional statistical metrics, while helpful, often fail to capture the complete picture of model performance revealed by spatial bias patterns. For example, Figure 5.6 shows the cosine similarity between observed and modeled wind fields-essentially a pattern correlation-for all 11 models. During winter (DJF; Figure 5.6a), all models yield cosine similarity values on the order of 0.98 (ranging approximately from 0.976 to 0.987), indicating that the modeled and observed wind vectors are nearly parallel on average. Similarly, high cosine similarity values occur for each season (Figure 5.6b–d), implying that all models reproduce the general spatial pattern of winds exceptionally well. At first glance, this suggests excellent performance; however, such uniformly high scores make it nearly impossible to distinguish which model is more faithful to reality. In other words, cosine similarity is overly insensitive in this context-it emphasizes directional agreement and broad spatial patterns but neglects the magnitude of biases that differentiate the models (as seen in Figures 5.2–5.5).

This illustrates a broader issue with many single-number metrics like global correlation or domain-averaged error: Different models can score similarly on these metrics despite having very different spatial bias distributions. In our analysis, even models with significant regional biases (for instance, large errors up to ± 8 m/s in parts of the Japan region) end up with nearly identical aggregate statistics, such as mean error or pattern correlation. These conventional metrics mask crucial information about where and when a model performs well or poorly. As a result, relying solely on such metrics can be misleading – they might suggest that all models are equivalently good when the bias maps tell a different story.

One common approach to overcome this problem is to compute multiple performance indices (e.g., mean bias, RMSE, correlation) for each model across various sub-regions or seasons. While this multi-metric approach is more informative than relying on a single metric,

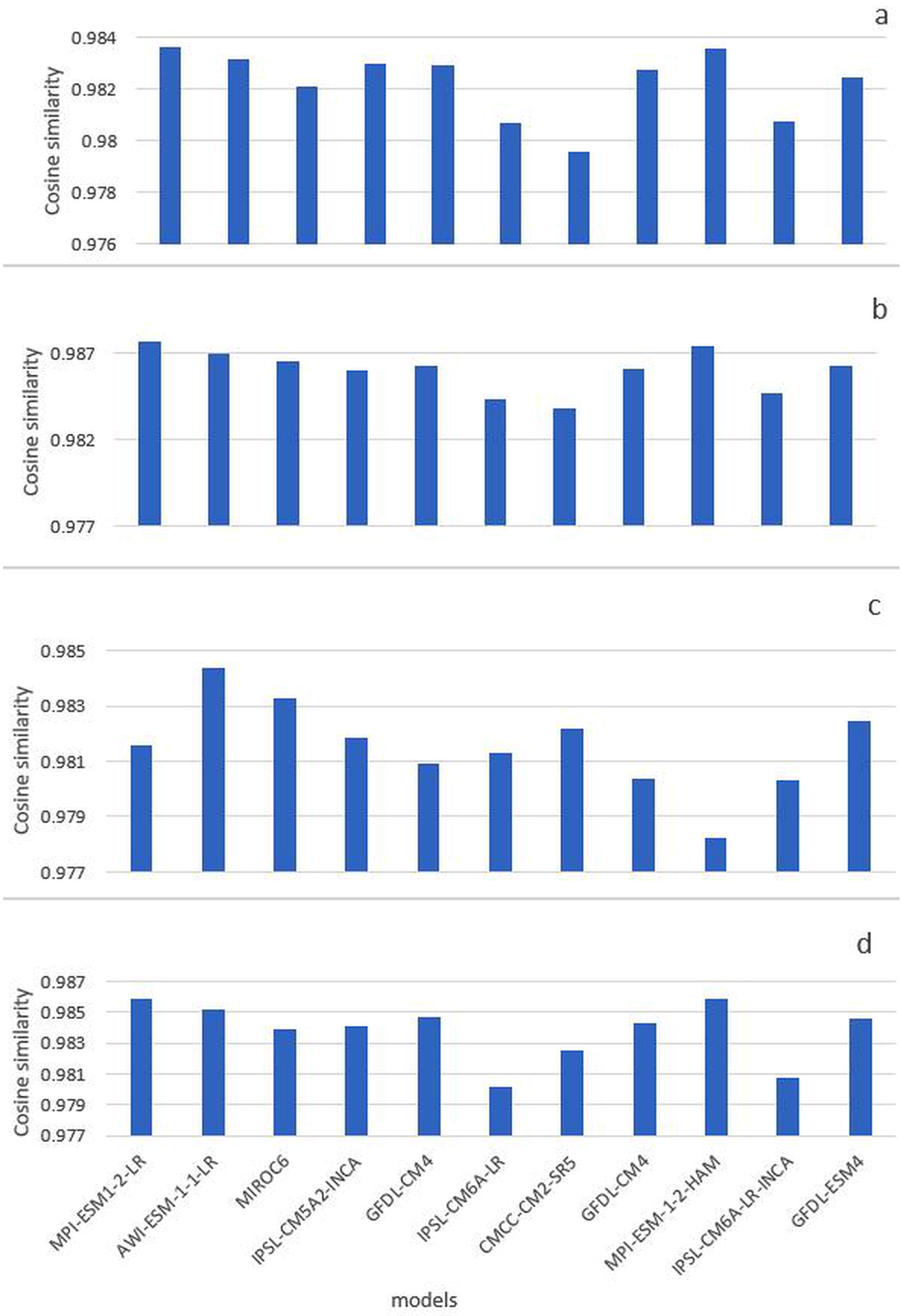

Figure 5.6 Cosine similarity of wind magnitude (in m/s) of 11 CMIP6 datasets and CMEMS satellite datasets at 10m above sea level for all the seasons from 1992–2014. (a) DJF, (b) MAM, (c) JJA, (d) SON.

it can become unwieldy and inconclusive. Different models often excel in metrics, creating a conflicting picture of "best" performance. For example, one model might have the most minor root-mean-square error while another has the highest correlation with observations, making it unclear which model is superior overall. Moreover, without a unified framework, there is no single quantitative measure of a model's overall skill – the analyst is left to weigh the importance of each metric subjectively. In summary, traditional evaluation methods struggle to provide a definitive ranking or clear selection of the best model, especially when model skill is uneven across regions and seasons. These limitations point to the need for a more robust, objective technique that can synthesize multiple aspects of performance into one coherent assessment.

The traditional error metrics were first used to examine the spatial distribution and magnitude of model biases. However, over a large domain such as Europe, these metrics are difficult to translate into a single model choice because positive and negative biases occur in different regions and seasons. Spatial averaging can therefore mask compensating errors, while visual interpretation of bias maps remains subjective. For this reason, the KDTree-based approach was introduced as an objective point-by-point comparison method. At each location and time step, the wind value from each climate model is compared with the corresponding satellite or reanalysis reference value, and the model with the smallest Euclidean distance is identified as the closest representation. Repeating this procedure across the full space–time domain provides an aggregated score of model proximity to the reference dataset. In this way, the method avoids relying only on domain-averaged statistics and provides a more systematic basis for selecting climate-model wind forcing for wave simulations.

5.3.3 Model Ranking with the KD-Tree Approach (Japan Region)

We applied this KD-tree ranking procedure separately for each observational reference dataset used for validation-the satellite-based CMEMS product and the ERA5 reanalysis. In each case, the models' bias, RMSE, and correlation were calculated against that reference, and a KD-tree nearest-neighbor search was performed to rank the models concerning the reference point $(0, 0, 1)$. The model rankings produced using the two different references were consistent with each other, indicating that the identification of the top-performing model is robust to the choice of observational dataset. This KD-tree–based framework thus provides a concise and objective way to integrate multiple error metrics into a single ranking, enabling the selection of an optimal climate model for subsequent wave simulations based purely on its bias and error characteristics.

The KD-tree nearest-neighbor evaluation in the Japan region identifies a single model as most skillful. IPSL-CM6A-LR-INCA emerges as the closest match to the observational baseline (CMEMS), exhibiting the lowest Euclidean distance (indicating minimal overall error; Figure 5.7) and the lowest Chebyshev distance (indicating the smallest peak error; Figure 5.8) among all CMIP6 models. This result implies that IPSL-CM6A-LR-INCA best reproduces both the average wind field and the extremes within this domain. Crucially, the model's top ranking remains unchanged when ERA5 reanalysis is used as the reference dataset, confirming the robustness of its superior performance across independent observational datasets. Other models exhibit larger distances (greater discrepancies), with some performing better on one metric but worse on another; none match the comprehensive fidelity of IPSL-CM6A-LR-INCA in capturing Japan's wind climate.

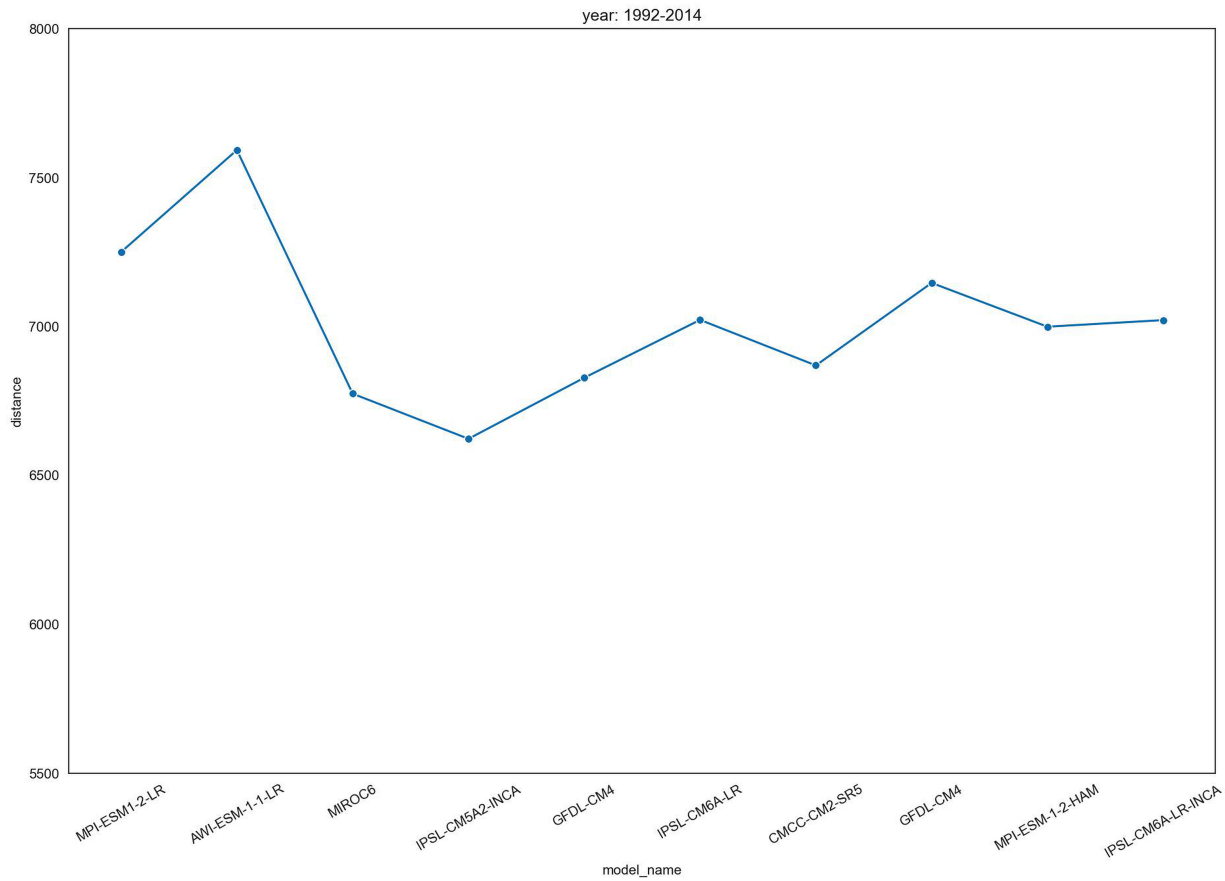

Figure 5.7 Kdtree Euclidean distance calculated (m/s) between CMIP6 datasets and CMEMS satellite merged dataset for 1992-2014. The points represent each distance of the respective model.

5.3.4 Global and European Performance Analysis

Having identified the optimal model for the Japan region, we extended the model evaluation to broader domains to see if the same model excels globally or in other regions. The KD-tree selection procedure was applied to two larger-scale domains: (1) the entire global ocean, and (2) the European and North Atlantic sector (a region of separate interest). This broader analysis reveals a notable contrast: MIROC6 emerges as the top-performing model for the global ocean winds *and* for the European/North Atlantic region, outperforming all others by the composite metrics.

In the KD-tree results for the global domain, MIROC6 consistently shows the smallest aggregated distance to the observational datasets, meaning that its overall error profile is closest to the "truth" when considering all oceans together. This holds true regardless of whether we measure distance by the Euclidean metric or by the Chebyshev metric, and it is consistent across both the satellite-based observations and the ERA5 reanalysis. In practical terms, MIROC6's wind speed errors are the least pronounced on a global scale, and it captures the observed spatial variability of winds better than its peers. A similar outcome is found for the European and North Atlantic region: MIROC6 again yields the best agreement with observations. As summarized in Figure 5.9, which compares model performance in the European domain, MIROC6 has the shortest distance to the observed wind field among all models, indicating the highest fidelity to the real regional winds.

Other models in the ensemble do show competitive performance in certain aspects or regions, but none match the across-the-board skill of MIROC6 when all evaluation criteria are considered simultaneously. For instance, one model might have slightly lower bias in a

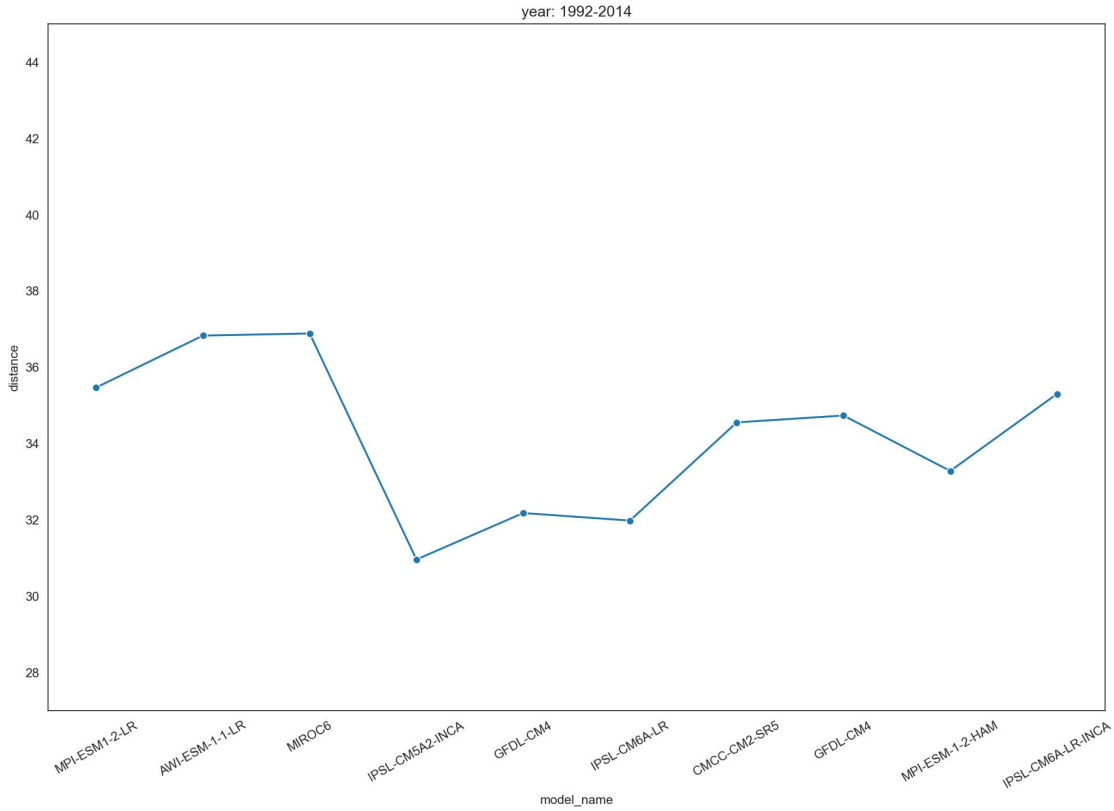

Figure 5.8 Kdtree Chebyshev distance calculated(m/s) between CMIP6 datasets and CMEMS satellite merged dataset for the period 1992-2014. The points represent each distance of the respective model.

particular sub-region or season, but at the cost of larger errors elsewhere, whereas MIROC6 achieves an excellent overall balance. The superior performance of MIROC6 at these broader scales is a significant finding. It suggests that the physical parameterizations and dynamics in MIROC6 are particularly well-suited for simulating surface wind climates on a global and mid-latitude scale, yielding realistic wind speed distributions and temporal variability. This result also validates the need for a multi-metric, spatially resolved evaluation: MIROC6 may not have the very lowest error in every single grid cell or season, but the KD-tree's holistic assessment shows that it provides the best compromise of accuracy across the entire domain.

5.3.5 Regional Dependence of Model Skill and Selection

The contrast between the Japan-focused analysis and the global/European analysis underscores a strong regional dependence in model skill. The model that performed best for the Japan coastal region (IPSL-CM6A-LR-INCA) is not the same as the one that performs best at global and European scales (MIROC6). This divergence highlights that no single climate model is universally superior for all regions; rather, each model's performance can depend on the region's particular climate features. It emphasizes the necessity of targeted regional model validation – a model should ideally be tested in the specific region of interest (and with region-specific metrics) before being chosen for impact studies in that area. Relying only on global performance metrics could lead to suboptimal choices for regional applications.

In summary, for the Japan region, IPSL-CM6A-LR-INCA was found to provide the most accurate representation of observed historical wind patterns, exhibiting the smallest errors

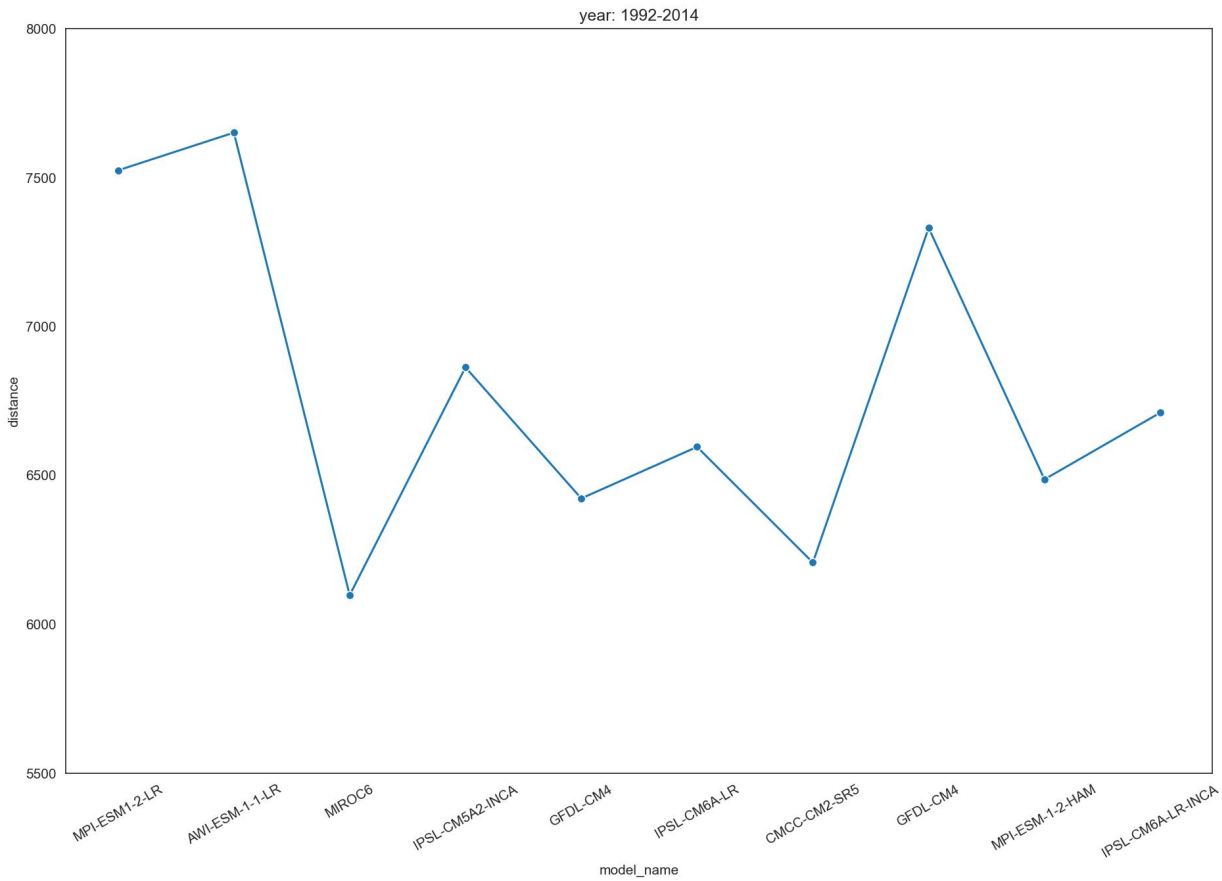

Figure 5.9 Performance of CMIP6 models in European and North Atlantic regions. MIROC6 shows the closest agreement with observed wind fields.

among the models tested. However, when evaluating across much larger scales (the global oceans and Europe), MIROC6 consistently ranked as the best-performing model. This outcome illustrates that the "best" model can vary by region: it is possible for one model to excel in a localized domain while another excels in a broader or different domain. Given MIROC6's strong overall performance across multiple metrics and its particular success in the European and global analyses, it has been selected as the preferred model to drive further analyses. In fact, MIROC6 will be used to force the wave model in the next phase of this research 6. By carrying forward the wind field from the top-ranked CMIP6 model, the subsequent wave modeling study is ensured the most reliable wind input available from our ensemble, providing a sound foundation for assessing wave climate and energy potentials without introducing unnecessary wind model biases.

5.4 Summary and Conclusion

This study set out to evaluate the performance of state-of-the-art climate models in simulating surface wind speeds and to identify a model that best represents observed wind conditions for use in wave energy research. The research was motivated by the need to include reliable climate change information in regional energy studies, given that ocean surface winds drive wave generation and thus directly impact wave energy potential. We focused on the latest CMIP6 climate models, which the IPCC 6th Assessment reports as having improved fidelity over the previous generation. The objectives were to quantify the variability of 10-m wind speeds globally and in a specific region (coastal Japan and EU), to

validate model outputs against real measurements (ERA5 reanalysis and satellite data), and to select the most suitable climate model for accurately representing regional wind climate. By addressing these aims, the study answers the key research questions on how well current climate models reproduce observed wind patterns and how a best-fit model can be efficiently identified for regional applications.

To achieve these goals, we conducted a comprehensive analysis of 11 CMIP6 historical simulations (3-hourly 10m winds) in comparison with observational datasets from 1992–2014. We applied multiple statistical metrics – including bias error and cosine similarity – to assess each model's accuracy in capturing seasonal and annual wind patterns in the Japan coastal region. The results revealed notable discrepancies: models exhibited both overestimation and underestimation of wind speeds up to about ±8 m/s when compared to the satellite-based reference, indicating significant model biases that vary by season. Interestingly, all models showed a high degree of pattern similarity to observations (cosine similarity 0.98), which means the general wind directionality and spatial patterns were well captured. However, this uniformly high similarity also implied that distinguishing the "best" model using conventional metrics alone was challenging. In other words, no single model outright dominated across all metrics, underscoring the need for a more robust selection technique.

We addressed this challenge by introducing a k-dimensional tree (KD-tree) based nearest-neighbor search as an optimal model selection method. This machine learning approach efficiently searches through the multi-dimensional space of model error metrics to find the model that is closest to the "real" data. By using distance measures (Euclidean and Chebyshev distances) on the bias-corrected wind data, the algorithm objectively identified which climate model's wind time series had the smallest overall discrepancy from observations. The KD-tree method – essentially combining k-nearest neighbors with a decision-tree search structure – dramatically reduced the computational burden of comparing every model against every data point. Through this approach, we found that one model (IPSL-CM5A2-INCA) consistently had the least error distance to the observed winds, marking it as the most faithful representation of the historical wind climate in the region. This selected model was therefore deemed pre-eminent for the study area and was used for further regional analysis.

In addition to the regional analysis over Japan, the evaluation was extended to two broader spatial domains: the global oceans and the European/North Atlantic region. In these domains, MIROC6 was found to have the lowest aggregated distance to both satellite and reanalysis datasets when assessed using multiple statistical metrics. This suggests that MIROC6 more closely represents the observed wind field at larger scales. The results highlight the spatial dependence of model performance, as the model performing best in one region may not be optimal elsewhere. While IPSL-CM6A-LR-INCA was selected for the Japan region, MIROC6 was identified as more suitable for global and European applications and was therefore used to drive the subsequent wave model simulations.

In conclusion, the study successfully met its objectives: it provided a detailed evaluation of climate model winds against real-world data and demonstrated a novel, efficient technique for model selection. These findings not only answer the research questions but also contribute to the broader field of climate model evaluation by showing how targeted regional validation and intelligent algorithms can improve confidence in using climate model outputs for renewable energy applications.

5.5 Key Takeaways

The main findings of this study are summarised below:

Region-specific evaluation Climate model skill is spatially heterogeneous. A simulation that performs well in global mean statistics can still exhibit systematic deviations at regional

scales. Evaluation against in-situ and remote-sensing observations from the target domain is essential for applications such as wave energy assessment, where regional wind speed and directional climatology influence resource estimates.

Machine learning as an objective ranking tool Rather than relying on subjective weighting of multiple performance metrics, the study uses a machine-learning–assisted nearest-neighbour approach (KD-tree) to rank CMIP6 models in a multi-metric error space. The method is training-free and fully interpretable: models are selected based on their distance to an ideal reference point (zero bias, zero RMSE, and maximum pattern agreement). This provides a transparent and computationally efficient way to synthesise several evaluation criteria into one defensible model ranking.

Relevance to wave energy modelling Selecting a model that has been regionally evaluated increases confidence in the representativeness of the wind forcing used to drive wave models. This improves the consistency of simulated wave climate statistics and subsequent energy potential estimates, which are critical for resource characterisation and marine spatial planning.

Future applications The methodology can be extended to other regions, climate variables (e.g., significant wave height, surface currents), and evaluation metrics (e.g., extreme-event frequency, calm-period duration). It can also be coupled with dynamical or statistical downscaling and ensemble approaches. Periodic re-evaluation with new climate model generations will maintain the relevance of the assessment framework.

6

Regional Wave Climate Hindcast for the North Sea and Northeast Atlantic

"The purpose of computing is insight, not numbers."

- Richard Hamming

"All models are wrong, but some are useful."

- George E. P. Box

This chapter develops and evaluates a regional wave hindcast for the North Sea and Northeast Atlantic using WaveWatch III (WW3) on a 0.25° *grid, forced by raw CMIP6 MIROC6 10-m winds for 2003–2012. Without bias correction or data assimilation, the setup provides a direct test of whether objectively selected climate-model winds can reproduce observed wave-climate statistics when dynamically downscaled through a third-generation spectral wave model. Model skill is assessed against ERA5 using complementary metrics (bias, RMSE, scatter index, IOA, and KGE), and the resulting wave-power distribution is examined to quantify regional gradients relevant for offshore renewables. Strengths, limitations, and pathways for improvement (e.g., boundary swell, wave–ice coupling, and wind refinement) are discussed to establish a consistent framework that bridges historical hindcasts and future projections.*

This chapter is based on:

MAYA, P., LAVIDAS, G., METRIKINE, A. V., & GONZÁLEZ, M. A. (2023).
CMIP6 wave climate simulation in the European North-East Atlantic Basin using WW3.
Proceedings of the 15th European Wave and Tidal Energy Conference (EWTEC 2023).

6.1 Introduction

Understanding and simulating long-term ocean wave climate is important for the design of offshore renewable energy systems and for managing coastal infrastructure. The accuracy of wave climate information directly affects structural performance, operational safety, and planning of marine installations such as wave energy converters, floating wind turbines, and coastal defences. A 10% error in significant wave height can lead to about a 20% difference in wave energy flux estimates, which affects both economic assessments and safety margins *[Osman et al., 2023]*. Wave modelling with sufficiently fine spatial and temporal resolution is therefore needed to capture regional wave patterns, coastal processes, and extreme events *[Stopa et al., 2016, Meucci et al., 2020]*.

Climate change has been associated with shifts in wave power distribution and a higher frequency of extreme wave events, often linked to changes in storm intensity and tracks *[Reguero et al., 2019, Morim et al., 2019]*. Capturing these variations remains challenging, as global climate models provide atmospheric forcing at coarse scales that do not explicitly resolve the spatial and temporal variability relevant for coastal and offshore wave simulations. This creates the need for downscaling approaches and regional wave modelling to connect global climate projections to applications at engineering scales.

Previous wave climate studies have mostly used wave models forced by atmospheric reanalysis wind datasets derived from numerical weather prediction systems and observations, or by bias-corrected climate model winds. Global wave reanalyses such as ERA5 are widely used as benchmarks for model evaluation *[Hersbach et al., 2020, Morim et al., 2022]*. In European waters, including the North Atlantic and the North Sea, reanalysis winds and direct measurements from buoys and satellites are often used to describe seasonal and interannual variability *[Wolf and Woolf, 2006, Charles et al., 2012]*. While bias correction improves agreement with observations, it also limits the evaluation of raw climate model winds and may underestimate the range of uncertainty in climate projections.

This chapter investigates the suitability of raw CMIP6 climate model winds for regional wave climate simulations, explores whether unsupervised machine learning can objectively identify better-performing climate forcings than those selected subjectively in Chapter 5, and assesses whether simulations with finer spatial resolution ($\sim$0.25°) capture key regional wave characteristics and reveal the impact of wind forcing resolution on model performance.

This study focuses on the North Sea, a region exposed to strong storms, important for offshore renewable energy, and shaped by complex coastal geometry. MIROC6, selected in 5 as the most suitable CMIP6 model for this area using a KD-tree approach, provides the wind forcing. These winds are used without bias correction or data assimilation to drive a $\sim$0.25° WW3 hindcast for the period 2003–2012, allowing the model to capture coastal effects, fetch limitations, and bathymetric influences.

The hindcast is evaluated against ERA5 wave reanalysis using multiple metrics: bias, RMSE, scatter index, Kling–Gupta Efficiency (KGE; Gupta et al., 2009), and the Index of Agreement (IOA; Willmott, 1981). This approach combining machine learning-based model selection, raw climate forcing, high-resolution wave modelling, and multi-metric evaluation offers a way to better understand climate model biases and assess how suitable raw winds are

for future wave simulations.

Section 6.2 describes the study area, MIROC6 winds, and WW3 setup. Section 6.4.2 covers the validation datasets and evaluation metrics. Section 6.5 presents the hindcast results. Section 6.5 discusses the findings in the context of climate projections and renewable energy. Section 6.6 summarises the main outcomes and suggestions for future work.

6.2 Numerical Methods and Model Configuration

The model used in this study is WW3 version 6.04, a third-generation spectral wave model. The general theoretical formulation of the spectral action balance equation solved by WW3 is described in Appendix 8.2.

For this application, the model is run on a fixed (Eulerian) latitude–longitude grid with a spatial resolution of 0.25°. Spatial propagation is computed using the third-order `PR3/UQ` finite-difference scheme, which applies a flux-based, control-volume approach to ensure conservation of wave action. A base time step of 1 h is used, chosen to satisfy the Courant–Friedrichs–Lewy (CFL) stability condition for all propagation components. The single-pass propagation algorithm in WW3 imposes the most restrictive stability requirement, as noted in the model documentation.

The third-order scheme reduces numerical diffusion compared to a first-order discretisation while mitigating the garden-sprinkler effect at high frequencies. This configuration prioritises stability, conservation, and reduced phase error, which is appropriate for a deep-water hindcast focusing on wave climate rather than fine-scale coastal processes.

6.2.1 Model configuration for the North-East Atlantic hindcast

The overall model workflow is illustrated in Figure 6.1, which summarises the numerical scheme, domain setup, atmospheric forcing, wave physics, initialization, integration, and validation procedure.

6.2.1.1 Domain and grid

The hindcast domain spans 18°N–80°N and 21°W–10°E, covering the Northeast Atlantic, European shelf seas, and the North Sea. Bathymetry is taken from the GEBCO dataset and interpolated to a 0.25° regular latitude–longitude grid (∼25 km). Coastlines are derived from GSHHS with sub-grid obstruction enabled. Open boundaries use radiative conditions, and shorelines are treated with partial reflection (`REF1`). This resolution balances computational cost and spatial detail, capturing regional gradients without the need for nested grids.

6.2.1.2 Atmospheric forcing

Surface winds are obtained from the MIROC6 climate model (CMIP6 historical run; native 2°, 3-hourly). This dataset was selected in Chapter 5 using a KD-tree–based evaluation of regional wind performance. The fields are interpolated to the WW3 grid (0.25°) using bilinear spatial interpolation (`WNX1`) and quadratic temporal interpolation (`WNT2`) to obtain hourly values. No bias correction is applied, and land points are masked to zero. No additional forcings such as currents, tides, or sea ice are included.

6.2.1.3 Wave physics and numerics

The model employs the ST4 source term package with the `STAB0` flux formulation for wind input and whitecapping *[Ardhuin et al., 2010]*, together with the DIA (`NL1`) for nonlinear

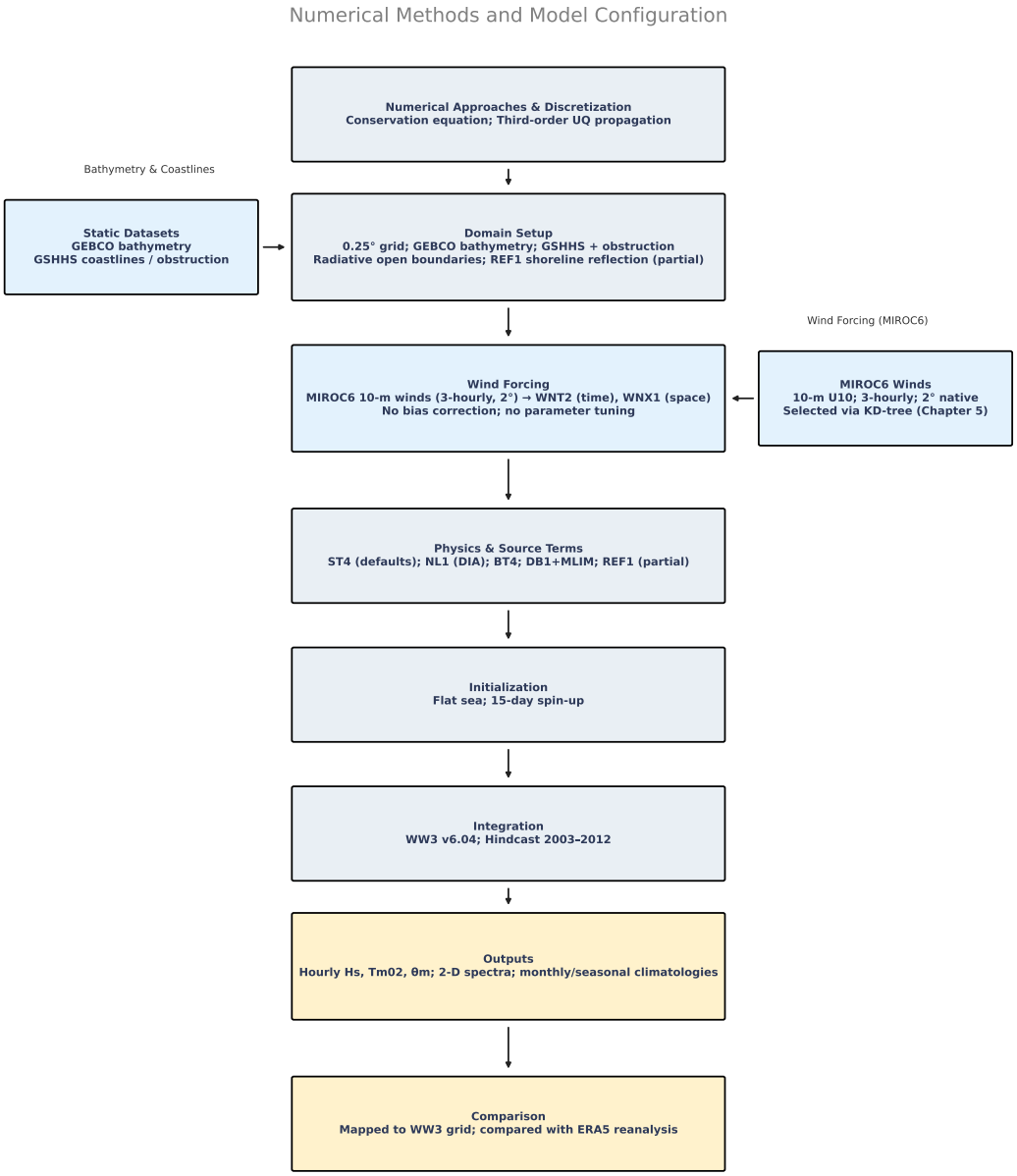

Figure 6.1 Numerical methods and model configuration for the WW3 hindcast. The workflow illustrates the setup steps: discretization and numerical scheme, domain definition with bathymetry and coastlines, MIROC6 wind forcing, wave physics and source terms, model initialization, integration period (2003–2012), and validation against ERA5.

quadruplet interactions. Wave advection is computed using the third-order PR3/UQ scheme. Bottom friction follows the SHOWEX formulation (BT4), and depth-induced breaking is represented by the Battjes–Janssen scheme (DB1) with MLIM. Triad interactions (TR0) and bottom scattering (BS0) are disabled. Wave–ice options (IC2, IS2) are compiled but not applied, as no sea-ice forcing is provided.

6.2.1.4 Initialization and spin-up

The model is initialized from a calm sea state (zero-energy spectrum). A 15-day spin-up (December 2002) is run using MIROC6 winds to allow the wave field to reach quasi-equilibrium with the forcing.

6.2.1.5 Outputs and validation

Hourly outputs include significant wave height (H_s), energy-weighted mean period (T_{m02}), mean wave direction, and full frequency–direction spectra, stored in NetCDF format. Validation is performed against ERA5 reanalysis, which assimilates buoy and satellite altimeter observations. ERA5 fields are interpolated to the WW3 grid to provide a consistent basis for evaluation during the 2003–2012 hindcast.

Table 6.1 summarises the complete model configuration, including grid setup, forcing, and physics options.

6.3 Pre-processing of input data

Accurate pre-processing ensures that the wave model receives consistent forcing and bathymetry inputs. Two primary datasets were prepared: MIROC6 10-m wind fields and the model domain bathymetry/land mask.

6.3.1 Wind forcing

Wind fields were obtained from the MIROC6 climate model (CMIP6 historical experiment; 10 m winds, 3-hourly, 2° resolution), selected for the region using the KD-tree evaluation described in Chapter 5. No bias correction was applied; winds were used in their raw form to directly assess climate model performance. Temporal interpolation to hourly resolution used WW3's quadratic scheme (WNT2), and bilinear spatial interpolation (WNX1) mapped winds to the 0.25° computational grid. Land points were masked to zero to prevent spurious forcing.

6.3.2 Bathymetry and land mask

Bathymetry was taken from the GEBCO 2021 dataset (15 arc-sec native resolution) and interpolated to the 0.25° grid, with a maximum depth of 6000 m imposed for numerical stability. The shoreline and land–sea mask were derived from GSHHS, with sub-grid obstruction enabled to represent partially blocked cells. Manual checks ensured accurate representation of major coastal features such as the British Isles and the Azores.

6.4 Post-processing and Model Validation Approach

After the 10-year hindcast, model outputs were compared with the ERA5 wave reanalysis *[Hersbach et al., 2020]*, which assimilates satellite altimeter and buoy observations and provides

Table 6.1 Key WW3 Model Configuration
(This table summarises the main setup parameters for the WW3 hindcast.)

Component	Setting / Description
Model version	WW3 v6.04 (NOAA/NCEP release)
Domain	NE Atlantic (18°N – 80°N, 21°W – 10°E)
Spatial grid	0.25° × 0.25° latitude–longitude (regular grid)
Bathymetry	GEBCO 2021 bathymetric grid (interpolated to 0.25° resolution)
Land mask	GSHHS coastline with sub-grid obstruction enabled
Time span	10-year hindcast, 1 Jan 2003 – 31 Dec 2012
Spin-up	15-day spin-up (Dec 2002)
Wind forcing	MIROC6 CMIP6 historical run; 10-m winds (3-hourly, 2°); interpolated to 0.25° and hourly resolution using `WNX1/WNT2`; no bias correction
Boundary conditions	Open boundaries (radiative; no incoming wave spectra, free wave exit)
Spectral grid	36 directions; 30 frequencies (0.04–0.5 Hz, geometric progression)
Source term package	ST4 with `STAB0` flux formulation for wind input and whitecapping *[Ardhuin et al., 2010]*
Nonlinear interactions	DIA scheme (`NL1`) for quadruplet interactions
Bottom friction	SHOWEX formulation (`BT4`)
Depth-induced breaking	Battjes–Janssen scheme (`DB1`) with `MLIM` limiter
Wave–ice interactions	Compiled (`IC2`, `IS2`) but not applied (no ice forcing provided)
Advection scheme	Third-order propagation scheme (`PR3/UQ`)
Time stepping	1-hour base time step with adaptive sub-stepping for source term integration
Parallelization	MPI-based domain decomposition for high-performance computing
Output interval	1-hourly
Output variables	H_s, T_{m02}, mean wave direction, and full 2-D spectra (NetCDF)

global wave parameters at hourly, 0.5° resolution. To enable a direct comparison, ERA5 fields were bilinearly interpolated onto the WW3 computational grid. Grid cells with more than 10% sea-ice concentration were excluded from the analysis, since waves are not reliably represented in partially ice-covered regions and the WW3 configuration did not include wave–ice interactions.

6.4.1 Model Output and Derived Products

Hourly outputs included H_s, T_{m02}, θ_m, and full spectra at each grid point. From these, monthly and seasonal climatologies and variability statistics were calculated for H_s to characterise spatial patterns and temporal variability.

6.4.2 Validation Data and Strategy

We assess whether the MIROC6-driven hindcast reproduces the observed climatological and seasonal variability of H_s in ERA5, used here as a reference dataset. This comparison does not constitute a full validation of the WW3 model itself, which would require simulations forced by reanalysis winds or direct buoy/altimeter data. Rather, the focus is on testing the capability of MIROC6 wind fields, when downscaled through WW3, to represent natural variability in the North Sea wave climate.

Spatial bias maps (WW3 – ERA5) and representative time series (e.g., near the Dutch coast, central North Atlantic) were used to assess systematic and temporal differences. Seasonal cycles were examined to verify the expected winter maxima and summer minima *[Semedo et al., 2011]*. Extreme value analysis and high-percentile event evaluation were outside the scope of this study and were not performed.

6.4.3 Performance Metrics

The quantitative assessment of model performance employed several statistical metrics commonly used in wave modeling studies:

Bias and Normalized Mean Bias (NMB)

Bias quantifies the mean deviation between modeled (H_s^{model}) and observed (H_s^{obs}) significant wave heights:

$$\text{Bias} = \frac{1}{N}\sum_{i=1}^{N}\left(H_{s,i}^{\text{model}} - H_{s,i}^{\text{obs}}\right) \tag{6.1}$$

Normalized Mean Bias (NMB) provides a relative measure of bias, calculated as:

$$\text{NMB} = \frac{\sum_{i=1}^{N}\left(H_{s,i}^{\text{model}} - H_{s,i}^{\text{obs}}\right)}{\sum_{i=1}^{N} H_{s,i}^{\text{obs}}} \tag{6.2}$$

An NMB within ±0.25 (±25%) is generally considered acceptable for wave modeling applications *[Zieger et al., 2009]*.

Mean Absolute Error (MAE) and Skill Score (SSMAE)

Mean Absolute Error (MAE) measures the average magnitude of model errors:

$$\mathrm{MAE} = \frac{1}{N}\sum_{i=1}^{N}\left|H_{s,i}^{\mathrm{model}} - H_{s,i}^{\mathrm{obs}}\right| \tag{6.3}$$

This error is transformed into a skill score (SS_MAE), a relative accuracy metric defined as:

$$\mathrm{SS\_MAE} = 1 - \frac{\sum_{i=1}^{N}\left|H_{s,i}^{\mathrm{model}} - H_{s,i}^{\mathrm{obs}}\right|}{\sum_{i=1}^{N}\left|H_{s,i}^{\mathrm{obs}} - \overline{H_s^{\mathrm{obs}}}\right|} \tag{6.4}$$

Skill scores approaching 1 indicate superior model performance, whereas values approaching 0 imply substantial deviations from observations.

Index of Agreement (IOA)

The IOA provides a normalized measure (ranging from 0 to 1) assessing the agreement between modeled and observed values, considering both systematic and unsystematic errors *[Willmott, 1981]*:

$$\mathrm{IOA} = 1 - \frac{\sum_{i=1}^{N}\left(H_{s,i}^{\mathrm{model}} - H_{s,i}^{\mathrm{obs}}\right)^2}{\sum_{i=1}^{N}\left(\left|H_{s,i}^{\mathrm{model}} - \overline{H_s^{\mathrm{obs}}}\right| + \left|H_{s,i}^{\mathrm{obs}} - \overline{H_s^{\mathrm{obs}}}\right|\right)^2} \tag{6.5}$$

where $\overline{H_s^{\mathrm{obs}}}$ is the mean of the observed significant wave heights. An IOA near 1 reflects high model accuracy.

Kling-Gupta Efficiency (KGE)

The Kling-Gupta Efficiency (KGE) integrates correlation (r), bias, and variability into a single metric, defined as *[Gupta et al., 2009]*:

$$\mathrm{KGE} = 1 - \sqrt{(r-1)^2 + (\beta-1)^2 + (\gamma-1)^2} \tag{6.6}$$

where $\beta = \frac{\overline{H_s^{\mathrm{model}}}}{\overline{H_s^{\mathrm{obs}}}}$ represents the bias ratio and $\gamma = \frac{\sigma_{H_s^{\mathrm{model}}}}{\sigma_{H_s^{\mathrm{obs}}}}$ represents the variability ratio. Here, $\overline{H_s^{\mathrm{model}}}$ and $\overline{H_s^{\mathrm{obs}}}$ denote the mean of the modeled and observed significant wave heights, respectively, and $\sigma_{H_s^{\mathrm{model}}}$ and $\sigma_{H_s^{\mathrm{obs}}}$ denote their standard deviations.

KGE values above approximately 0.5 indicate acceptable skill for climate-scale wave modeling, while values exceeding 0.8 represent high model fidelity.

6.5 Results and Discussion

6.5.1 Interpretation of Wave Hindcast Results

The 10-year hindcast (2003–2012), forced by MIROC6 winds, demonstrates reasonable agreement in reproducing the climatological mean state and seasonal-to-interannual variability of significant wave height (H_s) across the Northeast Atlantic. Within this broader domain, the North Sea emerges as a focal region due to its semi-enclosed geometry and relevance for coastal infrastructure and renewable energy applications. Bias patterns (Figure 6.2a) indicate that the hindcast systematically underestimates H_s by approximately 0.3–0.5 m along coastal and shallow shelf areas of the North Sea, consistent with fetch-limited growth and reduced swell penetration from the open Atlantic. Comparable underestimations occur in the Bay of

Biscay and southern English Channel. Conversely, a moderate positive bias is evident in the northwestern sector of the domain (e.g., near Iceland and Greenland), likely influenced by unresolved wave–ice interactions. While localized errors elsewhere reach magnitudes of up to ±1.5 m, the North Sea biases remain modest relative to the regional climatology, underscoring the robustness of the simulation in this key basin.

Two physical factors plausibly explain the observed bias structures. First, the absence of explicit wave–ice coupling in the WW3 setup leads to overestimation in the Norwegian and Barents Seas, where seasonal ice exerts a dampening effect on long-period swells. Second, the open boundary conditions exclude incoming swell spectra from the wider North Atlantic storm track, limiting the representation of swell penetration into semi-enclosed basins such as the North Sea and Bay of Biscay. These effects are consistent with earlier findings that boundary forcing constraints and missing ice–wave interactions can degrade hindcast fidelity at high latitudes and along enclosed shelves. Importantly, normalized mean bias (NMB; Figure 6.3a) across the North Sea remains within –0.2 to +0.2, indicating that model deviations scale to less than 20% of observed magnitudes-well within the envelope typically considered acceptable for regional wave hindcasts.

Beyond systematic bias, the hindcast exhibits moderate-to-good skill across independent statistical metrics. Annual performance scores (Table 6.2) highlight strong temporal coherence and amplitude fidelity relative to ERA5. The Index of Agreement (IOA) ranges from 0.80–0.89, reflecting consistent reproduction of the observed seasonal cycle and interannual variability with minimal phase and amplitude errors. Kling–Gupta Efficiency (KGE) values fall between 0.60 and 0.80, exceeding the widely cited climate-scale threshold of 0.5, and confirm the model's ability to capture correlation, bias ratio, and variability ratio simultaneously. Spatial skill fields (Figure 6.2b) reveal that the North Sea predominantly exhibits KGE values of 0.55–0.75, signifying moderate-to-high skill even in marginal seas. Notably, skill scores remain positive along nearshore zones where localized biases occur, confirming added predictive value relative to a persistence climatology.

In summary, the MIROC6-driven WW3 hindcast credibly reproduces the North Sea wave climate at climatological and seasonal-to-interannual scales. Bias magnitudes are modest and largely confined to shallow, fetch-limited coastal regions, while independent skill measures (IOA, KGE, and NMB) attest to credible basis with the ERA5 reference reanalysis. These findings reinforce the model's ability to represent dominant wave generation and propagation processes under climate-model wind forcing, providing a reliable framework for evaluating the suitability of MIROC6 winds in regional wave energy and coastal impact assessments.

Another important result is the spatial distribution of wave power derived from the hindcast. The model's average wave power map (Figure 6.3b) highlights distinct high and low wave energy regions consistent with known climatological patterns. Peak wave power, reaching up to ∼60 kW/m of wave crest, occurs along the exposed Atlantic margins-particularly west of Ireland, Scotland, and in the Norwegian Sea-and aligns well with global wave resource assessments that report values of 40–60+ kW/m within these storm-track corridors. Conversely, lower wave power (<20 kW/m) is observed in more sheltered or fetch-limited regions, such as the North Sea and the inner Bay of Biscay. The accurate reproduction of these spatial gradients suggests that the hindcast captures significant wave heights effectively and reasonably accurately represents the underlying energy flux distribution. This consistency with established patterns enhances the credibility of the WW3–MIROC6 setup for practical wave energy resource assessments. In particular, the model's ability to reproduce low-energy conditions in the North Sea, alongside high-energy Atlantic regions, confirms its skill in capturing key spatial dynamics. Combined with its strong statistical performance, this lends credibility to the model as a reliable tool for historical wave climate reconstruction and future scenario analysis. Such validated modeling frameworks are essential for offshore renewable energy planning, coastal infrastructure design, and long-term climate

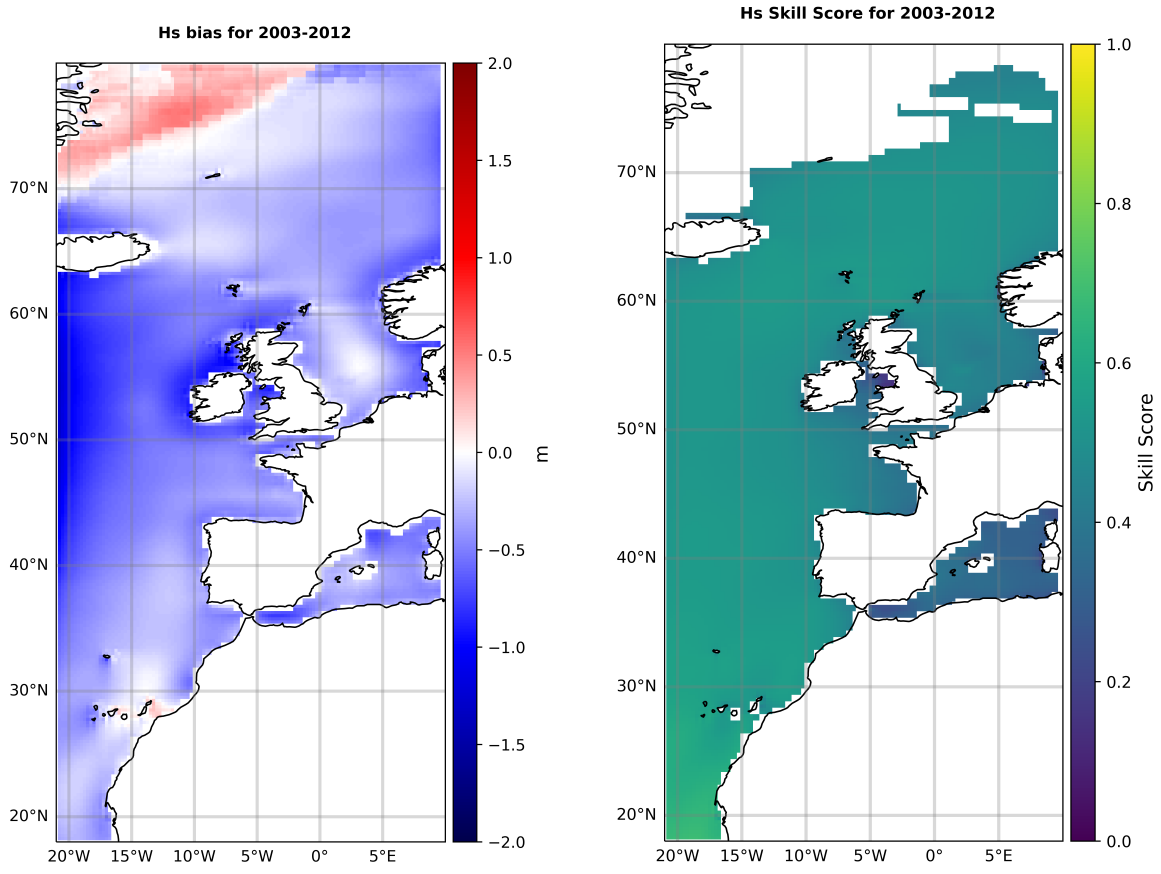

(a) Bias (m)

(b) Skill Score

Figure 6.2 Spatial evaluation of significant wave height (H_s) performance using WW3 with CMIP6 forcing: (a) bias and (b) skill score for 2003–2012.

risk assessments. By demonstrating that raw climate model winds can drive high-resolution wave simulations with realistic spatial patterns, this study supports the broader use of similar approaches for projecting future changes in wave energy potential and extreme events under climate change.

Table 6.2 Yearly aggregated spatial mean values of significant wave height for IOA, KEG scores, and all metrics

Year	IOA	KEG	Bias	RMSE	SI	MAE
2003	0.85	0.73	-0.31	0.47	0.21	0.39
2004	0.83	0.64	-0.46	0.55	0.24	0.48
2005	0.88	0.80	-0.23	0.34	0.15	0.27
2006	0.85	0.72	-0.28	0.46	0.20	0.38
2007	0.80	0.61	-0.46	0.59	0.25	0.52
2008	0.80	0.60	-0.51	0.62	0.29	0.55
2009	0.82	0.70	-0.37	0.53	0.22	0.44
2010	0.89	0.80	-0.15	0.31	0.14	0.24
2011	0.81	0.60	-0.54	0.62	0.25	0.56
2012	0.85	0.75	-0.36	0.43	0.19	0.38

6.5.2 Influence of Climate Model Wind Forcing on Wave Simulations

This subsection evaluates how the use of MIROC6 climate model winds influences the WW3 hindcast. MIROC6 is a global climate model with an atmospheric resolution of $\sim 2^{\circ}$, without assimilation of observations, and the outputs used here span 2003–2012. The wind fields represent the large-scale atmospheric conditions of the early 21st century but do not reproduce the exact phasing or trajectories of individual storms. Consequently, storm systems in the simulation can occur on different days or follow displaced tracks relative to reality, leading to temporal and spatial mismatches in wave conditions. These discrepancies elevate absolute error metrics even when the overall storm frequency and statistical distributions remain realistic.

Despite these limitations, wave model skill scores remain consistently high. Across the domain, the Index of Agreement (IOA) ranges from 0.80–0.89 and Kling–Gupta Efficiency (KGE) from 0.60–0.80, values that exceed typical thresholds for climate-scale hindcasts. The North Sea exhibits similar skill levels, indicating that MIROC6 forcing is capable of sustaining reliable wave climate simulations across both open-ocean and semi-enclosed basins.

Systematic biases in H_s can be attributed directly to characteristics of the MIROC6 wind fields. Underestimations in the North Sea and English Channel arise from the model's coarse resolution and smoothed land–sea interface, which suppress local wind gradients and orographic effects. In contrast, overestimations in high-latitude regions such as the Norwegian Sea reflect the absence of wave–ice coupling in WW3, whereas ERA5 accounts for partial ice cover and its dampening effects. Negative biases in the Bay of Biscay and along the Iberian coast are linked to boundary forcing constraints: the simulation excludes incoming long-period swell generated by remote North Atlantic storms, and wave growth in these regions therefore relies solely on local MIROC6 winds. The North Sea is less affected due to its semi-enclosed geometry and dominance of local wind forcing.

The use of MIROC6 in this hindcast provides a direct test of climate-model-derived wind fields for historical wave modeling. The simulation reflects the climate background of 2003–2012, incorporating both greenhouse gas concentrations and internal variability of that decade, and thus avoids reliance on synthetic or idealized conditions. Importantly, MIROC6 was selected through the KD-tree–based comparison described in Chapter 5, which objectively matched model winds to observational references. Its demonstrated skill justifies its application as the driver for both hindcast evaluation and forward-looking climate scenario simulations.

In summary, MIROC6 winds, when dynamically downscaled through WW3, produce wave fields that align with observed climatological statistics over a decadal period. While unsuitable for reproducing event-level chronology, the forcing is robust for long-term wave climate studies and provides a consistent framework for extending the analysis to future projections.

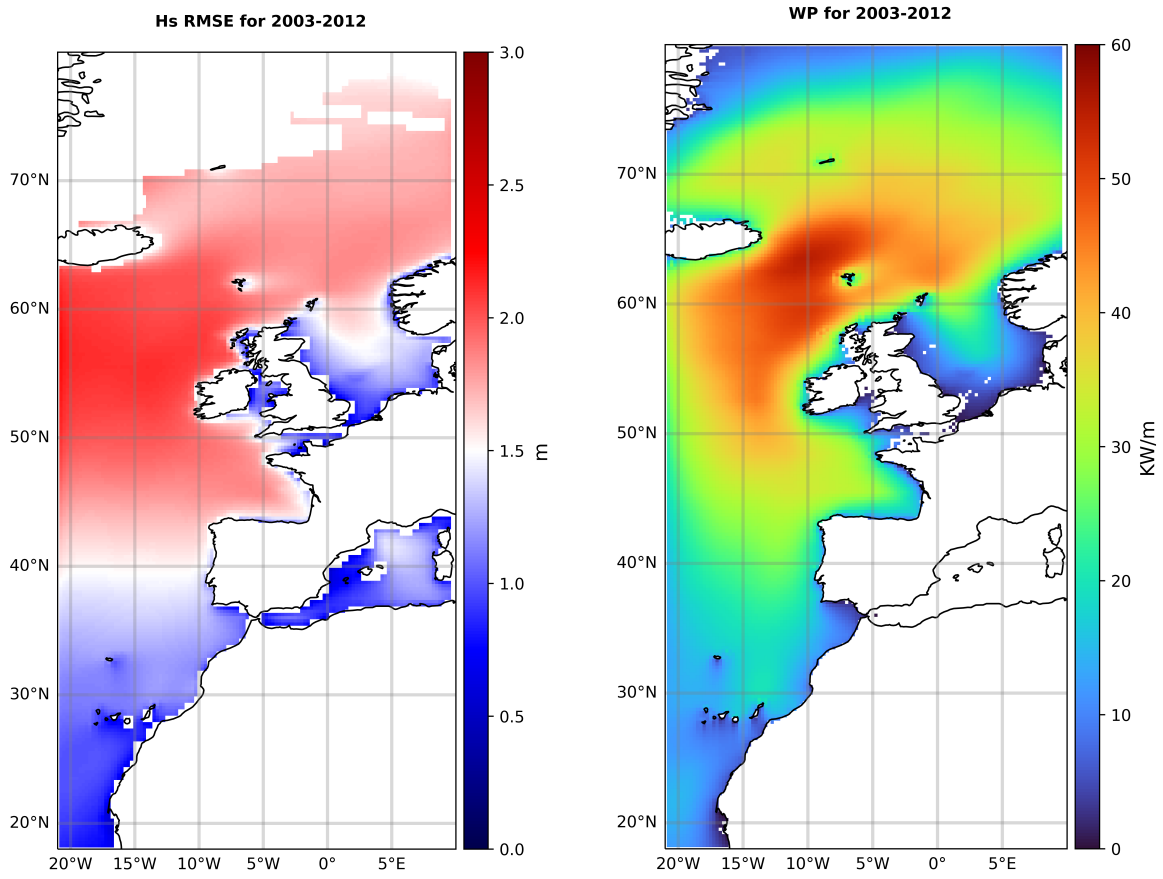

(a) RMSE (m)

(b) Wave Power (kW/m)

Figure 6.3 Evaluation of WW3 performance and energy output using CMIP6 forcing: (a) RMSE of significant wave height (H_s) and (b) spatial distribution of mean wave power for 2003–2012.

6.5.3 Strengths and Limitations of the Modelling Approach

The modelling framework adopted here a regional WW3 hindcast driven by raw CMIP6 climate model winds offers clear advantages but also inherent constraints that must be acknowledged.

Strengths: A primary strength lies in the moderate-to-good skill demonstrated over the 10-year period. Validation against ERA5 yielded IOA values of ∼0.85 and KGE values of ∼0.7 (Table 6.2), alongside stable annual skill scores, confirming consistent model behaviour through time. Importantly, multiple performance metrics were applied, capturing correlation, variability, and bias jointly rather than focusing on a single aspect of model performance.

This comprehensive evaluation ensures that the hindcast reproduces both the mean state and the temporal variability of wave conditions.

Another strength is the physical realism afforded by a third-generation spectral model. WW3 explicitly resolves energy across frequencies and directions, enabling the representation of processes such as swell propagation, fetch-limited growth, and coastal sheltering. The 0.25° (∼25 km) grid dynamically downscales the coarse MIROC6 winds, yielding spatial detail relevant for shelf seas and nearshore regions, while the large model domain (18°–80°N) encompasses the principal North Atlantic storm tracks that influence the North Sea. The hindcast therefore provides a spatially rich dataset of wave spectra and derived parameters (e.g. H_s, wave power, peak period), at finer resolution than the parent climate forcing, and suitable for practical applications such as coastal engineering and renewable energy planning. Finally, the use of a decade-long integration with hourly output allows the computation of climatological indicators and interannual variability, reducing sensitivity to anomalous years.

Limitations: The most significant constraint stems from the atmospheric forcing. MIROC6 is a free-running global model that does not assimilate observations, and its coarse resolution smooths wind gradients along coastlines and semi-enclosed basins. As a result, wind speeds are underestimated in regions such as the North Sea and English Channel, directly propagating into wave height underestimations. Conversely, overestimation of H_s in the Norwegian Sea reflects the absence of wave–ice interactions in WW3, which in ERA5 dampen winter wave growth. The use of open boundaries without incoming swell spectra also limits realism in regions like the Bay of Biscay, where long-period waves generated by remote North Atlantic storms play a significant role.

Spatial resolution imposes further limitations. A 0.25° grid cannot resolve estuaries, islands, or complex coastal geometries, and thus omits fine-scale processes such as local wave amplification and sheltering. For site-specific impact assessments, nested or higher-resolution modelling would be required. Similarly, the physics parameterisations employed ST4 for wind input and dissipation and DIA for nonlinear interactions are standard defaults rather than tuned to MIROC6 characteristics. While this avoids overfitting, it limits potential optimisation for local conditions. Finally, this study focused on H_s and derived wave power; other critical parameters such as mean period, directionality, and extremes were not evaluated. Validation against buoy spectra in the North Sea would be necessary to confirm skill across the full wave climate spectrum.

Overall, the hindcast is methodologically robust for assessing climatological wave variability under climate-model forcing, but caution is warranted for event-level analysis, fine-scale coastal applications, and high-latitude processes.

6.5.4 Comparison with Previous Studies and Literature

Placing the hindcast in the context of existing work highlights both points of convergence and unique contributions. Most wave hindcasts are traditionally forced with reanalysis winds (e.g. ERA5, CFSR), which assimilate observations and therefore achieve very high agreement with buoy data, often reporting IOAs ∼0.9 and minimal bias. Remarkably, our climate-model-driven hindcast reaches comparable performance levels: domain-wide IOA values lie between 0.80–0.89, and biases remain moderate, with localised deviations of 0.3–0.5 m in complex regions such as the North Sea and Norwegian Sea. This outcome is notable because the atmospheric forcing was objectively selected via a machine-learning approach (Chapter 5), demonstrating that carefully chosen climate model winds can approach the accuracy of reanalysis-driven hindcasts.

Only a limited number of studies have tested CMIP-era climate model winds for wave hindcasting. Prior work has largely focused on projections rather than historical validation. A recent global ensemble by *Meucci et al. [2024]* showed that CMIP6 models outperform earlier

CMIP5 winds, yielding improved skill. Our results reinforce that trend, but at a regional scale: even a single CMIP6 model (MIROC6), when dynamically downscaled with WW3, produces wave fields on par with conventional reanalysis-forced hindcasts. This finding closes a gap between traditional hindcasts and future projections by rigorously validating climate-model forcing in a historical setting.

Bias patterns observed in our simulation align with well-documented issues in the literature. Underestimation in semi-enclosed basins such as the North Sea has been reported by multiple studies and linked to coarse wind forcing or limited fetch representation *[Caires and Sterl, 2005, Bidlot et al., 2002, Cavaleri et al., 2020, Wang et al., 2004]*. Our hindcast reproduces this behaviour, consistent with earlier findings. At higher latitudes, overestimation of H_s reflects the omission of wave–ice coupling, echoing specialised high-latitude studies emphasising its importance *[Liu et al., 1991, Rogers et al., 2016]*. In terms of magnitude, our domain-averaged errors remain within ±25%, in line with thresholds considered acceptable for wave climate applications *[Ardhuin et al., 2010]*. Previous regional hindcasts using reanalysis winds typically report mean biases of a few centimetres to a few decimetres *[Stopa and Cheung, 2014]*, corresponding to relative errors of ∼5–15%. Our values (10–20%) therefore fall within the envelope of state-of-the-art validations, despite using non-assimilated climate model winds.

The simulated wave power distribution is also consistent with global resource assessments. *Reguero et al. [2015, 2019]* identify the Northeast Atlantic as one of the world's highest-energy regions, with values exceeding 40 kW/m and winter peaks of 60–70 kW/m. Our hindcast reproduces this gradient, showing ∼60 kW/m along exposed Atlantic storm-track corridors and much lower values (<20 kW/m) in sheltered seas such as the North Sea. These results validate the model's ability to represent not only significant wave heights but also the integrated energy flux that underpins wave energy exploitation.

Finally, our use of Kling–Gupta Efficiency (KGE) provides a novel perspective relative to most wave studies, which typically emphasise correlation or RMSE. A KGE of ∼0.7 demonstrates internally consistent skill across correlation, bias, and variability, and aligns with thresholds considered high in hydrological and climate contexts *[Knoben et al., 2019]*. By adopting this metric, our study introduces a more holistic framework for wave model evaluation. Furthermore, the approach straddles both hindcast and projection domains *[Morim et al., 2019]*: while rooted in a historical period, it directly informs the credibility of CMIP6-forced future simulations. Together with the ensemble evidence of *Meucci et al. [2024]*, our findings affirm the potential of CMIP6 atmospheric outputs for advancing wave climate research. In summary, the WW3–MIROC6 hindcast reproduces key climatological features and error magnitudes consistent with established literature, while pioneering the rigorous validation of a climate-model-driven simulation. This strengthens confidence in applying such approaches for both resource assessments and climate change impact studies.

6.5.5 Significance for Wave Climate Research and Applications

The successful decade-long hindcast using MIROC6 winds provides clear significance for wave climate research and applied sectors, especially in the context of climate change and the expansion of renewable ocean energy.

Advancing Climate-Driven Wave Modeling: The ability of a climate-model-forced simulation to reproduce observed wave conditions demonstrates that GCM outputs can function as reliable drivers for wave climate assessment. This opens the way for seamless integration of historical and scenario-based projections within a single modelling framework. Employing the same climate model for both hindcast and projection avoids discontinuities between datasets and ensures that biases remain internally consistent across time. Such methodological continuity is crucial for isolating genuine climate change signals in wave conditions, thereby enhancing confidence in projected changes to extremes, variability, and

mean states. This consistency is particularly important for climate impact assessments of coastal infrastructure, where direct comparisons between baseline and future wave climates underpin robust design and adaptation strategies.

Wave Energy and Offshore Engineering: For resource assessment and engineering practice, the hindcast's wave power maps provide a view of spatial variability across the Northeast Atlantic. Such information is essential for identifying promising locations for wave energy converters and for quantifying resource availability. The close alignment of our results with previous regional and global assessments strengthens their credibility for stakeholders considering energy potential. A key advantage of using climate model winds (i.e. free-running global climate model 10-m winds without data assimilation) is that long-term atmospheric variability is inherently embedded in the hindcast, creating a consistent baseline against which future scenario simulations can be compared. This enables "stress-testing" of offshore infrastructure under changing conditions. For example, if mean wave power at a site increases from 50 kW/m to 60 kW/m in future scenarios, design thresholds may need to be revised accordingly. Conversely, projected reductions in semi-sheltered seas could affect the performance of coastal protection measures and port operations. By demonstrating that climate-model forcing can reproduce present-day resources with realistic fidelity, this study enhances confidence in applying the same framework for forward-looking energy planning and climate adaptation.

Physical Insights and Climate Processes: The hindcast also provides process-level insights into the drivers of the regional wave climate. Bias diagnostics revealed the influence of missing long-period swell and the absence of wave–ice interactions. These results highlight the sensitivity of European seas both to remote storm activity and to Arctic ice cover. Swell propagation from distant storms exerts a strong control on Atlantic coastlines, indicating that projected shifts in storm tracks could modify regional wave regimes even without local wind changes. Similarly, the overestimation of H_s in the Norwegian and Barents Seas reflects the lack of ice–wave coupling, reinforcing that declining sea-ice extent under climate change is likely to amplify wave activity in sub-Arctic basins. In this sense, the hindcast serves as an analogue for future low-ice conditions, offering a process-based understanding of how large-scale climate drivers translate into regional wave responses.

Integrated Modeling and Stakeholder Relevance: This study shows that one-way coupled atmosphere–wave frameworks can be applied effectively for regional climate research. The performance of this setup suggests that fully coupled models, where waves influence the atmosphere through processes such as surface roughness, would be a logical next step. Such approaches would allow waves to be treated as an active part of the climate system rather than only as outputs. For stakeholders, the usefulness is practical. Hindcasts of this type provide input for updating design standards, such as extreme wave heights and return periods, and can also be extended to scenario analysis. This enables coastal planners and energy developers to assess possible future wave climates under consistent model biases. The identification of bias sources (e.g., underestimation in the North Sea due to coarse wind forcing, overestimation at high latitudes due to missing ice–wave interactions) also highlights key processes that merit closer monitoring, including North Atlantic swell activity and Arctic sea-ice extent.

6.5.6 Recommendations for Future Work and Improvements

Building on the insights gained and acknowledging the limitations discussed, we propose several recommendations for future work to enhance and expand this wave hindcasting approach:

1. **Bias Correction and Wind Field Refinement:** Future work should evaluate methods for correcting systematic biases in raw climate model winds before forcing the wave model. Statistical approaches such as quantile mapping or linear scaling, using reanalysis as a reference, could reduce mean biases and improve the representation of

extremes (e.g., MIROC6 underestimation of strong gusts). Dynamical downscaling with a regional atmospheric model may also help bridge the resolution gap, though at greater computational cost. Simpler alternatives, such as adding stochastic gustiness factors, could compensate for the smoother wind fields of GCMs and better capture high-frequency variability. Testing these approaches could reduce wind-related errors and improve the realism of simulated wave heights.

2. **Enhanced Wave Model Physics and Coupling:** Improvements to wave model configuration should be explored, particularly for processes currently simplified or omitted. Incorporating wave–ice interactions would reduce overestimation in high-latitude seas and is essential for future projections where declining sea-ice cover will play a major role. Alternative source term packages (e.g., ST6) or tuning of ST4 parameters could also be tested, while replacing the DIA approximation with more accurate methods (e.g., full Boltzmann integration or machine-learning surrogates) may improve spectral fidelity. Looking ahead, two-way coupled atmosphere–wave systems should be considered, where wave feedbacks modify surface roughness and momentum fluxes, potentially improving the representation of extreme storms. Intermediate steps, such as coupling WW3 with a regional atmospheric model, would provide valuable insights.

3. **Data Assimilation and Machine Learning Integration:** To improve alignment with observed chronology, future hindcasts could assimilate satellite altimetry or buoy data into WW3, even when forced by climate model winds. While assimilation risks obscuring some wind-driven biases, running both free and assimilated hindcasts would allow systematic errors to be separated from random noise. Machine learning also offers promising opportunities: bias-correction models trained on observational datasets could adjust GCM-driven hindcasts, while emulators of wave model physics could reduce computational cost for long-term or ensemble simulations. Such tools could enable rapid Monte Carlo experiments of wave climate under different scenarios once trained on physics-based runs.

4. **Longer and Future Period Simulations:** Extending the temporal scope is a natural next step. Multi-decadal hindcasts (e.g., from the 1980s to present) would allow assessment of decadal variability and provide more robust extreme value statistics. Forcing WW3 with MIROC6 historical winds over this longer period would test the model's ability to capture large-scale climate influences such as the North Atlantic Oscillation. More importantly, applying the validated setup to future scenario runs (e.g., SSP2-4.5, SSP5-8.5) will provide direct projections of changes in mean wave climate, extremes, and wave power by mid- and late-century. Such simulations could reveal shifts in storm tracks, northward migration of wave energy, or changes in return periods critical for engineering design.

5. **Broadened Validation Metrics and Variables:** Validation should move beyond significant wave height to include mean and peak wave period, wave directionality, and spectral shape. Buoy records provide valuable benchmarks for these parameters, which are essential for applications such as device response studies. Seasonal cycle amplitude and interannual variability should also be tested against reanalyses (e.g., whether winter waves are $\sim$50% larger than summer, or whether year-to-year variability aligns with observed anomalies). Satellite altimetry could provide independent spatial validation, complementing ERA5 comparisons and ensuring that model skill generalises beyond the reanalysis reference.

6. **Improved Representation of Extreme Events:** Finally, targeted evaluation of extremes is required. The tail of the wind distribution and the wave model's handling

of fully developed seas determine how well extreme events are captured. Analysis of the top 1% of waves, or of 50- to 100-year return levels, would indicate whether biases remain in rare but critical conditions. If underestimation is detected, gust factor corrections or targeted high-resolution coupling during storms may be necessary. Given the reliance of offshore design criteria on extreme statistics, improving model skill in this regime is essential for both hindcasts and projections.

In summary, while the present modelling approach provides a solid foundation, future work should focus on refining wind inputs, enhancing physical process representation, broadening validation scope, and extending the temporal and scenario coverage. Such advances will strengthen the reliability of climate-model-driven hindcasts and projections, ultimately supporting coastal engineering, renewable energy planning, and climate adaptation planning.

6.6 Conclusions

This chapter presented a 10-year wave hindcast for the North Sea and Northeast Atlantic using the WW3 model forced by raw MIROC6 climate-model winds. The simulation reproduced the main large-scale features of the historical wave climate, indicating that climate-model wind fields can provide a credible basis for regional wave-climate assessment. At the same time, the results should be interpreted as a test of the forcing–wave-modelling chain rather than as a full validation of the WW3 model itself.

Model errors were generally modest and spatially coherent. Biases typically remained within ±0.5 m across large parts of the domain, with underestimations of 0.3–0.5 m in semi-enclosed regions such as the North Sea and Bay of Biscay. These discrepancies are mainly linked to limitations in the atmospheric forcing and model setup, including underestimation of peak wind speeds, omission of sea-ice effects, and the absence of incoming swell at the open boundaries. As shown in Figure 6.2a, the hindcast captured the broad spatial structure of significant wave height, although local and event-scale errors remain important.

The central objective of this chapter was to evaluate whether raw CMIP6 climate-model winds can be used for regional hindcasting at higher spatial resolution. This aim was addressed by comparing the MIROC6-forced WW3 simulation against ERA5 reanalysis using multiple statistical metrics. Table 6.2 shows that the Index of Agreement (IOA) for H_s remained in the range 0.80–0.89 and the Kling–Gupta Efficiency (KGE) between 0.60 and 0.80, indicating moderate-to-good skill at climatological and seasonal timescales. However, these metrics do not imply event-level agreement, since free-running climate-model winds do not reproduce the exact timing and tracks of observed storms. The results therefore support the use of MIROC6 winds for broad wave-climate assessment, while also showing that wind-forcing biases propagate directly into the simulated wave field.

In summary, this chapter shows that a carefully configured WW3 hindcast driven by raw MIROC6 winds can reproduce the broad features of the observed wave climate with credible skill over a 10-year period. The results suggest that climate-model winds, even without bias correction or assimilation, can be informative for regional wave-climate studies when their limitations are explicitly considered. This provides a basis for linking historical hindcasts with future projections, while highlighting the need for longer simulations, improved wind forcing, incoming swell boundary conditions, wave–ice coupling, and validation against independent buoy or satellite observations before applying the framework to site-specific engineering or extreme-event assessment.

7

Discussion

"Water is the driving force of all nature."

- Leonardo da Vinci

"What we observe is not nature itself,
but nature exposed to our method of questioning."

- Werner Heisenberg

In this section, we discuss a number of cross-cutting themes that emerge from the individual chapters of the thesis. The aim is to place the results in a broader perspective and to reflect on their general implications across the different stages of the analysis.

We first focus on the integrated interpretation of wind–wave climate variability across European seas (Section 7.1). Subsequently, we discuss the physical drivers that shape regime structure and transitions (Section 7.2). Section 7.3 reflects on the methodological implications of using a fixed multivariate regime framework, while Section 7.4 addresses how uncertainty propagates across atmospheric forcing, model choice, and spatial scales. Section 7.5 discusses the consequences of these findings for offshore wind–wave energy assessment. Finally, Section 7.6 considers how the approach may be extended and applied in future, climate-oriented studies.

7.1 A Regime-Based Perspective on European wind–wave Climate

Confidence in wave climate projections, particularly for site-specific applications, depends on how well the key physical processes governing wave generation and transformation are represented. These processes are commonly represented through the spectral action balance equation, which describes the evolution of the wave spectrum under the combined influence of wind input, nonlinear wave–wave interactions, and dissipation processes such as whitecapping, bottom friction, and depth-induced breaking. In practice, this equation must be solved numerically, and several source and sink terms are parameterised to ensure numerical stability and computational feasibility, particularly in climate-scale simulations. As a consequence, no single wave or wind variable can fully characterise the complexity of wave generation and transformation encoded in the wave spectrum. Wind speed, significant wave height, wave period, and directional properties each capture different aspects of this coupled system, with their relative importance varying across regions, seasons, and time scales. Analysing these variables jointly, together with their seasonal and inter-annual variability, therefore provides a more integrated description of dominant wind–wave behaviour without explicitly resolving all underlying physical processes. By contrast, analyses based on single variables and common summary statistics, such as long-term mean significant wave height, offer a rapid overview but neglect information on variability, directionality, and coupling with atmospheric forcing. Accordingly, such single-variable approaches were not adopted as the primary analytical framework in this thesis. Instead, the first three chapters focus on the joint behaviour of wind and wave variables to characterise dominant wind–wave states across European seas. This analysis is not formulated as a region-specific framework, but is structured to remain applicable across different ocean basins, with the understanding that variables, parameter settings, or thresholds (e.g. wave-period definitions, directional binning, seasonal aggregation, or clustering parameters) may require regional adjustment to reflect local wind forcing, fetch, and basin geometry. Climate model simulations are incorporated to examine how dominant wind–wave regimes respond under future CMIP6 scenario conditions, which reflect changes in radiative forcing, land use, and broader socio-economic pathways, with renewable energy applications used as a contextual lens to interpret wind–wave behaviour, variability, and change across historical and future climates.

Approaching multiple wind and wave variables simultaneously, together with their seasonal and annual characteristics, increases descriptive completeness but also introduces practical challenges related to data volume and handling. The analysis involves large, high-dimensional datasets, requiring careful organisation to ensure that dominant large-scale patterns and physically interpretable wind–wave relationships are preserved, rather than being masked by noise or secondary variability. In addition to the variables themselves, large-scale ocean–atmosphere

circulation patterns influence wind–wave variability, and testing their imprint within a unified framework adds further complexity. The availability of along-track satellite observations and point-based in situ measurements therefore motivated the use of reanalysis data as a consistent reference, providing spatial and temporal continuity across the study domain. At the same time, the methodology was not intended to be rigid or regionally fixed; rather than developing a framework that is tightly bound to a specific dataset or configuration, the aim was to maintain adaptability by applying a fixed ERA5-derived regime structure across reanalysis and climate-model simulations, while allowing variables, thresholds, or settings to be adjusted as required to reflect regional wind–wave characteristics without altering the underlying structure.

The analysis therefore begins with what is readily available and well constrained, namely the reanalysis dataset, which provides a consistent and observation-informed reference for describing the current wind–wave climate. Extending the framework to include CMIP6 climate models was a stated objective of this work, but doing so introduces additional challenges related to differences in spatial resolution, internal variability, and the fact that climate-model simulations are not directly constrained by assimilated observations. Applying the same multivariate, regime-based analytical structure-derived from ERA5 and defined in a fixed wind–wave phase space-across reanalysis and climate model simulations requires the methodology to remain adaptable while preserving a common interpretive reference. This balance introduces further complexity, as the framework must accommodate heterogeneous datasets without becoming either overly tuned to a single source or insensitive to physically meaningful differences.

7.2 Robustness, Transferability, and Resolution Sensitivity of the Regime Framework

Applying the ERA5-derived regime framework to climate-model simulations shows that the large-scale organisation of coupled wind–wave regimes is retained across datasets. Regimes associated with open-ocean storm-track exposure, transitional margins, and semi-enclosed basins remain identifiable in both standard- and higher-resolution simulations, indicating that the dominant wind–wave regimes are not specific to a single model configuration, scenario, or spatial resolution.

Differences between simulations arise primarily in the spatial expression and internal variability of regimes. Diagnostics related to regime spatial extent, centroid dispersion, and boundary sharpness show that coastal and semi-enclosed regions are more sensitive to resolution than open-ocean areas. Higher-resolution simulations resolve stronger spatial gradients and more localized regime structure, whereas standard-resolution simulations tend to smooth these features, leading to broader regime boundaries and reduced internal variability. In contrast, open-ocean regimes display comparatively limited sensitivity, consistent with their control by large-scale atmospheric circulation rather than local geometric constraints.

Comparisons across ScenarioMIP and HighResMIP simulations indicate that regime identity is preserved, while regime occupancy and seasonal persistence vary. These variations are consistent with differences in simulated atmospheric variability, particularly in the representation of storm-track intensity and coastal wind gradients, and their interaction with basin geometry. As a result, changes in regime behaviour reflect both physical variability and resolution-dependent representation, rather than a redefinition of the coupled wind–wave system.

These findings demonstrate that the regime framework can be applied consistently across different datasets, while its spatial expression depends on the level of detail with which atmospheric forcing and regional constraints are resolved. This resolution sensitivity is most

relevant in regions where regime redistribution and stability are examined in subsequent analyses, and therefore provides context for interpreting near-term changes in wind–wave regimes.

7.3 Reorganisation of wind–wave Regimes under Near-Term Climate Forcing

This section examines how previously identified wind–wave regimes respond under near-term climate forcing. The analysis does not address the emergence of new regimes or structural changes to the classification. Instead, changes are evaluated in terms of redistribution, persistence, and internal variability of existing regimes. Regime geometry is held fixed, so differences between historical and future simulations are interpreted relative to a common reference space.

Changes are first expressed through modifications in the spatial footprint of existing regimes. Several regimes show shifts in geographic extent, most commonly along latitudinal gradients. These changes are not spatially uniform and are more evident in open-ocean and transitional regions than in semi-enclosed basins, where spatial adjustment is limited. At this stage, the analysis focuses on describing where redistribution occurs, while detailed attribution of the underlying physical drivers is beyond the scope of this work and would form a natural focus for future research.

In addition to spatial extent, changes are observed in regime occupancy. The relative frequency with which certain regimes occur varies between historical and near-term simulations, with some changes appearing seasonally rather than annually. These differences are expressed as shifts in relative occurrence among regimes, rather than as trends in individual wind or wave variables. Framing the response in this way avoids reliance on magnitude-based interpretation and instead reflects changes in coupled wind–wave behaviour.

Further insight is provided by examining changes in internal regime variability. In some regimes, centroid dispersion within the multivariate wind–wave feature space (defined by the joint variability of wind and wave variables) increases or decreases, indicating differences in stability and persistence. These variations are interpreted as changes in the expression of atmospheric variability within regimes, rather than as responses to a uniform external forcing.

The representation of spatial reorganisation is influenced by model resolution. Finer spatial resolution allows sharper gradients and regional transitions to be resolved more clearly, particularly near coastlines. However, the overall structure of regime organisation remains consistent across climate model configurations with different spatial resolutions. Resolution is therefore treated as affecting how changes are expressed spatially, rather than determining their presence.

Several aspects remain unchanged under near-term forcing. Regime identities, their association with dominant circulation patterns, and the overall structure of the multivariate space are preserved. Observed differences occur within the existing framework and do not indicate a redefinition of regime types. The use of fixed regime geometry constrains interpretation and limits the risk of classification-induced artefacts.

Finally, the scope of interpretation is bounded by the near-term nature of the simulations and by model uncertainty. The analysis does not address longer-term evolution or potential structural change beyond the examined period. Results are therefore interpreted as indicating reorganisation within an established wind–wave climate structure. This framing provides the basis for examining implications for wind–wave energy relevance in the following section.

7.4 Implications for Coupled wind–wave Energy Systems

This section interprets the implications of regime behaviour for wind–wave energy systems. Rather than analysing energy metrics in isolation, energy relevance is examined through the characteristics of the wind–wave regimes identified in previous chapters. In this context, energy is understood not only in terms of magnitude, but also in terms of variability, persistence, and spatial coherence. The discussion therefore builds directly on the regime reorganisation described in Section 7.3 and remains within the same interpretive framework.

Different wind–wave regimes are associated with distinct ranges of wind and wave energy. Open-ocean regimes, characterised by sustained exposure to large-scale circulation and long fetch, tend to correspond to higher wave energy levels. Transitional regimes occupy intermediate conditions, while enclosed and semi-enclosed regimes are associated with lower energy states constrained by basin geometry and limited fetch. These contrasts reflect underlying physical controls-such as differences in fetch length, exposure to large-scale storm tracks, basin geometry, and prevailing wind regimes-rather than differences in individual variables, and they are consistently observed in ERA5 reanalysis for the historical period (1979–2014) as well as in CMIP6 climate model simulations for both the historical and near-term period (2020–2050) examined in this study.

Energy relevance is also shaped by regime persistence and internal variability. Regimes that occur frequently and exhibit limited dispersion in multivariate space tend to correspond to more stable energy conditions, while regimes with higher internal variability are associated with less consistent energy availability. This distinction is particularly relevant for climate-scale assessments, where reliability and seasonal consistency may be as important as mean energy magnitude. As such, higher energy regimes are not necessarily more suitable from an energy perspective if they are accompanied by large variability or intermittent occurrence.

The spatial redistribution of regimes under near-term forcing, discussed in Section 7.3, has direct implications for the distribution of energy relevance. Changes in regime footprint alter where particular combinations of energy magnitude and stability are expressed, leading to a redistribution of energy characteristics rather than a uniform increase or decrease. These effects are regionally uneven, with clearer signals in open-ocean and transitional zones than in enclosed basins. Importantly, these shifts reflect changes in regime presence rather than changes in the intrinsic energy properties of the regimes themselves.

Within this framework, the distinction between Primary, Secondary, and Hotspot regions emerges from the combined consideration of energy magnitude and regime stability. Primary regions are characterised by relatively high energy levels and persistent regime behaviour, while Secondary regions exhibit either lower energy levels or greater internal variability. Hotspot regions correspond to areas where elevated energy levels coincide with higher variability or stronger seasonal sensitivity compared to more stable regimes. These categories are intended as an interpretive tool rather than a prescriptive classification, providing a structured way to relate regime persistence and variability to differences in energy reliability and consistency at climate scales.

Compared to conventional energy assessments based on long-term mean wave power, the regime-based perspective provides additional context by distinguishing between stable and variable energy states. Mean-based maps remain useful for broad resource estimation, but they do not capture differences in persistence, seasonal dominance, or sensitivity to atmospheric variability. The regime framework therefore complements existing approaches by placing energy metrics within a physically interpretable structure linked to wind–wave dynamics.

Finally, interpretation of the results is bounded by the climate-scale nature of the analysis and by the intent of the regime-based framework. Selection of offshore locations for wind

and wave energy farms is inherently multi-dimensional and involves physical, environmental, jurisdictional, and engineering considerations. Within this thesis, several of these dimensions are already addressed at regional and climate-relevant scales, including wind and wave energy magnitude, temporal stability, bathymetric and coastal constraints, and spatial context provided by ecological (MEOW) and jurisdictional (EEZ) boundaries. By examining how coupled wind–wave regimes persist and reorganise under historical and near-term climate forcing, the framework provides a structured, physically interpretable basis for understanding long-term resource reliability and variability. At the same time, final project-level site selection requires additional inputs-such as detailed seabed properties, infrastructure availability, regulatory processes, and device-specific performance-that lie beyond the scope of this work. Within the broader decision chain, the analysis presented here functions as a climate-informed screening and contextual layer, supporting robust interpretation of offshore energy potential rather than prescriptive site selection.

7.5 Uncertainty, Limitations, and Interpretational Boundaries

The analyses presented in this thesis are subject to several sources of uncertainty that must be acknowledged to place the results in their proper context. These uncertainties arise from the choice of datasets, model configurations, analytical assumptions, and the inherent variability of the climate system. Rather than detracting from the results, clarifying these limitations defines the scope within which the findings can be interpreted with confidence.

A primary limitation concerns the use of a single climate model configuration for future analysis. While the benchmarking exercise demonstrated that the selected model provides a reasonable representation of historical wind–wave behaviour, it cannot capture the full range of uncertainty associated with structural differences among climate models. Internal variability, parameterisation choices, and resolution differences across the CMIP6 ensemble are therefore not fully sampled. As a result, the future reorganisation of regimes described here should be interpreted as conditional on the selected forcing, rather than as an ensemble-robust outcome.

The use of a fixed regime geometry introduces an additional interpretational constraint. Holding regime boundaries constant enables consistent comparison across datasets and time periods, but it also assumes that the dominant modes of coupled wind–wave behaviour identified in the historical climate remain relevant under near-term forcing. While this assumption is reasonable for the examined time horizon, it limits the ability to detect potential emergence of fundamentally new regimes or structural changes beyond redistribution within the existing phase space. The framework is therefore designed to assess reorganisation rather than transformation.

Uncertainty is also introduced by the atmospheric forcing itself. Climate-model winds do not assimilate observations and are subject to biases in magnitude, variability, and spatial structure. These limitations propagate into the wave simulations, particularly in semi-enclosed basins and regions where local wind gradients or orographic effects are important. The absence of bias correction preserves consistency between historical and future simulations, but it also means that some systematic errors remain unresolved. Consequently, results are interpreted at climate scales rather than at the level of individual events or locations.

The wave modelling setup imposes further constraints. The WW3 configuration does not include wave–ice interactions, incoming swell at open boundaries, or two-way coupling with the atmosphere. These omissions affect high-latitude regions and basins influenced by remote wave generation, and contribute to biases in specific areas. In addition, the spatial resolution of the model limits representation of fine-scale coastal processes, restricting the

applicability of the results for site-specific engineering assessments. The analysis therefore focuses on regional patterns and variability rather than local extremes.

Data-related uncertainties also play a role. Reanalysis products, while observationally constrained, are themselves model-based and subject to assimilation assumptions. Using ERA5 as a reference provides consistency and broad observational grounding, but it does not represent an absolute truth. Validation against reanalysis therefore supports interpretation of relative behaviour and variability, rather than definitive accuracy.

Finally, the near-term focus of the climate simulations bounds the temporal interpretation of the results. The analysis does not address long-term evolution beyond the examined period, nor does it attempt to assess changes under stronger forcing scenarios. Conclusions regarding future behaviour are therefore limited to the persistence and redistribution of existing regimes under near-term conditions, and should not be extrapolated to longer horizons without additional evidence.

Taken together, these limitations define clear interpretational boundaries. The framework is suited to examining coupled wind–wave behaviour, variability, and reorganisation at regional and climate scales, but not to predicting local extremes, optimising energy sites, or quantifying long-term structural change. Recognising these boundaries ensures that the results are interpreted consistently and provides a transparent basis for future extensions of the work.

7.6 What This Thesis Changes — Scientific and Practical Perspective

This thesis contributes a structured way of interpreting wind–wave climate as a coupled system, rather than as a collection of individual variables or region-specific indicators. By adopting a fixed, multivariate regime framework, the work provides a consistent reference through which variability, model performance, and near-term change can be examined together. This perspective does not replace existing approaches, but offers an additional layer of interpretation that connects physical processes, spatial organisation, and temporal behaviour within a single analytical structure.

From a scientific standpoint, the thesis demonstrates that dominant wind–wave states can be identified in a physically interpretable manner and that these states persist across datasets and modelling configurations. Treating wind and wave variables jointly allows the influence of circulation, fetch, and basin geometry to be examined without isolating individual processes or relying on trend-based diagnostics alone. The framework supports comparison across reanalysis and climate-model simulations without redefining classifications, enabling changes to be interpreted as reorganisation within a shared phase space rather than as artefacts of shifting methodology.

The integration of climate models into this framework extends its relevance beyond present-day description. By benchmarking climate-model winds prior to wave simulation and applying a consistent wave-modelling setup, the thesis establishes a transparent pathway from atmospheric forcing to wave response. This approach bridges the gap between reanalysis-driven hindcasts and future projections, allowing climate-model uncertainty to be examined in a controlled and interpretable way. The results show that climate-model-driven simulations can reproduce key aspects of wind–wave variability at regional scales, while also clarifying where limitations arise.

In practical terms, the regime-based perspective provides context for interpreting wave energy relevance beyond mean resource estimates. By linking energy magnitude to regime persistence and variability, the framework highlights differences between stable and intermittent energy states that are not captured by conventional maps. The classification of Primary, Secondary, and Hotspot regions is not intended as a planning tool, but as a way to structure

discussion around energy consistency, seasonal behaviour, and sensitivity to atmospheric variability. This distinction is particularly relevant for regional assessments where long-term reliability is as important as peak values.

More broadly, the thesis provides a methodological foundation that can be adapted to other ocean basins and applications. While the analysis focuses on European seas, the framework is not tied to a specific region, dataset, or variable set. Variables, thresholds, and parameter choices can be adjusted to reflect regional conditions or alternative research questions without altering the underlying structure. This flexibility allows the approach to be extended to different climate regimes, time horizons, or coupled systems, including future work on extremes, directional persistence, or interactions with other marine processes.

Finally, the work establishes clear interpretational boundaries alongside its contributions. It does not claim predictive skill at local scales, optimisation of energy sites, or comprehensive sampling of climate-model uncertainty. Instead, it provides a consistent way to examine how wind–wave behaviour is organised, how it responds under near-term forcing, and how these responses can be interpreted across models and datasets. In doing so, the thesis offers a framework that supports cautious, physically grounded interpretation of wind–wave climate and its relevance for future applications.

8

Conclusions and Recommendations

"Everything changes, nothing endures,
and no conditioned thing is fully satisfying."

- The Buddha

"Live the questions now.
Perhaps you will then gradually,
without noticing it,
live along some distant day
into the answer."

- Rainer Maria Rilke

In this chapter, the main conclusions of the thesis are summarised (Section 8.1) by addressing the research questions formulated in Chapter 1, and the topics that require further research are outlined (see Section 8.2).

8.1 Conclusions

Our objective was to develop and apply a multivariate, regime-based framework to describe wind–wave climate variability across datasets and climate forcing conditions, in the context of renewable energy applications. In Section 1.4, the following research questions were formulated:

1. How can coupled wind–wave climate variability be described within a physically interpretable, regime-based framework that is robust across space, seasons, and timescales, and suitable for offshore energy and engineering applications?
2. How reliably can CMIP6 EC-Earth3 climate simulations reproduce the spatial coherence, variability, and energy relevance of European wind–wave climate when evaluated using a fixed ERA5-derived multivariate regime framework, and how does model resolution influence confidence in regime representation and offshore renewable-energy classification?
3. How will European coupled wind–wave regimes-and the associated hybrid offshore wind–wave renewable potential-reorganise under near-term climate forcing (2020–2050), when future EC-Earth3P-HR projections are mapped onto a fixed, physically interpretable ERA5-derived multivariate regime framework?
4. How can CMIP6 wind forcing be objectively selected for wave modelling, and does that selection translate into credible regional wave-climate simulations when dynamically downscaled through a spectral wave model?

These questions are addressed in the following sections.

8.1.1 A Multivariate Regime Framework for European wind–wave Climate

In this section, we answer the first research question:

> How can coupled wind–wave climate variability be described within a physically interpretable, regime-based framework that is robust across space, seasons, and timescales, and suitable for offshore energy and engineering applications?

This question is examined through the following aspects:

- How can joint wind and wave statistics be formulated to represent coupled wind–wave climate variability across European seas?
- What spatially coherent wind–wave regimes can be identified from long-term ERA5 reanalysis using a multivariate spatio-temporal clustering approach?
- To what extent are the identified regimes internally coherent and mutually distinct in multivariate feature space?
- How do the wind–wave regimes differ in their seasonal and interannual variability of wave height, wave period, wind speed, and directional characteristics?

- Under which large-scale atmospheric circulation patterns is regime-level wind–wave variability most strongly conditioned?

Coupled wind–wave climate variability across European seas can be represented through a unified multivariate descriptor that combines bulk wave and wind conditions with their variability and directionality. In this work, seasonal (DJF, MAM, JJA, SON) and annual statistics of significant wave height (H_s), mean wave period (T_{02}), 10 m wind speed (W_{s10}), mean wave direction (θ_w), and wind direction (W_{d10}) were formulated as a single feature set at each spatial location. For each variable, both the mean state and the associated standard deviation were included, while circular statistics were applied to the directional parameters. This formulation captures not only differences in mean conditions, but also regime-specific dispersion and directional persistence or rotation, providing a physically interpretable representation of the coupled wind–wave system rather than a collection of separate, single-variable climatologies.

A multivariate PCA–k-means framework applied to ERA5 data for the period 1979–2014 identifies nine spatially coherent wind–wave regimes that persist across multi-decadal variability and align with major European basin-scale structures. These regimes exhibit a clear geographic organization spanning (i) open-ocean, Atlantic-dominated sectors, (ii) transitional shelf and ocean–basin interface regions, and (iii) enclosed and semi-enclosed basins. This partitioning is not a simple re-expression of latitude or coastline geometry; instead, it reflects consistent multivariate signatures in wind speed, wave height, wave period, and directional behaviour that remain stable when summarised across seasons and years.

The nine-regime solution exhibits a defensible balance between internal coherence and mutual separation when evaluated within the PCA feature space used for clustering. Within-regime cohesion is supported by comparatively compact distributions of grid-cell-to-centroid distances in regimes characterised by more homogeneous forcing, notably in open-ocean sectors and several southern regimes. In contrast, broader intra-regime dispersion is observed in semi-enclosed basins, where fetch limitation, complex coastline geometry, and heterogeneous wind forcing enhance local variability. Between-regime distinctness is demonstrated by clear centroid-to-centroid separation, which highlights a robust Atlantic–Mediterranean contrast and identifies transitional regimes as intermediate "bridges" rather than ambiguous boundary artefacts. Taken together, these diagnostics indicate that the identified regimes are not arbitrary spatial patterns, but represent separable structures in multivariate space with physically interpretable differences.

The identified regimes exhibit systematic and physically consistent contrasts in both their seasonal cycles and interannual variability. Open-Atlantic regimes are characterised by the highest energy levels and the strongest seasonality, with pronounced winter enhancement in significant wave height (H_s), mean wave period (T_{02}), and 10 m wind speed (W_{s10}), together with comparatively broad interannual spreads. Enclosed and semi-enclosed basins display lower median energy levels and reduced variability, consistent with geometric confinement and predominantly locally forced short-sea conditions. Transitional shelf regimes occupy an intermediate energy range and are distinguished not only by moderate magnitudes, but also by pronounced directional structure: seasonal rotation and broader directional dispersion reflect the combined influence of locally generated seas and remotely forced swell. These contrasts demonstrate that regime separation is expressed in both magnitude-based metrics (wave height, period, and wind speed) and directional behaviour (persistence versus rotation), which is critical for engineering interpretation.

Regime-level variability is most strongly conditioned by North Atlantic–European circulation modes, with clear spatial selectivity. The North Atlantic Oscillation (NAO) and Arctic Oscillation (AO) provide the dominant associations for Atlantic-exposed regimes, particularly during winter and the shoulder seasons, where they co-vary with wind speed, significant wave height, mean wave period, and, in several regimes, directional shifts. Additional patterns,

including the East Atlantic (EA), East Atlantic–Western Russia (EAWR), Scandinavian (SCAND), and selected Eurasian- and Pacific-linked indices, act more regionally and often manifest more clearly in directional behaviour and/or wave period within transitional shelf regimes. This behaviour is consistent with modulation of storm-track pathways, swell exposure, and synoptic sequencing. Overall, the results support a state-aware interpretation in which teleconnection influence is not spatially uniform, but depends on regime exposure, basin geometry, and the balance between swell-dominated and locally forced conditions.

8.1.2 Benchmarking CMIP6 wind–wave Climate with Relevance for Renewable Energy Applications

In this section, we answer the second research question:

> How reliably can CMIP6 EC-Earth3 climate simulations reproduce the spatial coherence, variability, and energy relevance of European wind–wave climate when evaluated using a fixed ERA5-derived multivariate regime framework, and how does model resolution influence confidence in regime representation and offshore renewable-energy classification?

This question is examined through the following aspects:

- To what extent can an ERA5-derived multivariate wind–wave regime framework be transferred to independent EC-Earth3 historical simulations (ScenarioMIP and HighResMIP, 1979–2014) to enable consistent regime-scale benchmarking?
- How consistently do EC-Earth3 ScenarioMIP and HighResMIP reproduce the large-scale spatial organization of ERA5 wind–wave regimes, and where are the dominant regime disagreements located (e.g., coastal and transition zones)?
- How does horizontal resolution (ScenarioMIP 1° vs HighResMIP 50 km) alter regime boundaries, coastal transitions, and the representation of mesoscale wind–wave structure within the fixed ERA5 regime space?
- How does regime-membership confidence, quantified using softmax probabilities in the ERA5 PCA space, vary across regions and between EC-Earth3 configurations, and what does this reveal about spatial uncertainty and ambiguity?
- How well do EC-Earth3 simulations reproduce ERA5 patterns of seasonal and regime-scale variability in wind energy density and wave power, and how do biases differ between ScenarioMIP and HighResMIP?
- How do depth-resolved energy–stability classes (Primary, Secondary, Hotspot, Low) for wind, wave, and hybrid resources distribute across European seas, and how are these zones structured when aggregated by jurisdictional (EEZ) and ecological (MEOW) regions?

The ERA5-derived multivariate wind–wave regime framework is shown to be highly transferable to EC-Earth3 historical simulations from both ScenarioMIP and HighResMIP for the period 1979–2014. By projecting each EC-Earth3 configuration into the fixed ERA5-based PCA space, the same nine physically interpretable regimes are reproduced, enabling consistent regime-scale benchmarking across independent datasets. High regime-membership confidence and strong cross-dataset agreement demonstrate that the framework provides a robust common reference for evaluating wind–wave climate behaviour beyond traditional grid-point skill metrics.

EC-Earth3 consistently reproduces the large-scale spatial organisation of ERA5-derived wind–wave regimes across the Northeast Atlantic and European seas. Quantitatively, 36.4% of collocated grid points exhibit full three-dataset agreement (ERA5, ScenarioMIP, and HighResMIP), while 58.5% show agreement between two datasets; only 5.1% of locations disagree across all three. This implies that approximately 95% of the domain exhibits at least partial regime consistency. Residual disagreements are primarily concentrated along regime transition zones, coastal boundaries, and continental shelf regions, where sharp spatial gradients and unresolved sub-grid-scale processes exert the strongest influence.

Horizontal resolution exerts a first-order control on regime geometry. The coarser ScenarioMIP configuration (approximately 1°) tends to smooth spatial gradients, broaden regime boundaries, and partially merge or dilute narrow coastal and transitional regimes, thereby reducing the definition of fetch-limited and nearshore structures. In contrast, the HighResMIP configuration (approximately 50 km) sharpens coastal transitions, improves separation between neighbouring regimes-particularly along complex margins such as the North Sea–Baltic and Iberian–western Mediterranean interfaces-and better resolves mesoscale wind–wave features within the fixed ERA5 regime space. These results demonstrate that increased horizontal resolution enhances spatial fidelity primarily through improved representation of near-surface wind gradients and coastal complexity.

Regime-membership confidence is high overall, but exhibits clear spatial structure. ERA5 displays very strong membership strength, with a mean softmax probability of 0.98, reflecting persistent and well-separated regimes. EC-Earth3 retains similarly high confidence, albeit with a clear dependence on horizontal resolution: ScenarioMIP exhibits a lower mean confidence (0.90), while HighResMIP shows an improvement (0.93). Reduced confidence is primarily concentrated in coastal and shelf transition zones and within semi-enclosed basins, where wind forcing is more heterogeneous and wave development is strongly fetch-limited. The resulting softmax probability fields therefore provide a practical spatial diagnostic of ambiguity, highlighting regions where regime assignment is inherently less distinct and where model representation is correspondingly more uncertain.

EC-Earth3 reproduces the dominant ERA5 spatial patterns of wind energy density and wave power, including maxima along the North Atlantic storm track-most notably within the NWAC and EAC regimes-and minima in semi-enclosed basins such as the Baltic Sea and the eastern Mediterranean. Across all datasets, a consistent seasonal cycle is observed, with energy maxima during DJF and SON and minima in JJA, while the relative ranking of regimes remains stable. The primary difference lies in magnitude: ScenarioMIP systematically exhibits broader and, in many regions, higher wintertime energy levels, consistent with resolution-related smoothing and stronger effective forcing. In contrast, HighResMIP reduces this amplitude bias, sharpens nearshore gradients, and achieves closer alignment with ERA5. Importantly, even where absolute magnitudes differ, the regime framework demonstrates that EC-Earth3 preserves the spatial and seasonal structure most relevant for interpreting climate-driven wind–wave energy variability.

The depth-resolved energy–stability classification reveals a clear and physically consistent hierarchy across European seas. Primary zones, characterised by high energy and high stability, are concentrated within deep-water Atlantic regimes (NWAC and EAC), where persistent westerly forcing and long fetch support strong and steady resources. Secondary zones dominate transitional shelf regions (e.g. WENS and WMIC), while Low classes prevail in shallow and enclosed basins such as the Baltic Sea and the eastern Mediterranean, reflecting limited fetch, enhanced frictional effects, and constrained synoptic exposure. Hotspot (variable) areas are primarily located along energetic margins and regime transition zones, where mean energy levels are high but temporal stability is reduced. The hybrid classification identifies fewer Primary areas than wind-only or wave-only maps, highlighting the stricter requirement for concurrent persistence of both resources. Aggregation by Exclusive Economic Zones (EEZs)

and Marine Ecoregions of the World (MEOW) further demonstrates a consistent concentration of higher-class resources in high-latitude Atlantic jurisdictions and ecoregions (e.g. Iceland, Faroe Islands, Ireland; Faroe Plateau, Celtic Seas, North Sea), while Mediterranean and other enclosed regions remain dominated by Low and Hotspot fractions.

8.1.3 Near-Term Reorganisation of European wind–wave Regimes Under Climate Forcing

In this section, we answer the third research question:

> How will European coupled wind–wave regimes-and the associated hybrid offshore wind–wave renewable potential-reorganise under near-term climate forcing (2020–2050), when future EC-Earth3P-HR projections are mapped onto a fixed, physically interpretable ERA5-derived multivariate regime framework?

This question is examined through the following aspects:

- To what extent can future EC-Earth3P-HR wind–wave conditions (2020–2050) be consistently projected onto a fixed ERA5-derived principal-component space, enabling direct comparison with historical conditions (1979–2014) without redefining regime geometry?
- How do European wind–wave regimes reorganise under near-term climate forcing in terms of regime transitions, centroid migration, and changes in spatial footprint, and what does this reveal about spatial persistence versus dynamical redistribution within the fixed regime framework?
- Which changes in significant wave height and near-surface wind speed drive the observed future regime transitions, and how do these anomalies relate to shifts in atmospheric forcing and wave-generation processes across European seas?
- How does the seasonal coherence of wind–wave regimes evolve under future climate forcing, as quantified by the Seasonal Regime Stability Index, and do seasonal states become more or less consistent with their annual mean behaviour?
- How do offshore wind and wave energy resources evolve within the historical regime structure under future forcing, as measured by changes in deep-water wave power and hub-height wind energy?
- How does a hybrid classification combining energy magnitude and seasonal stability reorganise Primary, Secondary, Hotspot, and Low wind–wave resource zones under future climate conditions?
- What insights does a regime-based, multivariate framework provide into future offshore renewable potential, resource stability, and climate-aware planning across European seas?

Future EC-Earth3P-HR wind–wave conditions (2020–2050) can be consistently projected into the fixed ERA5 principal-component space, enabling like-for-like comparison with 1979–2014 without redefining regime geometry. The PCA–centroid mapping provides a stable multivariate reference, so diagnosed changes represent true shifts in regime occupancy within a common feature space, rather than artefacts of re-clustering. The fact that future states are expressible within the ERA5-derived space supports the framework's transferability and interpretability for near-term projection analysis.

Under near-term forcing, the European wind–wave climate shows partial persistence with substantial reorganisation. Most grid points retain their historical regime label (domain-mean RTI $\approx$ 0.18, i.e. $\sim$18% transition), but transitions concentrate in dynamic margins and gateways (Norwegian Sea, northern North Sea entrance, Northeast Atlantic shelf), indicating that regime change is spatially structured rather than uniform. The future classification consolidates into fewer occupied regimes, with strong redistribution toward mixed/open-ocean conditions (notably WENS and WMIC), while several transitional and semi-enclosed regimes contract sharply or become negligible. Overall, the system expresses high large-scale pattern continuity combined with regional dynamical redistribution in sensitive transition zones.

The observed regime transitions are primarily driven by coherent increases in wind and wave forcing in northern basins and weaker or negative changes in parts of the southern domain. Positive anomalies in 10 m wind speed (ΔU_{10}) and significant wave height (ΔH_s) align with the expanding footprints and centroid shifts of the dominant future regimes, consistent with enhanced storm-track influence and stronger wave generation in the Northeast Atlantic–North Sea–Norwegian Sea corridor. Conversely, reduced forcing in the subtropical eastern Atlantic and parts of the western Mediterranean aligns with contraction of southern and semi-enclosed regime expressions. These patterns indicate that regime redistribution is physically linked to changes in atmospheric circulation intensity and regional wave-growth conditions (fetch and exposure).

Seasonal coherence changes are regionally asymmetric. The Seasonal Regime Stability Index indicates reduced seasonal stability (positive ΔSRSI) across northern and northeastern regions-most strongly in summer-implying that seasonal states diverge more from the annual mean in areas experiencing the greatest forcing increases. In contrast, parts of the southern domain, including the western Mediterranean and subtropical eastern Atlantic, show little change or increased seasonal coherence (negative ΔSRSI). This reveals that future wind–wave intensification in northern corridors is accompanied by lower temporal persistence, increasing the relevance of stability metrics alongside mean energy.

Offshore wind and wave energy increase most clearly in the northern basins and open-ocean or mixed regimes. Both deep-water wave power ($H_s^2 T_{02}$) and hub-height wind energy (U_{100}^3) exhibit coherent positive changes across the Northeast Atlantic, northern North Sea, and Norwegian Sea. When sampled on historical regime footprints, the largest positive regime-mean changes occur for northern and open-ocean regimes, while southern and semi-enclosed regimes show small, mixed, or negative changes, reflecting weaker forcing changes and limited wave-growth potential. The regime-based view therefore indicates a northward concentration of future energy gains, rather than a uniform strengthening across Europe. Importantly, higher energy magnitude is not inherently beneficial; its relevance depends on accompanying changes in temporal stability, variability, and regime persistence.

The hybrid classification shows that future conditions shift toward greater high-energy potential but with more variability in key northern corridors. Primary zones expand modestly into northern basins, while Hotspot zones increase around energetic margins, such as the northern British Isles and the northern North Sea entrance, where energy is high but seasonal stability declines. Low-resource areas contract, often transitioning into Secondary, indicating either modest energy increases, improved stability, or both. Secondary remains the most widespread and persistent class, but with increased transitions toward Hotspot in mid- to high-latitude transition areas. Overall, future hybrid potential becomes more concentrated and more heterogeneous, emphasising the combined role of magnitude and stability.

A regime-based multivariate framework provides planning-relevant insight that conventional mean-field analyses miss. It separates persistent spatial structure from redistribution within a fixed regime geometry, identifies where change concentrates-at gateways and margins rather than uniformly-and links projected resource evolution to both energy strength and temporal robustness. The results suggest that near-term offshore opportunities may strengthen

in northern corridors, but with increasing stability challenges in some high-energy areas, highlighting the need for climate-aware planning that considers co-variability, persistence, and regime transitions rather than relying solely on mean wind or wave trends.

8.1.4 Objective Wind-Forcing Selection and Implications for Regional Wave Modelling

In this section, we answer the fourth research question:

> How can CMIP6 wind forcing be objectively selected for wave modelling, and does that selection translate into credible regional wave-climate simulations when dynamically downscaled through a spectral wave model?

This question is examined through the following aspects:

- How accurately do CMIP6 historical near-surface wind simulations reproduce observed and reanalysis wind climatology across seasons and regions relevant for wave modelling?
- Do conventional single-metric evaluations adequately discriminate between CMIP6 wind models, or do they obscure important magnitude and seasonal errors relevant for wave generation?
- Can a multi-metric, machine-learning–based framework (KD-tree nearest-neighbour ranking) objectively identify the most suitable CMIP6 wind forcing for a given region?
- Does the objectively selected CMIP6 wind forcing, when used without bias correction, produce a regional wave hindcast that reproduces observed wave-climate statistics?
- How do biases in climate-model wind forcing propagate into simulated wave heights and wave power, and which physical processes dominate the resulting errors?
- Is a wave modelling framework driven by objectively selected CMIP6 winds suitable for regional wave-climate analysis and for providing climate context relevant to offshore renewable-energy studies at climate timescales?

CMIP6 historical near-surface wind simulations reproduce the large-scale spatial structure and directional patterns of observed and reanalysis wind climatology with high consistency across seasons, as indicated by uniformly high spatial pattern agreement (cosine similarity typically 0.97). However, substantial magnitude-dependent biases remain, with seasonal and regional variations reaching up to ± 8 $\mathrm{m\,s^{-1}}$ in some areas. These biases are particularly pronounced in winter and in dynamically complex regions such as coastal margins and semi-enclosed basins. While overall climatological patterns are well captured, the results demonstrate that CMIP6 winds exhibit systematic seasonal and regional errors in wind-speed magnitude that are critical for wave generation and cannot be neglected in wave-modelling applications.

Conventional single-metric evaluations, particularly correlation- or pattern-based measures such as cosine similarity, do not adequately discriminate between CMIP6 wind models. Although these metrics consistently indicate strong agreement with observations, they obscure large and spatially structured magnitude errors that vary by season and region. Models with markedly different bias distributions often receive nearly identical correlation scores, masking deficiencies that are critical for downstream wave simulations. This finding demonstrates that single-metric approaches are insufficient for wind-forcing assessment and can lead to misleading conclusions regarding model performance for wave-modelling purposes.

The multi-metric, machine-learning–based KD-tree nearest-neighbour framework successfully integrates bias, RMSE, and spatial agreement into a single, objective ranking in error space. This approach overcomes the ambiguity inherent in conventional evaluations and enables robust, reproducible identification of the most suitable wind forcing for specific regions. The analysis reveals a clear regional dependence of optimal model choice, with MIROC6 emerging as the most suitable CMIP6 wind forcing for the European and Northeast Atlantic domain. The consistency of this selection across independent reference datasets (CMEMS and ERA5) confirms the robustness of the framework and its suitability for systematic climate-model forcing selection.

When used without bias correction to force a 0.25° WW3 regional hindcast, the objectively selected MIROC6 wind forcing produces a credible reproduction of observed wave-climate statistics over the North Sea and the Northeast Atlantic. Validation against ERA5 demonstrates credible basis at climatological and seasonal-to-interannual timescales, with Index of Agreement values of approximately 0.80–0.89 and Kling–Gupta Efficiency values between 0.6 and 0.8. These results confirm that the wind-forcing selection derived in Chapter 7 translates into physically meaningful wave-model performance, thereby validating the selection strategy through dynamical downscaling.

Biases in climate-model wind forcing propagate directly into the wave simulations, manifesting as systematic underestimations of significant wave height in semi-enclosed and fetch-limited regions such as the North Sea, and overestimations in high-latitude regions. These errors are primarily attributed to coarse atmospheric resolution, which smooths coastal wind gradients, as well as to missing physical processes in the wave-model configuration. In particular, the absence of incoming swell at open boundaries limits wave growth in regions influenced by remote storm activity, while the omission of wave–ice interactions leads to overestimated wave heights at high latitudes. Despite these limitations, error magnitudes remain moderate and spatially coherent, indicating that the dominant source of uncertainty lies in the atmospheric forcing rather than in wave-model instability.

The results demonstrate that a wave-modelling framework driven by objectively selected CMIP6 winds is suitable for regional wave-climate and renewable-energy assessments at climate timescales. The MIROC6-driven WW3 hindcast reproduces realistic spatial gradients in significant wave height and wave power, consistent with established climatological patterns and previous resource assessments. Although the framework is not designed to reproduce event-level chronology, it provides a robust and internally consistent representation of long-term wave-climate variability, making it appropriate for applications such as wave-energy resource characterisation, offshore planning, and climate-change impact assessment. The approach establishes a defensible pathway for extending historical hindcasts to future scenario projections within a unified modelling framework.

8.2 Recommendations

This thesis demonstrates that a fixed, ERA5-derived multivariate regime framework provides a robust and physically interpretable basis for assessing future wind–wave climate evolution and offshore renewable potential across European seas. Building on these findings, the following recommendations and future research directions are identified.

First, the regime-based projection methodology should be extended to multi-model climate ensembles. Applying the fixed ERA5 PCA–cluster framework consistently across other CMIP6 HighResMIP and ScenarioMIP models would enable separation of robust climate signals from model-specific behaviour and allow quantification of inter-model uncertainty in regime transitions, stability, and energy evolution.

Second, future studies should investigate the temporal evolution of regime transitions

rather than relying on comparisons between two fixed periods. Analyses using sliding or decadal windows would clarify whether regime changes occur gradually, episodically, or in response to specific circulation anomalies, and would help identify emerging transition zones and regions of heightened dynamical sensitivity.

Third, a deeper attribution of regime changes to large-scale atmospheric drivers is recommended. Linking regime transitions, centroid migration, and footprint changes to variations in storm-track activity, cyclone frequency, jet-stream position, and dominant climate modes (e.g. NAO-like variability) would strengthen the mechanistic understanding of projected wind–wave reorganisation.

Fourth, the assessment of temporal stability should be expanded beyond seasonal coherence. Incorporating interannual persistence, variability of extremes, and regime-dependent stability metrics would provide a more comprehensive picture of resource reliability, particularly for offshore energy systems sensitive to prolonged variability or episodic extremes.

Fifth, the energy diagnostics could be refined toward more application-oriented indicators. Future work may integrate regime-based wind and wave energy estimates with capacity-factor proxies, joint wind–wave operability metrics, and downtime statistics, thereby strengthening the connection between climate projections and offshore engineering design, operation, and grid integration.

Sixth, the hybrid wind–wave resource classification should be further tested under alternative thresholds and planning constraints. Sensitivity analyses using different percentile definitions, stability metrics, or weighting between wind and wave components would improve robustness. Integrating bathymetry, distance-to-shore, environmental protection zones, and infrastructure constraints would enhance relevance for marine spatial planning.

Finally, translating regime-based diagnostics into stakeholder-oriented decision tools represents an important next step. Aggregating regime transitions and hybrid resource classes by Exclusive Economic Zones and marine ecoregions, and combining projected energy gains with indicators of variability and uncertainty, would support climate-aware offshore planning, risk assessment, and adaptive energy strategies across European seas.

Chapters 7 and 8 demonstrate that reducing uncertainty in atmospheric forcing is a necessary step for reliable wave-climate modelling, and that an objectively selected CMIP6 wind forcing can successfully drive regional wave hindcasts. Based on these findings, the following recommendations and directions for future work are proposed.

The use of raw CMIP6 winds proved sufficient for climate-scale wave hindcasting, but systematic biases remain, especially in coastal and semi-enclosed regions such as the North Sea. Future work should examine whether simple bias-correction approaches, applied seasonally or regionally, can reduce these errors without compromising physical consistency. In addition, dynamical downscaling of CMIP6 winds using a regional atmospheric model may improve the representation of coastal wind gradients and extreme wind events. Comparing wave simulations forced by raw, bias-corrected, and downscaled winds would help clarify the balance between realism, uncertainty reduction, and computational cost.

The KD-tree–based selection framework provided a clear and reproducible way to rank CMIP6 wind models using multiple performance metrics. This framework can be extended by including additional wind characteristics relevant for wave generation, such as extreme wind percentiles, directional stability, or persistence. Rather than selecting a single model, future studies could also retain a small subset of high-performing models to better represent forcing uncertainty. Exploring alternative machine-learning approaches may further improve the robustness of model ranking, but any extension should preserve the transparency and interpretability of the current method.

Several systematic wave-model biases identified in Chapter 8 are linked to simplified or missing physical processes. Future simulations should include incoming swell at open boundaries, particularly for regions influenced by remote storm systems, and wave–ice interac-

tions in high-latitude seas. Sensitivity tests using alternative source-term parameterisations could also help assess how model physics influence wave height and energy estimates. These improvements would allow a clearer separation between errors originating from wind forcing and those related to wave-model configuration.

The present hindcast focused on a 10-year historical period to validate the methodology. Extending the simulations to longer historical periods would allow analysis of decadal variability and more robust estimates of extremes. Most importantly, the framework should be applied to CMIP6 future scenarios, using the same objectively selected wind forcing. This would enable consistent assessment of projected changes in wave climate and wave energy potential, without introducing discontinuities between historical and future simulations.

Validation in this study focused primarily on significant wave height. Future work should include wave period, direction, and spectral characteristics, which are important for offshore engineering and wave-energy applications. Direct comparisons with buoy observations and satellite altimeter data would strengthen confidence in model performance beyond reanalysis-based validation. Assessing seasonal variability, interannual variability, and high-percentile events would further improve the robustness of the evaluation.

The wave-power distributions derived in Chapter 8 show clear relevance for offshore renewable-energy assessment. Future studies should link the modelling framework to energy yield estimates, device response, and marine spatial planning. Extending the analysis to coastal impacts, such as wave-driven erosion or operational constraints, would further enhance its practical value. Using a consistent climate-model-driven framework makes it possible to assess how wave-energy resources and coastal conditions may evolve under future climate forcing.

Finally, future work could explore coupled or hybrid modelling approaches, where waves interact with the atmosphere through surface roughness and momentum exchange. While computationally demanding, such approaches may improve the representation of extreme events. Hybrid strategies combining physics-based models with machine learning may offer a practical way to scale simulations while retaining physical interpretability.

References

O. J. Aarnes, M. Reistad, Ø. Breivik, E. Bitner-Gregersen, L. I. Eide, O. Gramstad, and E. Vanem. Projected changes in significant wave height toward the end of the 21st century: Northeast atlantic. Journal of Geophysical Research: Oceans, *122(4):3394–3403, 2017.*

Nima Afshar-Kaveh, Abbas Ghaheri, Vahid Chegini, Amir Etemad-Shahidi, and Mohammad Nazarali. Evaluation of different wind fields for storm surge modeling in the persian gulf. Journal of Coastal Research, *33(3):596–606, 2017. doi: 10.2112/JCOASTRES-D-15-00151.1.*

A. A. Akinsanola, K. O. Ogunjobi, A. T. Abolude, and S. Salack. Projected changes in wind speed and wind energy potential over west africa in CMIP6 models. Environmental Research Letters, *16(4):044033, 2021. doi: 10.1088/1748-9326/abe37c.*

A. Akpınar, P. J. Rosa-Santos, and D. Carvalho. Offshore wind and wave energy and climate change impacts. Frontiers in Energy Research, *10:1002690, 2022. doi: 10.3389/fenrg.2022.1002690.*

Fabrice Ardhuin, Eric Rogers, Alexander V. Babanin, Jean-François Filipot, Rudy Magne, Aron Roland, André van der Westhuysen, Pierre Queffeulou, Jérôme Lefevre, Lotfi Aouf, and Fabrice Collard. Semiempirical dissipation source functions for ocean waves. part i: Definition, calibration, and validation. Journal of Physical Oceanography, *40(9):1917–1941, 2010.*

Fabio Barbariol, Sarah Davison, Federico M. Falcieri, Rossella Ferretti, Andrea Ricchi, Mauro Sclavo, and Alvise Benetazzo. Wind waves in the Mediterranean Sea: an ERA5 reanalysis wind-based climatology. Frontiers in Marine Science, *8:760614, 2021. doi: 10.3389/fmars.2021.760614.*

A. G. Barnston and R. E. Livezey. Classification, seasonality and persistence of low-frequency atmospheric circulation patterns. Monthly Weather Review, *115(6):1083–1126, 1987.*

A. Benetazzo, A. Bergamasco, D. Bonaldo, F. M. Falcieri, M. Sclavo, L. Langone, and S. Carniel. Response of the adriatic sea to an intense cold air outbreak: dense water dynamics and wave-induced transport. Progress in Oceanography, *128:115–138, 2014. doi: 10.1016/j.pocean.2014.08.015.*

J. L. Bentley. Multidimensional binary search trees used for associative searching. Communications of the ACM, *18(9):509–517, 1975. doi: 10.1145/361002.361007.*

R. J. Bergillos, C. Rodriguez-Delgado, and G. Iglesias. Ocean Energy and Coastal Protection: A Novel Strategy for Coastal Management Under Climate Change. *Springer Nature, 2019. doi: 10.1007/978-3-030-31318-0.*

J. R. Bidlot, D. J. Holmes, P. A. Wittmann, R. Lalbeharry, and H. S. Chen. Intercomparison of the performance of operational ocean wave forecasting systems with buoy data. Weather and Forecasting, *17(2):287–310, 2002. doi: 10.1175/1520-0434(2002)017<0287:IOTPTO>2.0.CO;2.*

Harriet C. Bingham, Daniela Juffe Bignoli, Emma Lewis, Brian MacSharry, Neil D. Burgess, Piero Visconti, and Naomi Kingston. Sixty years of tracking conservation progress using the world database on protected areas. Nature Ecology & Evolution, *3(5):737–743, 2019. doi: 10.1038/s41559-019-0869-3.*

Christopher M. Bishop. Pattern Recognition and Machine Learning. *Information Science and Statistics. Springer, New York, 2006. ISBN 978-0-387-31073-2.*

Antonio Bonaduce, Joanna Staneva, Arno Behrens, Jean-Raymond Bidlot, and Ralf A. I. Wilcke. Wave climate change in the North Sea and Baltic Sea. Journal of Marine Science and Engineering, *7(6):166, 2019. doi: 10.3390/jmse7060166.*

S. Caires and A. Sterl. 100-year return value estimates for ocean wind speed and significant wave height from the era-40 data. Journal of Climate, *18(7):1032–1048, 2005. doi: 10.1175/JCLI3312.1.*

D. Carvalho, A. Rocha, X. Costoya, M. DeCastro, and M. Gómez-Gesteira. Wind energy resource over Europeunder CMIP6 future climate projections: What changes from CMIP5 to CMIP6. Renewable and Sustainable Energy Reviews, *151:111594, 2021. doi: 10.1016/j.rser.2021.111594.*

M. Casas-Prat and J. P. Sierra. Projected future wave climate in the nw Mediterranean Sea. Journal of Geophysical Research: Oceans, *118(7):3548–3568, 2013. doi: 10.1002/jgrc.20233.*

M. Casas-Prat, M. A. Hemer, G. Dodet, J. Morim, X. L. Wang, N. Mori, and Y. Feng. Wind-wave climate changes and their impacts. Nature Reviews Earth & Environment, *5 (1):23–42, 2024a.*

M. Casas-Prat, M.A. Hemer, G. Dodet, J. Morim, X.L. Wang, N. Mori, I. Young, L. Erikson, B. Kamranzad, P. Kumar, and M. Menéndez. Wind-wave climate changes and their impacts. Nature Reviews Earth & Environment, *5(1):23–42, 2024b.*

L. Cavaleri, F. Barbariol, and A. Benetazzo. Wind–wave modeling: Where we are, where to go. Journal of Marine Science and Engineering, *8(4):260, 2020. doi: 10.3390/jmse8040260.*

Luigi Cavaleri, Baylor Fox-Kemper, and Mark Hemer. Wind waves in the coupled climate system. Bulletin of the American Meteorological Society, *93(11):1651–1661, 2012.*

Environmental Modeling Center. User manual and system documentation of wavewatch iii® version 6.07. Technical report, NOAA/NCEP/MMAB, 2019.

E. Charles, D. Idier, P. Delecluse, M. Déqué, and G. Le Cozannet. Climate change impact on waves in the bay of biscay, france. Ocean Dynamics, *62:831–848, 2012.*

Arun Chawla, David Spindler, and Hendrik L. Tolman. A thirty year wave hindcast using the latest ncep climate forecast system reanalysis winds. In Proceedings of the 12th International Workshop on Wave Hindcasting and Forecasting*, volume 310, October 2011.*

Witold Cieślikiewicz and Aleksandra Cupial. Long-term statistics of atmospheric conditions over the Baltic Sea and meteorological features related to wind wave extremes in the Gulf of Gdańsk. Oceanologia*, 66(2):180–195, 2024. ISSN 23007370. doi: 10.1016/j.oceano.2023.10.002.*

K. Deng, C. Azorin-Molina, L. Minola, G. Zhang, and D. Chen. Global near-surface wind speed changes over the last decades revealed by reanalyses and CMIP6 model simulations. Journal of Climate*, 34(6):2219–2234, 2021. doi: 10.1175/JCLI-D-20-0344.1.*

Guillaume Dodet, Angélique Melet, Fabrice Ardhuin, Xavier Bertin, Déborah Idier, and Rafael Almar. The contribution of wind-generated waves to coastal sea-level changes. Surveys in Geophysics*, 40(6):1563–1601, 2019. doi: 10.1007/s10712-019-09557-5.*

A. I. Elshinnawy and J. A. Antolínez. A changing wave climate in the Mediterranean Sea during 58-years using uerra-mescan-surfex high-resolution wind fields. Ocean Engineering*, 271:113689, 2023. doi: 10.1016/j.oceaneng.2023.113689.*

V. Eyring, S. Bony, G. A. Meehl, C. A. Senior, B. Stevens, R. J. Stouffer, and K. E. Taylor. Overview of the coupled model intercomparison project phase 6 (CMIP6) experimental design and organization. Geoscientific Model Development*, 9(5):1937–1958, 2016. doi: 10.5194/gmd-9-1937-2016.*

I. Fairley, M. Lewis, B. Robertson, M. Hemer, I. Masters, J. Horrillo-Caraballo, and D. E. Reeve. A classification system for global wave energy resources based on multivariate clustering. Applied Energy*, 262:114515, 2020. doi: 10.1016/j.apenergy.2020.114515.*

P. J. Gleckler, K. E. Taylor, and C. Doutriaux. Performance metrics for climate models. Journal of Geophysical Research: Atmospheres*, 113(D6):D06104, 2008. doi: 10.1029/2007JD008972.*

R. Goyal, A. Sen Gupta, M. Jucker, and M. H. England. Historical and projected changes in the southern hemisphere surface westerlies. Geophysical Research Letters*, 48(4):e2020GL090849, 2021. doi: 10.1029/2020GL090849.*

Robert M. Graham, Stephen R. Hudson, and Marion Maturilli. Improved Performance of ERA5 in Arctic Gateway Relative to Four Global Atmospheric Reanalyses. Geophysical Research Letters*, 46(11):6138–6147, 2019. ISSN 19448007. doi: 10.1029/2019GL082781.*

The WAMDI Group. The wam model—a third generation ocean wave prediction model. Journal of Physical Oceanography*, 18(12):1775–1810, 1988.*

Y. Guanche, R. Guanche, P. Camus, F. J. Mendez, and R. Medina. A multivariate approach to estimate design loads for offshore wind turbines. Wind Energy*, 16(7):1091–1106, 2013. doi: 10.1002/we.1532.*

H. V. Gupta, H. Kling, K. K. Yilmaz, and G. F. Martinez. Decomposition of the mean squared error and nse performance criteria: Implications for improving hydrological modelling. Journal of Hydrology*, 377(1-2):80–91, 2009.*

R. J. Haarsma, M. J. Roberts, P. L. Vidale, C. A. Senior, A. Bellucci, Q. Bao, P. Chang, S. Corti, N. S. Fučkar, V. Guemas, J. von Hardenberg, W. Hazeleger, C. Kodama, T. Koenigk, L. R. Leung, J. Lu, J.-J. Luo, J. Mao, M. S. Mizielinski, R. Mizuta, P. Nobre, M. Satoh, E. Scoccimarro, T. Semmler, J. Small, and J.-S. von Storch. High resolution model intercomparison project (HighResMIP v1.0) for CMIP6. Geoscientific Model Development*, 9(11):4185–4208, 2016. doi: 10.5194/gmd-9-4185-2016.*

Mark A. Hemer, John A. Church, and John R. Hunter. Variability and trends in the directional wave climate of the southern hemisphere. International Journal of Climatology: A Journal of the Royal Meteorological Society*, 30(4):475–491, 2010. doi: 10.1002/joc.1900.*

Mark A. Hemer, Yalin Fan, Nobuhito Mori, Alvaro Semedo, and Xiaolan L. Wang. Projected changes in wave climate from a multi-model ensemble. Nature Climate Change*, 3(5): 471–476, 2013. doi: 10.1038/nclimate1791.*

Hans Hersbach, Bill Bell, Paul Berrisford, Shoji Hirahara, András Horányi, Joaquín Muñoz-Sabater, Julien Nicolas, Carole Peubey, Raluca Radu, Dinand Schepers, Adrian Simmons, Cornel Soci, Saleh Abdalla, Xavier Abellan, Gianpaolo Balsamo, Peter Bechtold, Gionata Biavati, Jean Bidlot, Massimo Bonavita, Giovanna De Chiara, Per Dahlgren, Dick Dee, Michail Diamantakis, Rossana Dragani, Johannes Flemming, Richard Forbes, Manuel Fuentes, Alan Geer, Leo Haimberger, Sean Healy, Robin J. Hogan, Elías Hólm, Marta Janisková, Sarah Keeley, Patrick Laloyaux, Philippe Lopez, Cristina Lupu, Gabor Radnoti, Patricia de Rosnay, Iryna Rozum, Freja Vamborg, Sebastien Villaume, and Jean Noël Thépaut. The ERA5 global reanalysis. Quarterly Journal of the Royal Meteorological Society*, 146(730):1999–2049, 2020. ISSN 1477870X. doi: 10.1002/qj.3803.*

Leo H. Holthuijsen. Waves in Oceanic and Coastal Waters*. Cambridge University Press, Cambridge, 2010.*

J. W. Hurrell and C. Deser. North Atlantic climate variability: the role of the North Atlantic oscillation. Journal of Marine Systems*, 79(3-4):231–244, 2010.*

James W. Hurrell. Decadal trends in the North Atlantic oscillation: Regional temperatures and precipitation. Science*, 269(5224):676–679, 1995. doi: 10.1126/science.269.5224.676.*

Anil K. Jain. Data clustering: 50 years beyond k-means. Pattern Recognition Letters*, 31(8): 651–666, 2010. doi: 10.1016/j.patrec.2009.09.011.*

P. A. E. M. Janssen. The Interaction of Ocean Waves and Wind*. Cambridge University Press, Cambridge, UK, 2004.*

I. T. Jolliffe. Principal component analysis for special types of data. In Principal Component Analysis*, pages 338–372. Springer New York, 2002.*

W. J. Knoben, J. E. Freer, and R. A. Woods. Inherent benchmark or not? comparing nash–sutcliffe and kling–gupta efficiency scores. Hydrology and Earth System Sciences*, 23 (10):4323–4331, 2019. doi: 10.5194/hess-23-4323-2019.*

Boma Kresning, M. Reza Hashemi, Amir Shirvani, and Javad Hashemi. Uncertainty of extreme wind and wave loads for marine renewable energy farms in hurricane-prone regions. Renewable Energy*, 220(December 2022):119570, 2024. ISSN 18790682. doi: 10.1016/j.renene.2023.119570. URL https://doi.org/10.1016/j.renene.2023.119570.*

H. Kutiel and Y. Benaroch. North Sea-caspian pattern (ncp)–an upper level atmospheric teleconnection affecting the eastern mediterranean: Identification and definition. Theoretical and Applied Climatology*, 71:17–28, 2002.*

J. L. Li, K. M. Xu, J. H. Jiang, W. L. Lee, L. C. Wang, J. Y. Yu, and Y. H. Wang. An overview of CMIP5 and CMIP6 simulated cloud ice, radiation fields, surface wind stress, sea surface temperatures, and precipitation over tropical and subtropical oceans. Journal of Geophysical Research: Atmospheres*, 125(15):e2020JD032848, 2020. doi: 10.1029/2020JD032848.*

J. H. Liang, X. Wan, K. A. Rose, P. P. Sullivan, and J. C. McWilliams. Horizontal dispersion of buoyant materials in the ocean surface boundary layer. Journal of Physical Oceanography*, 48(9):2103–2125, 2018. doi: 10.1175/JPO-D-18-0025.1.*

A. K. Liu, B. Holt, and P. W. Vachon. Wave propagation in the marginal ice zone: Model predictions and comparisons with buoy and synthetic aperture radar data. Journal of Geophysical Research: Oceans*, 96(C3):4605–4621, 1991. doi: 10.1029/90JC02368.*

S. Lloyd. Least squares quantization in PCM. IEEE Transactions on Information Theory*, 28 (2):129–137, 1982. doi: 10.1109/TIT.1982.1056489.*

Hector Lobeto, Melisa Menendez, and Iñigo J. Losada. Future behavior of wind wave extremes due to climate change. Scientific Reports*, 11(1):7869, 2021. doi: 10.1038/s41598-021-87267-z.*

Hector Lobeto, Alvaro Semedo, Gil Lemos, Ali Dastgheib, Melisa Menendez, Roshanka Ranasinghe, and Jean Raymond Bidlot. Global coastal wave storminess. Scientific Reports*, 14(1):1–18, 2024. ISSN 20452322. doi: 10.1038/s41598-024-51420-0. URL https://doi.org/10.1038/s41598-024-51420-0.*

A. Martinez and G. Iglesias. Climate change impacts on wind energy resources in north america based on the CMIP6 projections. Science of The Total Environment*, 806:150580, 2022. doi: 10.1016/j.scitotenv.2021.150580.*

A. Martínez-Asensio, M. N. Tsimplis, M. Marcos, X. Feng, D. Gomis, G. Jordà, and S. A. Josey. Response of the North Atlantic wave climate to atmospheric modes of variability. International Journal of Climatology*, 36(3), 2016.*

P. Maya and J. A. A. Antolínez. Multivariate spatio-temporal clustering of wind–wave variability across european seas. Atmosphere*, 2025. Under review for the Special Issue "Wind and Wave Climate Variability and Its Impacts on Coastal and Marine Environments".*

Ponni Maya, George Lavidas, Alexander Metrikine, and Marta Alvarez Gonzalez. CMIP6 wave climate simulation in the european north east atlantic basin using wavewatch iii. In Proceedings of the European Wave and Tidal Energy Conference*, volume 15, September 2023.*

A. Meucci, I. R. Young, C. Trenham, and M. Hemer. An 8-model ensemble of CMIP6-derived ocean surface wave climate. Scientific Data*, 11(1):100, 2024.*

Andrea Meucci, Ian R. Young, Mark Hemer, Erkan Kirezci, and Roshanka Ranasinghe. Projected 21st century changes in extreme wind-wave events. Science Advances*, 6(24): eaaz7295, 2020. doi: 10.1126/sciadv.aaz7295.*

J. Morim, M. Hemer, X. L. Wang, N. Cartwright, C. Trenham, A. Semedo, I. Young, L. Bricheno, P. Camus, M. Casas-Prat, and L. Erikson. Robustness and uncertainties in global multivariate wind-wave climate projections. Nature Climate Change*, 9(9):711–718, 2019. doi: 10.1038/s41558-019-0542-5.*

J. Morim, L. H. Erikson, M. Hemer, I. Young, X. Wang, N. Mori, and T. Wahl. A global ensemble of ocean wave climate statistics from contemporary wave reanalysis and hindcasts. Scientific Data*, 9(1):358, 2022.*

M. H. Mousa and M. K. Hussein. Toward high-performance computation of surface approximation using a gpu. Computers and Electrical Engineering*, 99:107761, 2022. doi: 10.1016/j.compeleceng.2022.107761.*

Walter H. Munk. Origin and generation of waves. Technical Report SIO Ref. 51-57, Scripps Institution of Oceanography, 1951.

Farshid Najafzadeh, Marcin Z. Jankowski, Andrea Giudici, Risto Männikus, Ülo Suursaar, Maido Viška, and Tarmo Soomere. Spatiotemporal variability of wave climate in the gulf of riga. Oceanologia*, 66(1):56–77, 2024. doi: 10.1016/j.oceano.2024.01.003.*

Jon Olauson. ERA5: The new champion of wind power modelling? Renewable Energy*, 126: 322–331, 2018. doi: 10.1016/j.renene.2018.03.056.*

Intergovernmental Panel on Climate Change (IPCC). Climate Change 2013: The Physical Science Basis. Contribution of Working Group I to the Fifth Assessment Report of the Intergovernmental Panel on Climate Change. *Cambridge University Press, Cambridge, 2013.*

A. I. Osman, L. Chen, M. Yang, G. Msigwa, M. Farghali, S. Fawzy, and P. S. Yap. Cost, environmental impact, and resilience of renewable energy under a changing climate: a review. Environmental Chemistry Letters*, 21(2):741–764, 2023.*

F. Pedregosa, G. Varoquaux, A. Gramfort, V. Michel, B. Thirion, O. Grisel, M. Blondel, P. Prettenhofer, R. Weiss, V. Dubourg, J. Vanderplas, A. Passos, D. Cournapeau, M. Brucher, M. Perrot, and É. Duchesnay. Scikit-learn: Machine learning in python. Journal of Machine Learning Research*, 12:2825–2830, 2011.*

J. Perez, M. Menendez, P. Camus, F. J. Mendez, and I. J. Losada. Statistical multi-model climate projections of surface ocean waves in europe. Ocean Modelling*, 96:161–170, 2015.*

Owen M. Phillips. The Dynamics of the Upper Ocean*. Cambridge University Press, 1977.*

Elizabeth P. Pike, Jennifer M. MacCarthy, Summer O. Hameed, Nicole Harasta, Kirsten Grorud-Colvert, Jessica Sullivan-Stack, and Lance Morgan. Ocean protection quality is lagging behind quantity: Applying a scientific framework to assess real marine protected area progress against the 30 by 30 target. Conservation Letters*, 17(3):e13020, 2024. doi: 10.1111/conl.13020.*

J. Pérez, M. Menéndez, F. J. Méndez, and I. J. Losada. Evaluating the performance of cmip3 and CMIP5 global climate models over the north-east atlantic region. Climate Dynamics*, 43(9):2663–2680, 2014. doi: 10.1007/s00382-014-2078-8.*

Borja G. Reguero, Iñigo J. Losada, and Fernando J. Méndez. A global wave power resource and its seasonal, interannual and long-term variability. Applied Energy*, 148:366–380, 2015. doi: 10.1016/j.apenergy.2015.03.114.*

Borja G. Reguero, Iñigo J. Losada, and Fernando J. Méndez. A global wave power resource and its seasonal, interannual and long-term variability. Applied Energy*, 148:366–380, 2019. doi: 10.1016/j.apenergy.2015.03.114.*

C. Rodriguez-Delgado, R. J. Bergillos, and G. Iglesias. Dual wave farms for energy production and coastal protection under sea level rise. Journal of Cleaner Production, *222:364–372, 2019. doi: 10.1016/j.jclepro.2019.03.061.*

W. E. Rogers, J. Thomson, H. H. Shen, M. J. Doble, P. Wadhams, and S. Cheng. Dissipation of wind waves by pancake and frazil ice in the autumn beaufort sea. Journal of Geophysical Research: Oceans, *121(11):7991–8007, 2016. doi: 10.1002/2016JC012251.*

Aron Roland, Yinglong J. Zhang, H. V. Wang, Ying Meng, Y. C. Teng, Vladimir Maderich, Ivan Brovchenko, Mirela Dutour-Sikiric, and Ulrich Zanke. A fully coupled 3d wave-current interaction model on unstructured grids. Journal of Geophysical Research: Oceans, *117 (C11), 2012. doi: 10.1029/2012JC007952.*

Suranjana Saha, Shrinivas Moorthi, Hua-Lu Pan, Xingren Wu, Juhua Wang, Sudhir Nadiga, and Mitchell Goldberg. The ncep climate forecast system reanalysis. Bulletin of the American Meteorological Society, *91(8):1015–1058, 2010. doi: 10.1175/2010BAMS3001.1.*

Divya Sardana, Prashant Kumar, and Rajni. Influence of climate variability modes over wind-sea and swell generated wave energy. Ocean Engineering, *291(June 2023):116471, 2024. ISSN 00298018. doi: 10.1016/j.oceaneng.2023.116471. URL https://doi.org/10.1016/j.oceaneng.2023.116471.*

J. Sarmiento, A. Iturrioz, V. Ayllón, R. Guanche, and I. J. Losada. Experimental modelling of a multi-use floating platform for wave and wind energy harvesting. Ocean Engineering, *173:761–773, 2019. doi: 10.1016/j.oceaneng.2018.12.046.*

A. Semedo, K. Sušelj, A. Rutgersson, and A. Sterl. A global view on the wind sea and swell climate and variability from era-40. Journal of Climate, *24(5):1461–1479, 2011.*

Jian Shi, Xiangbo Feng, Ralf Toumi, Chi Zhang, Kevin I. Hodges, Aifeng Tao, Wei Zhang, and Jinhai Zheng. Global increase in tropical cyclone ocean surface waves. Nature Communications, *15(1), 2024. ISSN 20411723. doi: 10.1038/s41467-023-43532-4.*

Youn L. Shin and Hyeon J. Song. Normative challenges in addressing climate-induced maritime distress and search-and-rescue operations within exclusive economic zones (eezs). Journal of the Society of Disaster Information, *21(1):241–248, 2025.*

T. Song, H. Liao, and G. Subbarayan. Efficient local refinement near parametric boundaries using kd-tree data structure and algebraic level sets. Algorithms, *15(7):245, 2022. doi: 10.3390/a15070245.*

Mark D. Spalding, Helen E. Fox, Gerald R. Allen, Nick Davidson, Zadie A. Ferdaña, Max A. X. Finlayson, Benjamin S. Halpern, Melanie A. Jorge, Andrea Lombana, Sara A. Lourie, Kenneth D. Martin, Ed McManus, Jennifer Molnar, Catherine A. Recchia, and James Robertson. Marine ecoregions of the world: A bioregionalization of coastal and shelf areas. BioScience, *57(7):573–583, 2007. doi: 10.1641/B570707.*

J. E. Stopa and K. F. Cheung. Intercomparison of wind and wave data from the ecmwf reanalysis interim and the ncep climate forecast system reanalysis. Ocean Modelling, *75: 65–83, 2014. doi: 10.1016/j.ocemod.2014.01.002.*

Justin E. Stopa, Fabrice Ardhuin, and Fanny Girard-Ardhuin. Wave climate in the arctic 1992–2014: Seasonality and trends. The Cryosphere, *10(4):1605–1629, 2016. doi: 10.5194/tc-10-1605-2016.*

S. Susini, M. Menendez, P. Eguia, and J. M. Blanco. Climate change impact on the offshore wind energy over the North Sea and the irish sea. Frontiers in Energy Research*, 10:881146, 2022. doi: 10.3389/fenrg.2022.881146.*

Lynne D. Talley. Descriptive Physical Oceanography: An Introduction*. Academic Press, 2011.*

The WAM Group. The wam model—a third generation ocean wave prediction model. Journal of Physical Oceanography*, 18(12):1775–1810, 1988.*

D. W. J. Thompson and J. M. Wallace. The arctic oscillation signature in the wintertime geopotential height and temperature fields. Geophysical Research Letters*, 25(9):1297–1300, 1998.*

D. W. J. Thompson and J. M. Wallace. Annular modes in the extratropical circulation. part i: Month-to-month variability. Journal of Climate*, 13(5):1000–1016, 2000.*

K. B. Tokarska, M. B. Stolpe, S. Sippel, E. M. Fischer, C. J. Smith, F. Lehner, and R. Knutti. Past warming trend constrains future warming in CMIP6 models. Science Advances*, 6(12): eaaz9549, 2020. doi: 10.1126/sciadv.aaz9549.*

Hendrik L. Tolman. A third-generation model for wind waves on slowly varying, unsteady, and inhomogeneous depths and currents. Journal of Physical Oceanography*, 21(6):782–797, 1991.*

Hendrik L. Tolman. User manual and system documentation of wavewatch iii™ version 3.14. Technical Note MMAB Contribution 276, NOAA / National Weather Service, National Centers for Environmental Prediction, 2009. 276 pp.

Hendrik L. Tolman. User manual and system documentation of wavewatch iii version 4.18. Technical Note MMAB Contribution 316, NOAA / National Weather Service, National Centers for Environmental Prediction, 2014. NOAA/NWS/NCEP/MMAB.

Tim Toomey, Angel Amores, Marta Marcos, and Alejandro Orfila. Coastal sea levels and wind-waves in the Mediterranean Sea since 1950 from a high-resolution ocean reanalysis. Frontiers in Marine Science*, 9(September):1–16, 2022. ISSN 22967745. doi: 10.3389/fmars.2022.991504.*

Kevin E. Trenberth, John T. Fasullo, and Jeffrey Kiehl. Earth's global energy budget. Bulletin of the American Meteorological Society*, 90(3):311–324, 2009.*

G. Varlas, V. Vervatis, C. Spyrou, E. Papadopoulou, A. Papadopoulos, and P. Katsafados. Investigating the impact of atmosphere–wave–ocean interactions on a mediterranean tropical-like cyclone. Ocean Modelling*, 153:101675, 2020.*

J. M. Wallace and D. S. Gutzler. Teleconnections in the geopotential height field during the northern hemisphere winter. Monthly Weather Review*, 109(4):784–812, 1981.*

X. L. Wang, F. W. Zwiers, and V. R. Swail. North Atlantic ocean wave climate change scenarios for the twenty-first century. Journal of Climate*, 17(12):2368–2383, 2004. doi: 10.1175/1520-0442(2004)017<2368:NAOWCC>2.0.CO;2.*

A. F. Waterhouse, J. A. MacKinnon, J. D. Nash, M. H. Alford, E. Kunze, H. L. Simmons, K. L. Polzin, L. C. St. Laurent, O. M. Sun, R. Pinkel, and L. D. Talley. Global patterns of diapycnal mixing from measurements of the turbulent dissipation rate. Journal of Physical Oceanography*, 44(7):1854–1872, 2014. doi: 10.1175/JPO-D-13-0104.1.*

C. J. Willmott. On the validation of models. Physical Geography, *2:184–194, 1981.*

WindEurope. Wind energy in europe: 2022 statistics and the outlook for 2023-2027, 2022. URL https://windeurope.org/intelligence-platform/product/wind-energy-in-europe-2022-statistics-and-the-outlook-for-2023-2027/. Accessed: 2025-01-11.

J. Wolf and D. K. Woolf. Waves and climate change in the north-east atlantic. Geophysical Research Letters, *33(6), 2006. doi: 10.1029/2005GL025113.*

D. Woolf and J. Wolf. Impacts of climate change on storms and waves. MCCIP Science Review, *2013:20–26, 2013.*

D. Xu and Y. Tian. A comprehensive survey of clustering algorithms. Annals of Data Science, *2(2):165–193, 2015. doi: 10.1007/s40745-015-0040-1.*

I. R. Young and A. Ribal. Multiplatform evaluation of global trends in wind speed and wave height. Science, *364(6440):548–552, 2019.*

Ian R. Young. Wind Generated Ocean Waves. *Elsevier, 1999.*

Ian R. Young, Stefan Zieger, and Alexander V. Babanin. Global trends in wind speed and wave height. Science, *332(6028):451–455, 2011. doi: 10.1126/science.1197219.*

M. D. Zelinka, T. A. Myers, D. T. McCoy, S. Po-Chedley, P. M. Caldwell, P. Ceppi, and K. E. Taylor. Causes of higher climate sensitivity in CMIP6 models. Geophysical Research Letters, *47(1):e2019GL085782, 2020. doi: 10.1029/2019GL085782.*

S. Zhang and J. Chen. Uncertainty in projection of climate extremes: A comparison of CMIP5 and CMIP6. Journal of Meteorological Research, *35(4):646–662, 2021. doi: 10.1007/s13351-021-1026-0.*

Stefan Zieger, Jayaram Vinoth, and Ian R. Young. Joint calibration of multiplatform altimeter measurements of wind speed and wave height over the past 20 years. Journal of Atmospheric and Oceanic Technology, *26(12):2549–2564, 2009. doi: 10.1175/2009JTECHA1327.1.*

Epilogue

At the beginning of this Ph.D., I carried a familiar thought: if there is a will, there is a way. I understood will as the intention to contribute something careful and useful, trusting that patience would allow a path to form.

With time, that belief became more measured. There were periods when persistence mattered more than momentum, and moments when not acting was as important as acting—*"patience is the companion of wisdom,"* as Saint Augustine observed. Progress was often subtle. Some directions unfolded slowly; others needed to be paused or reconsidered. What sustained me was not confidence in outcomes, but the ability to remain resilient as expectations shifted.

I learned that effort alone does not guarantee clarity. Continuing often meant returning to first assumptions, adjusting pace, or accepting that understanding arrives unevenly. I began to see the difference between endurance that sharpens insight and effort that simply exhausts it. Looking back, even delays and detours carried meaning, though not always at the time.

Not all refinement is gentle. Some lessons arrive through resistance, silence, humiliation, or being underestimated. Yet certain experiences cut deeply enough to refine rather than diminish. Looking back, I recognise that many of the moments that appeared destructive at first were, in fact, sharpening something quieter and more enduring. Eventually, the need to defend oneself disappears, and the work begins to speak alone.

During this process, I often returned to a thought that reflects the limits of intention and control:

> *"The last thing one discovers in composing a work is what one must put first."*
> — T. S. Eliot

I read this not as a statement about finishing, but about orientation. Understanding tends to emerge only after experience has altered the questions themselves. By the end of this Ph.D., I was less concerned with arriving at conclusions, and more attentive to how judgment had changed—how confidence had given way to care.

This thesis marks a point of transition rather than an ending. What remains is not resolution, but a steadier direction—one that allows uncertainty without urgency, and effort without force. I am grateful to those who have taken the time to read this work; whatever value it holds exists only through that attention.

Perhaps fittingly, a study centered on renewable energy resources also taught me how to use my own "resources" more wisely.

The reader who has accompanied me through this journey will recognise that it is not finished, and that what remains is a reminder of responsibility—to use, with patience and care, the knowledge we have gained.

Appendix

Supplementary Material

A.1 WW3 Model Setup and Theoretical Foundation

WW3 is a state-of-the-art numerical model developed for predicting wind-generated ocean waves. Initially created by the National Oceanic and Atmospheric Administration's National Centers for Environmental Prediction (NOAA/NCEP) during the 1990s, WW3 is classified as a third-generation spectral wave model Tolman [2009]. It was designed as a successor to earlier versions of WW3 and draws substantial theoretical inspiration from the pioneering WAM model The WAM Group [1988].

WW3 simulates the growth and evolution of the wave energy spectrum based on wind input, incorporating the current understanding of air–sea interactions and wave physics Tolman [1991]. A key advancement of WW3 over previous models lies in its improved governing equations, sophisticated numerical schemes, and updated physical parameterizations that enhance forecast accuracy and operational flexibility Tolman [2014].

At its core, WW3 solves the spectral action balance equation - a fundamental conservation law for wave energy - which allows it to simulate wind-driven wave generation, propagation, and dissipation Ardhuin et al. [2010]. The model incorporates multiple physical processes including wind input, nonlinear wave–wave interactions, dissipation due to whitecapping, bottom friction losses, and shallow-water breaking Afshar-Kaveh et al. [2017]. These make the model versatile enough to handle conditions from global oceans to shallow coastal zones, including wetting and drying processes for coastal grid cells Roland et al. [2012].

WW3 is widely used for operational wave forecasting by NOAA and other meteorological services globally Chawla et al. [2011], producing outputs such as significant wave height, mean wave period, direction, and spectral distributions. Beyond operational forecasting, it serves as a robust research tool for hindcasting wave climates, studying extreme storm events, and testing new wave physics schemes Morim et al. [2019].

Its open-source nature and community-driven development have made it the preferred choice in both research and industry. In the sections that follow, we explore the theoretical foundations of WW3 and the practical aspects of its implementation.

A.1.1 Theoretical Framework of WW3: Governing Spectral Action Balance Equation

In third-generation wave models such as `WAVEWATCH III` (WW3), the sea state is described by the wave energy spectrum $E(f, \theta; \mathbf{x}, t)$ or equivalently the variance density spectrum $F(k, \theta; \mathbf{x}, t)$, which distributes wave energy variance across wavenumber (k) or frequency (f) and direction (θ). For practical modeling purposes, the wave action spectrum $N(k, \theta; \mathbf{x}, t)$ is

used, defined as $N = E/\sigma$, where $\sigma = 2\pi f$ is the intrinsic angular frequency. Wave action N is conserved in the presence of currents or depth variations, whereas energy E is not, making N the appropriate quantity for the governing equation. WW3 is based on linear wave theory, such that σ and k are related by the dispersion relation $\sigma^2 = gk\tanh(kd)$, where g is the gravitational acceleration and d is the local water depth.

Conservation Equation. The evolution of the action density spectrum is governed by the spectral action balance equation, which in compact conceptual form can be written as:

$$\frac{DN}{Dt} = \frac{S_{\text{tot}}}{\sigma} \tag{1}$$

where D/Dt is the total (or material) time derivative following a wave group, and S_{tot} represents the net source term-the sum of all energy source and sink processes. This equation expresses that the rate of change of wave action following the propagation of waves equals the combined effect of all wave generation, dissipation, and nonlinear transfer processes.

For implementation in an Eulerian model, this is expanded into a partial differential equation. In a Cartesian (flat-earth) coordinate system with spatial coordinates $\mathbf{x} = (x, y)$, wavenumber k, and direction θ, the action balance equation can be written in conservation form as:

$$\frac{\partial N(k,\theta;\mathbf{x},t)}{\partial t} + \nabla_{\mathbf{x}} \cdot (\dot{\mathbf{x}}\, N) + \frac{\partial}{\partial k}(\dot{k}\, N) + \frac{\partial}{\partial \theta}(\dot{\theta}\, N) = \frac{S_{\text{tot}}}{\sigma} \tag{2}$$

Each term on the left-hand side of the spectral action balance equation represents transport of spectral action in a different domain: time, geographic space, wavenumber (or frequency), and direction. The quantities $\dot{\mathbf{x}}$, $\dot{k}$, and $\dot{\theta}$ are the characteristic propagation velocities in physical and spectral space.

In the absence of ambient currents or depth variations, $\dot{\mathbf{x}}$ corresponds to the wave group velocity c_g (with components c_{gx}, c_{gy}), while $\dot{k} = 0$ and $\dot{\theta} = 0$, implying that energy propagates without changes in k or θ. In general, however, these terms account for wave advection by currents, refraction, and shoaling due to spatial variation in depth or currents. Specifically:

$$\dot{\mathbf{x}} = c_g + \mathbf{U}(\mathbf{x}) \tag{3}$$

where $\mathbf{U}$ is the ambient current vector, indicating that current advection carries wave energy with the flow.

The term $\dot{k}$ represents the rate of change of wavenumber (or frequency) following the wave and arises due to spatial gradients in depth and currents. In `WW3`, this is modeled as:

$$\dot{k} = -\frac{\partial \sigma}{\partial d} \cdot \frac{\partial d}{\partial s} - k \cdot \frac{\partial \mathbf{U}}{\partial s} \tag{4}$$

where $\partial/\partial s$ denotes the derivative along the direction of wave propagation. The first term, $-\frac{\partial \sigma}{\partial d} \cdot \frac{\partial d}{\partial s}$, represents shoaling-i.e., how waves speed up or slow down due to changes in depth d. The second term, $-k \cdot \frac{\partial \mathbf{U}}{\partial s}$, is the Doppler refraction term arising from current gradients along the wave path; waves propagating into opposing currents shorten, while waves in following currents lengthen.

Similarly, the turning rate $\dot{\theta}$ describes the change in wave direction due to gradients in depth and current perpendicular to the wave direction:

$$\dot{\theta} = -\frac{1}{k}\left(\frac{\partial \sigma}{\partial d} \cdot \frac{\partial d}{\partial m} + k \cdot \frac{\partial \mathbf{U}}{\partial m}\right) \tag{5}$$

where $\partial/\partial m$ is the derivative perpendicular to the wave heading. This causes wave refraction: waves bend toward shallower regions or lower current speeds. For example, waves approaching a beach turn to become more shore-normal as depth decreases.

On a spherical Earth, additional geometric terms are introduced. The advection terms include corrections for latitude convergence, and the turning rate $\dot{\theta}$ gains an extra term:

$$-\frac{c_g \tan\phi \cos\theta}{R} \tag{6}$$

which accounts for great-circle propagation, where ϕ is the latitude and R is Earth's radius.

`WW3` supports both Cartesian and spherical coordinate systems; in the spherical mode, the full action balance equation includes all these geometry-related corrections.

The right-hand side of the balance equation represents the source term S_{tot}/σ, i.e. the sum of all energy input and dissipation terms (divided by σ because $N = E/\sigma$ is used in the model). In deep water, S_{tot} is traditionally decomposed into three dominant contributions:

- **Wind input (S_{in})**: energy added to waves by wind forcing at the sea surface (can be negative for swell losing energy to the atmosphere);
- **Nonlinear wave-wave interactions (S_{nl})**: conservative redistribution of energy across the spectrum by resonant wave interactions;
- **Wave dissipation (S_{ds})**: energy lost due to wave breaking (whitecapping) and other dissipative mechanisms in deep water.

In shallow water (finite depth), additional terms must be included. Wave energy can be lost through bottom friction (S_{bot}) as waves interact with the seabed, and in very shallow depths through depth-induced breaking (S_{db}) in the surf zone where waves become too steep for the given depth. Nonlinear triad interactions (S_{tr}) among three-wave groups can also transfer energy between frequencies in shallow water. Other processes that may be represented in S_{tot} include: wave–ice interactions (S_{ice}) in ice-covered regions, which attenuate wave energy; wave scattering by bathymetric features (S_{bs}); energy reflection from shorelines or obstacles (S_{ref}); and a catch-all user-defined term (S_{user}) for any additional processes.

In WW3, all these source and sink terms can be activated or deactivated depending on the physical environment (e.g. S_{bot} and S_{db} are set to zero in deep water, S_{ice} only applies in the presence of sea ice, etc.). The full expression for the total source term in WW3 (for the energy spectrum) is given by:

$$S_{\text{tot}} = S_{ln} + S_{in} + S_{nl} + S_{ds} + S_{bot} + S_{db} + S_{tr} + S_{bs} + S_{ice} + S_{ref} + S_{user} \tag{7}$$

where S_{ln} is an optional linear wind input term used for initial wave growth (discussed below). Each of these terms represents a specific physical process, discussed in detail next. We will describe the form of each source/sink term, their physical interpretations, and the conditions under which they are active in WW3.

A.1.2 Wave Spectral Energy Source and Sink Terms

Overview. In the spectral balance equation, S_{tot} represents the combined effect of sources and sinks of wave energy. Each term $S_i(f,\theta)$ on the right-hand side injects or removes energy at a given frequency–direction (f,θ) in the spectrum. Figure 2.16 of the WW3 manual (WW3DG 2019) enumerates all source terms implemented in WW3. The dominant source/sink processes can be grouped by physical regime:

- **Deep water (no depth influence):** wind input (S_{in}) pumps energy into the waves, balanced by whitecap dissipation (S_{ds}). Nonlinear spectral transfer (S_{nl}) redistributes energy internally but does not add or remove net energy.

- **Finite depth (shallow water):** bottom friction (S_{bot}) and depth-limited breaking (S_{db}) become additional sinks of energy, and triad interactions (S_{tr}) provide additional internal transfers.
- **Ice-covered seas:** wave–ice interactions (S_{ice}, and scattering S_{is}) attenuate and scatter wave energy in the presence of sea ice.
- **Miscellaneous processes:** e.g. scattering by unresolved seabed roughness (S_{bs}), partial wave reflection at coasts (S_{ref}), etc., which are usually minor or situation-specific terms.

Below, we detail each major source/sink term in WW3, including their theoretical formulation and typical parameterizations. Table 1 summarizes when each process is relevant. Many of these terms have multiple available formulations or parameterizations in WW3; for clarity, we indicate the WW3 "switch" names (in parentheses) for key options (e.g. the default wind input parameterization is referred to as ST4 in WW3).

Table 1 Major Source/Sink Terms in WW3 and Activation Conditions
Adapted from WW3DG (2019); outlines key physical processes and typical activation scenarios.

Source Term	Physical Process	Active / Relevant When...
S_{in} (wind input)	**Wind energy input to waves**. Positive (growth) or negative (damping) transfer depending on wind–wave speed relation.	Wind over water surface. *Negative* S_{in} for swell in light/opposing wind.
S_{nl} (nonlinear 4-wave interactions)	**Spectral energy redistribution** via resonant wave-wave quartets. No net gain or loss.	Always active. Dominant in deep water shaping, but negligible effect on total energy.
S_{ds} (whitecapping dissipation)	**Dissipation due to deep-water breaking** (whitecaps). Parametrizes energy cascade to turbulence.	Active in all wind-driven seas. Balances S_{in} in steady state.
S_{bot} (bottom friction)	**Loss from seabed drag** (viscous/-turbulent).	Shallow water where orbital motion touches seabed ($d < L/2$). Negligible in deep water.
S_{db} (depth-induced breaking)	**Energy loss via surf breaking** in shallow water.	Surf zone, when H/d0.5–0.8. Not used in deep water.
S_{tr} (nonlinear triad interactions)	**Three-wave energy transfers** (triads). Transfers to higher frequencies.	Shallow/intermediate depths. Shapes nearshore spectrum.
S_{ice} (wave–ice attenuation)	**Loss from wave–ice interactions**: damping, scattering, frazil/-grease ice.	Only active in sea ice regions. Inactive in open water.
Additional terms: S_{bs}, S_{ref}, S_{ln}, S_{user}	**Special cases**: bottom scattering, reflection, linear growth, user-defined losses.	S_{bs}: complex bathymetry; S_{ref}: coasts/icebergs; S_{ln}: calm starts; S_{user}: custom.

A.1.2.1 Wind Energy Input (S_{in})

Physical mechanism: Wind blowing over the ocean transfers energy to the waves through pressure fluctuations and shear stress at the air–sea interface. This atmospheric input term S_{in} is typically positive, representing wave growth, and is the primary source of energy for wind waves. Physically, when wind speed at the surface exceeds the wave phase speed, pressure variations along the wave profile do positive work on the waves (the Miles mechanism of wind–wave resonance). Conversely, if waves propagate faster than the wind (swell outrunning a weak wind), S_{in} can become negative – the atmosphere then extracts energy from the waves (causing swell damping).

In WW3, the wind input source term is often conceptually split into two parts: a positive input from wind to waves ($S_{\text{atm-in}}$) and a possible negative input or drag on the waves ($S_{\text{atm-out}}$) due to swell. The total wind–wave interaction term is $S_{in} = S_{\text{atm-in}} + S_{\text{atm-out}}$. Most modern parameterizations inherently allow negative values for swell, though older formulations simply set $S_{in} = 0$ when wind cannot drive growth.

Formulation: The exact physics of wind–wave growth are complex, so S_{in} is parameterized empirically or semi-empirically. A widely used early formulation is that of Snyder et al. (1981) as adapted by Komen et al. (1984) for the first-generation WAM model. In this formulation (used in WAM Cycle 3, WW3 switch `ST1`), the wind input growth rate is proportional to the ratio of friction velocity u_* to phase speed c minus a threshold, and concentrated in waves traveling in the wind direction.

For example, WAM Cycle 3 uses:

$$S_{in}(k,\theta) = C_{in}\,\frac{\rho_a}{\rho_w}\,\max\left[0,\,28\,\frac{u_*}{c}\cos(\theta-\theta_w)-1\right]\sigma\,N(k,\theta) \tag{8}$$

where $C_{in} = 0.25$ is a tunable constant, ρ_a/ρ_w is the air/water density ratio, u_* is the wind friction velocity, $c = \sigma/k$ the wave phase speed, θ_w the wind direction, and the $\max[0,\cdot]$ ensures no negative growth for swell.

The friction velocity u_* is related to the 10 m wind speed U_{10} via a drag law (e.g. $u_* \approx 0.001(0.8 + 0.065U_{10})$, for moderate winds). This exponential growth form ($S_{in} \propto \sigma N$ when active) reflects Miles' theory where growth rate $\sim 28\,u_*/c - 1$ (with a threshold of $c \approx 28\,u_*/\cos\Delta\theta$ for wave components aligned with the wind).

Newer wind-input formulations improve upon this basic form. `WAVEWATCH III` offers several alternative S_{in} parameterizations (often coupled with matching S_{ds} dissipation parameterizations), selected as "ST" switch options. For instance, ST2 is the Tolman and Chalikov (1996) scheme, and ST3 corresponds to WAM Cycle 4 (Janssen 1991 feedback mechanism). The default in WW3 for many applications is ST4, the Ardhuin et al. (2010) source term package. ST4 uses a variant of the ECMWF wave model (ECWAM) wind input (based on Janssen's theory) with adjustments to limit input at high frequencies and high winds.

In ST4, the wind input term is expressed in terms of a non-dimensional growth rate β that depends on wave age and a wave-number-dependent friction velocity $u'_*(k)$. This allows ST4 to explicitly tune the momentum transfer at different scales (e.g. incorporating a sheltering effect for shorter waves in strong winds). The net effect is a more flexible wind input term that, together with a corresponding dissipation term, can be calibrated to observations across a range of conditions.

Other source term packages include ST5 (Rogers et al. 2012 and Zieger et al. 2015 adjustments) and a recently developed ST6 (by a consortium including Donelan, Babanin, Rogers, and Young) which is based on Lake Ocean Wave experiments and introduces explicit swell decay and other refinements.

In summary, all S_{in} formulations share the feature of injecting energy primarily into waves moving in the wind direction, with a growth rate that increases with wind speed and decreases with wave phase speed (i.e. favoring slower, shorter waves).

Linear growth term S_{ln}: In very low-energy conditions (e.g. the initial growth of waves from calm water), some models include a linear wind input term S_{ln} in addition to the exponential S_{in}. This accounts for the earliest stages of wave development where the exponential growth law might underpredict energy input. WW3 allows an optional S_{ln} based on Cavaleri and Malanotte-Rizzoli (1981). This term is proportional to the wave spectrum (thus "linear") and provides growth even for very low-amplitude waves. It is typically small and only active at the start of a simulation or in very young sea states, and is usually turned off once waves reach sufficient energy levels.

A.1.2.2 Nonlinear Wave–Wave Interactions (S_{nl})

Physical mechanism: S_{nl} represents conservative nonlinear energy transfers within the wave spectrum due to resonant interactions among wave quartets (groups of four wave components). In deep water, the dominant nonlinear process is the resonant four-wave interaction (often called the Hasselmann resonance after Hasselmann 1962). In essence, waves can exchange energy with other waves if certain resonance conditions on frequency and direction are satisfied (e.g. $f_1 + f_2 = f_3 + f_4$ and $\mathbf{k}_1 + \mathbf{k}_2 = \mathbf{k}_3 + \mathbf{k}_4$). This results in a redistribution of energy: typically, energy is transferred from the peak of the spectrum toward both lower frequencies (longer waves) and higher frequencies (shorter waves), in a process that maintains total energy and momentum. These nonlinear transfers are crucial for the equilibrium shape of the wave spectrum, allowing a balance between input and dissipation (e.g. driving the -4.5 power-law tail of the spectrum). The S_{nl} term itself has zero net energy input ($\int S_{nl}\, df\, d\theta = 0$), acting only to reshuffle energy across frequencies and directions.

Formulation: The exact expression for four-wave interactions is given by the Boltzmann collision integral derived by Hasselmann (1962, 1963). It is a high-dimensional integral (involving a quadruple integral over interacting wave components) and is extremely expensive to compute directly. The integral can be written schematically as:

$$S_{nl}(f,\theta) = \frac{2\pi g^2}{(2\pi)^4} \iiint G(k_1,k_2,k_3,k_4)\, N_1 N_2 (N_3 + N_4) \times \delta(\mathbf{k}_1 + \mathbf{k}_2 - \mathbf{k}_3 - \mathbf{k}_4)\, \delta(\sigma_1 + \sigma_2 - \sigma_3 - \sigma_4)\, dk_2\, dk_3\, dk_4 \tag{9}$$

where G is a nonlinear coupling coefficient and the delta-functions enforce the resonant conditions (here indices 1 and 2 denote the "sending" waves that lose energy, while 3 and 4 gain energy). While we do not expand this in detail, it is important to note this integral conserves action and ensures the correct nonlinear flux of energy.

Because computing the full integral at every time step is prohibitive, practical models use approximations. WW3 provides multiple options for computing S_{nl}. The traditional approach is the Discrete Interaction Approximation (DIA) of Hasselmann et al. (1985), which greatly simplifies the integral by assuming energy exchanges occur in a fixed configuration of four waves with pre-set frequency ratios. The DIA yields a reasonable qualitative representation of nonlinear transfers at a tiny fraction of the cost of the exact solution.

WW3's default for efficiency is often the DIA (switch `NL1`), but it also includes the more accurate Webb–Resio–Tracy (WRT) method to compute the exact Boltzmann integral (within numerical limits). The WRT method uses a sophisticated algorithm to evaluate the 4-wave interactions with discrete integration in k-space and is much more computationally intensive, but can be used for research or high-precision applications.

Intermediate schemes are also available: the Generalized Multiple DIA (GMD) and Two-Scale Approximation (TSA) are improved approximate methods that aim to capture interactions more accurately than the original DIA while remaining faster than WRT. Regardless of the method, all S_{nl} implementations ensure that energy is conserved and only redistributed within the spectrum.

The presence of a realistic S_{nl} term is what defines a third-generation wave model (i.e. the model allows the spectrum to evolve freely toward its equilibrium shape rather than imposing a fixed shape). In summary, S_{nl} is a sink for energy at the spectral peak and a source at both lower and higher frequencies: it transfers energy from where wind input is concentrated to other parts of the spectrum. This spread is what allows waves to grow in height (energy moves to low frequencies, lengthening the waves) and develop a high-frequency tail (energy cascades to short waves that eventually dissipate). Without S_{nl}, a wave model cannot correctly simulate fetch-limited growth or spectral shapes; hence WW3 includes robust options to calculate it, balancing accuracy and computational cost.

A.1.2.3 Wave Breaking Dissipation (S_{ds})

Physical mechanism: Not all wave energy added by the wind remains in the wave field indefinitely – waves lose energy through breaking. In deep water, wave breaking usually occurs in the form of whitecaps (white foam patches) when waves become too steep. This process, known as whitecapping, is a primary sink balancing wind input in the open ocean. S_{ds} represents the rate at which wave energy is dissipated (converted into turbulence and heat) by breaking. Unlike depth-limited breaking in the surf zone, whitecapping can occur in deep water due to wave–wave interactions that cause some waves to exceed a steepness threshold and spill energy. It is a highly nonlinear, scale-dependent process: typically the highest, sharpest waves in a spectrum will break. Because it is impractical to predict individual wave breaking events in a spectral model, S_{ds} is parameterized as a bulk dissipation acting continuously on the spectrum. It predominantly removes energy from the high-frequency part of the spectrum (where waves are shorter and more prone to breaking), but the details of how it acts must be tuned so that the integrated effect matches observed wave growth and decay rates.

Formulation: The true physics of whitecap dissipation are complex and involve wave instability and airflow separation; therefore S_{ds} is formulated empirically with parameters adjusted to close the energy balance with S_{in} and S_{nl}. In the WAM Cycle 3 (Komen) formulation (WW3 switch `ST1`, paired with the Snyder input above), S_{ds} is modeled to be proportional to the spectral density N and to a steepness parameter measuring the wave's energy level relative to a fully developed sea. Specifically, Komen et al. (1984) used a dissipation term of the form:

$$S_{ds}(k,\theta) = C_{ds}\,\hat{\sigma}\,\hat{k}\left(\frac{\hat{\alpha}}{\hat{\alpha}_{PM}}\right)^2 N(k,\theta) \tag{10}$$

where C_{ds} is a negative constant ($C_{ds} \approx -2.36\times10^{-5}$ in WAM), and the hatted variables are normalized quantities (in WAM terms) – $\hat{\alpha}$ is a measure of the wave spectrum's energy density (a nondimensional wave steepness), and $\hat{\alpha}_{PM} = 3.02\times10^{-3}$ is its value for a Pierson–Moskowitz fully developed spectrum. The ratio $(\hat{\alpha}/\hat{\alpha}_{PM})^2$ thus represents how saturated the spectrum is relative to a mature sea state, and $\hat{\sigma}/\hat{k}$ is related to the group velocity (since $\hat{\sigma} = \sigma$ for deep water and $\hat{k} = k$ in the Komen notation). In essence, this formulation says dissipation is stronger when the spectrum's energy level (steepness) exceeds that of a fully developed sea, and it increases with frequency (through the σ/k factor) so that high-frequency waves suffer proportionally more dissipation.

The S_{ds} term is negative definite (always removes energy) and its magnitude grows rapidly with wave steepness, effectively capping the growth of the spectrum to prevent a runaway cascade. The constant C_{ds} is tuned along with C_{in} so that for steady wind conditions, a balance $S_{in} + S_{nl} + S_{ds} = 0$ is achieved at the correct wave energy level and spectrum shape.

Many refinements to the dissipation term have been developed, and WW3 includes several options linked to the chosen wind input scheme. The `ST4` package (Ardhuin et al. 2010) uses a saturation-based dissipation approach: rather than the $(\alpha/\alpha_{PM})^2$ form, it uses the concept of wave spectral saturation $B(k) = k^3E(k)$ and limits the growth of $B(k)$ at high frequencies. ST4's S_{ds} is formulated to dissipate energy at a rate tied to the spectral saturation and includes a cumulative breaking effect (accounting for multiple breaking events of different scales). It also introduces tunable parameters for swell dissipation and steepness thresholds. The ST4 dissipation is paired with a reduced high-frequency wind input (through $u'_*(k)$ as noted earlier) to produce a physically consistent balance.

Another advanced dissipation option is the one in `ST6` (developed from Lake George experiments). ST6 unifies deep and shallow breaking mechanisms and explicitly includes a threshold steepness for wave breaking onset (based on Babanin et al. 2010). Below the steepness threshold, $S_{ds} = 0$; above it, dissipation kicks in. It also accounts for the cumulative

effect of breaking and wave–turbulence interactions for very young waves. These improvements allow ST6 to capture phenomena like reduced breaking in young wind seas and enhanced swell decay in very old seas.

Summary: S_{ds} is modeled such that small, steep waves are efficiently damped, preventing unlimited growth at high frequencies, while allowing larger waves to develop until a balance with wind input is reached. The exact mathematical form of S_{ds} varies by parameterization, but it always serves as a negative feedback on wave growth. All dissipation formulations contain empirical coefficients that are calibrated against wave growth curves and observations (e.g. fetch growth experiments, wave spectra measurements). In WW3, these coefficients (like C_{ds}, $\hat{\alpha}_{PM}$, or their analogues in ST4/ST6) can be adjusted via namelist parameters, allowing tuning for specific conditions if necessary. Typically, the chosen default (such as ST4 in WW3 v6) has been calibrated to perform well over a wide range of conditions.

A.1.2.4 Bottom Friction (S_{bot})

Physical mechanism: When waves travel in shallow water, the orbits of water particles under the waves extend to the sea floor. This interaction causes bottom friction: the wave's motion induces shear stress in the bottom boundary layer, dissipating wave energy as heat. S_{bot} represents the loss of spectral energy due to this wave–seabed friction. The efficiency of bottom dissipation depends on the seabed roughness and the wave orbital velocity near the bed. In sandy or muddy areas, substantial energy can be absorbed, especially for shorter-period waves which have stronger near-bed velocities. In very deep water, $S_{bot} \approx 0$ because wave-induced motion decays exponentially with depth (negligible at the bottom).

Formulation: WW3 provides multiple formulations for bottom friction, from simple empirically constant models to complex physics-based models. The simplest is the JONSWAP parameterization (from the 1973 JONSWAP experiment analysis), which assumes a linear wave energy decay with a constant friction coefficient. In WW3 this is labeled `BT1`. Using Tolman's (1991) notation, the JONSWAP bottom friction source term is written as:

$$S_{bot}(k,\theta) = 2\,\Gamma\, n^{-0.5}\, g\, d\, N(k,\theta) \tag{11}$$

where Γ is an empirical drag coefficient and $n = c/c_g$ is the ratio of phase to group velocity (related to how much energy is "stored" in a wave; in deep water $n = 1/2$). The constant Γ is typically set to -0.067 m^{2}s^{-3} for wind sea and -0.038 m^{2}s^{-3} for swell. (The negative sign indicates energy removal.) These values were determined by Hasselmann et al. (1973) and by Bouws & Komen (1983) from field observations.

Essentially, this formula produces a sink term proportional to the action density N (hence linear in the spectrum) with a magnitude that increases for lower group velocity waves (via $n^{-0.5}$) – implying higher dissipation for shorter period waves, which is physically consistent (short waves have higher orbital velocities near the bed for a given energy level).

While the JONSWAP/`BT1` model is simple, real bottom friction can depend on wave amplitude and bottom roughness in a nonlinear way. WW3's `BT4` option implements a more complex bottom friction model based on the SHOWEX experiment and the theory of Grant & Madsen (1979). This formulation considers a turbulent boundary layer over a rough seabed, including effects of sediment ripples and sheet flow at high wave energies. The dissipation in `BT4` is frequency-dependent and is often expressed in terms of an equivalent bottom friction coefficient that depends on wave orbital Reynolds number. In the WW3 manual, the `BT4` source term is given by:

$$S_{bot}(k,\theta) = -f_{eub}(k)\,\frac{\sigma^2}{2g\sinh^2(kd)} \tag{12}$$

where $f_{eub}(k)$ is an effective energy dissipation factor that encapsulates the bottom roughness and wave amplitude effects, and the $\frac{\sigma^2}{2g\sinh^2(kd)}$ term relates to the near-bed orbital velocity variance for a wave of frequency σ at depth d. Thus, dissipation is proportional to the square of orbital velocity (since $u_{\text{orb}}^2 \sim \frac{\sigma^2}{\sinh^2(kd)}E$) – a fundamentally quadratic friction law. The factor f_{eub} is calculated from the bottom drag coefficient, which in turn depends on grain roughness, ripple geometry, etc. If the seabed is rougher or the wave orbital amplitude is larger, f_{eub} increases, enhancing dissipation. In practice, `BT4` is tuned to perform better for sandy bottoms by accounting for the increase in friction as waves get larger (e.g., mobilizing sediment into ripples that increase roughness).

Between these extremes, other bottom friction formulations exist (e.g., Collins (1972) drag law, or a modified eddy-viscosity approach). WW3 also includes specialized dissipation terms for muddy bottoms (S_{mud}), where energy loss is due to viscous absorption in a soft mud layer rather than turbulent grain roughness. These are implemented as separate source terms (e.g., based on Dalrymple & Liu 1978, and Ng 2000 models for mud).

For most applications with a solid sandy bottom, however, users choose either a constant friction coefficient (`BT1`) for simplicity or the more advanced formulation (`BT4`) if site-specific calibration data are available.

Summary: S_{bot} is always a negative term (dissipative) and primarily affects shorter waves in shallow water. It becomes significant when the water depth is such that waves "feel" the bottom (roughly when depth $dL/2$ where L is wavelength). WW3's flexible formulations allow S_{bot} to be tuned from simple uniform damping to highly realistic, environment-specific damping. By default, a moderate value of bottom friction (e.g., JONSWAP with $\Gamma = -0.067$) might be used for coastal regions, but for detailed hindcasts in shallow bays or continental shelves, the SHOWEX (`BT4`) option can improve accuracy by representing the physics of the bottom boundary layer more faithfully.

A.1.2.5 Depth-Induced Breaking (S_{db})

Physical mechanism: As waves propagate into very shallow water (surf zone), their height is limited by the water depth. When the wave steepness or height-to-depth ratio becomes too large, waves break in the surf (plunging or spilling breakers), rapidly dissipating energy. This depth-induced breaking is distinct from whitecapping (S_{ds}) – it is primarily controlled by the seabed shallowness rather than wind or wave steepness alone. Depth-induced breaking typically affects waves as they approach the shore (e.g., on shoals, reefs, or beach slopes) and is responsible for the large loss of energy between deep water and the shoreline. In spectral models, S_{db} is included to handle this nearshore wave energy dissipation that S_{ds} (tuned for deep water) may not adequately capture in very shallow depths.

Formulation: WW3 uses an approach based on the empirical model of Battjes and Janssen (1978) for breaking waves in shallow water (WW3 switch `DB1`). The Battjes & Janssen (B&J) model does not predict individual wave breaking; instead, it assumes that at any given time a certain fraction Q_b of waves are actively breaking. The breaking fraction Q_b is determined by assuming the distribution of wave heights follows a Rayleigh distribution truncated by a maximum possible wave height $H_{\max}$ (which is depth-limited). B&J derive an implicit equation for Q_b in terms of the root-mean-square wave height H_{rms} and $H_{\max} = \gamma d$ (where γ is an empirical breaking index, typically around 0.73 for random waves on a flat bottom).

In WW3, γ is a tunable parameter with default $\gamma = 0.73$ (though other studies suggest values from 0.55 to 0.8 depending on bottom slope and wave spectra). Once Q_b is found (iteratively from the B&J equation), the total energy dissipation per unit surface area due to breaking, δ, is computed as proportional to Q_b and $H_{\max}^2$ (reflecting that larger waves dissipate more energy when breaking). B&J gave an expression $\delta = \frac{3}{4}\rho_w g Q_b H_{\max}$ (for monochromatic

waves), which WW3 adapts for the spectrum.

The spectral sink term $S_{db}(f,\theta)$ is then formulated by distributing the total dissipation δ across the frequency spectrum in proportion to the energy density at each (f,θ). In other words, it assumes all parts of the wave spectrum break equally (a crude assumption, but common in spectral models):

$$S_{db}(f,\theta) = -\alpha\,\delta\,\frac{E(f,\theta)}{E_{\text{tot}}} \tag{13}$$

where $E_{\text{tot}} = \int E(f,\theta)\,df\,d\theta$ is the total wave energy, and α is a calibration coefficient (WW3 default $\alpha = 1.0$). This ensures that the integrated S_{db} equals $-\delta$ (i.e., the correct total energy removal) while preserving the spectral shape (since each spectral component is reduced by the same fraction in a breaking event).

In the WW3 manual, this is expressed as equation (2.169), for which a simplified form is:

$$S_{db}(k,\theta) = -0.25\,\alpha\,Q_b\,f_m\,H_{\max}^2\,\frac{E(f,\theta)}{E_{\text{tot}}} \tag{14}$$

where f_m is an empirical factor related to mean frequency. The factor 0.25 arises from assumptions in the derivation and α can be tuned slightly (though typically left at 1). The B&J depth-limited breaking model is widely used (also in SWAN and other nearshore models) because it provides a realistic bulk dissipation that matches observed wave decay over reefs and surf zones with a suitable choice of γ.

WW3 allows the user to choose between the B&J method (`DB1`) and an alternative "microwave limiter" (MLIM) approach. The limiter approach (not described in detail in the manual snippet) likely caps the spectrum when a wave height to depth criterion is met, rather than explicitly computing a source term. By default, WW3 uses the B&J explicit source term (Eq. 2.169) with $\gamma = 0.73$. Users can adjust γ if needed (e.g., on very mild slopes, a smaller γ like 0.55 might be more appropriate, per Nelson 1994).

Summary: S_{db} acts as a strong sink activated in shallow water when waves approach the depth breaking limit (typically $H_{\text{rms}}/d > 0.5$ or so). It is usually zero in deeper water and only becomes nonzero as depth decreases to the point of incipient breaking. In such cases it can dissipate a large portion of wave energy in a narrow coastal region (the surf zone). The inclusion of S_{db} in WW3 allows the model to simulate wave height saturation near the shore, complementing the deep-water S_{ds} term which on its own would not fully dissipate waves in very shallow depths.

A.1.2.6 Triad Wave–Wave Interactions (S_{tr})

Physical mechanism: In shallow water, nonlinear triad interactions (three-wave interactions) become possible and can significantly shape the wave spectrum. Unlike deep-water four-wave interactions, triads involve two primary waves interacting to generate a third wave (often a frequency that is the sum or difference of the two). This process is important in shoaling waves: for example, energy from a dominant wave at frequency f can be partially transferred to a higher harmonic at $2f$ (and sometimes to a subharmonic). Triad interactions are a conservative (energy-preserving) nonlinear transfer, typically transferring energy from the primary spectral peak to higher frequencies (and sometimes to infragravity frequencies) as waves enter shallow water. This leads to the characteristic spectral widening and development of harmonic peaks observed near shore. Triad interactions are most pronounced when the water depth is such that the wave steepness is moderate and the dispersion is weak (usually in intermediate depths where kd is small enough for nonlinear effects but not so small that waves have broken).

Formulation: WW3 includes an optional triad interaction term S_{tr} (switch `TR1`), which uses a Lumped Triad Approximation (LTA) based on the work of Eldeberky (1996). The

LTA is a spectral implementation derived from Boussinesq wave model equations (Madsen & Sørensen 1993) averaged to yield a stochastic source term for spectral energy transfers. In essence, it parameterizes the collective effect of many triad interactions in a simplified way.

The model assumes that triad interactions predominantly transfer energy to the frequency around $2f_p$ (double the peak frequency) and perhaps to a small degree to a difference frequency (infragravity waves). The LTA requires specification of a cutoff frequency (often 2.5 times the mean frequency) up to which interactions are computed. The WW3 manual notes that Eldeberky (1996) suggests limiting triad computations to $f_{\max,\mathrm{EB}} \approx 2.5 f_{m01}$ (2.5 times the mean frequency) to capture the important harmonic generation without excessive computations.

The specific formulation of S_{tr} is somewhat complex: it involves an integral of the product of three N terms and a coupling coefficient, but LTA simplifies it to an algebraic source term that is a function of the local spectrum. Typically, it will have the form of a source at the harmonic frequency and a sink at the primary frequency (ensuring no net energy change). The WW3 implementation was adopted from the SWAN model's triad module, as indicated by "Provided by A. van der Westhuysen" (who contributed to SWAN). This suggests it is the same formulation used in SWAN, which was tuned to reproduce observed spectral energy transfer in nearshore environments.

Effect and usage: When activated, S_{tr} will drive energy from the spectral peak to higher frequencies as depth decreases, simulating the generation of harmonics (e.g., the development of a secondary peak at twice the frequency of the primary swell). It does not add or remove total energy, only redistributes it. However, modeling triads in a phase-averaged model is challenging, and the accuracy of current parameterizations is limited. The WW3 manual cautions that present triad parameterizations have "limited accuracy", so this term is used with care.

In practical applications, S_{tr} might be enabled for detailed nearshore wave modeling when the spectral shape (e.g., wave period distribution) is important, such as for calculating wave run-up or surf beat. In large-scale models or when focusing only on integral wave height, S_{tr} can often be neglected.

Summary: S_{tr} provides WW3 with a capability to simulate nonlinear spectral evolution in shallow water beyond what four-wave interactions can do, capturing some of the energy transfer to higher frequencies that occurs before waves break. It is a conservative source term (zero net energy) that, when activated, complements S_{bot} and S_{db} in shaping the nearshore spectrum. It is usually only significant in depths on the order of one to a few wavelengths, and it ceases to be important in deep water (where quadruplet interactions dominate instead).

A.1.2.7 Wave–Ice Interaction Losses (S_{ice})

Physical mechanism: Ocean surface waves traveling into ice-covered waters experience attenuation through various processes. If the sea is partially covered by sea ice (e.g., floes, pancake ice, or continuous ice cover), wave energy can be dissipated by viscous damping, scattering, and wave–ice elastic interactions. For example, ice floes can flex and absorb wave energy, or waves propagating under a continuous ice sheet are damped by friction in the underlying water layer and by the bending of the ice. Also, irregularities in the ice edge or floe distribution can scatter wave energy, redistributing it directionally (and to a lesser extent in frequency). These processes are represented by source terms generally denoted S_{ice} (for energy losses due to ice) and sometimes S_{is} for scattering. In WW3, wave–ice interactions are treated via additional sink terms that become active when an ice concentration is present in a grid cell.

Formulation: WW3 includes a suite of wave–ice source term options (switches `IC1` through `IC5`, etc.), reflecting ongoing research in this area.

- **Simple exponential damping (IC1):** This approach applies an exponential decay of wave energy with distance into the ice, characterized by an attenuation rate $\kappa(f)$ that can be specified or tuned. In spectral form, this manifests as:

$$S_{ice}(f,\theta) = -2\kappa(f)\, c_g\, E(f,\theta) \tag{15}$$

  since $\partial E/\partial x = -2\kappa E$ gives an energy sink. This simple model can be calibrated to observations of wave decay in ice fields.

- **Viscoelastic plate models (e.g., IC2 – Liu et al.):** These are based on treating the ice cover as a viscoelastic layer that interacts with the waves. Liu et al. (1991) provided a model where the ice layer's flexural motion leads to energy loss. Such models yield frequency-dependent attenuation rates that often scale as a power of frequency (e.g., higher-frequency waves attenuate faster under ice). WW3's "Liu et al." option implements this theory, producing S_{ice} terms that remove energy at a rate consistent with an assumed viscosity or elastic modulus of the ice.

- **Wave–ice drag models (e.g., IC3 – Shen et al.):** Shen et al. (1987) developed models for wave damping in pancake or frazil ice, where a turbulent layer under the ice causes dissipation. WW3 includes such a formulation, which might treat the ice-covered water as a two-layer viscous fluid. The resulting S_{ice} is again a frequency-dependent sink term.

- **Empirical and combination models:** WW3 also has an empirical/parametric damping option (`IC4`), where the user can input observed attenuation curves or use simple power-law fits. Additionally, `IC5` (Mosig et al. 2015) likely combines scattering and dissipation in a more advanced way, possibly partitioning the energy loss into components due to scattering versus true dissipation.

Scattering (S_{is}): WW3 distinguishes pure scattering processes as S_{is} (these redistribute energy in direction or space without net loss). For example, an ice floe scattering model will take incident wave energy and scatter it into other directions (and perhaps slightly lower frequencies). This doesn't directly remove energy but can effectively cause local reductions as energy spreads out. WW3's `IC6`/`IC7` options include such scattering, including floe-size dependent scattering where smaller floes scatter high-frequency waves, etc. In the model, scattering might be treated by a diffusion term in spectral space or by adding a directional spread in the source term (so it is not a simple negative sink like others).

Practical considerations: In practice, wave attenuation in ice is often modeled as an exponential decay with distance. The various S_{ice} formulations in WW3 are calibrated so that the overall decay of wave energy in an ice field matches observations or theory. For example, if measurements show that wave height is reduced by 50% over 100 km of marginal ice zone for 10 s period waves, the S_{ice} term will be tuned accordingly. The presence of S_{ice} is conditional on the model's ice concentration or ice mask – it is only active where ice is present (often defined by an ice concentration threshold, e.g., >0.1).

Summary: S_{ice} (and S_{is}) provide frequency-dependent damping of the wave spectrum in ice-covered regions. High-frequency waves are usually attenuated more strongly than low-frequency swells, so $S_{ice}(f)$ typically increases with f. These terms are important for high-latitude and winter wave modeling, ensuring that the model does not propagate unrealistically large waves through ice fields. By including multiple options, WW3 allows users to choose a wave–ice interaction model suited to the ice conditions of their simulation (e.g., thick continuous ice vs. broken floes vs. slush ice). The ultimate effect of S_{ice} is a sink of energy that can be substantial – large wave events can be markedly reduced in energy after passing through hundreds of kilometers of ice. Scattering terms S_{is} redistribute some of that energy

(e.g., scattering can spread wave energy to wider angles, reducing the peak energy), and a portion of scattered energy may eventually be lost (e.g., via repeated scattering or dispersion).

A.1.2.8 Additional Source/Sink Terms and Features

Beyond the major source terms described above, WW3 includes a few specialized terms and mechanisms:

- **Bottom Scattering (S_{bs}):** This term accounts for scattering of wave energy by unresolved small-scale bathymetric variations (such as seabed rocks, coral heads, or sand bars). It does not directly remove energy, but redistributes it in direction (and possibly frequency). In WW3 it is labeled S_{bs} (or S_{sc} in some documentation). The effect is similar to having a rough sea floor that scatters wave rays – energy from a wave traveling in one direction might be partially scattered into other directions, leading to a more diffuse wave field. This term is usually small and is often omitted unless modeling regions with very irregular bottom features.

- **Unresolved Obstacles (S_{uo}):** WW3 can account for blocking and reflection by sub-grid obstacles (small islands, atolls, breakwaters) through a dedicated source term S_{uo} (unresolved obstacle term). Instead of explicitly masking out energy behind an obstacle, a sink term can be applied to simulate the wave energy removed by the obstacle's shadow. This term is scenario-specific and requires specifying obstacle locations and transmission coefficients.

- **Wave Reflection (S_{ref}):** When waves hit a solid boundary like a coastline or a large iceberg, some energy is reflected back seaward. WW3 can include a source term S_{ref} to represent reflected wave energy added back into the model domain. S_{ref} can also generate low-frequency waves (e.g., infragravity waves) if the reflection involves downshifting of energy – for instance, waves breaking on a shoreline can induce infragravity oscillations that travel back as long-period waves. In practice, reflection is often handled through boundary conditions rather than a source term, but WW3's S_{ref} provides a way to inject reflected energy within the spectral model itself. This is particularly useful in partially enclosed domains or for iceberg-rich seas where random reflection occurs not at a single boundary but throughout an area.

- **Swell Decay due to Air–Sea Friction:** While negative wind input was discussed under S_{in}, it is worth noting that WW3 can impose additional damping on swell via a gentle negative source term when waves outrun the wind. Some source term packages (e.g., `ST6`) explicitly include a swell dissipation term representing wave energy lost to the atmosphere or ocean turbulence for very low-curvature waves. This is not a separate S in the equation (it is lumped into S_{in} or S_{ds} depending on implementation), but conceptually it is an additional sink for very old waves.

- **User-Defined (S_{user}):** WW3 provides a placeholder where users can plug in any custom source term (S_{xx} in the code, labeled S_{user}). This can be used for experimental source functions, such as wave–current interaction terms (if one wanted to add an additional coupling term beyond the conservative Doppler shift already in the left-hand side), or wave emission from moving vessels, etc. By default, $S_{user} = 0$ unless a specific mechanism is coded by the model user.

Finally, it is important to note that in WW3's numerical solution, some of these source terms can be handled with special techniques. For example, spectrum limiting or filtering is sometimes applied to prevent the model from producing non-physical negative spectra

or overshoots when sources are strong. Depth-induced breaking S_{db} often uses a limiter to ensure the spectrum after breaking is physically plausible (e.g., not removing too much at one frequency). These algorithmic details ensure stability and physical fidelity.

The source and sink terms in the WW3 action balance equation encapsulate all the important physical processes in wind–wave evolution. The governing equation presented at the start of this section, together with the detailed source term formulations described here, form the theoretical backbone of WW3. Wind input (S_{in}) and dissipation (S_{ds}) govern wave growth and decay, nonlinear transfers (S_{nl} and S_{tr}) shape the spectrum, and bottom and ice terms (S_{bot}, S_{db}, S_{ice}) handle interactions with the environment.By selecting appropriate parameterizations (e.g., `ST4` for open ocean, adding `BT4` and `DB1` for coastal shallow waters, `ICx` for ice, etc.), the model can be tuned to a wide range of scenarios. This framework, originally laid out by the WAM model developers *[Group, 1988]* and continuously refined in later developments of WW3 *[Center, 2019]*„ allows WW3 to simulate the life cycle of ocean waves from generation by winds, through nonlinear evolution, to eventual dissipation by breaking, bottom drag, or ice. The next section will apply this theoretical framework to specific modeling case and discuss the performance of these source term choices in practical wave hindcast.

Acknowledgements

Each morning, without exception, there was a message waiting for me—a short voice note from my dad, wishing me good morning. It arrived before the day began. It carried a warmth that did not ask for response, only presence. I rarely replied, but it stayed with me, warming the hours that followed. I am certain that on the rare mornings he forgot, my mother was there to remind him. Without such a family—their care, their support, and much more than I could ever name—I would not be the person I am today.

With that quiet assurance, I would begin my day. Somewhere between the first light filtering through the window and the rhythm of getting ready, their presence remained—not as instruction, but as steadiness. From my mother, I learned patience and a sense of inward calm, shaped by belief and reflection. From my father, I learned that care can take many forms at once—discipline and humor, emotion and practicality, firmness and reassurance. These lessons were never spoken aloud, yet they followed me into adulthood, into work, into silence.

As I stepped outside, the world was different from where I grew up. The air was colder, the streets quieter, the rhythm unfamiliar. Living far from home meant learning to carry my family with me in subtler ways. My brother, though often far away, was always part of that background certainty—the kind that does not demand constant checking in, only trust. Knowing he would be there if needed was enough.

I am also grateful to Vijith, who taught me during my Master's studies and whose friendship, encouragement, and support have remained with me throughout the years.

Some mornings, as I moved through my day, memories surfaced unexpectedly. I would think of my father's elder brother, who, during my bachelor's studies, used to take me shopping each year when the university reopened, making sure I had what I needed without ever making it feel like an obligation. Years later, after I began working, I returned home and found myself able to do the same for him. The joy he felt—and the tears he did not hide—stayed with me long after I returned. It reminded me that care has its own sense of timing, and that giving back often arrives quietly, when one is finally ready.

These moments—past and present—wove themselves into the ordinary structure of my days. My cousin brothers, my relatives, and the wider circle of family remained present not through constant contact, but through an enduring sense of belonging. Even while building a life far from home, I never felt untethered. The day could unfold—uncertain, demanding, unfinished—yet beneath it all was the same foundation that had always been there.

By the time I stepped outside, the day had fully begun. Delft revealed itself slowly—canals still, streets orderly, the air carrying a kind of calm that was unfamiliar at first but gradually became grounding. Walking the same paths each morning, I learned the discipline of repetition. The pace was unhurried, almost meditative. Somewhere between footsteps and thought, I found space to reflect—or sometimes, not to think at all.

Work did not begin abruptly. It accumulated. The building came into view, familiar and unremarkable in its appearance, yet filled with conversations, questions, and long stretches of concentration. Much of my PhD unfolded in my office—a shared space where I was the only woman among three men, a fact that never needed emphasis but quietly shaped the dynamic.

Yared, a postdoctoral researcher and also a friend, brought sharp thinking and a good sense of humour into the room. His questions were thoughtful, his suggestions usually came at the right time, and his teasing—often at my expense—made sure things never felt too serious for too long. Chimango had just started his PhD, carrying the curiosity and energy of someone at the very beginning, while Sajid blended into the steady rhythm of the office. Between work discussions, small jokes, and long quiet stretches of concentration, the office slowly became more than just a place to work—it became part of my everyday life.

Not all writing happened there. Some afternoons, I would leave the building and walk toward the station, to a small restaurant called Seven Hills. It became a quiet extension of my workspace—a place where chapters took shape, sentences were revised, and ideas were allowed to breathe. I had my own spot there, familiar and undisturbed. The people working there were always kind, unassuming, and present in a way that made it easy to stay for hours. Many pages of this thesis were written there, surrounded by ordinary life unfolding at nearby tables.

As the work deepened, so did the academic relationships that guided it. My promotor, Andrei Metrikine, was one of the first people to interview me at the start of this journey. Our discussions were often marked by both agreement and disagreement—moments of challenge that demanded clarity and rigor. His questions were never superficial; they pushed me to think more deeply, more structurally. Beneath that intellectual intensity, I always sensed care—the kind that does not soften expectations, but holds them steady. Over time, he became a fatherly presence in a place far from home.

If the structure of my PhD had a backbone, however, it was my daily supervisor, José. From the moment he entered my academic life, I learned what thoughtful supervision truly meant. He never rushed solutions, never imposed pressure where it was unnecessary. Instead, he approached problems from my perspective, helping me find clarity without losing confidence. Through him, I learned how to think strategically, how to prioritise myself alongside my work, and how to move forward without force. His intelligence, generosity, and genuine happiness in my progress shaped not only this thesis, but the way I understand mentorship itself.

I am also grateful to Ada van Gulik, my confidential advisor, whose guidance, understanding, and steady support during a challenging period of my PhD helped me navigate difficulties with greater clarity and made that part of the journey much smoother.

There was a period when the rhythm of my days became uncertain. Midway through the PhD, I changed my supervisor, and with that change came a stretch of confusion I had not anticipated. I was no longer sure whether I would be able to complete the PhD, or whether I would finish it on time. The work did not disappear, but my confidence did. Questions that once felt challenging began to feel heavy.

During that time, my body registered what my mind tried to ignore. Health issues emerged quietly at first, then more insistently. It became clear that persistence alone would not carry me forward. I had to learn something I had never prioritised before: myself. With guidance and steady support from my supervisor, I began to approach both work and life differently—more deliberately, with boundaries, and with care. There is a lot of you in what I carry ahead, José.

I started going to the gym, not as a solution but as a routine. Movement brought structure back into my days. Strength returned gradually, first physically and then mentally. Through that process, I realised that I carried more resilience than I had ever given myself credit for. I learned to recognise my own self-worth and to hold onto self-respect, even in moments of uncertainty.

As my confidence returned, so did my curiosity. Research that once felt overwhelming became engaging again. Ideas connected more quickly, and the work began to flow. Publications followed, not as a sudden breakthrough, but as a quiet accumulation of effort and focus. I realised that I had been underestimating my own capacity—that I was able to create meaningful work within shorter periods than I had believed possible.

Throughout this turning point, I was not alone. My external advisor, Laura, offered clarity and support when it was most needed, and her presence during this phase helped stabilise a difficult transition. I am also deeply grateful to Kai, my co-author from the United States Geological Survey, whose positivity, kindness, and commitment made the process of reviewing and refining our work both constructive and encouraging. Their support arrived without pressure, and it mattered more than they may know.

The day did not suddenly become easier after that, but it became steadier. I learned to walk forward without forcing certainty, trusting that progress could exist alongside doubt.

In many ways, the Netherlands became the place where my life unfolded through action. It was here that I learned what independence truly meant. Far from home, in a culture entirely different from where I grew up—in its language, food, climate, and social rhythms—I had to do everything on my own. There was no familiar structure to lean on, only the one I slowly built for myself.

Freedom arrived early, and with it came responsibility. Living alone taught me discipline: how to keep myself safe, how to choose carefully, how not to mistake loneliness for companionship. I learned to sit with myself without distraction, to understand what I wanted when no one else was shaping the answer. Over time, that freedom became clarifying rather than overwhelming.

The weather, too, became a teacher. I was used to rain—Kerala had given me that—but the cold was new. At first it felt refreshing, almost gentle. Over time, winter revealed itself more honestly. My body resisted its rhythm, and I learned that I was not made for long darkness. I realised, quietly and without disappointment, that I am something closer to a sunflower—responsive to light, lifted by warmth. Accepting this was also a form of self-knowledge. Who knows? perhaps my circadian rhythm is slowly recalibrating.

Walking through Delft each day, I became attentive to small things. A familiar face passing by. A brief greeting exchanged without expectation. Kindness offered in moments so ordinary they could easily be missed. I grew fond of these quiet recognitions—the way life acknowledges you without demanding explanation.

Some of the most meaningful moments came close to home. Over the years, I became close to my neighbours and to their daughter, Ivy. She was born around the time I began my PhD, and by the time I was nearing its end, she was already four. Being greeted by her on my walks to and from work—her running toward me with joy, calling my name, offering hugs and kisses—became one of the purest forms of happiness in my days. Her family often called me her godmother, a title I carried with quiet pride. Even their dog, Ponio, became part of this small world I learned to feel safe in.

These moments anchored me. They reminded me that life does not pause while a thesis is written—it continues, generously, alongside it.

Beyond home and work, friendships formed in gentle, unexpected ways. Some were longstanding, like Annie, whose friendship has been part of my life since kindergarten, and Shalot, whose presence has accompanied me since my bachelor's days. Others arrived through chance encounters and shared moments: Aravind, whose friendship began through creative work and carried me through difficult times; Raghavi, whose support and understanding came with the wisdom of someone who had already completed the journey; and friends such as Sreepriya, Milcah, Sarath, and Elsitta, whose presence, encouragement, and companionship enriched different stages of my life. And Maria, my neighbor, whose eye for style and everyday advice quietly shaped how I learned to carry myself here. There were others, too—colleagues

across departments, familiar faces in places I returned to often, people whose names I may not list but whose warmth made this place feel lived-in.

As days turned into years, I grew emotionally, mentally, and physically. I learned resilience not as a grand concept, but as a daily practice. I learned to walk forward without certainty, to trust effort without demanding immediate reward, and to recognize my own worth independent of outcomes.

As this chapter of my life comes to a close, I find myself grateful not only for the people and places that shaped it, but for time itself—for the slow unfolding that allowed me to become who I am. This thesis is a record of work completed, but more importantly, it is a trace of a life lived with care, discipline, and intention. For that, and for everything that carried me here, I am deeply thankful.

I believe we move through life together.
Every day is shaped by many people,
often without knowing it.
I carry their kindness with me,
and I remain thankful for it.

List of Abbreviations

AO	Arctic Oscillation
CDF	Cumulative Distribution Function
CMEMS	Copernicus Marine Environment Monitoring Service
CMIP	Coupled Model Intercomparison Project
CMIP6	Coupled Model Intercomparison Project Phase 6
DECK	Diagnostic, Evaluation and Characterisation of Klima experiments
DJF	December–January–February
EA	East Atlantic pattern
EAWR	East Atlantic–Western Russia pattern
EC-Earth3	EC-Earth version 3 climate model
ECMWF	European Centre for Medium-Range Weather Forecasts
EEZ	Exclusive Economic Zone
ERA5	ECMWF Reanalysis version 5
GCM	Global Climate Model
HighResMIP	High Resolution Model Intercomparison Project
IOA	Index of Agreement
JJA	June–July–August
KD-tree	k-dimensional tree
KDE	Kernel Density Estimation
KGE	Kling–Gupta Efficiency
LTA	Lumped Triad Approximation
MAE	Mean Absolute Error
MAM	March–April–May
MEOW	Marine Ecoregions of the World
MIROC6	Model for Interdisciplinary Research on Climate version 6
ML	Machine Learning
MPA	Marine Protected Area
NAO	North Atlantic Oscillation
NCEP	National Centers for Environmental Prediction
NMB	Normalized Mean Bias
NOAA	National Oceanic and Atmospheric Administration

PC	Principal Component
PCA	Principal Component Analysis
PDE	Partial Differential Equation
POLEUR	Polar–Eurasian pattern
RMSE	Root Mean Square Error
RTI	Regime Transition Index
SCAND	Scandinavian pattern
ScenarioMIP	Scenario Model Intercomparison Project
SI	Scatter Index
SON	September–October–November
SRSI	Seasonal Regime Stability Index
TSA	Two-Scale Approximation
WDPA	World Database on Protected Areas
WAM	WAve Model
WED	Wind Energy Density
WPD	Wave Power Density
WRT	Webb–Resio–Tracy exact nonlinear interaction method
WW3	WAVEWATCH III spectral wave model
WW3DG	WAVEWATCH III Development Group
H_s	Significant wave height
T_{02}	Mean zero-crossing wave period
U_{10}	Wind speed at 10 m height
U_{100}	Wind speed at 100 m hub height
W_{d10}	Wind direction at 10 m height
W_{s10}	Wind speed at 10 m height
θ_w	Mean wave direction
S_{in}	Wind energy input source term
S_{nl}	Nonlinear wave–wave interaction source term
S_{ds}	Whitecapping dissipation source term
S_{bot}	Bottom friction dissipation source term
S_{db}	Depth-induced breaking dissipation source term
S_{tr}	Triad wave–wave interaction source term
S_{ice}	Wave–ice interaction dissipation source term
S_{is}	Wave–ice scattering source term
S_{bs}	Bottom scattering source term
S_{ref}	Wave reflection source term
S_{ln}	Linear wind input growth source term
S_{user}	User-defined source or sink term
S_{uo}	Unresolved obstacle dissipation source term
ST1–ST6	WW3 wind input and dissipation source-term packages
BT1	JONSWAP bottom friction formulation
BT4	SHOWEX-based bottom friction formulation
DB1	Battjes–Janssen depth-induced breaking formulation
TR1	Triad interaction parameterisation
IC1–IC7	Wave–ice interaction parameterisations

List of Figures

List of Tables

About the Author

Ponni Maya was born in Thiruvananthapuram, Kerala, India, where she completed her schooling. She obtained her Bachelor's degree in Physics from All Saints' College, Thiruvananthapuram. In 2019, she commenced her Master's studies in Physical Oceanography at Cochin University of Science and Technology. During the final phase of her Master's programme, she carried out her Master's thesis in collaboration with the Indian Institute of Tropical Meteorology (IITM), Pune. Owing to the COVID-19 pandemic, this research was conducted remotely. She completed her Master's degree in 2021. After graduating from her Master's programme, she began her doctoral research in February 2022 at Delft University of Technology (TU Delft), the Netherlands. Her PhD research was conducted at the Faculty of Civil Engineering and Geosciences, within the Hydraulic Engineering department, under the Offshore Engineering section.

List of Publications

Peer-Reviewed Journal Articles

1. **Maya, P.**, Parker, K., Cagigal, L., Metrikine, A. V., & Antolínez, J. A. A. *Multivariate spatio-temporal clustering approach to assess wind–wave variability in European seas. Atmosphere*, under review.

2. **Maya, P.**, Parker, K., Cagigal, L., Metrikine, A. V., & Antolínez, J. A. A. *Benchmarking wind–wave resource variability across EC-Earth3 ScenarioMIP and HighResMIP experiments using ERA5-derived climate clusters. Journal of Ocean Engineering and Science*, under review.

3. **Maya, P.**, Parker, K., Cagigal, L., Metrikine, A. V., & Antolínez, J. A. A. *Assessing future transitions in European wind–wave regimes using a fixed ERA5-derived clustering framework and EC-Earth3P-HR simulations. Renewable Energy*, under review.

Conference Proceedings and Abstracts

1. Maya, P., Álvarez Antolínez, J. A., Js, D., & Gnanaseelan, C. (2024). *Interannual and decadal sea-level variability over the Indo-Pacific Oceans in reanalysis and CMIP6 historical simulations and projections. EGU General Assembly Conference Abstracts*, EGU24-9762.

2. Maya, P., Antolínez, J. A. A., & Metrikine, A. V. (2024). *The integrative analysis of wave and wind climate historical simulations and projections under shared socioeconomic pathways in the CMIP6 framework. 3rd International Conference on Natural Hazards and Risks in a Changing World: Addressing Compound and Multi-Hazard Risk*, Amsterdam, The Netherlands.

3. Maya, P., Lavidas, G., Metrikine, A. V., & González, M. A. (2023). *CMIP6 wave climate simulation in the European North-East Atlantic Basin using WAVEWATCH III. Proceedings of the 15th European Wave and Tidal Energy Conference (EWTEC 2023).*

Peer-Reviewed Technical Reports

1. Maya, P., & Lavidas, G. (2022). *Nearest-neighbour techniques for global and regional statistical analysis of high-temporal-resolution CMIP6 surface wind speed using ECMWF reanalysis and satellite winds. OTEC: Report of the Institute of Ocean Energy, Saga University*, 27, 113–125.

Honours and Awards

1. **Best Presentation Award**, International Platform on Ocean Energy for Young Researchers (IOES 2025), Saga University, Japan, for the presentation entitled *AI-Enhanced Offshore Wind and Wave Energy Mapping: A Multi-Resolution Analysis with ERA5, EC-Earth3 Scenarios, and High-Resolution EC-Earth.*

2. **Young Researcher Cash Award**, Institute of Ocean Energy, Saga University, Japan (2022), awarded for an outstanding research presentation on nearest-neighbour techniques for analysing high-resolution CMIP6 wind fields.

```
regimes = KMeans(9).fit_predict(PCA(30).fit_transform(X_std))
```